Characteristic Time Model Validation

Final Technical Report

K.V. Tallio, R.C. Prior, Jr., and A. M. Mellor*

U.S. Army Research Office

Contract Number DAAG29-84-K-0165

Department of Mechanical Engineering and Mechanics
Drexel University
Philadelphia, PA

September 1988

Approved for Public Release;
Distribution Unlimited

*All of the authors are now in the Department of Mechanical Engineering, Vanderbilt University, Nashville, TN.

ADA201374

UNCLASSIFIED
SECURITY CLASSIFICATION OF THIS PAGE

MASTER COPY - FOR REPRODUCTION PURPOSES

REPORT DOCUMENTATION PAGE

1a. REPORT SECURITY CLASSIFICATION Unclassified	1b. RESTRICTIVE MARKINGS NA
2a. SECURITY CLASSIFICATION AUTHORITY NA	3. DISTRIBUTION/AVAILABILITY OF REPORT Approved for public release; distribution unlimited.
2b. DECLASSIFICATION/DOWNGRADING SCHEDULE NA	
4. PERFORMING ORGANIZATION REPORT NUMBER(S) NA	5. MONITORING ORGANIZATION REPORT NUMBER(S) ARO 21743.4-EG
6a. NAME OF PERFORMING ORGANIZATION Drexel University 6b. OFFICE SYMBOL (If applicable) NA	7a. NAME OF MONITORING ORGANIZATION U. S. Army Research Office
6c. ADDRESS (City, State, and ZIP Code) Mechanical Engineering and Mechanics Depart. Philadelphia, PA 19104	7b. ADDRESS (City, State, and ZIP Code) P. O. Box 12211 Research Triangle Park, NC 27709-2211
8a. NAME OF FUNDING/SPONSORING ORGANIZATION U. S. Army Research Office 8b. OFFICE SYMBOL (If applicable)	9. PROCUREMENT INSTRUMENT IDENTIFICATION NUMBER DAAG29-84-K-0165
8c. ADDRESS (City, State, and ZIP Code) P. O. Box 12211 Research Triangle Park, NC 27709-2211	10. SOURCE OF FUNDING NUMBERS PROGRAM ELEMENT NO. / PROJECT NO. / TASK NO. / WORK UNIT ACCESSION NO.

11. TITLE (Include Security Classification)
Characteristic Time Model Validation (unclassified)

12 PERSONAL AUTHOR(S)
Tallio, K.V., Prior, R.C. Jr., Mellor, A.M.

13a. TYPE OF REPORT	13b. TIME COVERED	14. DATE OF REPORT (Year, Month, Day)	15. PAGE COUNT
Final	FROM 10/84 TO 6/88	1988 September	xiii + 168

16 SUPPLEMENTARY NOTATION
The view, opinions and/or findings contained in this report are those of the author(s) and should not be construed as an official Department of the Army position, policy, or decision, unless so designated by other documentation.

17. COSATI CODES		
FIELD	GROUP	SUB-GROUP

18. SUBJECT TERMS (Continue on reverse if necessary and identify by block number)
Two-dimensional confined shear layers; two-dimensional prefilming airblast atomizers; characteristic time model; finite difference model.

19 ABSTRACT (Continue on reverse if necessary and identify by block number)

An experimental program for validation of the semi-empirical characteristic time model (CTM) is described. A two-dimensional turbulent shear layer is generated in the experimental test section using a two-stream, vertically downflowing wind tunnel with a flat prefilming airblast atomizer fitted along its centerline. This facility simulates the shear layer around the recirculation zone found in the primary zone of a gas turbine combustor. Experimental results are used to investigate CTM parameters for turbulent mixing and droplet lifetime and to examine current finite difference modeling techniques.

Global mixing times evaluated at the origin of the shear layer and defined in terms of geometric macroscale and a reference velocity are compared with the locally measured values of turbulent mixing time. The results demonstrate that these global times, as defined for the CTM, do in fact accurately represent the events occurring on a local scale, as hypothesized. Modifications to the mixing time parameter to improve existing correlations are proposed. Due to restrictions imposed by the facility and instrumentation, validation of the (cont.)

20. DISTRIBUTION/AVAILABILITY OF ABSTRACT ☐ UNCLASSIFIED/UNLIMITED ☐ SAME AS RPT. ☐ DTIC USERS	21. ABSTRACT SECURITY CLASSIFICATION Unclassified
22a NAME OF RESPONSIBLE INDIVIDUAL D.M. Mann	22b. TELEPHONE (Include Area Code) 919-549-0641 / 22c. OFFICE SYMBOL

DD FORM 1473, 84 MAR 83 APR edition may be used until exhausted. All other editions are obsolete.

SECURITY CLASSIFICATION OF THIS PAGE
UNCLASSIFIED

Abstract .... continued

droplet lifetime parameter was not possible. Measurements were restricted to mean spray diameters. These data and others demonstrate that current correlations for Sauter mean diameter do not adequately account for changes in atomizer geometry or liquid properties. In addition, the present measurements show that the presence of a shear layer at the atomizer tip significantly degrades atomization quality.

Finite difference models for turbulent flows are shown to perform poorly for the gas-phase flows considered here. The problem appears to be rooted in the turbulence model, and suggestions for improving agreement with experimental data are suggested.

TABLE OF CONTENTS

List of Tables

List of Figures

NOMENCLATURE

a, b, c	Constants	
C_p	Specific heat	kJ kg^{-1} K^{-1}
C_v	Liquid Volume Concentration	dimensionless
d	Diameter, Height	m
D	Drop Diameter	μm
D	Hydraulic Diameter of Tunnel	m
D_p	Prefilmer Diameter	m
E	Voltage	volts
H	Latent Heat	kJ kg^{-1}
I	Intensity	W $Steridian^{-1}$
ITS	Integral Time Scale	ms
K	Mean Scattering Coefficient	dimensionless
k	Turbulent Kinetic Energy	kJ
k_A	Thermal Conductivity	W m^{-1} $°C^{-1}$
ℓ	Turbulent Length Scale, Characteristic Length	m
P	Pressure	kPa
R(τ)	Autocorrelation Coefficient	dimensionless
Re	Reynolds Number	dimensionless
S	Swirl Number, Sample Size	dimensionless
SMD	Sauter Mean Diameter	μm
T	Temperature	°C, K
t	Splitter Plate Thickness	m
U	Axial Velocity	m s^{-1}
U(t)	Instantaneous Axial Velocity	m s^{-1}
U_x	Mean Axial Velocity	m s^{-1}

u,v,w,V	Velocity	$m\ s^{-1}$
V	Change in Volume as a Function of Time	$m^3\ s^{-1}$
W	Mass Flow Rate	kg^{-1}
w_{tooth}	Tooth Width	m
Y	Distance From Origin	m
β	Effective Evaporation Coefficient	$m^2\ s^{-1}$
ϵ	Rate of Dissipation of Turbulence	$m^2\ s^{-3}$
λ	Shear Layer Strength	dimensionless
μ	Absolute Viscosity	$kg\ m^{-1}\ s^{-1}$
ρ	Density	$kg\ m^{-3}$
σ	Surface Tension, Prandtl Number	dyne cm^{-1}, dimensionless
τ	Characteristic Time	s
$1/\Phi$	Nozzle Efficiency Factor	dimensionless

Subscripts

a	Air
A	Average
AAS	Air Side
AFS	Fuel Side
ann	Annular
co	Carbon Monoxide
comb	Combustor
disc	Disc
eb	Evaporation
global	Global Value
hc	Chemical Kinetics
ℓ	Liquid

local	Local Value
max	Maximum Value
n	Normal
o	Initial Value
pri	Primary Dilution Holes
ref	Reference
rms	Fluctuating Component
s	Streamwise
sec	Secondary Dilution Holes
sl	Shear Layer
step	Step
t	Turbulent Quantity
xy	Value at xy Coordinates
∞	Maximum Value

Acknowledgements

Special thanks are due Messrs. David Wolf, William Frantz and Brian Royds for their assistance in data acquisition and analysis and Professor David L. Miller for his input in the latter stages of the program. For his efforts in design and development of the facilities and implementation of the gas-phase diagnostics, the authors wish to acknowledge Mr. Steven Marakovits. The generosity and support provided by Mrs. Frederic O. Hess in laboratory development and fellowships is sincerely appreciated.

The assistance of Professors J.E. Peters, of the University of Illinois at Urbana-Champaign, and E.D. Hirleman, of Arizona State University, in development of the spray diagnostics is gratefully acknowledged. Thanks also go to Dr. B. Farouk, of Drexel University, and Eric Bradley for their aid in the computational portion of this program.

A special note of appreciation is extended to Ms. Sharon Huff for preparing this manuscript.

The support of the Army Research Office, and in particular the assistance provided by Dr. David M. Mann as Technical Monitor, is appreciated.

Abstract

An experimental program for validation of the semi-empirical characteristic time model (CTM) is described. A two-dimensional turbulent shear layer is generated in the experimental test section using a two-stream, vertically downflowing wind tunnel with a flat prefilming airblast atomizer fitted along its centerline. This facility simulates the shear layer around the recirculation zone found in the primary zone of a gas turbine combustor. Experimental results are used to investigate CTM parameters for turbulent mixing and droplet lifetime and to examine current finite difference modeling techniques.

Global mixing times evaluated at the origin of the shear layer and defined in terms of geometric macroscale and a reference velocity are compared with the locally measured values of turbulent mixing time. The results demonstrate that these global times, as defined for the CTM, do in fact accurately represent the events occurring on a local scale, as hypothesized. Modifications to the mixing time parameter to improve existing correlations are proposed. Due to restrictions imposed by the facility and instrumentation, validation of the droplet lifetime parameter was not possible. Measurements were restricted to mean spray diameters. These data and others demonstrate that current correlations for Sauter mean diameter do not adequately account for changes in atomizer geometry or liquid properties. In addition, the present measurements show that the presence of a shear layer at the atomizer tip significantly degrades atomization quality.

Finite difference models for turbulent flows are shown to perform poorly for the gas-phase flows considered here. The problem appears to be rooted in the turbulence model, and suggestions for improving agreement with experimental data are suggested.

1.0. Introduction and Summary

Turbulent two-phase flows are found in many practical combustion systems. These include automotive fuel injected gasoline reciprocating engines and diesels, gas turbines used to power aircraft, vehicles, ships, and to generate electrical power, and liquid fueled ramjets used for military applications. To date the design and development of these engines has been mostly empirical in nature, a method that is both costly and time consuming. Because of the shortcomings of the empirical approach, recent interests in engine combustor design have focused on the modeling field. In principle, this approach has several potential advantages including reduced cost, time savings, and the ability to test a range of modifications quickly. Numerical models can provide detailed information about the flowfield within the engine which can be difficult to obtain experimentally. However, prior to gaining acceptance in the design community, these models must be validated experimentally to ensure that the physics of these flows are properly modeled.

As an illustration of a turbulent two-phase flow, consider continuous combustion systems where the liquid fuel can be injected directly into the shear layer surrounding the flameholding recirculation zone thus providing residence times that are sufficiently long to allow the fuel to evaporate, mix with air, and finally, ignite. Understanding the interaction between the liquid fuel spray and turbulent shear layer is crucial to developing high performance combustors for gas turbines and liquid fueled ramjets. For example, in the primary zone of a gas turbine combustor, this mixing region is thought to control flame stabilization (Plee and Mellor, 1979) and combustion efficiency (Leonard and Mellor, 1983). In dump-type ramjet combustors, Schadow et al. (1986) have shown that altering the characteristics of the shear layer can have a significant impact on the heat release rates, and consequently the flame stability, within the burner. Modifications to the geometry of the initial shear layer in the latter configuration have been shown to enhance mixing which will promote stable operation (Schadow et al., 1988).

The finite difference approach to modeling combustion systems involves discretizing the governing equations to yield a system of algebraic equations that can be solved numerically.

This method uses a number of physical/chemical submodels to account for the turbulence, turbulent transport, spray trajectories and fuel evaporation rates, and combustion chemistry. Rizk and Mongia (1986) note that although these models are useful in the design phase, significant improvements in the submodels are required to permit accurate prediction of complex reacting flows found in typical gas turbine combustors. In addition to these uncertainties, the long computational times required to accurately model these flows can make this method very expensive and thus not always competitive with combustor rig testing.

Semi-empirical models offer an alternative to numerical methods. Instead of computing the entire flowfield, this approach focuses on key regions within the flow and relates conditions there to known inlet conditions to the flow. Although this method is much simpler than the former approach it is a potentially powerful tool for preliminary design. An example of this type of model is the Characteristic Time Model (CTM) (Mellor, 1980).

The CTM isolates the processes responsible for the phenomenon of interest (e.g., lean blowoff, ignition, efficiency, emissions) and estimates the global time requirements for each in terms of combustor inlet conditions, geometry, and fuel and injector type. For example, Plee and Mellor (1979) have shown that three characteristic times are associated with flame stabilization: the fuel droplet evaporation time, τ_{eb}; the mixing time of the fuel vapor and air, $\tau_{s\ell}$; and the ignition delay time, τ_{hc}. The model suggests that if a stable flame is to exist, the mixing time of the fuel vapor and air mixture in the shear layer identified above must be greater than or equal to the time required to evaporate the liquid fuel plus the ignition delay time of the fuel vapor with air. Thus the equation for the lean blowoff limit is:

$$\tau_{s\ell} = a(\tau_{hc} + b\tau_{eb}) \tag{1.1}$$

Equation 1.1 must be calibrated against actual engine data to determine the values for the slope and y-intercept, as well as a value for the constant b (Leonard and Mellor, 1983; Jarymowycz and Mellor, 1986; Derr and Mellor, 1987). With the introduction of model constants a and b it

is only necessary that the characteristic times be proportional to the actual times in a combustor.

The primary objective of this program is to compare the global parameters (as defined for an engine) for turbulent mixing and droplet lifetime from the CTM with the corresponding experimental values in a representative flow. These data can then be used to establish that the global times are in fact proportional to the local parameters that they represent and to suggest improvements in their definitions to reduce the scatter in the correlations. The present study does not address the chemical kinetics time as its most significant parameter, the activation energy, is based on well established global approaches in the literature.

Measurements of these times in the three-dimensional, recirculating flow found in an engine would be difficult. Instead, we focus on an element of the engine flow, specifically the shear layer. The experimental configuration thus involves a non-reacting, two-dimensional shear layer in which by choice of conservative values of cross-stream velocity gradient and suitable design of the test tunnel recirculation is avoided. A flat, prefilming airblast nozzle used as the splitter plate injects liquid at the origin of the shear layer, with subsequent atomization providing the spray. Optical and probe access are available through the confining walls of the test section.

In addition to investigating semi-empirical models, spatially resolved experimental data obtained in this facility are also used for evaluating finite difference models of turbulent two-phase flows. Measurements in the gas-phase flow include mean velocity, turbulent intensity and turbulent length scale. Experimentally measured inlet conditions were used as input for a parabolic k-ϵ model and the computed gas-phase flowfield was compared with the experimentally measured one at several downstream stations to evaluate the predictive ability of the model. Local mean drop size measurements were also obtained for the spray, and measurements of turbulent dispersion and droplet evaporation rates were attempted. However, because the computed gas-phase flow was in poor agreement with the experimental data, no two-phase computations were performed.

Descriptions of the models investigated in this program are presented in Section 2. The CTM parameters for turbulent mixing and droplet lifetime are discussed, along with correlations for mean spray diameters used as an input for both types of models. In addition, the finite difference model employed is discussed in this section.

Section 3 provides a description of the air supply system, test section and atomizer, along with the instrumentation used to monitor the experimental conditions. The hot-film anemometry and forward scattering systems used for measurements in the gas and liquid-phase flows, respectively, are also discussed, as well as the data reduction techniques which were employed.

Results from the experimental program to be found in Section 4 have established that the global CTM parameter for turbulent mixing scales well with the locally measured time at the origin of the shear layer. Measurements used to investigate the droplet lifetime have shown that correlations for mean drop size cannot predict the effects of changes in airblast atomizer geometry and liquid properties; available data indicate that errors due to geometric factors can be as high as fifty percent, while the errors caused by changes in liquid properties can be as high as ten percent. In addition, the presence of a shear layer at the atomizer tip has been shown to have an adverse affect on atomization quality. Measurements have shown that increasing shear layer strength results in a significant increase in mean drop size. This effect is not included in the previously discussed correlations for mean drop size, and since detailed measurements of the exit plane flowfield for airblast atomizers in actual combustors are generally unavailable its effects on combustor performance are unknown. Turbulent dispersion of the spray perpendicular to the dominant flow direction was much stronger than anticipated. As a result, the liquid spray wetted the tunnel walls bounding the width of the sheet. This limited optical access, and therefore spray measurements, to those perpendicular to the liquid sheet.

Measurements of mean drop size were possible in spite of the restrictions noted above; however, problems were encountered in attempts to measure evaporation rates and turbulent dispersion. The initially proposed method for evaluating the former quantity called for measuring the length required for the spray to completely evaporate, and then, using a mean

droplet velocity, relating this distance to the time required to evaporate the spray. However, because of limitations on maximum test section temperature, the required length for evaporation could not be realized in the present facility. Methods to obtain evaporation rates using laser extinction measurements were investigated, but the effects of evaporation could not be decoupled from those due to laminar dispersion with available instrumentation (Tailio, 1987). As a result it was not possible to complete validation of the droplet lifetime parameter. Measurements of turbulent spray dispersion were not possible due to the previously mentioned problems encountered with spray impingement.

Comparison of experimental data with those predicted by the finite difference model employed here can be found in Section 5. The original two-phase flow code and modifications implemented during this program in an attempt to improve the predictions are discussed The code, developed by United Technologies Research Center, was intended to model the presence of fuel injectors and struts in an axisymmetric prevaporizing/premixing passage. Experimental values were used as input to the code. Mean velocity data were entered directly, and k and ϵ were computed from experimentally measured values of rms velocity and length scales. Direct comparison accomplished to date of computed and experimental profiles at several downstream stations has shown that the code performs poorly for this type of flow. Errors in mean velocity are as high as 25 percent and rms velocities deviated from experimental values by as much as 90 percent. Several explanations for these errors are discussed; chief among them may be the need to "calibrate" the turbulence model. Calculations were limited to the gas-phase. Because these predictions were poor, there was no justification for including the spray model at this time.

Validation of the CTM parameter for droplet lifetime could not be completed due to previously discussed restrictions imposed in part by the instrumentation. Section 6 outlines techniques that will be used to continue the experimental investigation of this parameter using a recently acquired Phase/Doppler Particle Analyzer that will make decoupling of the laminar dispersion and droplet evaporation possible. This section also discusses methods that will be

used to further the investigation of the turbulent mixing time parameter by investigating the effects of freestream length scale and efforts that will be undertaken to continue the investigation of finite difference models for two-phase flows.

2.0. Background and Scope

Prior to presenting the experimental results a discussion of two-phase turbulent flows, as they relate to continuous combustion systems, is warranted. This section will focus on the background of the problem studied here, provide a brief overview of current modeling techniques and outline the objectives of the program.

2.1 Introduction

Combustion of fuel and air in the primary zone of a gas turbine combustor is a complex process involving turbulent mixing, spray atomization and evaporation, heat transfer, and chemical kinetics. In order to predict the effects of changes in design parameters (inlet conditions, combustor geometry, fuel and injector type) on changes in engine performance (altitude relight, lean blowoff, emissions, efficiency, etc.) a number of models for the combustion process have been developed and are discussed in the literature (see, for example, Mellor, 1976, 1980; Rizk and Mongia, 1986).

The objective of these models is to provide a tool to aide in the development of new combustors and to improve the performance of existing ones. The advantage of utilizing models becomes apparent when one considers the cost and lead time associated with the "cut and try" method of combustor design. With the trend toward decreased computing costs realized over the last decade it may become more effective to implement mathematical models to predict the effect of proposed design changes than to construct and test prototypes that include these changes.

In order to properly model these complex systems it is essential that the physics of two-phase turbulent flows be properly understood. Areas of particular interest include: interactions between the gas and liquid-phase flows (turbulent dispersion of the spray, spatial distribution of fuel in the combustor, momentum exchange between the gas and liquid phase), evaporation of the fuel spray, and mixing of the resulting fuel vapor and air. None of these

aspects can be adequately described analytically for the complex flowfield found in a gas turbine engine, and, as such, modelers must rely on experimental data to form empirical correlations for parameters of interest.

A number of different combustor models have been developed to predict engine performance. These approaches range from the modular to the complex numerical techniques used to solve the basic conservation equations, as well as the simpler semi-empirical methods that define the parameters of interest in terms of the physical processes and obtain the model constants from empirical data. This study has focused on two model types, the semi-empirical characteristic time model (Mellor, 1976), and a parabolic finite difference code developed by Anderson et al. (1982). Therefore, the discussion here will be limited to continuum finite difference models and the semi-empirical characteristic time model.

2.2 Continuum Models

With the advent of large scale digital computers numerical solutions can be obtained for engineering problems that were previously intractable because no analytic solution existed. Utilizing the rapid computational speed and large storage available on these computer systems it is possible to discretize the governing equations for any given problem and recast it in an algebraic, as opposed to a differential, form which is easily handled computationally (Anderson et al., 1984).

The complex flowfield parameters and chemistry found in typical combustion applications are handled using chemical/physical submodels which are based on both experimental and analytical considerations. These submodels, however, require significant improvements in order to accurately predict the complex reacting flows found in typical gas turbine combustors (Rizk and Mongia, 1986). The only practical method for ascertaining the validity of these models it to develop a well defined experimental datum base that can be used to refine the current modeling techniques (Strahle and Lekoudis, 1985).

The primary advantage of using the continuum computational approach is that a detailed description of the time averaged flowfield can be obtained (see, for example, Rizk and Mongia, 1986). However, these computed results are strongly affected by the choice of initial conditions, among other things, used for the code. In typical gas turbine combustors it is generally a difficult task to obtain the detailed measurements required for input to the code.

There are several distinct disadvantages associated with the use of numerical schemes for predicting engine performance parameters. Because of the complexity of these codes long computational times and large amounts of computer storage are required resulting in significant computer costs. The previously mentioned difficulties encountered with the physical/chemical submodel accuracy brings the validity of the predictions into question. Strahle and Lekoudis (1985) also note that most turbulent reacting flow models are application specific resulting in the need for extensive modification to handle changes in geometry and/or chemistry. The predictive ability of turbulence models is particularly sensitive. In the two-equation turbulence model, a dissipation length can be defined:

$$l = \frac{C_\mu^x \, k^{1.5}}{\varepsilon} \qquad 2.1$$

There is disagreement in the literature with regard to the appropriate value of the exponent x. Gosman and Ioannides (1983) used a value of 0.5, while Faeth (1987) reports that 0.75 provided a better fit to experimental data. In both cases it was necessary to "calibrate" the turbulence model. However, these calibrations appear to be specific to the particular flow under investigation (Faeth, 1987).

2.3 Semi-Empirical Models

As discussed previously, semi-empirical models offer an alternative to continuum models. With this technique, the physical processes occurring within the combustor are identified and the time required for each process (e.g., fuel droplet evaporation) is computed. This approach has

been successful in correlating data for lean blowoff (Jarymowycz and Mellor, 1986; Derr and Mellor, 1987), combustion efficiency (Leonard and Mellor, 1983), and spark ignition (Peters and Mellor, 1982) from several engines operating on a wide range of fuels. These results appear to be independent of engine and fuel type, most likely because the models describe the essential physics of turbulent spray diffusion flames common to all conventional gas turbine combustors. The principle advantage of these characteristic time models (CTM) is that the entire flowfield need not be evaluated; instead only regions of key importance to the combustion process are considered.

Combustor performance is characterized with three principal characteristic times: the fluid mechanics time $\tau_{s\ell}$, to describe the mixing of the fuel vapor and air; a kinetics time, τ_{hc}, to account for the chemistry; and a droplet lifetime, τ_{eb}, to model the evaporation of liquid fuel. These times are estimated based on combustor geometry, inlet conditions, and fuel and injector types, and the model constants are evaluated using actual engine data. The times computed with the model are expected to be proportional to the time required for the actual process to occur, with the constant of proportionality obtained from experimental data.

These times are combined in the form of algebraic equations which permit rapid calculation to predict changes in engine performance for a given change in design. For example, the lean blowoff model states that the residence time of the fuel/air mixture in the shear layer adjacent to the flame holding recirculation zone must be sufficiently long to permit the liquid fuel to evaporate and kinetics to occur if a stable flame is to exist.

$$\tau_{s\ell} \geq a(\tau_{hc} + b\tau_{eb}) \qquad 2.2$$

The coefficients a and b are empirically derived. The results of correlations performed with the lean blowoff model (see, for example, Jarymowycz and Mellor, 1985 and Derr and Mellor, 1987) are shown in Fig. 2.1. Here, the solid line represents the limit of stable operation.

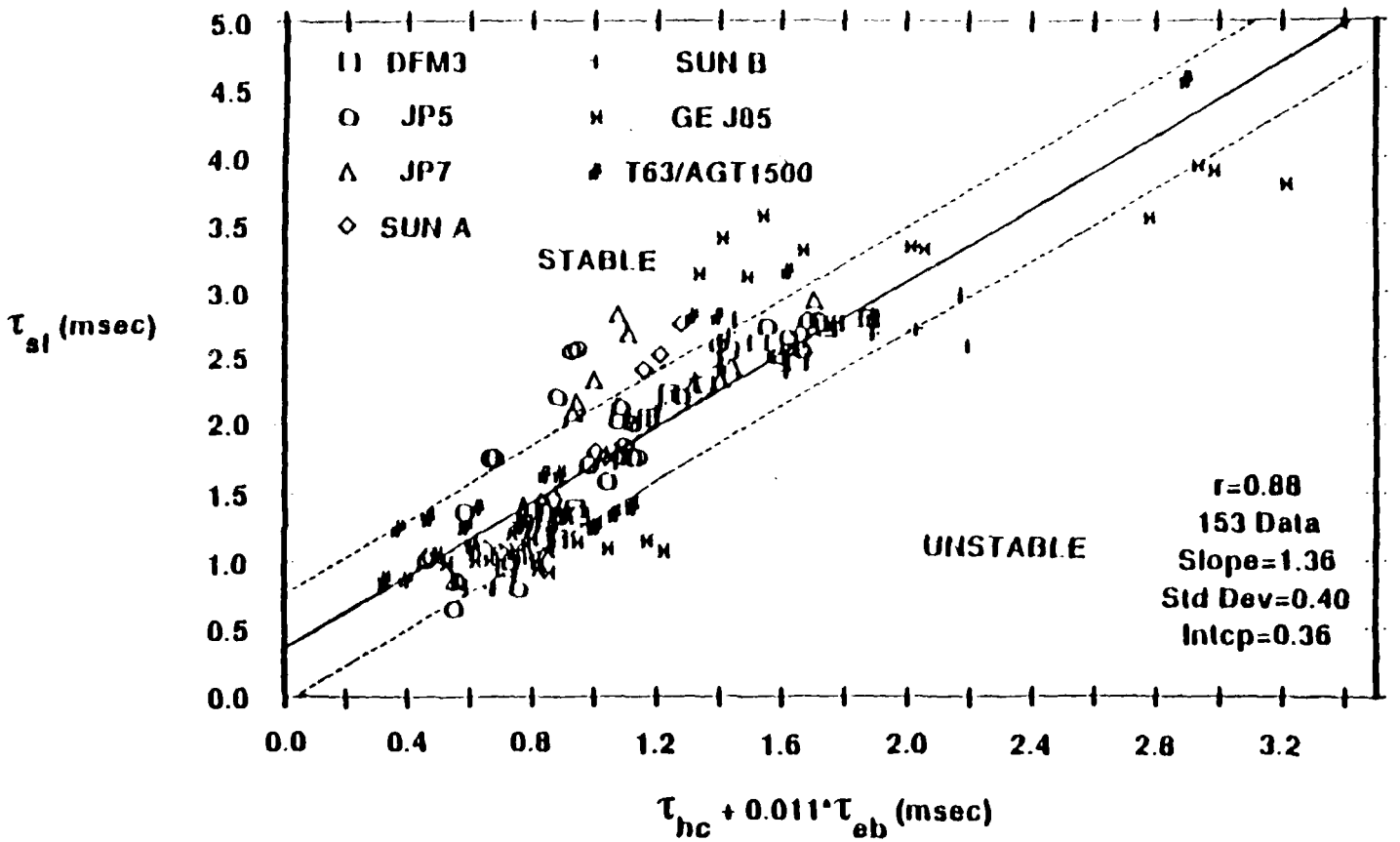

Figure 2.1 Lean Blowoff Results for Gas Turbine Combustors*

* From Derr and Mellor (1987)

Figure 2.1 Lean Blowoff Results for Gas Turbine Combustors

Other characteristic times which are used to describe pollutant formation and flame stabilization in two-phase turbulent flows are shown in Table 2.1. This table, taken from Mellor (1976), describes the processes associated with each of the times. The focus of the present study are the parameters for mixing time, $\tau_{s\ell}$, and for droplet lifetime, τ_{eb} (both are described in detail below). Detailed analysis of the other times can be found in Mellor (1976) and (1980).

There are several advantages to using the characteristic time approach to modeling a combustion system; the principle one is the ease of use of the technique. Since all of the quantities used as inputs to the model are design parameters (e.g., combustor geometry, fuel and injector type, etc.), their values are known. This is a significant advantage over the continuum model where the initial conditions (air flows through swirlers, holes, etc; fuel drop size and velocity distributions where the spray becomes dilute) must be measured in an actual rig or assumed. The computational times required to compute performance parameters with this model are minimal. The apparent universality of the model (i.e., independent of engine or fuel type) means that this method of predicting engine performance need not be modified significantly for changes in conventional combustor design since all of the design considerations are included in the model parameters. Finally, this modeling technique is the only type capable of predicting performance parameters (Lefebvre, 1983), unlike the numerical models which still require significant work to improve the turbulence-chemistry interaction submodel, for example.

Still another approach involves combining the computational and semi-empirical models. This method was employed by Rizk and Mongia (1986) to predict performance parameters for an advanced combustor. This technique is still in the developmental stages, and obviously suffers from the shortcomings associated with the computational model. That is, the semi-empirical model's accuracy is limited by the predicted flowfield values from the computational model. However, as computational predictions are improved this approach will be useful as a preliminary design tool.

2.4 Development of $\tau_{s\ell,co}$

Tuttle et al. (1977) using a disc-in-duct burner showed the important effect turbulent mixing has on the molecular diffusion process. They suggested CO emissions would scale with a time appropriate to the shear layer near the the rim of the disc where quenching occurs, provided the droplet lifetime is short. The appropriate time scale will be associated with the large scale turbulence (eddies) of this region and will be inversely proportional to the rms of the velocity.

$$\text{Time Scale} = \ell/u_{rms} \qquad 2.3$$

This fluid mechanic time is consistent with what has been used for similar turbulent flows (e.g., Tennekes and Lumley, 1972 or Abdalla et al., 1981). Tuttle et al. (1977) concluded that the turbulent time scale would be inversely proportional to the mean convective velocity if the rms is but some fraction of this velocity. They chose the disc diameter to be the length scale of this shear layer because it determines the initial size of the vortices that are shed from its edge. Thus, to correlate CO emissions data for a circular disc flameholder the following mixing time scale was used:

$$\tau_{s\ell,co} = \ell_{co}/U_{ann} \qquad 2.4$$

ℓ_{co} is the length scale equal to the diameter of the disc and U_{ann} is the velocity calculated from mass flow rates and the mass flow area around the disc.

A modification was made to their experimental setup by replacing the circular disc with a toothed disc flameholder. The length scale was altered to account for the additional vortices generated due to flow around the teeth. These vortices have initial size scales of the tooth width (equal to tooth height), and thus the appropriate turbulent scale was a weighted average

of the reciprocals of both initial eddy sizes.

$$\ell_{co}^{-1} = d_{disc}^{-1} + k(w_{tooth})^{-1} \qquad 2.5$$

The proportionality constant, k, represents a scaling relationship and was determined experimentally. Correlation with their CO emissions model for both flameholders using propane fuel was good (Tuttle et al., 1977).

TABLE 2.1*

Characteristic Times for Combustion and Pollutant Formation in Two-Phase Turbulent Flow

Time	Symbol	Physical or Chemical Process
Fuel droplet time	τ_{eb}	Droplet evaporation and/or combustion
Eddy dissipation time	τ_{fi}	Small-scale turbulent mixing for injected fluid near the fuel injector in the recirculation zone
Eddy dissipation time in the shear layer	$\tau_{s\ell}$	Large-scale turbulent mixing between fresh air and the recirculating burned gas-fuel mixture
Fuel ignition	τ_{hc}	Homogeneous combustion of the fuel to CO_2
NO formation time	τ_{no}	Homogeneous kinetics for NO formation

*Taken from Mellor (1976).

Altenkirch and Mellor (1975), following Zukoski and Marble (1956), proposed a flame stabilization model in which the hot turbulent eddies present in the shear layer region between the recirculating burned gases and the free stream must ignite before they are quenched by the relatively cold free stream; otherwise the shear layer flame extinguishes. Noting that the shear layer region dominant for flame stabilization was identical to the one for CO emissions and utilizing the mixing time of Tuttle et al. (1977), Plee and Mellor (1979) correlated lean blowoff data for simple geometries (e.g., tube-and-disc and disc-in-duct) and a variety of fuels. They assumed the mixing to correspond to the breakdown of large scale eddies and chose their length scales to be proportional to the flameholder width, which also is representative of the size of the recirculation zone. For three different geometries and 397 datum points the correlation coefficient for their lean blowoff model was 0.93 (Plee and Mellor, 1979).

The lean blowoff model of Plee and Mellor (1979) was modified and applied to both can-type combustors (Leonard and Mellor, 1983) and an annular combustor (Jarymowycz and Mellor, 1986). Since the combustor geometry is more complex than a simple flameholder, a length scale based on the CO emissions model for a can combustor (Mellor, 1977) was used. Here ℓ_{co} was inversely proportional to the sum of reciprocal diameter of the combustor and the reciprocal of quench length, ℓ_q, defined as the axial distance from the tip of the fuel injector to the centerline of the primary or secondary dilution holes.

$$\ell_{co}^{-1} = (\ell_{sec} \text{ or } \ell_{pri})^{-1} + d_{comb}^{-1} \qquad 2.6$$

where: ℓ_{sec} = axial distance from the tip of the fuel injector to centerline of the secondary dilution holes

ℓ_{pri} = axial distance from the tip of the fuel injector to centerline of the primary dilution holes

d_{comb} = diameter of combustor

Because ℓ_{sec}, ℓ_{pri}, and d_{comb} are all of the same order, k in Eq. 2.5 is taken as unity in Eq. 2.6. The reference velocity, U_{ref}, based on inlet conditions replaces U_{ann} because the area of

the dilution holes did not affect the CO emission data for the combustor studied by Mellor (1977). Thus, $\tau_{s\ell,co}$ for a combustor is defined as follows:

$$\tau_{s\ell,co} = \ell_{co}/U_{ref} \qquad 2.7$$

2.5 Droplet Lifetime

The expression for droplet lifetime is defined using the d^2 law of Godsave as:

$$\tau_{eb} = d_o^2/\beta \qquad 2.8$$

where d_o is the initial droplet diameter and β is the effective evaporation coefficient. The evaporation coefficient, modified for forced convection (Kanury, 1975), is defined as:

$$\beta = \frac{8\,k_a}{\rho_\ell\, C_{p,a}} \ln\left[1 + \frac{C_{p,a}\,(T_a - T_\ell)}{H}\right] (0.185\,Re^{0.6}) \qquad 2.9$$

Since sprays encountered in practical applications are polydisperse in nature, the initial droplet diameter in Eq. 2.8 is set equal to the Sauter mean diameter (SMD) of the spray and hence, τ_{eb} represents an average evaporation time for the spray (Mellor, 1976). The SMD of the spray is defined as the droplet size with the same volume to surface area ratio as that of the entire spray.

$$SMD = \frac{\int_0^{D_\infty} n(D)\,D^3\,dD}{\int_0^{D_\infty} n(D)\,D^2\,dD} \qquad 2.10$$

At first, this assumption may seem unjustified until one considers the correlation of Simmons (1977) which shows that for all "commercial quality" atomizers the SMD is uniquely related to the maximum drop diameter in the spray. Since the largest droplet will define the time required

for the spray to completely evaporate it is seen that, in fact, the characteristic evaporation time calculated with the model is proportional to the actual evaporation time, as hypothesized.

Empirical correlations are generally used to determine the initial mean spray diameter because of complexities involved with measuring it in an actual combustor. A number of correlations have been developed to predict the performance of both two-dimensional and axisymmetric airblast atomizers (see, for example, Gretzinger and Marshall, 1961; Wigg, 1964; Rizkalla and Lefebvre, 1975a,b; Rizk and Lefebvre, 1977, El Shannaway and Lefebvre, 1980; Jasuja, 1979; Simmons, 1979; Lefebvre, 1980). These correlations provide information on the dependence of mean drop size on initial conditions (air velocity and air and liquid mass flow rates), liquid properties (viscosity, surface tension, density) and atomizer scale (for example, prefilmer diameter). Lefebvre (1980) provides a review of previous work in the field of airblast atomization and the discussion here will be limited to his correlation.

Correlations for SMD are generally written as the sum of two components: the first is governed by the Weber number and the second by the Reynolds number of the liquid. The equation takes the following form:

$$SMD = SMD_1 + SMD_2 \qquad 2.11$$

The dominant term in Eq. 2.11 for liquids of moderate viscosity is SMD_1 which is defined in terms of the Weber number. The second term, SMD_2, is negligible for liquid of moderate viscosity (approximately that of kerosine). The final form of the correlation is written as:

$$SMD = \frac{1}{\Phi}\left(1 + \frac{W_l}{W_a}\right)\left[0.073\left(\frac{\sigma_l}{\rho_a U_a^2}\right)^{0.6}\left(\frac{\rho_l}{\rho_a}\right)^{0.1} D_p^{0.4} + 0.015\left(\frac{\mu_l^2 D_p}{\sigma_l \rho_l}\right)^{0.5}\right] \qquad 2.12$$

The term $1/\Phi$ is a nozzle efficiency factor and is included to account for differences in atomizer design. Lefebvre (1980) correlated data from six geometrically dissimilar prefilming airblast atomizers (both axisymmetric and two-dimensional) using this correlation and values of $1/\Phi$ between 0.61 and 1.0. Tallio (1987) added a seventh atomizer to the correlation using a value of 0.57 for $1/\Phi$.

2.6 Refinement of Characteristic Time Model Parameters

Although the characteristic time models have been successful in correlating engine performance parameters in terms of combustor geometry, inlet conditions and fuel type, two specific questions about the model still exist. First, can the method used to evaluate the parameters in the characteristic time model be improved to reduce the scatter in the correlations shown for example in Fig. 2.1, and second, why does such a simple model work?

Because of the practical limitations on probe access and the complex flowfield it is not possible to experimentally investigate the model parameters in an actual combustor. In order to obtain the detailed measurements necessary for model validation a specially designed wind tunnel was constructed. The tunnel uses two airstreams to produce a planar, two-dimensional, turbulent shear layer to permit investigation of the mixing time parameter and gas-phase flow properties. An airblast atomizer, located along the tunnel centerline and used to separate the two air flows, injects liquid into the origin of the shear layer so that the droplet lifetime parameter and the two-phase flow can be studied.

Although this geometry does not resemble that of an actual gas turbine combustor, the physics of the two flows are the same (i.e., turbulent shear layer with liquid injection). This facility is a logical extension of previous work by Tuttle et al. (1977) (Section 2.4) where the primary zone of a gas turbine combustor was simulated using a disc-in-duct configuration. Figure 2.2 shows a typical gas turbine combustor along with the simulations used by Tuttle and the present study. The previous program established a relationship between geometric macroscale and the turbulent mixing times of the fuel and air. Various disc geometries were

investigated using circular discs of different diameter, and by installing toothed discs. These changes in geometry produced changes in the initial turbulent length scale immediately downstream of the flameholder, and, the researchers hypothesized, thus affected the turbulent mixing times by changing the microscale of turbulence. The facility used in the present program was designed to investigate the link between the macroscopic parameters (i.e., mean velocity and geometry) and the microscopic turbulent mixing (actually, Taylor microscale) by simulating only the shear layer surrounding the flame holding recirculation zone (Fig. 2.2). A two-dimensional shear layer was selected because it possesses the velocity gradients found in the fully three-dimensional flow of an actual gas turbine combustor, but does not have a recirculation zone. This simplifies data acquisition and, since the flow is parabolic in nature, eliminates the need for an elliptic finite difference model to compute the flowfield.

The gas-phase flow was investigated using hot-film anemometry to measure mean (U) and rms (u_{rms}) velocity and turbulent length scale (ℓ). Detailed measurements of ℓ and u_{rms} were obtained at the shear layer origin to provide the data necessary to investigate the relationship between the globally computed characteristic mixing time and that found on the local scale in the flow. The objective here was to experimentally validate the turbulent mixing time parameter and to suggest improvements in its evaluation method that could be used reduce scatter in the model. To investigate finite difference models for turbulent flows measurements of gas-phase flow parameters were obtained downstream to examine the flow as it developed. Using the data obtained at the first station in the test section for initial conditions it was possible to investigate current methods used to model turbulent flows. To ensure that there was no ambiguity in the initial conditions, experimentally measured values of ℓ and u_{rms} were used to compute the inlet values of k and ϵ directly.

Forward scattering measurements were used for spray diagnostics. This technique provides mean drop size information, but no measurement of drop size or velocity distribution can be made. In addition, laser extinction measurements were used to determine liquid volume concentrations in the flow. The objectives of this phase of the program were to determine the

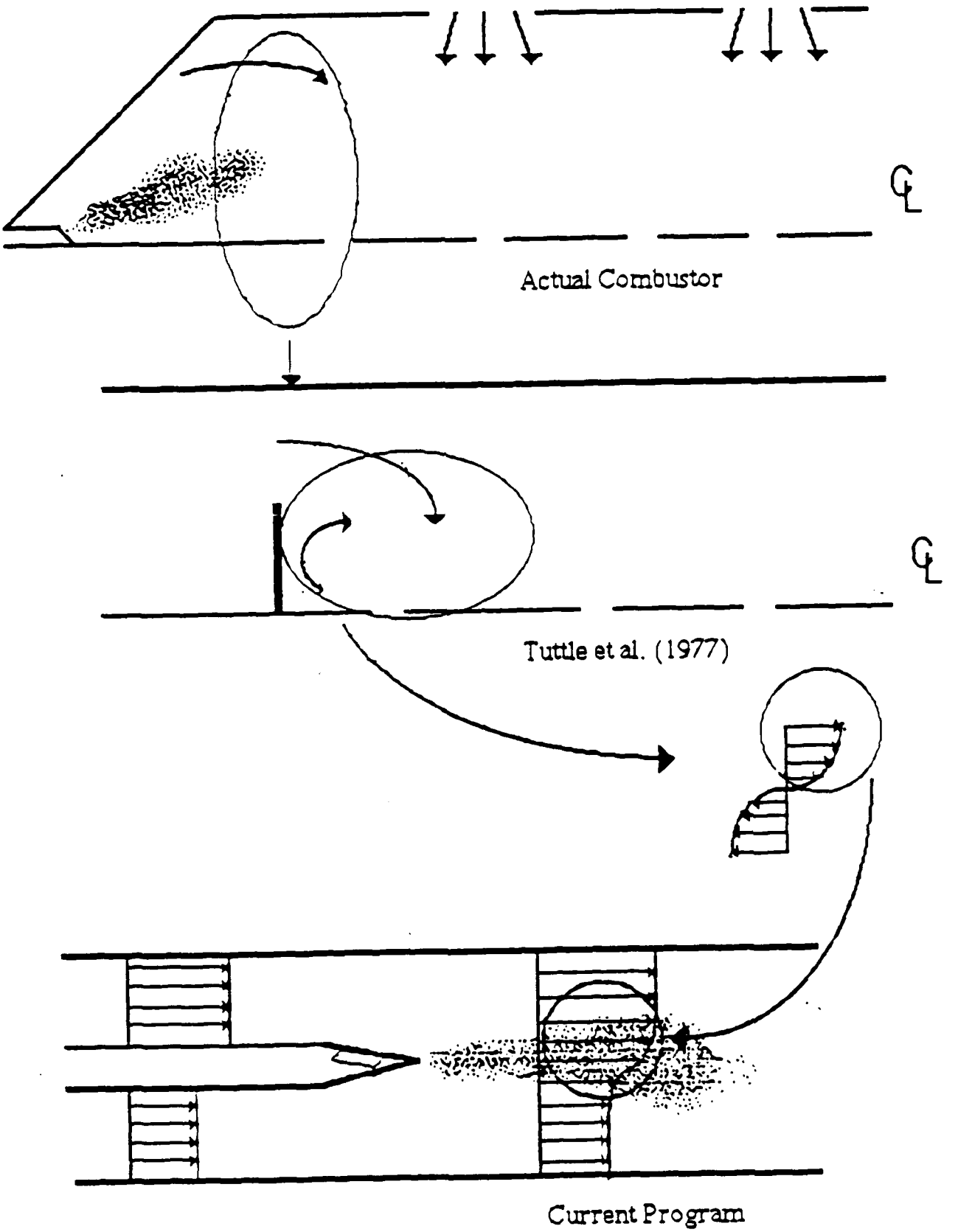

Figure 2.2 Subsection Simulations of Flowfields in the Primary Zones of Gas Turbine Combustors

accuracy of the drop size correlations used as an input to the droplet lifetime parameter and to compare the evaporation rates measured in a polydisperse spray with those predicted analytically. Since correlations for mean drop size cannot adequately account for changes in atomizer geometry and liquid properties (see for example, Lefebvre, 1980; Tallio, 1987) it is important that their contributions to scatter in the model be properly accounted for. Also, because the equation to predict droplet evaporation rate (Godsave, 1953) and the correlation for convective effects (Kanury, 1975) were developed for single droplets, the effects due to a polydisperse distribution of droplets must be investigated. Obtaining measurements of the previously noted parameters, as well as turbulent spray dispersion, as a function of axial location also provides a means of testing finite difference spray submodels used for turbulent two-phase flows. Finally, data were also obtained to extend the work of Sattlemayer and Wittig (1987) on the effects of shear layer strength on airblast atomization, an area that, until recently, had received little attention.

To evaluate methods of modeling two-phase turbulent flows a computer code developed for NASA-Lewis/AVSCOM , United Technologies Research Center (Anderson et al., 1982) was employed. This code uses a parabolic formulation and a two equation turbulence model for the gas-phase flow and imposes a dilute spray assumption for calculations of the liquid-phase flow. The dilute spray assumption is used to decouple the gas- and liquid-phase momentum equations and simplify the computational time required. The objectives of the numerical work were to compare the results of the computed flow parameters with those measured experimentally when detailed experimental values of initial conditions were provided for the code.

With the necessary background complete and the program objectives defined, the remainder of this report will focus on the experimental facility, validation of the characteristic time model parameters, and investigation of numerical techniques used to model two-phase turbulent flows.

3.0. Experimental Facility

This section describes the experimental facility developed to investigate the CTM parameters for turbulent mixing and droplet lifetime. The air supply system, test tunnel, and airblast atomizer are discussed first, followed by a description of both the hot-film anemometer and forward scattering systems used for gas and liquid-phase flow diagnostics, respectively.

3.1 CTM Test Tunnel

The test tunnel used in this program was designed to simulate the shear layer in a gas turbine combustor thought to be responsible for flame stabilization (Plee and Mellor, 1979) and efficient combustion (Leonard and Mellor, 1983). The fully three-dimensional flow field found in an actual burner has been modeled with a two-dimensional, planar turbulent shear layer into which liquid is injected as shown in Fig. 3.1. The simplification allows the relevant processes (i.e., the evaporation of fuel droplets and the mixing of fuel vapor and air necessary for combustion) to be studied in a well controlled laboratory environment that, as opposed to an actual combustor, is easily accessible to diagnostic instruments.

The two-stream vertically down-flowing wind tunnel is constructed from several square sections that, when bolted end to end, total 4.1 meters in length. The square sections, each 7.62 x 7.62 cm^2, are assembled from four 9.5 mm thick polished aluminum plates. To ensure a smooth transition and minimize flow disturbances, each section is fitted with pinned flanges and sealed with gaskets. The test section (the tunnel section which contains the windows) permits both optical and probe access using interchangeable plates which are inserted into the tunnel walls. Quartz windows are used for optical access, and hot-film/pitot tube insertion is provided with specially designed plates. The air flow is driven by a Lamson Model 608 multi-stage axial blower followed by a Chromalox Model GCH-45175 in-line electrical resistance heater providing mass flow rates to 1.17 kg/s and temperatures up to 450 K at atmospheric pressure.

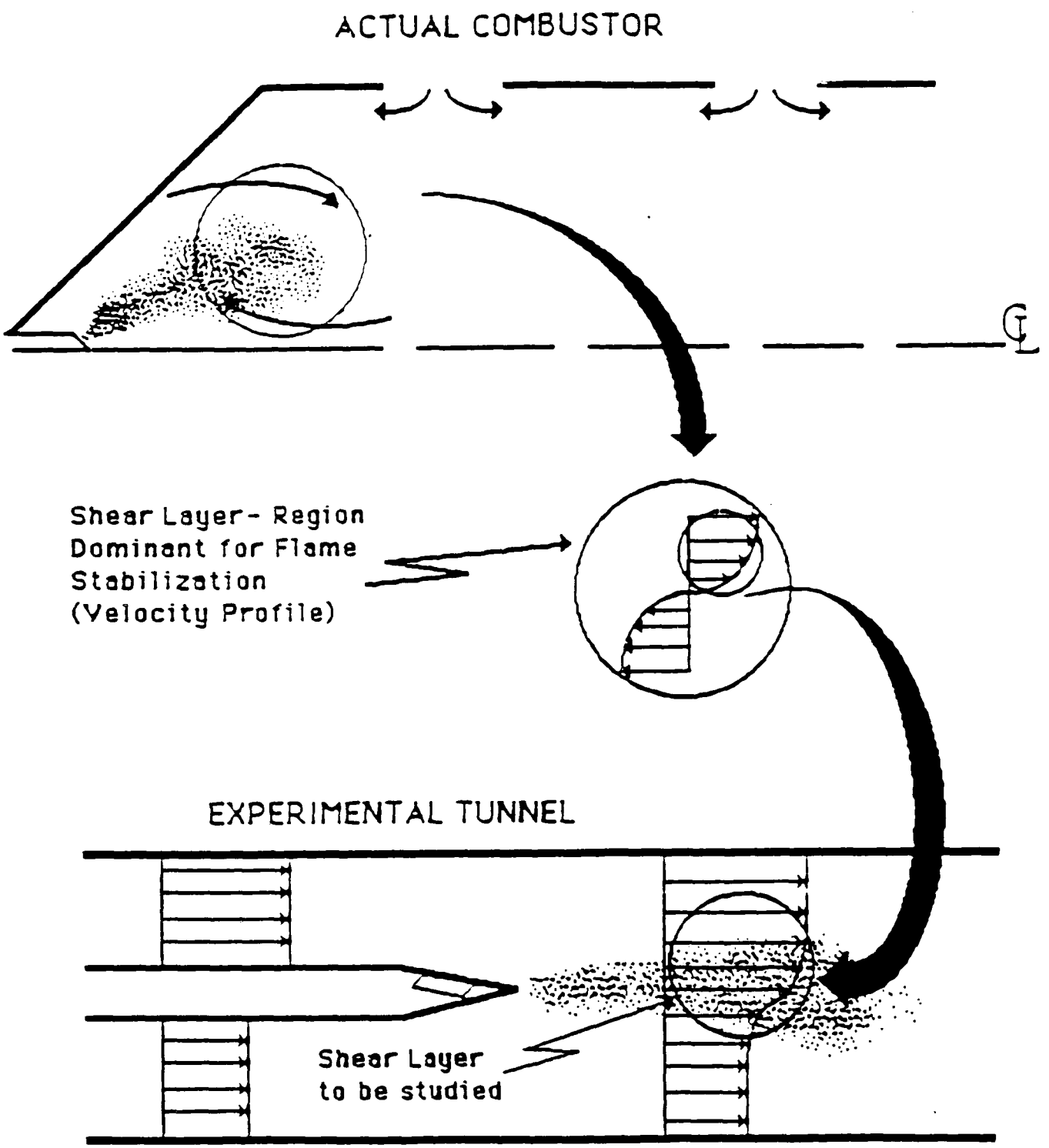

Figure 3.1 Comparison of Primary Zone of an Actual Combustor with Experimental Configuration

In order to create two different air velocities simultaneously from a single blower the specially designed piping system shown in Fig. 3.2 was necessary. At the point where the 15.24 cm diameter pipe from the air heater terminates, a "Y" fitting divides the flow into two 7.62 cm diameter pipes. One of the lines is fitted with a tee to a butterfly type diaphragm-actuated control valve which is used to bleed air from, and thus reduce, the flow in that pipe. The bleed valve is remotely controlled so that the velocity can be varied from the control panel in the lab. Each side has a globe valve 46 cm downstream of the "Y" section to allow for additional flow control. After a 90^{o} elbow, the piping is horizontal and has no disturbances until the orifice plates which are 229 cm away. At a distance of 56 cm downstream of the orifice plates both pipes have another 90^{o} elbow and then feed into a circular to rectangular duct transition section. Each duct, 7.62 x 5.0 cm^2, then feeds directly into its respective side of the tunnel. The distance from the top of the tunnel to the test section (the location used for data acquisition) is 241 cm.

Temperature and pressure access ports are available upstream and throughout the test tunnel. Upstream orifice plates provide mass flow measurements for each side of the tunnel. Pressures and temperatures are entered into an LSI-11 microcomputer which calculates the flow conditions of the tunnel.

Temperature measurements are obtained using iron-constantan grounded junction thermocouples and displayed with an Omega Model 650 multichannel digital thermometer. The sheath diameter of the thermocouples was .102 cm. Thermocouples are positioned at the air heater outlet, 40 cm downstream of the orifice plates, and on either side of the splitter plate 84 cm upstream of the test section. These positions were chosen to obtain local temperatures for the mass flow and density calculations.

The pressure measurement system uses four differential (Series 501) and one absolute (Series 502) Daytronic strain gage pressure transducers along with five signal conditioner/indicators. The pressure transducers were calibrated at the factory and are periodically checked. Two of the differential transducers are dedicated to the orifice plate taps

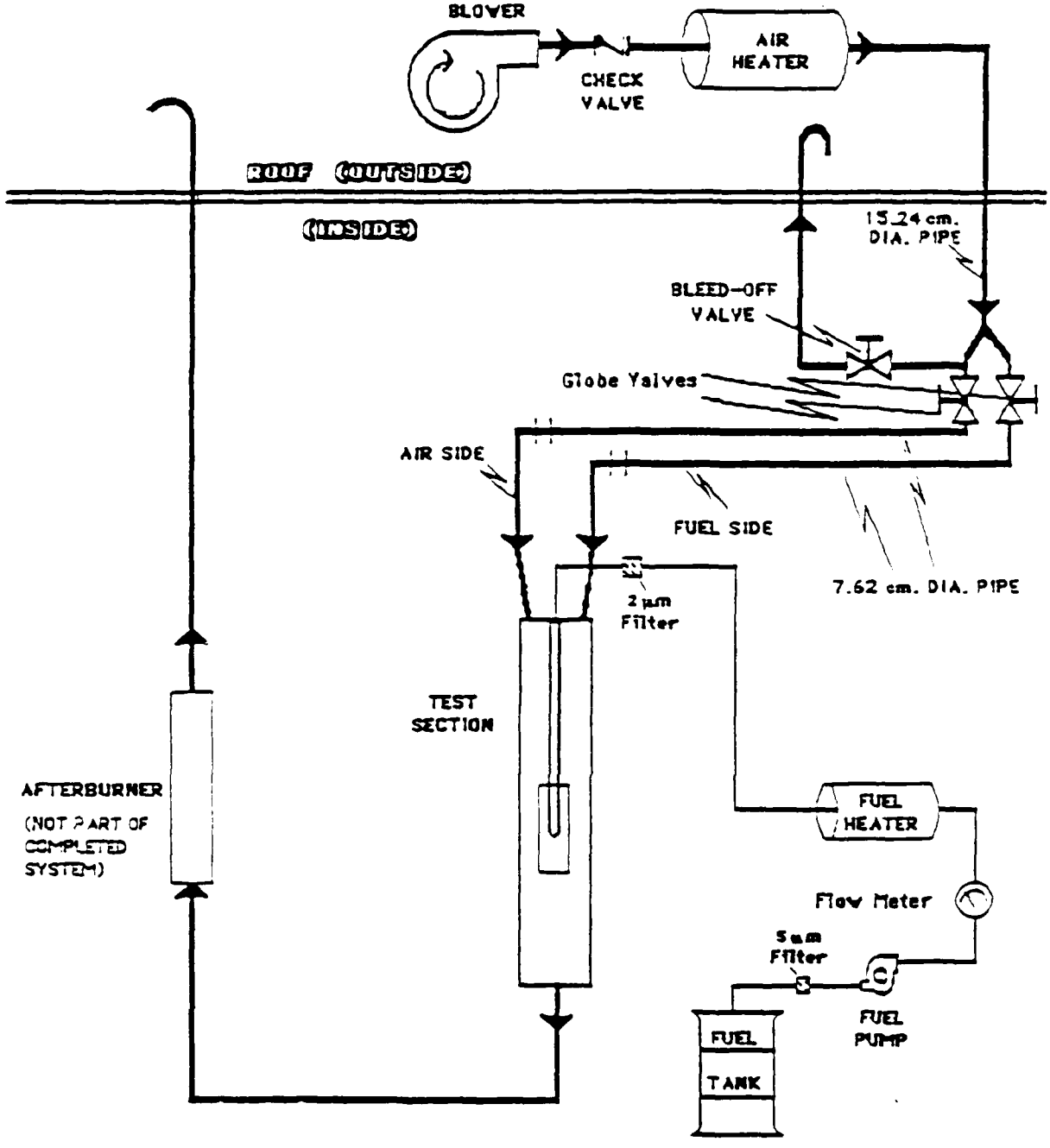

Figure 3.2 Schematic of Fuel and Air Supply System

and the other two to the pitot static tubes. The absolute transducer is used to measure a reference pressure which is the highest static pressure in the tunnel.

Three pitot static tubes are located in the CTM tunnel and are used to calculate velocities. The pitot static tube used for hot wire and orifice plate calibration is retractable and located in the test section. The other two are located 91 cm upstream and are used to obtain an estimate of the velocity of each side. Besides the pitot tubes there are other static pressure ports upstream of the atomizer tip that allow for measurement of a pressure profile.

The ASME standard orifice plates used in the tunnel have a diameter of 5.72 cm and are flange tapped. To check for proper alignment of the orifice plates, axial pitot tube velocity traverses were made upstream of the atomizer tip for various blower settings. These profiles were then integrated for mass flow and compared to the values calculated from the orifice plates. The difference between the integrated pitot velocity profiles and the orifice plates was less than 1.9% for both flows.

A splitter plate located along the tunnel centerline ensures that the two flows remain isolated prior to mixing at the atomizer tip where the shear layer is formed. As shown in Fig. 3.3, these flows are labelled "fuel side" (the side of the atomizer containing the porous plate used for liquid injection) and "air side". The shear layer strength, λ, is defined in terms of the mass average velocities of these two flows at the atomizer tip as:

$$\lambda = \frac{U_{AFS}-U_{AAS}}{U_{AFS}+U_{AAS}} \qquad 3.1$$

The laboratory reference frame was selected to simplify data acquisition by fixing the measurement locations for the gas and liquid-phase flows with respect to the wind tunnel. The coordinate system (Fig. 3.3) and atomizer can be traversed in the axial, X-direction, to examine both the spray and shear layer as they develop downstream. The Y-direction is perpendicular to the atomizer. Spray measurements along this axis are integral averages through the spray for both SMD and liquid volume concentration, C_v, and were used to establish the

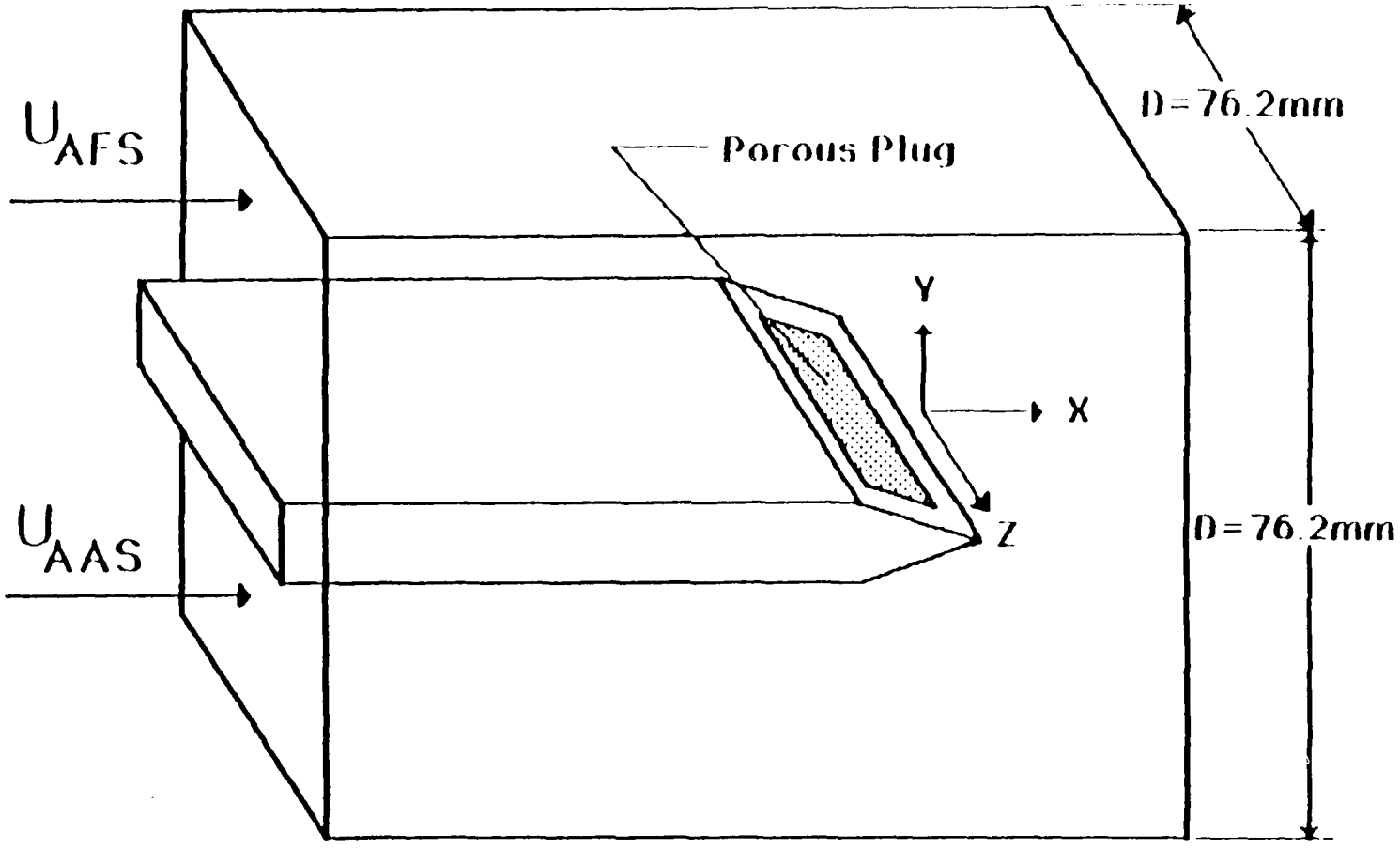

Figure 3.3 Tunnel Test Section and Coordinate System

two-dimensionality of the spray. Y-profiles of the gas-phase flow were used to probe the shear layer for mean and rms velocities, and length scale. Two-dimensionality of the gas-phase flow is established with hot-film measurements along the Z-axis (parallel to the atomizer), while spray measurements in this direction provide information about the spread rate of the spray perpendicular to the flow. For reporting purposes, each of the coordinate axes has been nondimensionalized by the hydraulic diameter, D (Fig. 3.3), of the tunnel downstream of the atomizer.

A specially designed probe drive mechanism is used to traverse the hot-film probe across the test section. The probes have a length of 45 mm and plug into a probe support which connects to a coaxial cable. Special plates were designed to allow for proper sealing of the probe and support shafts independent of the position of the probe support with respect to the tunnel walls. The probe assembly could be traversed manually or by a stepper motor. The accuracy of traverse motion was 0.2 mm. The rotation of the probe, for alignment purposes, is accomplished with a thumb wheel mounted on the support.

The probe drive assembly can be mounted on all sides of the tunnel so that both Y and Z velocity profiles can be measured. On each wall there are three locations available to insert the probe: Y/D or Z/D = -0.25, 0, + 0.25. These locations permit measurements along the tunnel centerline and at one-half the distance between the wall and centerline.

3.2 Airblast Atomizer and Fuel Supply System

The basic design objective for the atomizer was to produce a flat liquid sheet that could be injected at the origin of the shear layer. This was accomplished with a design similar to one used by Rizk (1976). The atomizer, shown in Fig. 3.4, has a total length of 69.9 cm and is 1.03 cm thick. The design is such that the atomizer can be traversed axially within the test tunnel a total of 56 cm. The tip of the atomizer is machined to a knife edge with an included ramp angle of 15°. This angle was selected to minimize the possibility of flow separation along the ramp.

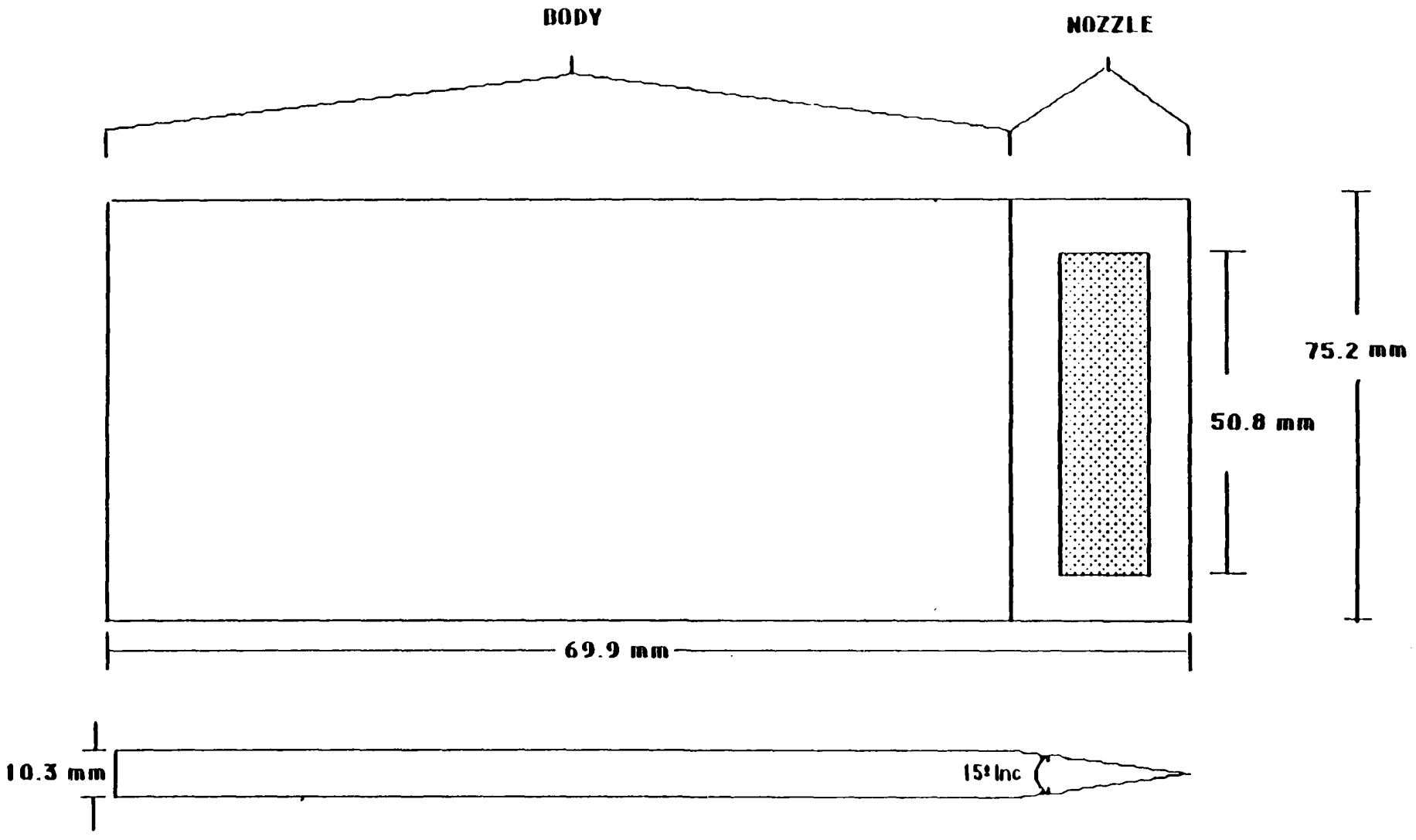

Figure 3.4 Airblast Atomizer

The section of the atomizer labelled "body" in Fig. 3.4 is 64.8 cm long and serves several purposes. It contains four tubes which run from end to end to permit liquid to flow into the nozzle, provide a passage for instrumentation wiring, and recirculate the fluid, if necessary. The body thickness was selected to allow it to be retracted into the splitter plates when positioning the atomizer. A specially designed fitting bolted to one end of this piece is attached to the nozzle positioning the system. The other end contains three stainless steel studs used to attach the body to the nozzle. The total width is 7.52 cm; teflon seals are located between the body and tunnel wall to eliminate metal to metal contact at the body/tunnel interface.

The nozzle is 5.1 cm long and its thickness varies from 1.03 cm where it connects to the body to 0.0 cm at the tip. A detailed drawing of this piece is shown in Fig. 3.5. A porous plate contained in one of the ramps is used to inject the liquid. The porous plate, manufactured by Mott Metallurgical, is constructed of sintered stainless steel, and porosities of 2 and 5 μm have been used for this study. Under the porous plate is a reservoir which is instrumented with both a thermocouple and miniature pressure transducer to monitor the pressure and temperature of the liquid prior to injection. The seal between the plate and nozzle is provided by an O-ring that is located in a groove on the nozzle body. Dove-tail joints are used to ensure a tight seal between the plate and nozzle to minimize leakage and flow disturbances.

The nozzle is sealed to the atomizer body with O-rings mounted on four fittings, each designed to accommodate instrumentation, or provide liquid access. Stainless steel nuts, located inside the reservoir, fix the nozzle to the atomizer body.

Two different porous plate designs were used in this study, but problems encountered with each resulted in minor leakage (<1% of the total mass flow rate) and spray impingement on the windows used for optical access. The first design, with the plate covering the entire reservoir, is shown in Fig. 3.5. The edges of the plate in contact with the O-ring were machined to seal the porous material (as recommended by the manufacturer) and prevent leakage. Although the leakage past the O-ring seal was reduced to a small percentage of the total liquid mass flow

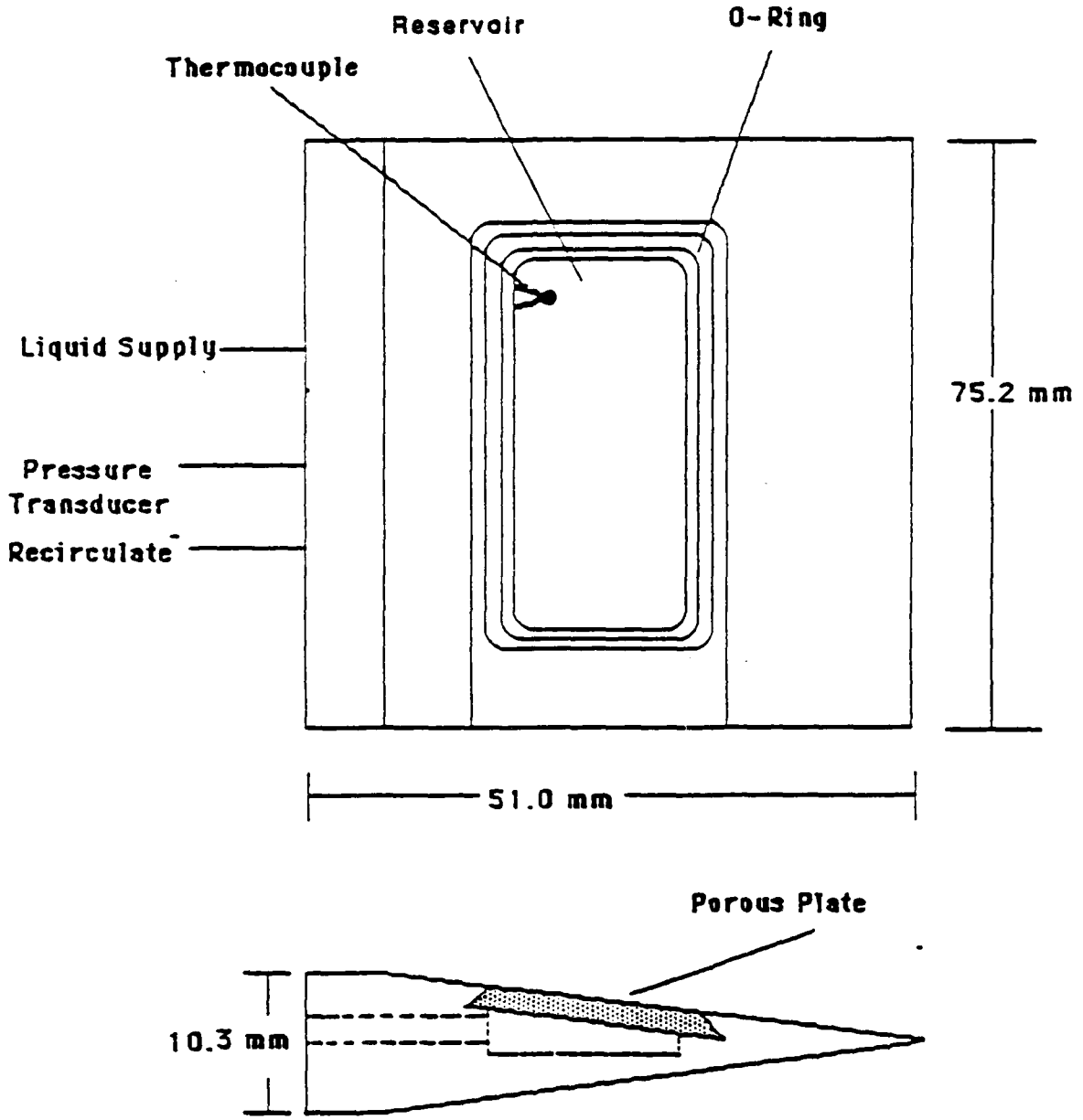

Figure 3.5 Airblast Atomizer Nozzle

rate it was not possible to completely eliminate it. The second design (not shown) consisted of a stainless steel plate that was machined to accept a smaller section of porous material. The stainless plate was in contact with the seals to eliminate the problems associated with sealing the porous material. This did not eliminate the problem since no acceptable method of bonding the porous material to the stainless plate could be found (welding caused severe warpage of the stainless plate, and conventional silicone sealants were inadequate).

The nozzle reservoir was instrumented to monitor conditions in the nozzle prior to injection. A type-J (iron-constantan) thermocouple was used to monitor the temperature of the liquid, while a Precision Measurements Model 150 miniature pressure transducer monitored the pressure. The temperature and pressure were displayed on an Omega Model 650 multichannel digital thermocouple readout and a Precision Measurements Model X strain indicator.

Accurate positioning of the atomizer was essential to reproducing experimental conditions. The nozzle drive system was comprised of a Slo-Syn Model M091-F006 stepper motor interfaced with an LSI-11/23 microcomputer using a Robot Synergy System A2 stepper motor controller. To connect the atomizer to the stepper motor a lead screw was attached to an adaptor (located on one end of the body) and then passed through a drive gear that is linked to the stepper motor with a chain. The stepper motor could position the atomizer with an absolute accuracy of $\pm$ 0.5 mm.

To prevent the velocity differential across the atomizer from displacing it in the Y-direction (due to the Bernoulli effect) wings are mounted along the atomizer body at 0.73 tunnel diameters upstream of the tip. The stabilizing wings are designed to minimize flow disturbances and have teflon edges to prevent marring the test section walls at the contact points.

The fuel supply system, also shown in Fig. 3.2, has been designed to deliver the liquid being atomized at mass flow rates up to 50 g/s. The liquid (only distilled water was used) was stored in a 55 gallon stainless steel drum. The piping system uses only plastic (low pressure/temperature) and stainless steel (high pressure/temperature) tubing to reduce problems

associated with corrosion. A stand-pipe was used in the fuel supply drum to eliminate contaminants that may have settled to the bottom. A Teel Model 1P777 pump, driven by a 1/2 Hp Dayton Model 2M169C electric motor, delivers the liquid to the atomizer. The motor speed and, hence, liquid flow rate were controlled with an SCR controller.

To ensure that microscopic contaminants (which could cause the atomizer to clog) were removed from the flow an Omni Model FW-5 filter was installed. This filter is rated as 99% efficient for particles with a diameter of 5μm and larger. After exiting the filter, the flow passed through a Brooks Model 1110-08H2G1R rotameter to monitor mass flow rate. The flow meter has an accuracy of ± 2% of the scale reading over the range of flow rates used in this study. To provide preheat for the liquid, a Chromalox Model NWHI-62515E3 in-line electrical resistance heater was used providing temperatures of up to 400 K. Positive displacement valves have been installed so that both the fuel heater and rotameter could be bypassed when required (e.g., during start-up).

All of the supply lines beyond the heater were insulated to minimize temperature loss. Prior to entering the atomizer, the liquid was again filtered with a Nupro Model SS-4FW-2 stainless steel mesh filter. This filter is rated 99% efficient for 2 μm particles and was used to remove any residual contaminants.

The liquid was delivered to the atomizer via a specially-designed feed tube. Because the atomizer was designed to translate axially within the test section the feed tube remains rigid and is inserted into the atomizer body.

3.3 Gas-Phase Measurements

A TSI Model IFA-100 hot-film anemometer system was chosen to obtain the velocity measurements. The IFA-100 is a high performance low noise constant temperature anemometer with a built-in microprocessor. The unit contains two channels, to handle cross-film probes, and is expandable to sixteen channels. The overheat ratio, the ratio of the sensor operating

temperature to the temperature of the air, is adjustable, and the IFA-100 can also interface with the LSI-11 microcomputer.

Initially hot wire probes (single and cross) were used for both the preliminary system verification and the gas-phase test matrix (for details, see Marakovits, 1987). However, the hot-wire probes were constantly damaged in the latter because of the environment inside the CTM tunnel. The wires used were tungsten with a sensor diameter of 4 microns, a frequency response of 600 kHz, and a maximum overheat ratio of 12 based on an ambient temperature of 25°C. Small particulate matter was believed to be causing the failure. The air supply system does have an inlet filter with a rating of 99 percent for filtering out particles 10 μm and larger. However, the smaller particles, probably scale from the pipes upstream of the Y section in Fig. 3.2, caused wire deterioration, i.e., continuous resistance change and eventual burnout. To alleviate the breakage problem quartz coated platinum films were used in the later stages of the program. The diameter of the film sensors was 25 μm, the frequency response was 300 kHz, and maximum overheat ratio was 17.

A TSI Model IFA-200 A-D converter was used to transfer the voltage signals from the IFA-100 to the LSI-11. The A-D converter has two channels and a maximum frequency response of 50 kHz. The data were then transferred to a VAX 11/750 where mean and rms velocities, and turbulent length scales were computed.

The instantaneous axial velocity, U(t), is calculated using the digitized output voltages (E) from the anemometer with a fourth order calibration curve fitted through the origin.

$$U(t) = a\,E^4 + b\,E^3 + c\,E^2 + d\,E \qquad (3.2)$$

The coefficients are evaluated prior to each experimental run using techniques discussed in

Marakovits (1987). The axial mean velocity is then calculated from the instantaneous values as:

$$U_x = \frac{1}{s} \sum_{i=1}^{s} U_i(t) \tag{3.3}$$

Here, s is the total sample size. Knowing U_x, it is now possible to calculate the rms velocity.

$$u^2_{rms} = \frac{1}{s} \sum_{i=1}^{s} (U_i(t) - U_x)^2 \tag{3.4}$$

Experimental values of length scale were computed using a two step procedure. First, an autocorrelation coefficient was calculated from the rms velocity data.

$$R(\tau) = \frac{\overline{[u(t)\ u(t+\tau)]}}{\overline{[u^2(t)]}} \tag{3.5}$$

Here, τ is the delay time and u is the rms velocity. Values of $R(\tau)$ are computed, by increasing the delay time, until it reaches zero (i.e., the rms data are no longer correlated). This function is then integrated to determine the intergral time scale (ITS).

$$ITS = \int_0^{\tau_{max}} R(\tau)\, d\tau \tag{3.6}$$

Then, using the mean velocity (Eq. 3.3) and Taylor's hypothesis (eddies are convected at the mean flow velocity) the length scale is calculated as:

$$\ell = (U_x)(ITS) \tag{3.7}$$

Parametric studies were conducted to determine optimum sampling times and frequencies for measurements of U_x, u_{rms}, and ITS (and, hence ℓ). Typically for these flows, mean and rms velocity data were acquired at 0.5 kHz for eight seconds, while length scale measurements required sampling at 5 kHz for five seconds.

Noise in the anemometer signal due to probe vibration was investigated and found to be minimal. With the film probe mounted, but the element concealed from the flow, mean and rms values of the output voltage were taken with and without the tunnel operating. For the non-operating condition the signal to noise ratio, S/N, was 376. The tunnel was then operated at three conditions, ranging from minimum to maximum velocity, and the S/N for each setting was within 1.5% of the non-operating condition, indicating probe vibration was not a problem.

3.4 Measurement of SMD and Liquid Volume Concentration

There are several optical techniques that have been developed to investigate fuel sprays. These include diffraction (Dobbins et al., 1963; Swithenbank et al., 1976) and extinction (Dobbins and Jizmagian, 1966) which provide, respectively, line-of-sight averages of SMD and liquid volume concentration through the fuel spray, and the more recently developed crossed-beam fringe methods (Bachalo et al., 1984) for point measurements of drop size and velocity distributions and liquid volume flux.

In this study, the optical technique developed by Dobbins et al. (1963), which is based on Fraunhoffer diffraction, was selected because it is a well established method of measuring mean drop sizes. It provides a direct relation between the intensity profile of the diffractively scattered light and the line-of-sight average of SMD through the spray. This technique, however, does not provide any information about the drop size or velocity distributions.

A Uniphase Model 1305 5 mW He-Ne laser provides the monochromatic light source required by these techniques. As illustrated in Fig. 3.6, the raw laser beam is passed through a 10X microscopic objective with a pinhole located at its focus to produce a clean expanding spherical wavefront. A collimating lens, placed at one focal length from the pinhole, is used to focus the wavefront at infinity. The diameter of the beam can be varied by changing the focal length of the collimating lens. This beam is then passed through an aperture before illuminating the spray where the light is scattered and absorbed. The scattered light and incident beam are focused at the focal plane of a 712.5 mm collecting lens. The detector, also located on the

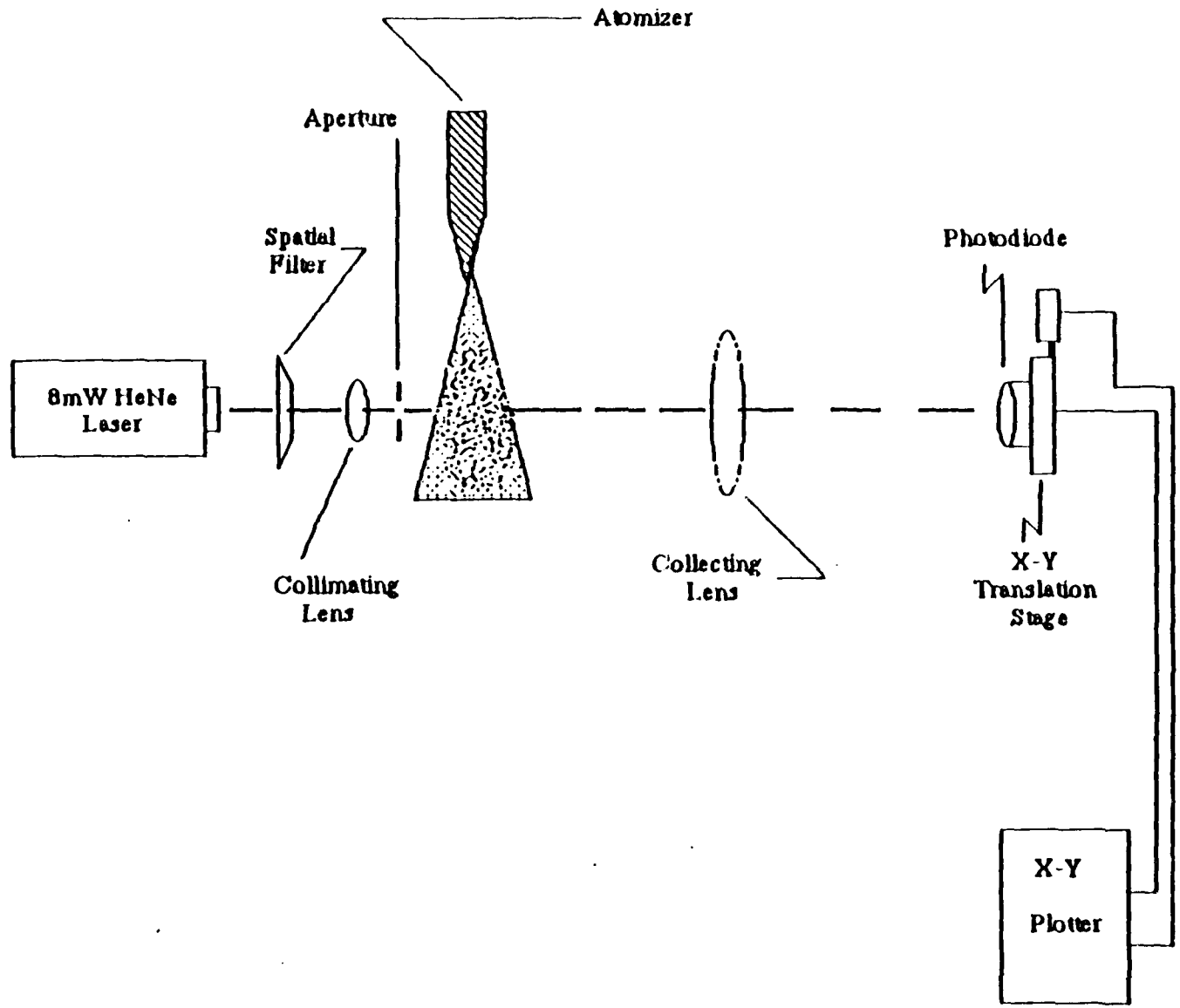

Figure 3.6 Droplet Sizing System

focal plane of the collecting lens, consists of a single photodiode (Hammamatsu Model S1087-1) mounted on a dual axis translation stage. The scattered and transmitted intensities are measured as functions of position on the focal plane by traversing the detector with a precision micrometer. A pinhole is mounted in front of the photodiode to increase the angular resolution of the detector and a red-line filter is used to remove extraneous light. The size of the pinhole is selected to optimize the detector's signal-to-noise characteristics. A reverse bias circuit, where the photodiode acts as a voltage gate (i.e., voltage output is proportional to the incident intensity), is used to measure the scattered light and the incident beam intensities. This circuit was selected because the low intensity of the scattered light (approximately two orders of magnitude less than the incident beam) necessitated large gains for current amplifiers, which tended to drive them unstable. The circuit output, along with the output from a linear potentiometer used to sense position, is fed into a Linseis Model LY17200 X-Y plotter which records the intensity profiles. The data from these profiles are then entered into a VAX 11/750 computer to calculate the SMD of the spray.

Extinction measurements were to be used to determine the liquid volume concentration, which is related to the extinction of the incident light via Beer's Law (Halliday and Resnick, 1974) suitably modified for polydisperse sprays (Dobbins and Jizmagian, 1966).

$$\frac{I}{I_0} = \exp\left[-\frac{3}{2} \frac{K C_v \ell}{SMD} \right] \qquad 3.8$$

Here, K, the mean scattering coefficient, is only a function of the SMD of the spray (Dobbins and Jizmagian, 1966), ℓ is the optical path length, and C_v is the liquid volume concentration, the parameter of interest.

Unfortunately, measurements of spray evaporation rates were not possible in the present facility. The initially proposed method of determining the evaporation rate called for using laser extinction measurements to determine a global value for this parameter. These measurements entailed obtaining a measure of the laser intensity without a spray, the spray was then to be

started and the intensity of the transmitted light would again be measured. The atomizer would then be retracted (hence the need for 56 cm of travel) until the measured intensity reached 99 percent of its initial value. The axial location would be noted, and using this distance in conjunction with a mean spray velocity would result in a value for τ_{eb} that was averaged over the entire spray. However, due to problems with the tunnel's sealant design, it was not possible to obtain air temperatures that were large enough to completely evaporate the spray.

In an attempt to resolve this problem another method of measuring τ_{eb} was proposed which entailed measuring the change in SMD as a function of distance from the injector ($d(SMD)/d(X/D)$). It was hoped that this parameter could be related to the evaporation coefficient using some mean spray velocity, if it behaved in a manner similar to a single droplet in terms of evaporation. That is, from the definition of β:

$$\beta = -\frac{d(D^2)}{dt} \qquad 3.9$$

This method, however, will not produce the desired results since in many cases SMD increases as a function of X/D (Dodge, 1984), a fact which may at first seem surprising until one considers that it simply means the average volume of the spray ($\int n(D)D^3dD$) is decreasing at a faster rate than the average surface area ($\int n(D)D^2dD$). Since this definition is not consistent with Godsave's (1953) d^2 law it was apparent that another method was required.

A final approach involved measuring the change in extinction (due to evaporation) as a function of distance from the injector. Here, the evaporation coefficient can be defined as:

$$\beta = \frac{4\dot{V}}{\pi D} \qquad 3.10$$

where $\dot{V}$ is the change in volume of the spray as a function of time and D is a mean diameter of the spray. Since $\dot{V}$ is related to $d(C_v)/dt$, transmission measurements should yield the desired results.

However, this method failed as well. First, measurement sensitivity makes transmission measurements difficult for small changes (on the order of $I/I_0 \geq 0.98$) in transmitted light. The second, and more difficult problem to overcome was decoupling changes in transmission due to evaporation from those due to laminar dispersion. An analysis of this problem is presented in Tallio (1987); the reader is referred there for details.

In addition to problems encountered with measuring r_{eb}, it was not possible to obtain extinction measurements as a function of Y/D due to the previously noted (Section 3.2) problems with spray impingement which restricted optical access.

The facility described in this chapter has been used to obtain data for turbulent two-phase flows to provide the information necessary to investigate both semi-empirical and finite difference models of these flows. Due to the restrictions noted previously, evaluation of turbulent spray dispersion and of droplet lifetime or evaporation coefficient was not completed. However, measurements to investigate gas-phase flow finite difference models and validate the turbulent mixing time parameter in the CTM were successful. Additionally, data to investigate the accuracy of correlations for mean drop size provided insight into difficulties associated with the CTM parameter for droplet lifetime. With the description of the experimental facility complete, the remaining chapters will focus on the results of the experimental program and complementary numerical studies.

4.0. Experimental Results and Discussion

The focus of this section is experimental flowfield and atomization studies. Preliminary experimental results pertaining to the current work are presented first, followed by mean and rms velocity and length scale measurements. Implications for the CTM based on these data are discussed as are mean drop size and spray attenuation results.

4.1 Preliminary Experimental Program

Preliminary experimental work was undertaken to characterize the gas-phase flow in the test tunnel and to ensure that the atomizer was functioning properly (i.e., that the sprays produced were similar to other two-dimensional and axisymmetric prefilming airblast atomizers reported in the literature). The objectives of this work were to establish a set of baseline operating conditions for the two-phase flow test matrix that would be used for investigating the models of these flows discussed in Section 2. This section of the report will simply highlight the findings of the previous work; the interested reader is referred to Marakovits (1987) and Tallio (1987) for details.

The gas-phase measurements revealed the flowfield in the experimental facility for the eight cases of the preliminary test matrix shown in Table 4.1. Shear layer strengths (λ) were selected to cover the range of conditions from a wake flow ($\lambda = 0$) to a fully recirculating flow ($\lambda = 1$). Fuel side air velocities (U_{AFS}) were chosen based on other work in the literature with flat prefilming airblast atomizers (Rizk, 1976); the choice of λ and U_{AFS} specified the air side air velocity U_{AAS}. The measurements established in which cases the flowfield was two-dimensional (i.e., flow parameters were only weak functions of Z/D) and nonrecirculating, and that the experimental conditions could be accurately reproduced. The coordinate system used throughout the following is shown in Fig. 3.3.

Table 4.1

Preliminary Test Matrix[1]

Case	U_{AFS} (m/s)	λ	U_{AAS} (m/s)
1	73.9	0.0	73.9
2	73.9	0.67	14.6
3	73.9	1.0	0.0
4	42.5	0.33	21.4
5	73.9	0.33	37.2
6	100.4	0.33	50.6
7	42.5	0.0	42.5
8	100.4	0.0	100.4

1. U_{AFS} and U_{AAS} are calculated from continuity for the matrix presented here, and correspond to cases numbered in a similar way by Marakovits (1987), who used an average peak velocity definition.

Two-dimensionality of the gas-phase flow and the lack of recirculation is desirable because a two-dimensional, parabolic finite difference code was selected to compute the flowfield. Further, if the air flow over the liquid sheet (from Z/D = -0.3 to + 0.3) is two-dimensional then the sprays generated by the atomizer may also be two-dimensional. The results demonstrated that the flow met this criterion over the entire measurement domain ($X/D \leq 2$) for shear layer strengths less than 0.67. For these cases (all but two and three) it was also shown that the Z velocities (those important for atomization) were constant for the range $-0.3 < Z/D < 0.3$; outside this range wall effects create boundary layer flow. This finding assisted in sizing the porous plate used to deliver the liquid for atomization.

To establish the measurement techniques used for the gas-phase flow the experimental velocity profiles were integrated to obtain mass flow rates, which were compared with those measured by the orifice plates upstream of the test section. In the nonrecirculating cases of the preliminary matrix the mass flow rates calculated by integration were within five percent of the orifice plate values (Marakovits, 1987).

Characterization of the prefilming atomizer was necessary to establish that the sprays were similar to those obtained by other researchers (e.g., Rizk, 1976; Lefebvre, 1980) and that the spray was two-dimensional. Both of these design objectives were met. The correlation developed by Lefebvre (1980) for SMD, Eq. 2.12, showed agreement that was as good or better ($R = 0.96$) than for the other six atomizers used to develop the correlation (Tallio, 1987). In addition, the results of Rizk (1976) revealed that correlations of this type are not accurate to better than 10 percent for changes in liquid properties, and errors as high as 50 percent can result for changes in the atomizer geometry (Tallio, 1987). Finally, the SMD was not a function of the liquid flow rate because the liquid to air ratio used in this work was below the critical value of 0.2 (Lefebvre, 1980). The results of this work, and those from the gas-phase flow studies discussed above, were used to refine inlet conditions for the subsequent studies.

4.2 Two-Phase Flow Matrix

The two-phase flow matrix, shown in Table 4.2, was chosen based on several criteria and constraints. It was desirable to repeat some cases of the preliminary test matrix to verify that flow conditions within the test section could be reproduced accurately. Accordingly, the two-phase flow matrix includes cases 1, 7, and 8 of the preliminary test matrix.

Secondly, it was necessary to eliminate cases which involved three dimensional or recirculating flow. As discussed in the previous section, preliminary results limited λ to less than 0.67. Another consistent constraint was that later atomization studies found that $\lambda = 0.33$ resulted in spray impingement on the windows, making accurate droplet sizing measurements impossible. Thus all the cases of the two-phase flow matrix have shear layer strengths less than 0.33 and, as seen from Table 4.2, the final values of shear layer strength selected were between 0.0 and 0.22.

The final constraint set air velocities. The cases in the two-phase flow matrix must have air velocities sufficiently large to ensure atomization will produce measurable Sauter mean diameters, but not so large as to cause frequent hot film probe breakage. These two velocity

requirements limited the allowable mass average velocity on either side of the splitter plate to a range varying from 40 m/s to 100 m/s.

TABLE 4.2
Two-Phase Flow Matrix

Case	U_{AFS} (m/s)	λ	U_{AAS} (m/s)
1	73.9	0.0	73.9
7	42.5	0.0	42.5
8	100.4	0.0	100.4
10	82.6	0.0	82.6
11	82.6	0.1	67.1
12	82.6	0.2	54.2
13	100.4	0.2	63.4
14	73.9	0.2	46.1

Of the eight cases from the two-phase flow matrix two were chosen to study the evolution of mean and rms velocities and length scales in detail. Case 1 is a repeated case from the preliminary test matrix, and so can be compared with preliminary test matrix results. Case 14 was selected for study for two reasons: to determine mixing times with a strong shear layer, and to maintain the same fuel side velocity as case 1, making comparisons between case 1 and case 14 possible.

Flowfield measurements were obtained 0.66 tunnel diameters upstream of the origin (X/D = -0.66) to observe the flow directly before the atomizer ramp. Measurements obtained at 0.33 tunnel diameters upstream revealed flow characteristics part way through the flow expansion due to the decreasing thickness of the ramp. Mean and rms velocity measurements taken at 0.03 tunnel diameters downstream of the atomizer tip enabled the flow at the geometric origin of the shear layer to be observed and provided data for the calculation of initial mixing times. These

data also served as inlet conditions for the finite difference model discussed in Section 5. It should be noted that the inlet conditions were determined at X/D = 0.03 and not X/D = 0.00 due to restrictions inherent in traversing a hot film probe beneath the atomizer tip. Downstream of the atomizer gas-phase measurements were taken at X/D = 0.50, 1.00, 1.50, and 2.00 to observe the shear layer growth as the flow progressed, and to obtain downstream mixing times for comparison with the mixing time at the shear layer origin.

Flowfield measurements at each axial location involved three probe traverses in the direction perpendicular to the plane of the atomizer (Y-profiles) and three traverses parallel to the plane of the atomizer (Z-profiles). Those taken perpendicular to the atomizer were located at the centerline (Z/D = 0.00) and at one-quarter tunnel diameter on either side of the centerline (Z/D = ± 0.25). Likewise, traverses parallel to the atomizer were located at Y/D equal to 0.00 and ±0.25.

At each axial location gas-phase flow data were obtained both with and without spray. In the former case, measurements were restricted to the freestream as any liquid which impinged on the hot film probe yielded erroneous results and caused damage to the probe. Gas-phase flow data with liquid injection into the flowfield determine insofar as possible with the current instrumentation the validity of assuming the two-phase flow is dilute.

For all eight cases of the two-phase flow matrix, length scale and rms and mean velocity measurements at the inlet station (X/D = 0.03) were obtained for characteristic time model validation.

Mean droplet size (SMD) and transmission measurements were also conducted for selected cases from X/D = 0.50 to X/D = 2.00 in one-half tunnel diameter increments for those cases where spray impingement did not restrict optical access. At each downstream location both optical measurements were attempted at the centerline locations (Z/D = 0.00) and at 5 mm (0.066D) increments on either side of the centerline, for a total of five measuring locations. Figure 4.1 shows the locations of incident laser light for integral measurements, or those taken

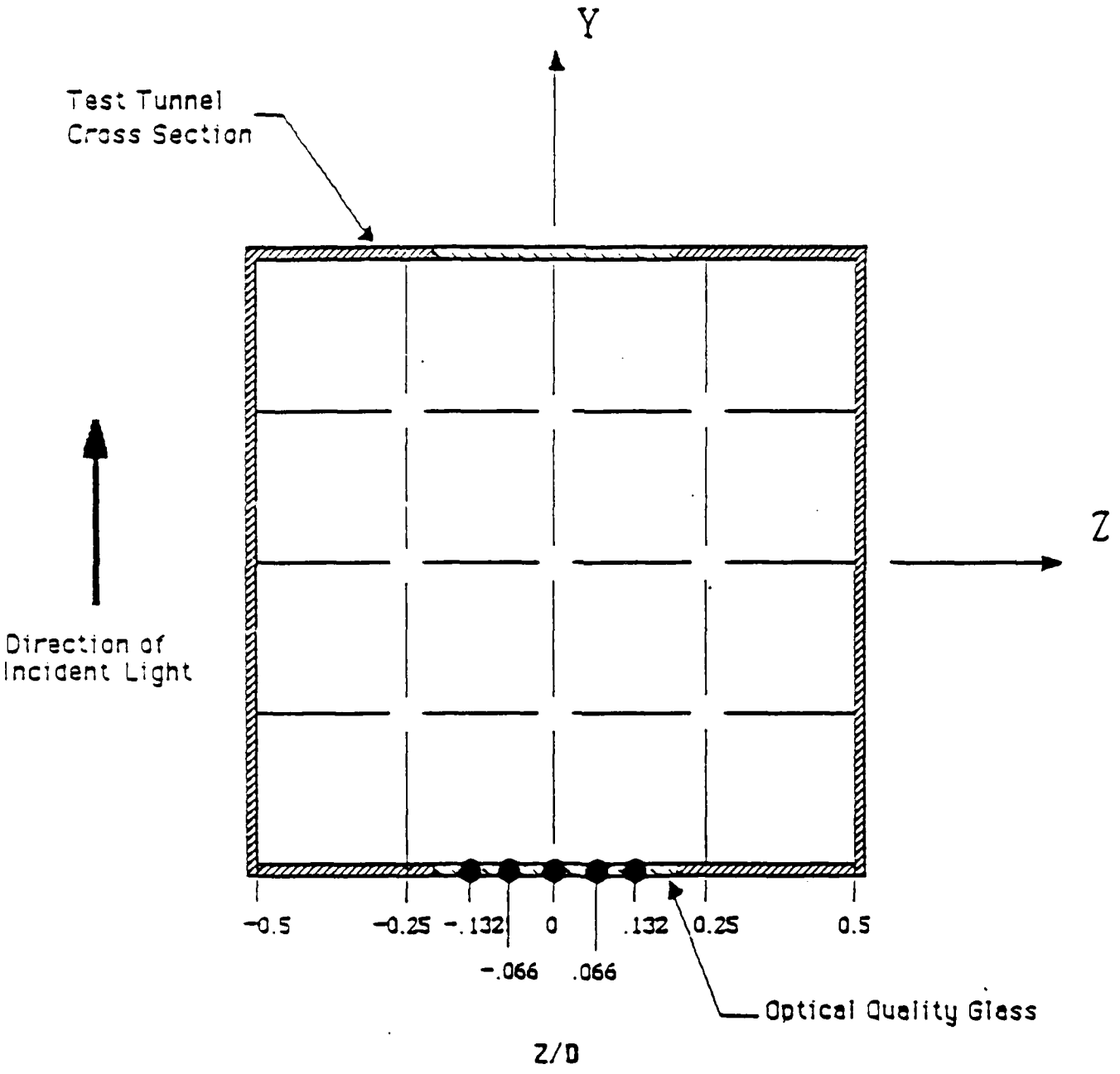

Figure 4.1 *Incident Beam Locations for Integral SMD and Transmission Measurements*

in the Y-direction. In the direction parallel to the spray sheet, optical measurements were precluded by droplet impingement which occurred on the Z-walls at X/D less than 0.5.

As discussed in Section 3.2, problems with sealing the porous plate were encountered in this study. All of the data reported here were obtained using the wide porous plate (first design) described previously and are presented in tabular form in Appendix A. Consult Marakovits (1987) for a listing of the preliminary test matrix data.

4.3 Gas-Phase Results

4.3.1. Consistency of the Data

Figures 4.2 through 4.4 compare mean and rms velocity data from case 1 of both the preliminary test matrix and the two-phase flow matrix. Each plot shows the Z-averaged mean or rms velocity profile perpendicular to the atomizer tip (Y-profile) from case 1 of the two-phase flow matrix and the centerline (Z/D = 0.00) velocity profile from case 1 of the preliminary test matrix at successive downstream locations. The deviation bars placed at representative points on the average velocity curve show the minimum and maximum values of the three measurements along the Z-axis at that corresponding Y/D location.

At all three axial stations the mean velocity profiles from the two matrices show good agreement except in the boundary layers near the outer walls approaching Y/D = ±0.50. The deviation bars for the present work demonstrate freestream and wake velocity variations of less than 7 percent along the Z-axis, further verifying the two-dimensionality of the flow in these regions. In these same regions rms velocity measurements from the preliminary test matrix show values consistently less than and outside the rms velocity range defined by the deviation bars of the two-phase flow matrix case. Although a specific explanation cannot be offered at this time, these differences are apparently a result of using a cross-film probe for data acquisition in the latter experiments. The only other parameter varied between the two sets of data was the airblast atomizer (preliminary measurements used a blank atomizer, i.e., one without a porous plate; the data reported here used the actual atomizer containing a porous

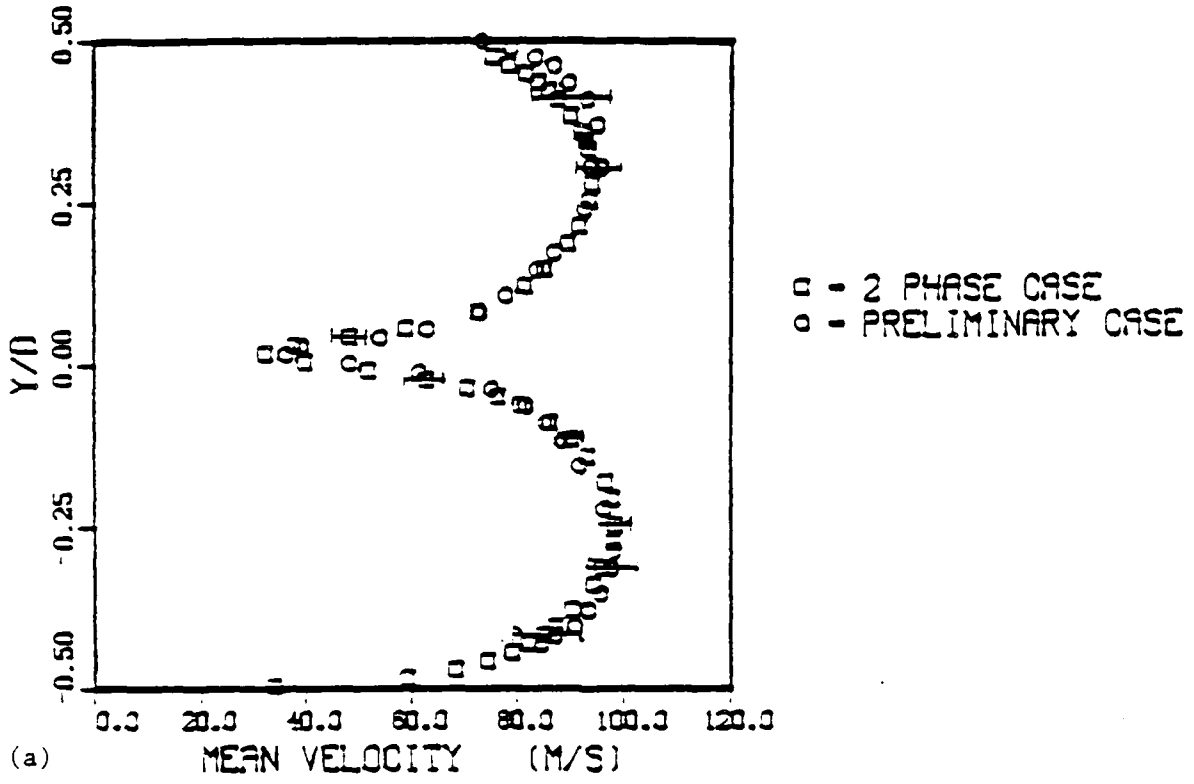

(a)

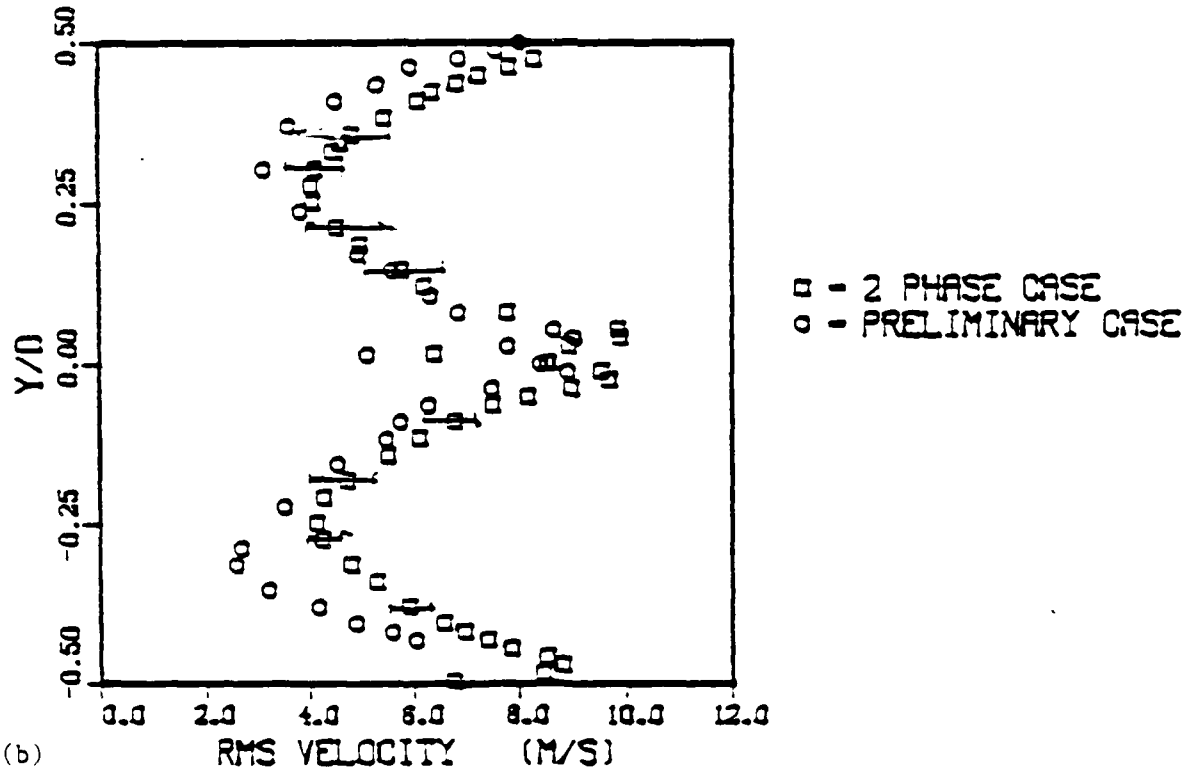

(b)

Figure 4.2 Comparison of Experimental Z-Averaged (a) Mean and (b) rms Velocity for Case 1 of Two-Phase Flow Matrix with Experimental Centerline Values for Case 1 of the Preliminary Test Matrix at X/D = 0.03

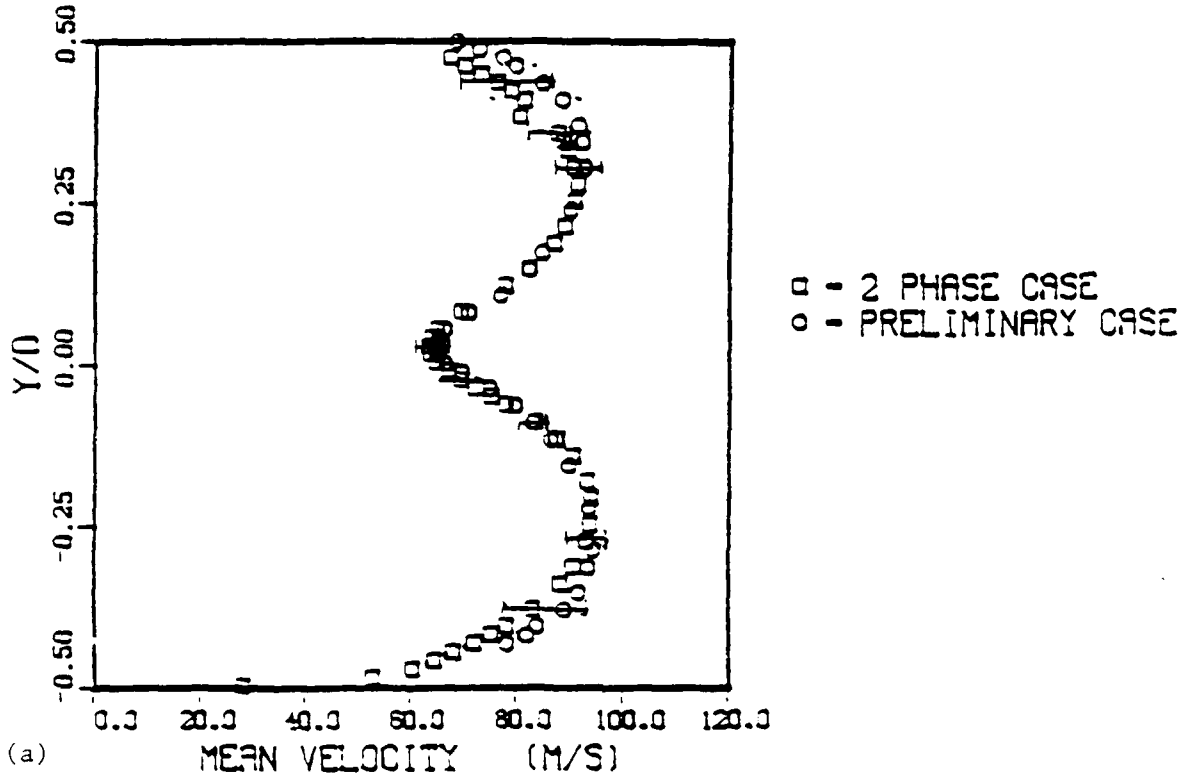

(a)

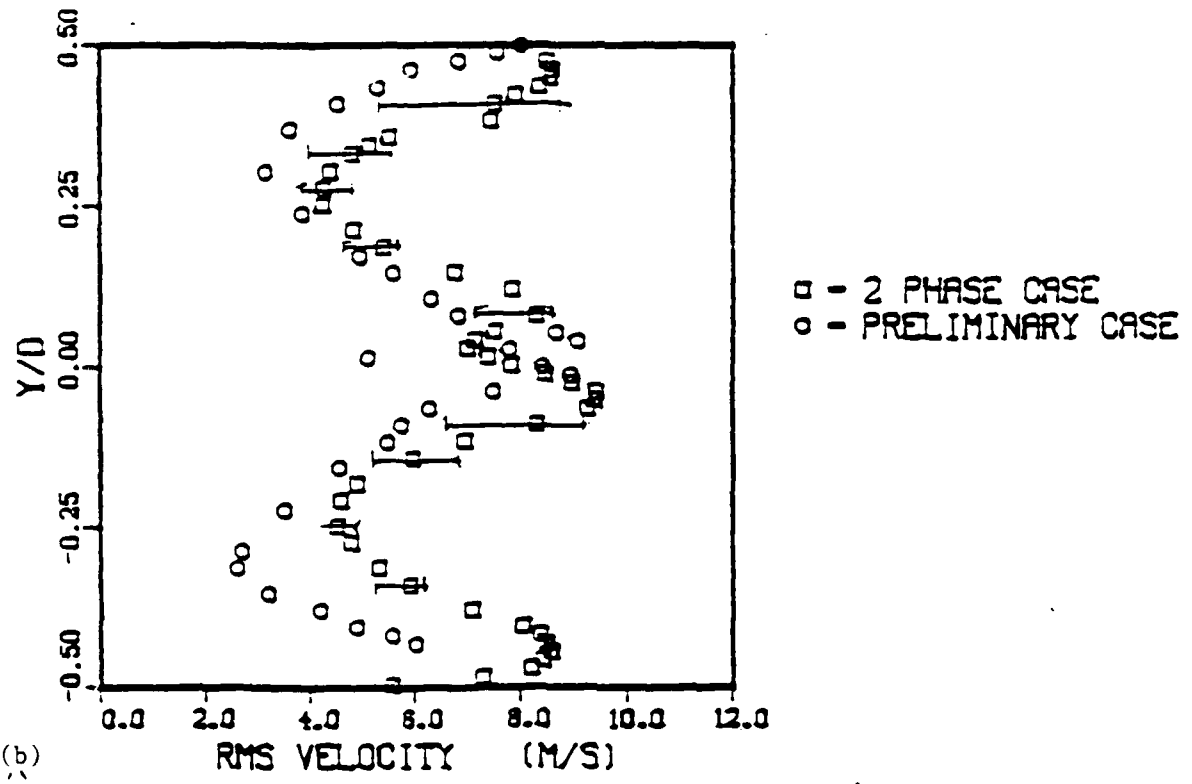

(b)

Figure 4.3 Comparison of Experimental Z-Averaged (a) Mean and (b) rms Velocity for Case 1 of Two-Phase Flow Matrix with Experimental Centerline Values for Case 1 of the Preliminary Test Matrix at X/D = 1.0

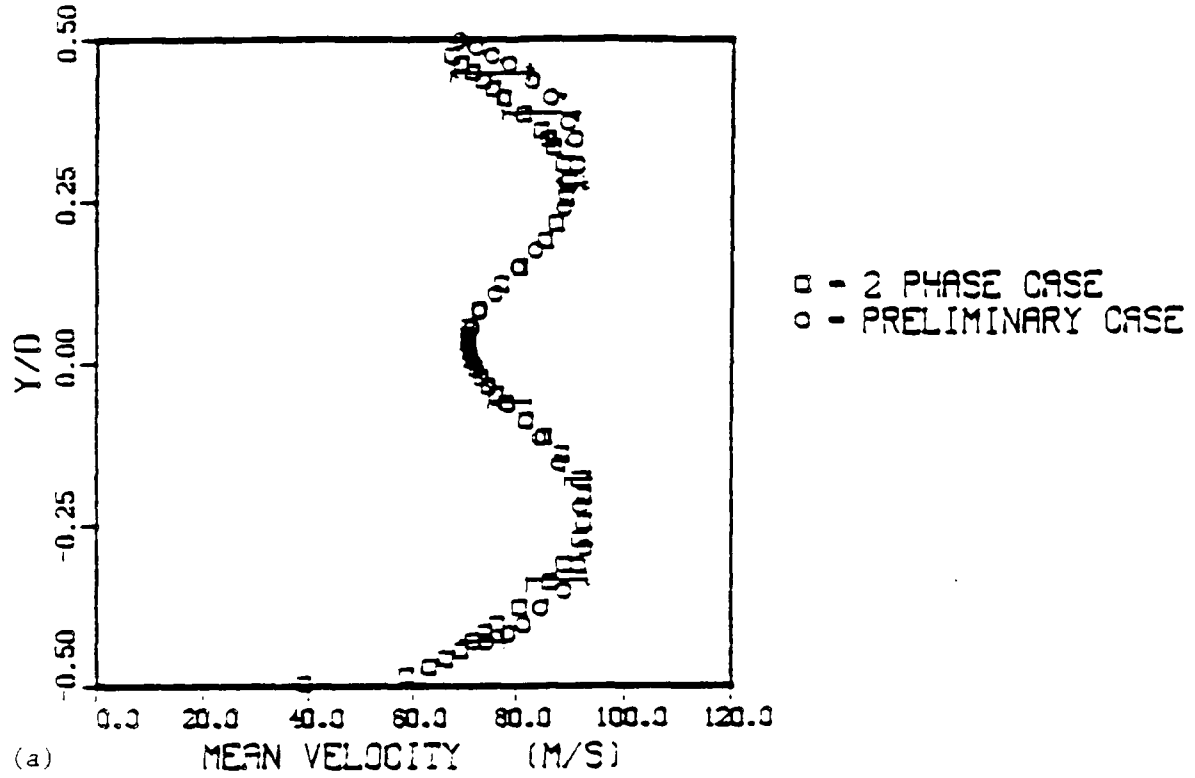

(a)

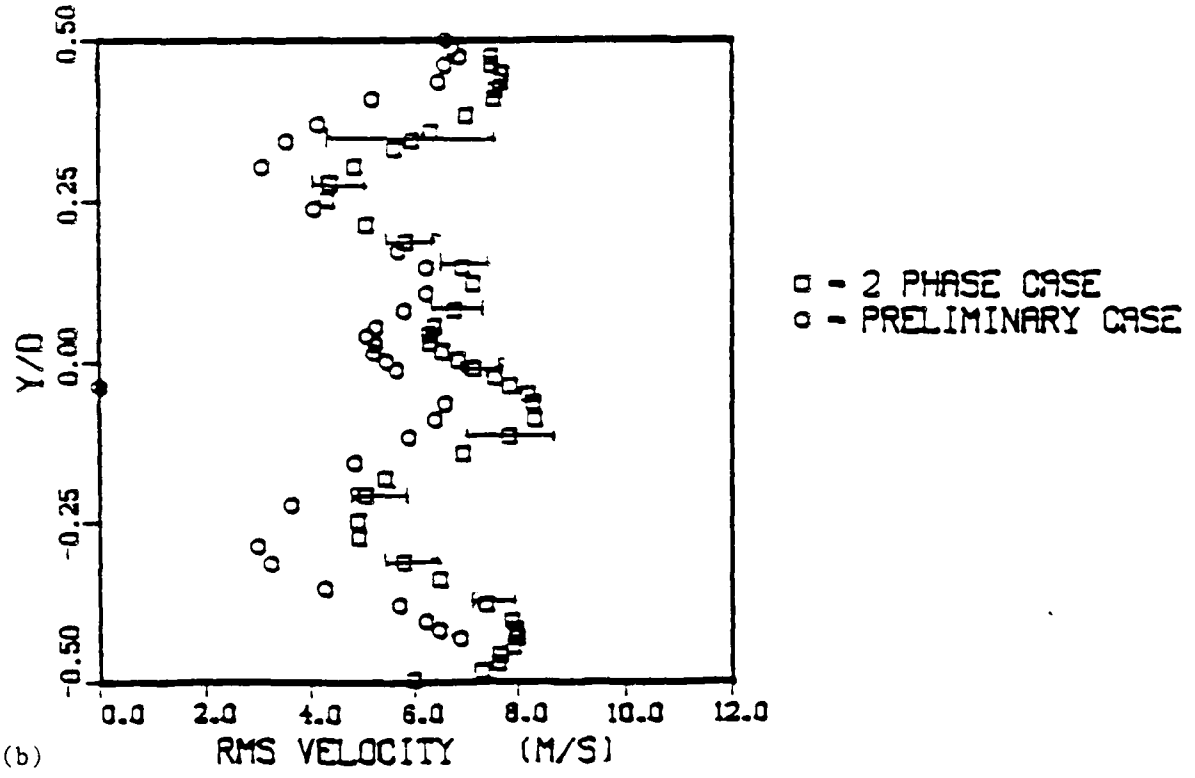

(b)

Figure 4.4 Comparison of Experimental Z-Averaged (a) Mean and (b) rms Velocity for Case 1 of Two-Phase Flow Matrix with Experimental Centerline Values for Case 1 of the Preliminary Test Matrix at X/D = 2.0

plug). Marakovits (1987) shows that the effect of this change on the freestream rms velocities is less than four percent.

Air mass flow rates calculated from the orifice plates upstream of the test section are comparable with those obtained by integrating the experimental mean velocity profiles at each axial station. For the data reported here, six velocity profiles were used, three parallel (Y/D = 0.00, and ±0.25), and three perpendicular (Z/D = 0.00 and ±0.25) to the atomizer. These calculations for case 1 (and 14 discussed below) of the two-phase flow matrix show a worst case discrepancy of 2.03 percent, well within the 5 percent tolerance limit established for our data. Calculations for case 1 of the preliminary test matrix were found to deviate by 1.12 percent (Marakovits, 1987), but those integrated air mass flow rates were calculated using only four mean velocity profiles, three in the Y-direction and one in the Z-direction.

4.3.2. Detailed Measurements

Figures 4.5 through 4.15 present Z-averaged mean and rms velocity data for cases 1 and 14 for all axial locations where measurements were made. Centerline (Z/D = 0) Y-profiles of length scale are alsc shown for these cases in Fig. 4.16 to 4.26. At and downstream of X/D = 0.03, profiles computed with the finite difference code are indicated as well, but will be discussed in Section 5.

For case 1, Fig. 4.5 and 4.6 verify that a condition of $\lambda = 0$ has been produced, as the peak velocities of both airstreams vary by less than 4.4% at the first upstream measurement location (X/D = -0.66) and at the origin (X/D = 0.03). The mean and rms velocity profiles are also reasonably symmetric about the centerline. A comparison of mean velocity profiles from Figs. 4.5 to 4.8 shows freestream mean velocity decreasing downstream, as expected, due to first the flow expansion past the atomizer and then the momentum transfer from the freestream flow to the wake region. Concurrently, wake turbulence decays and spreads into the freestream as a result of turbulent mixing of the two flows. Figs. 4.9 through 4.15 for case 14 ($\lambda = 0.22$) show similar results with reference to flow expansion and momentum transfer, except that the

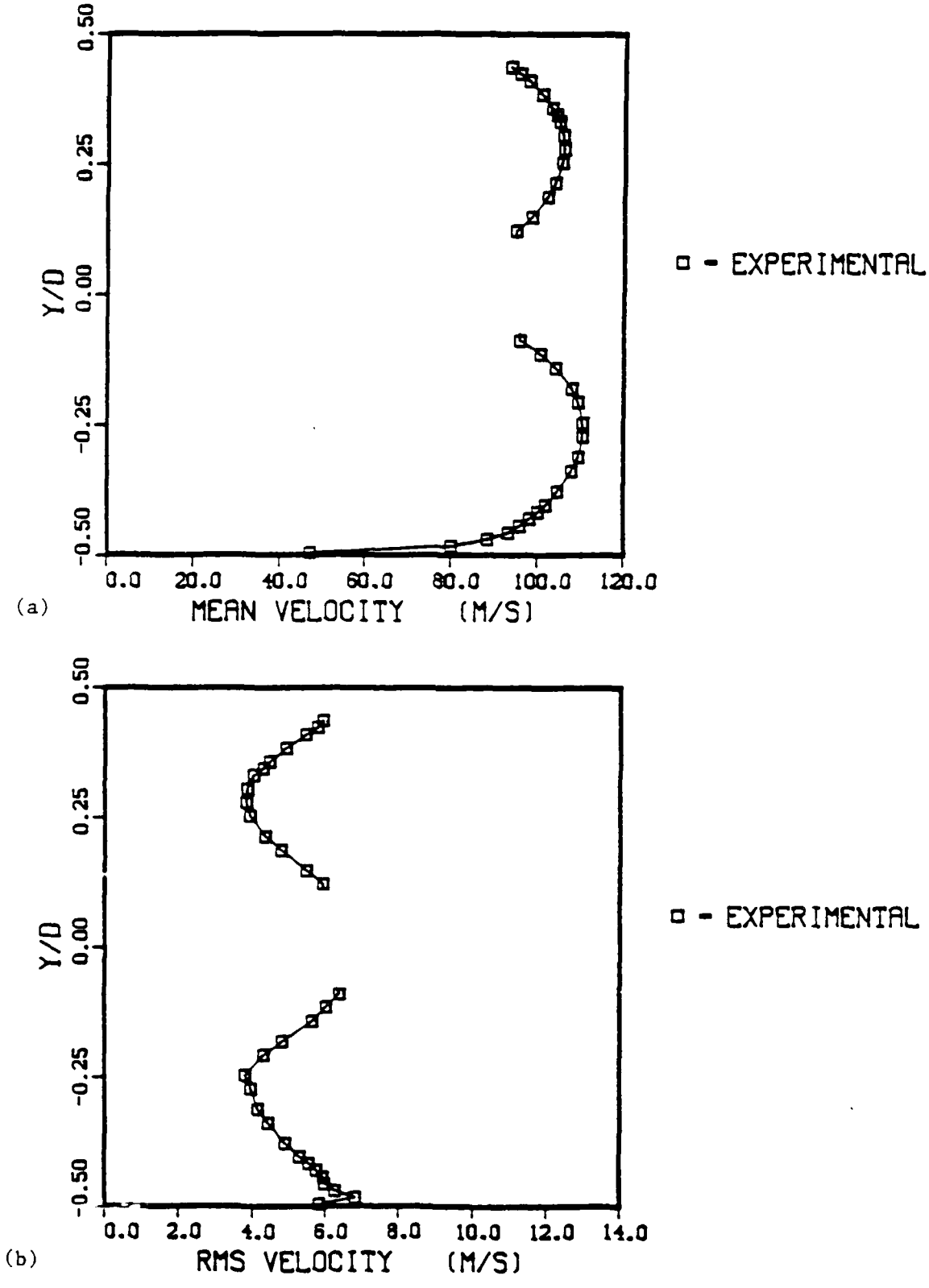

Figure 4.5 Experimental Z-Averaged (a) Mean and (b) rms Velocity for Case 1 at X/D = -0.66

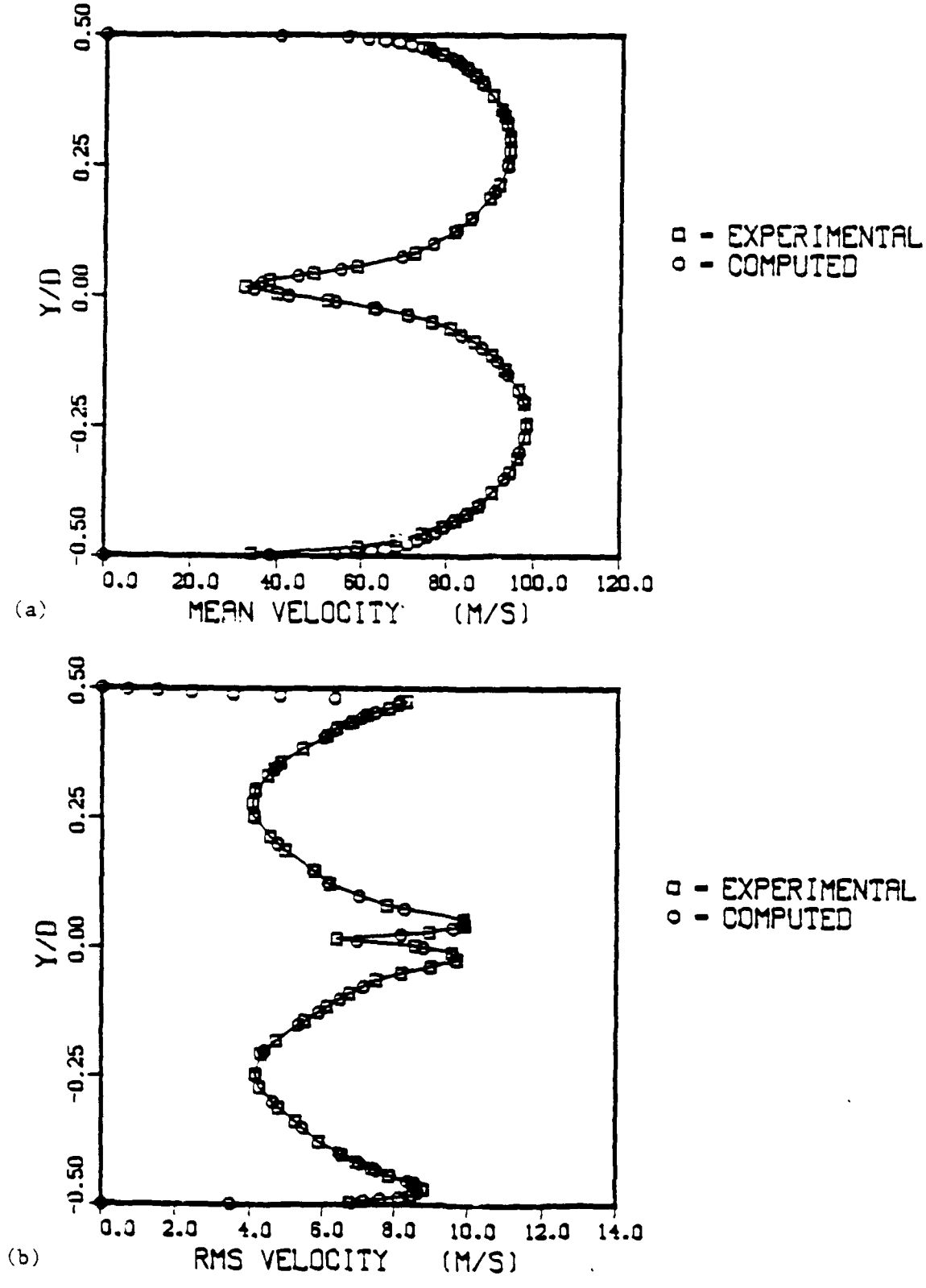

Figure 4.6 Comparison of Experimental Z-Averaged (a) Mean and (b) rms Velocity with Computed Values for Case 1 at X/D = 0.03

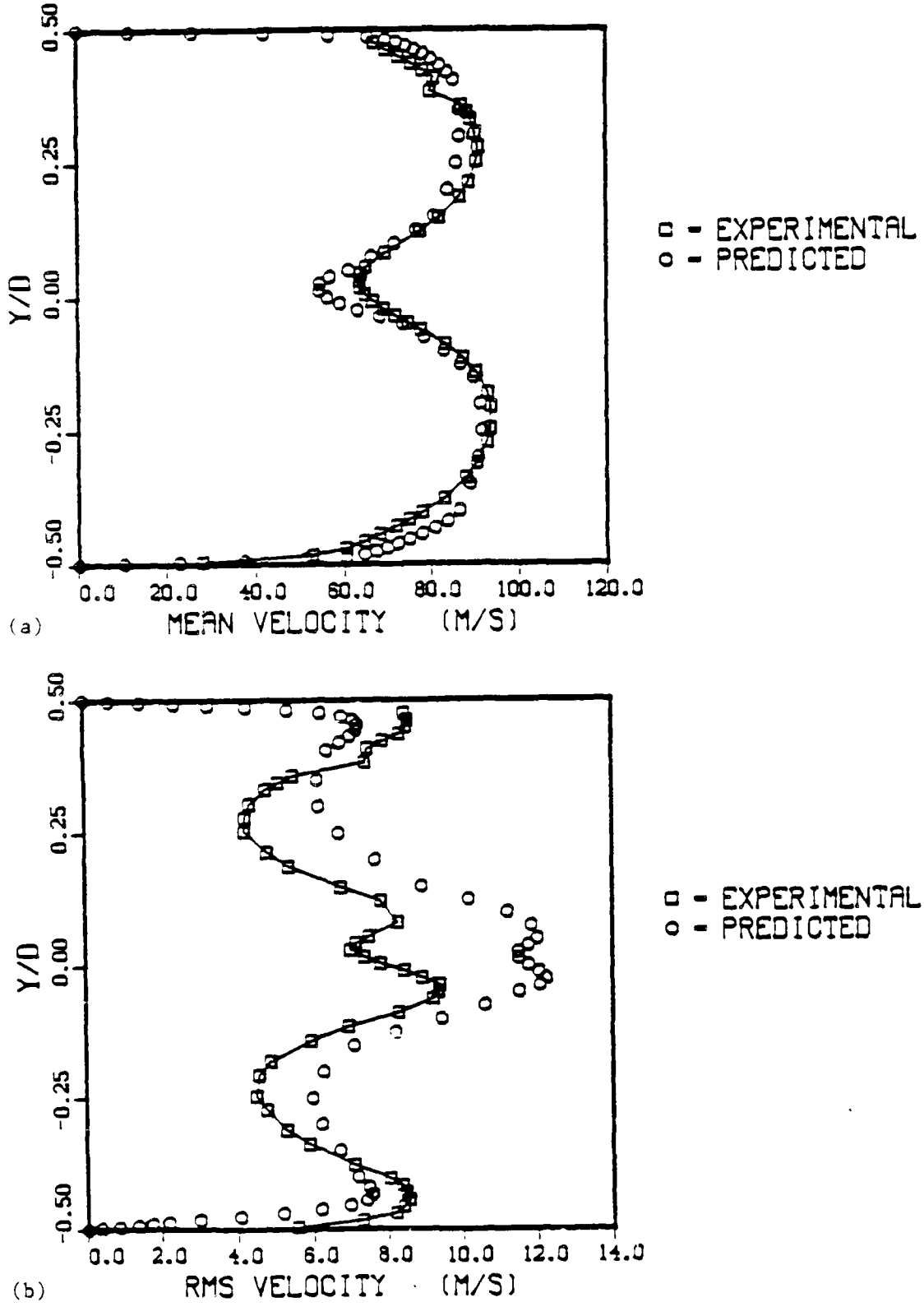

Figure 4.7 Comparison of Experimental Z-Averaged (a) Mean and (b) rms Velocity with Predicted Values for Case 1 at X/D = 1.0

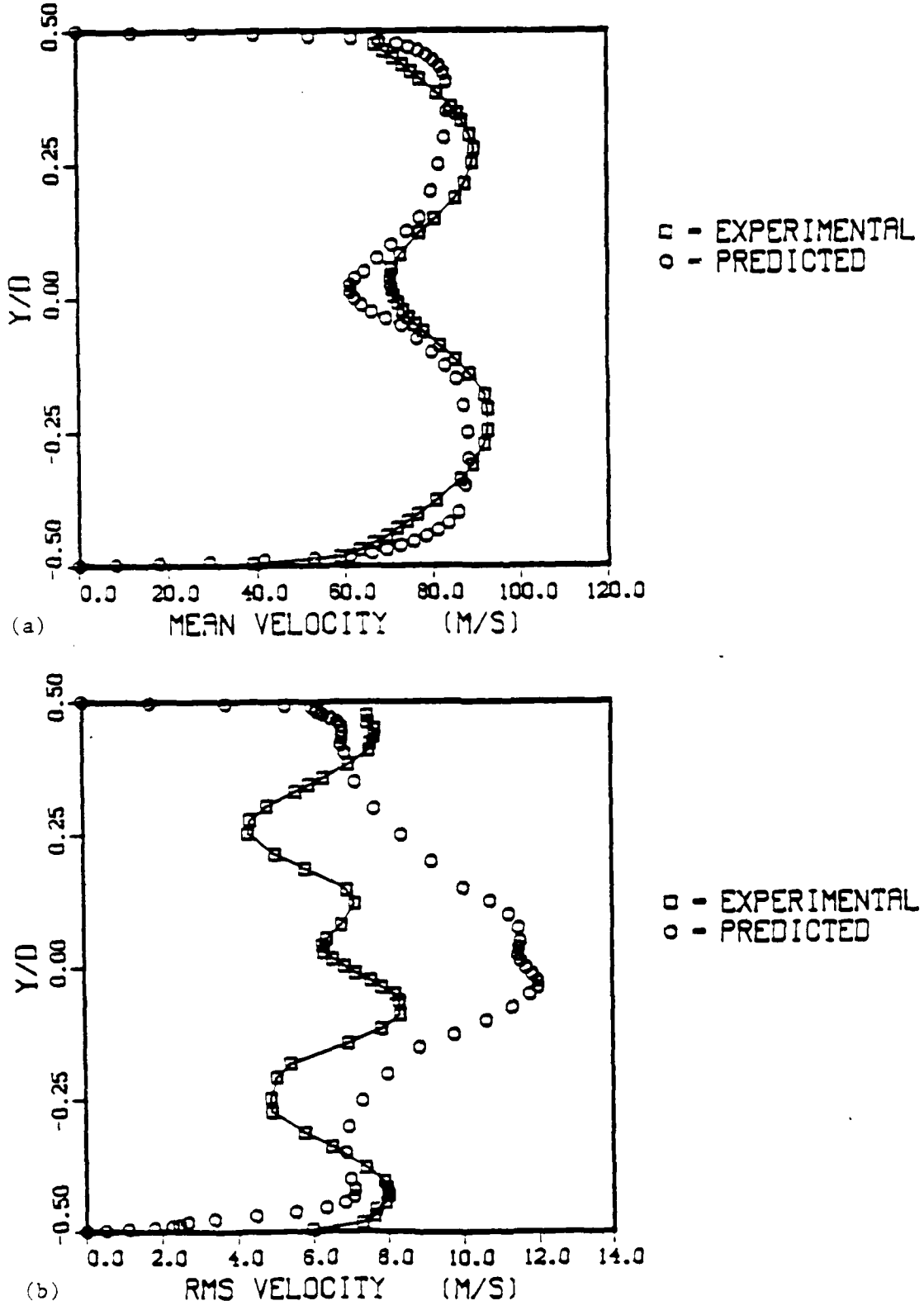

Figure 4.8 Comparison of Experimental Z-Averaged (a) Mean and (b) rms Velocity with Predicted Values for Case 1 at X/D = 2.0

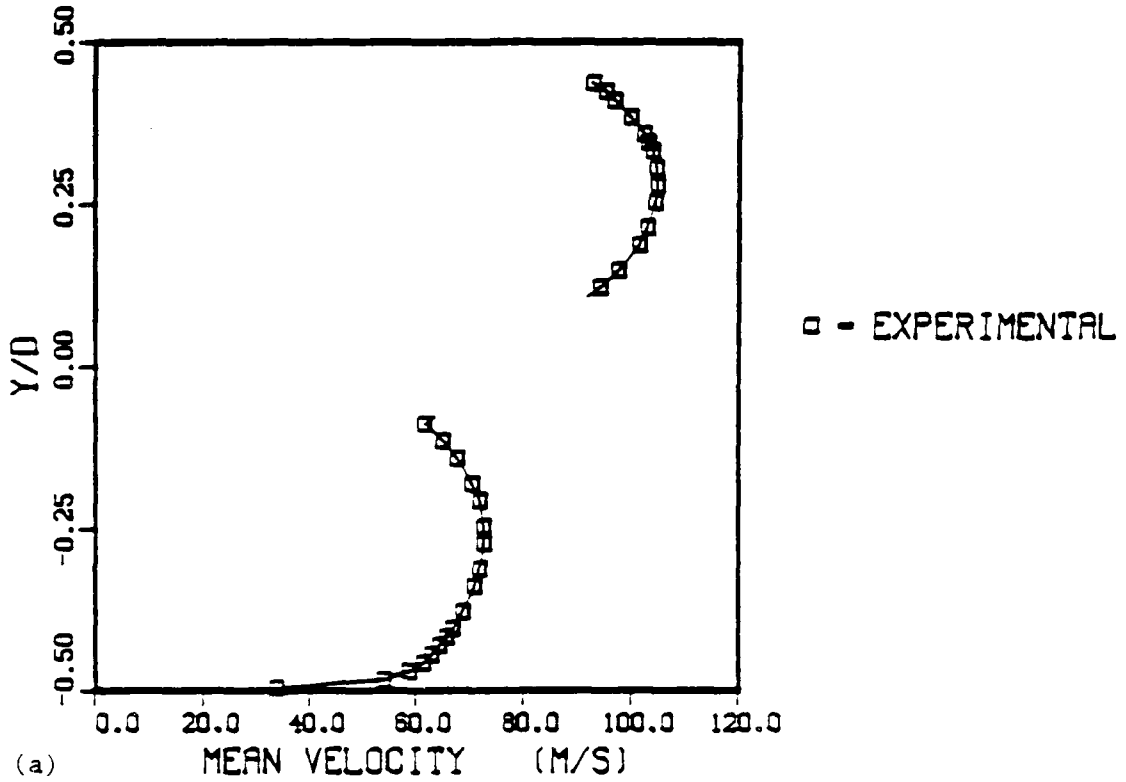

(a)

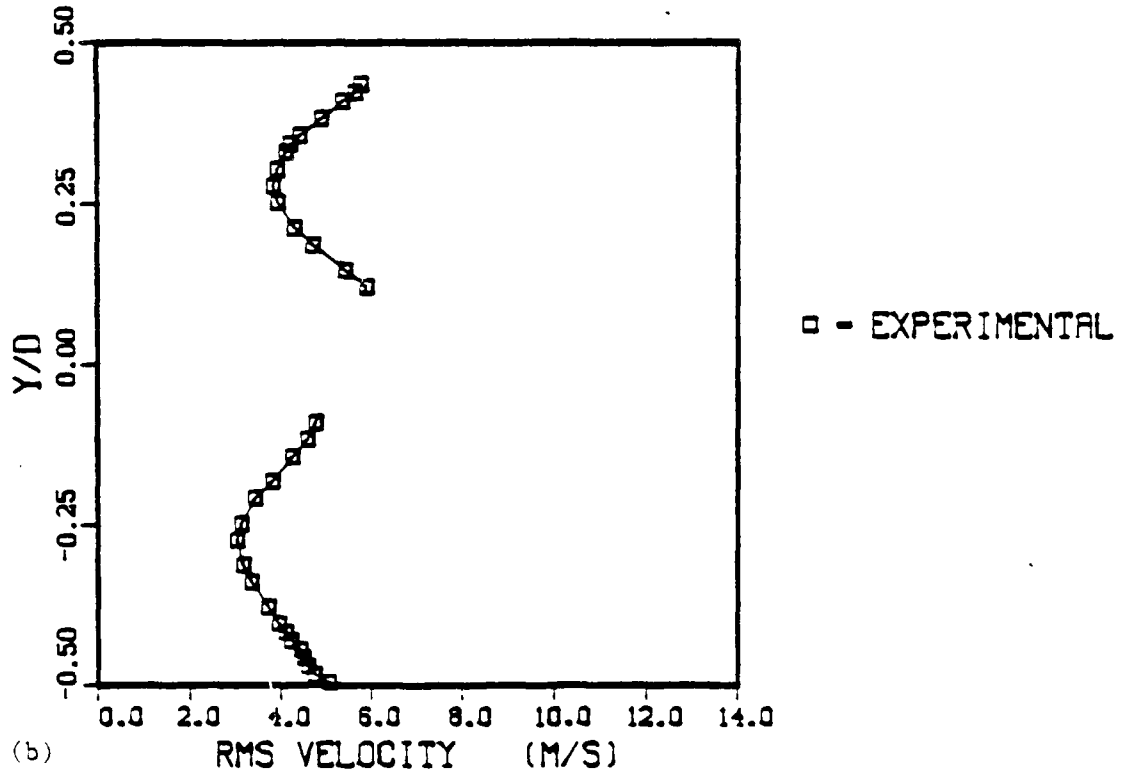

(b)

Figure 4.9 Experimental Z-Averaged (a) Mean and (b) rms Velocity for Case 14 at X/D = -0.66

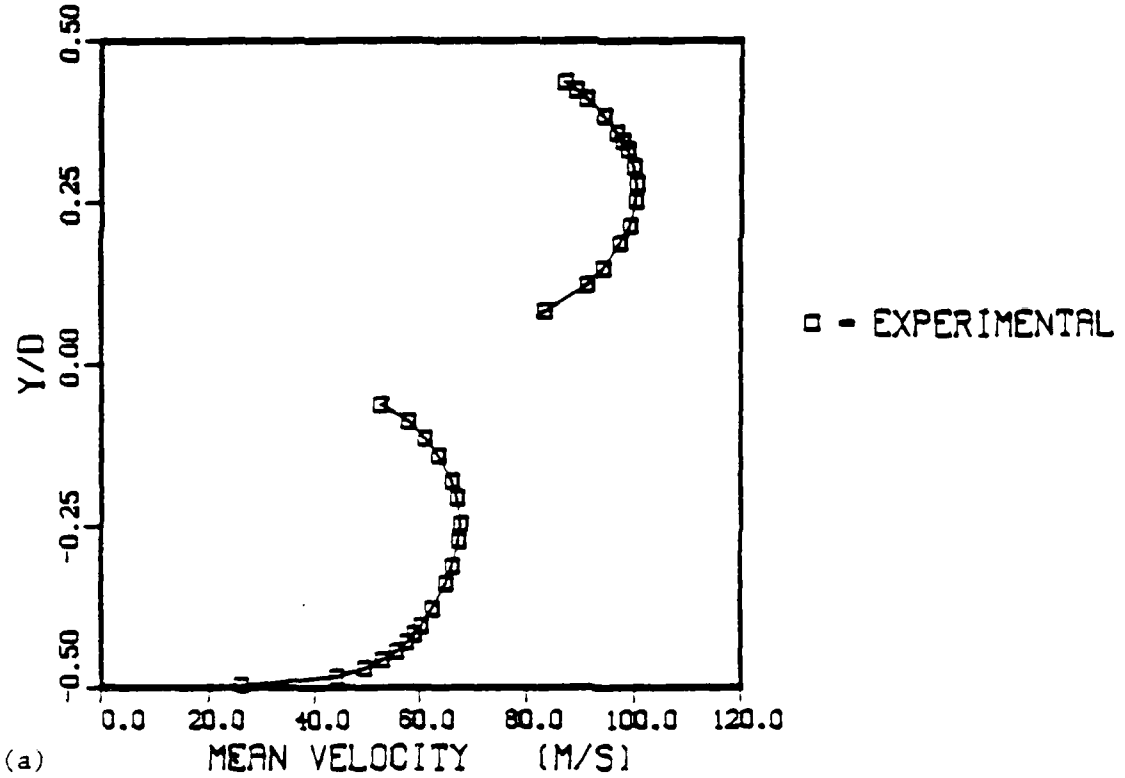

(a)

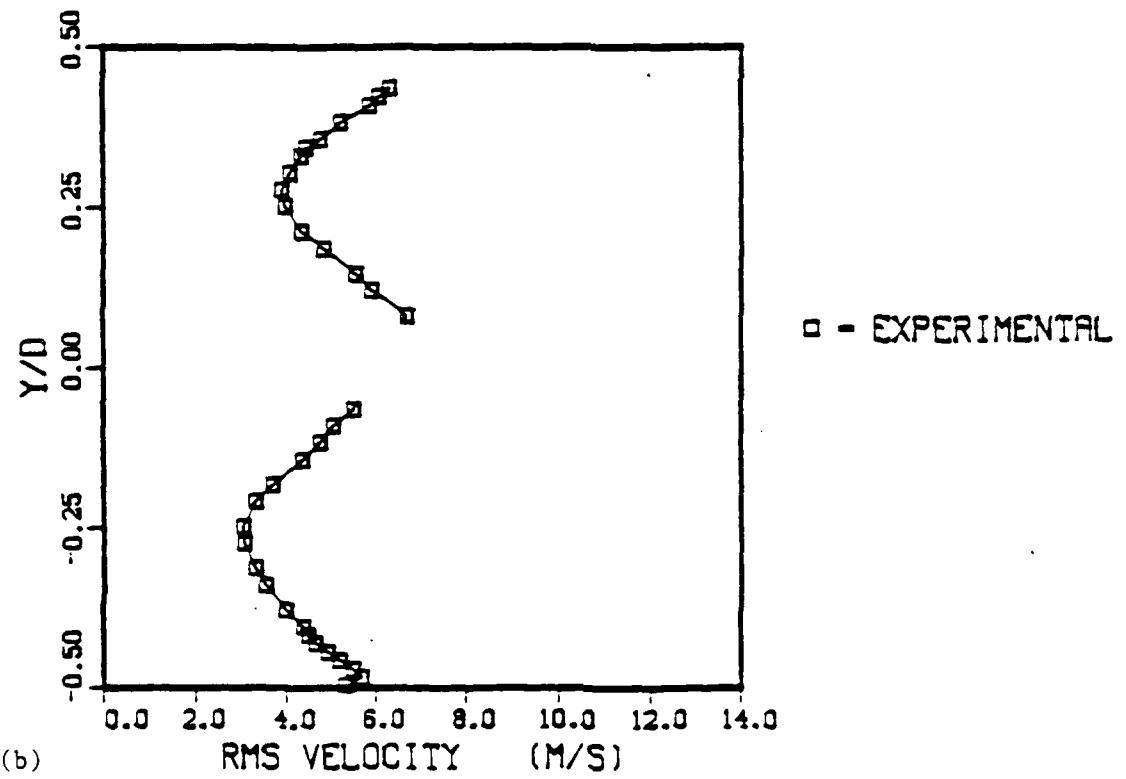

(b)

Figure 4.10 Experimental Z-Averaged (a) Mean and (b) rms Velocity for Case 14 at X/D = -0.33

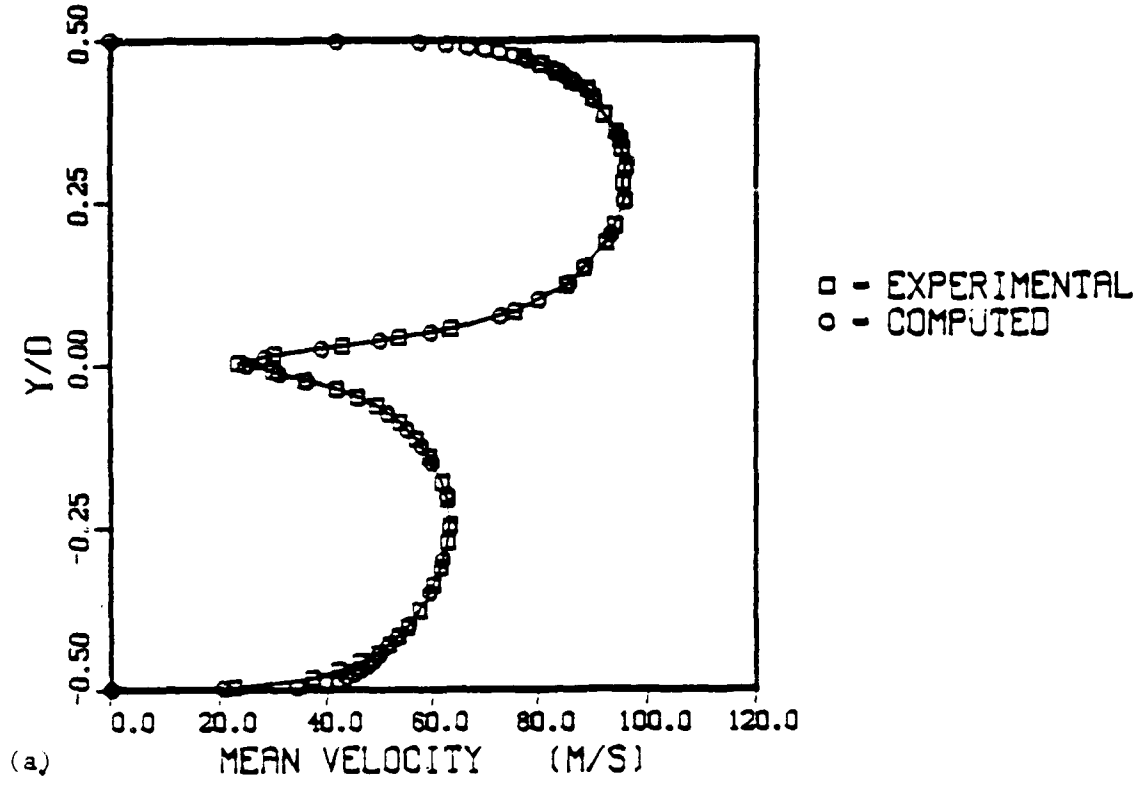

(a)

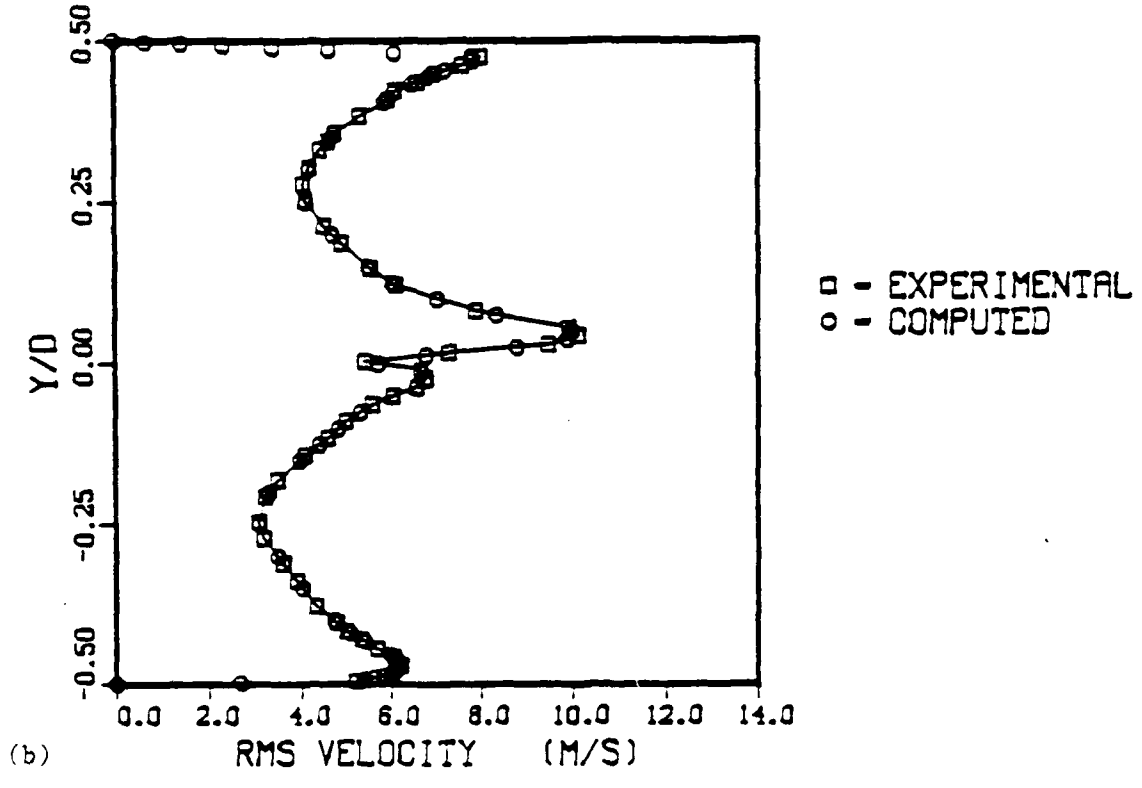

(b)

Figure 4.11 Comparison of Experimental Z-Averaged (a) Mean and (b) rms Velocity with Computed Values for Case 14 at X/D = 0.03

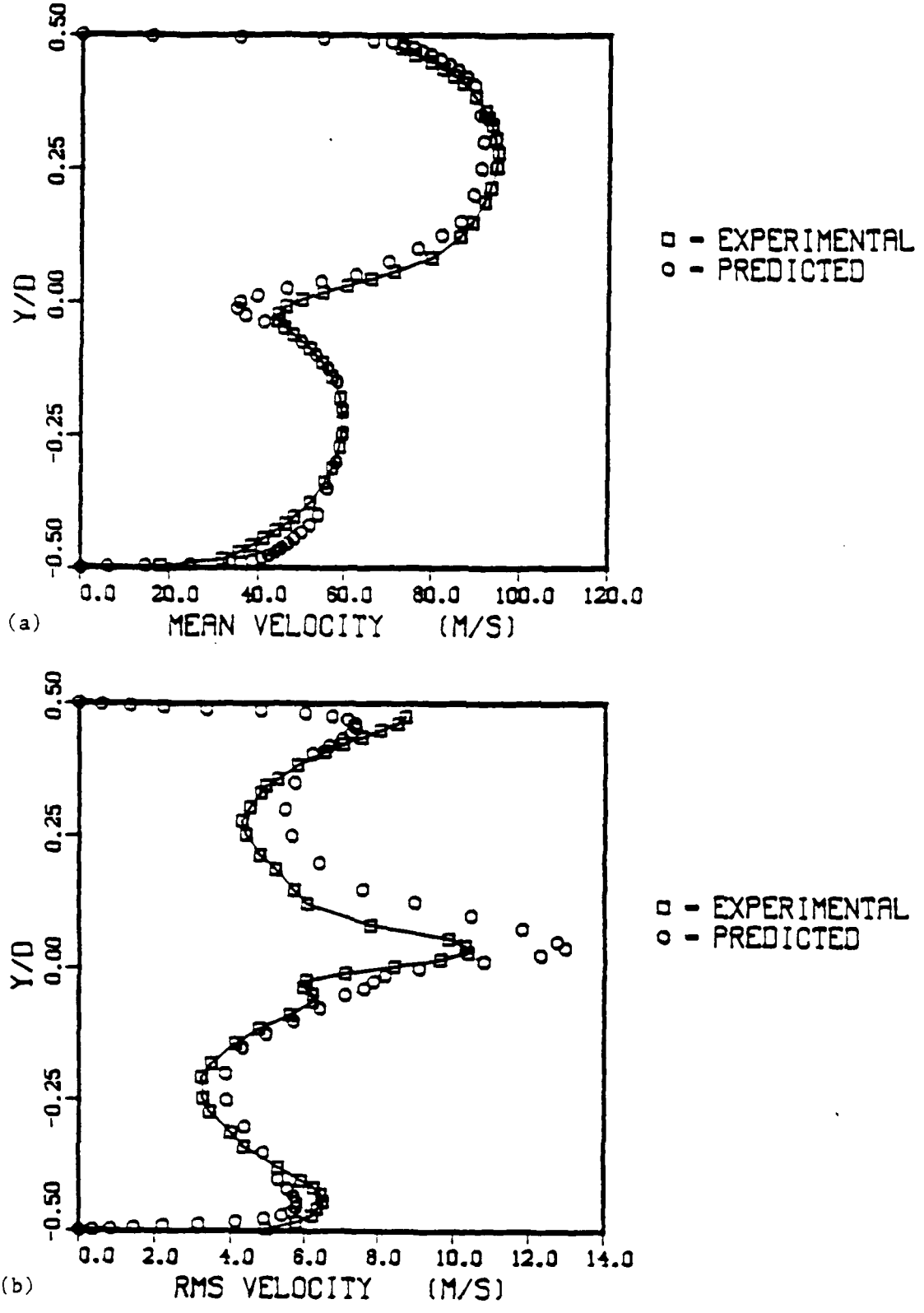

Figure 4.12 Comparison of Experimental Z-Averaged (a) Mean and (b) rms Velocity with Predicted Values for Case 14 at X/D = 0.5

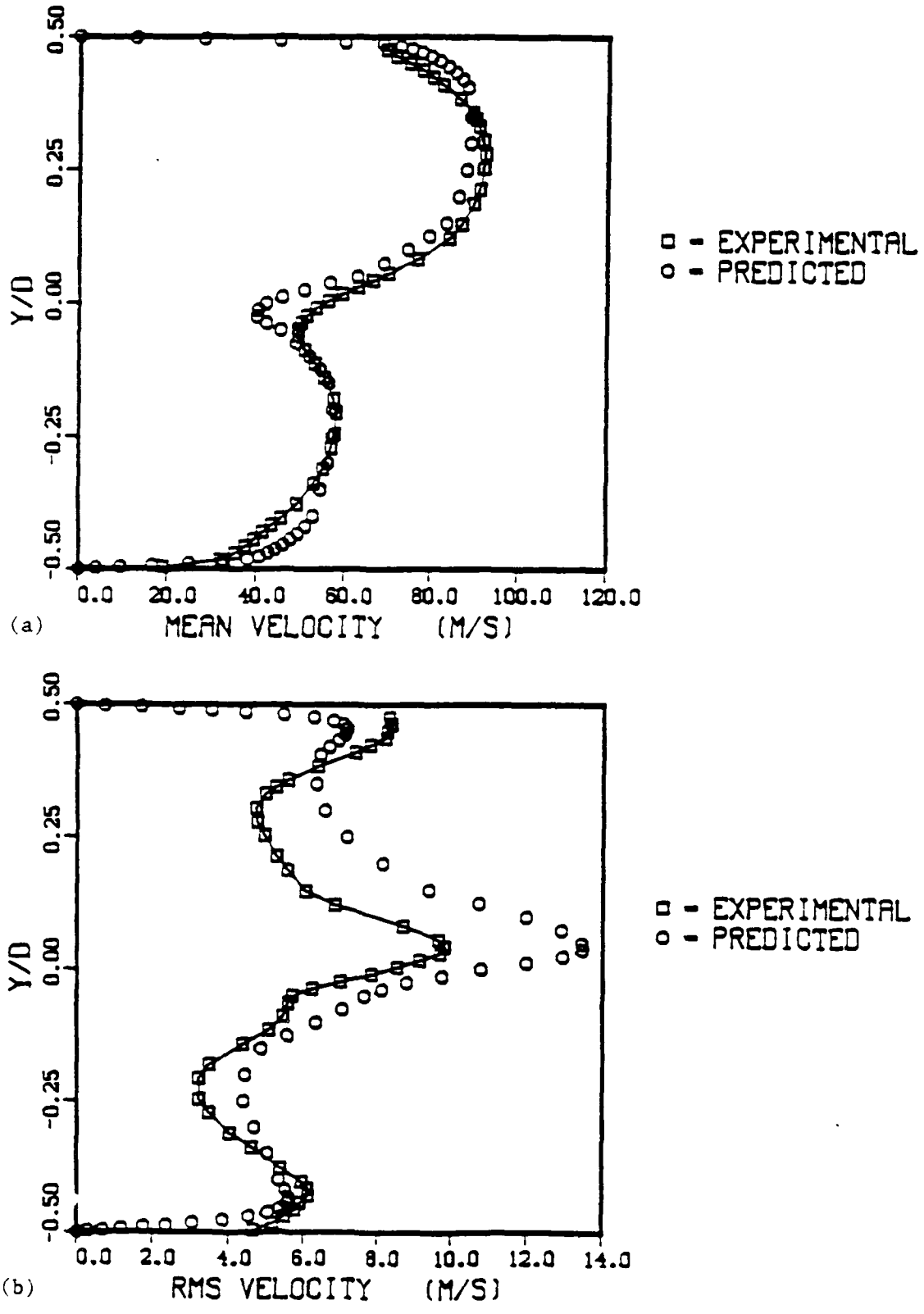

Figure 4.13 Comparison of Experimental Z-Averaged (a) Mean and (b) rms Velocity with Predicted Values for Case 14 at X/D = 1.0

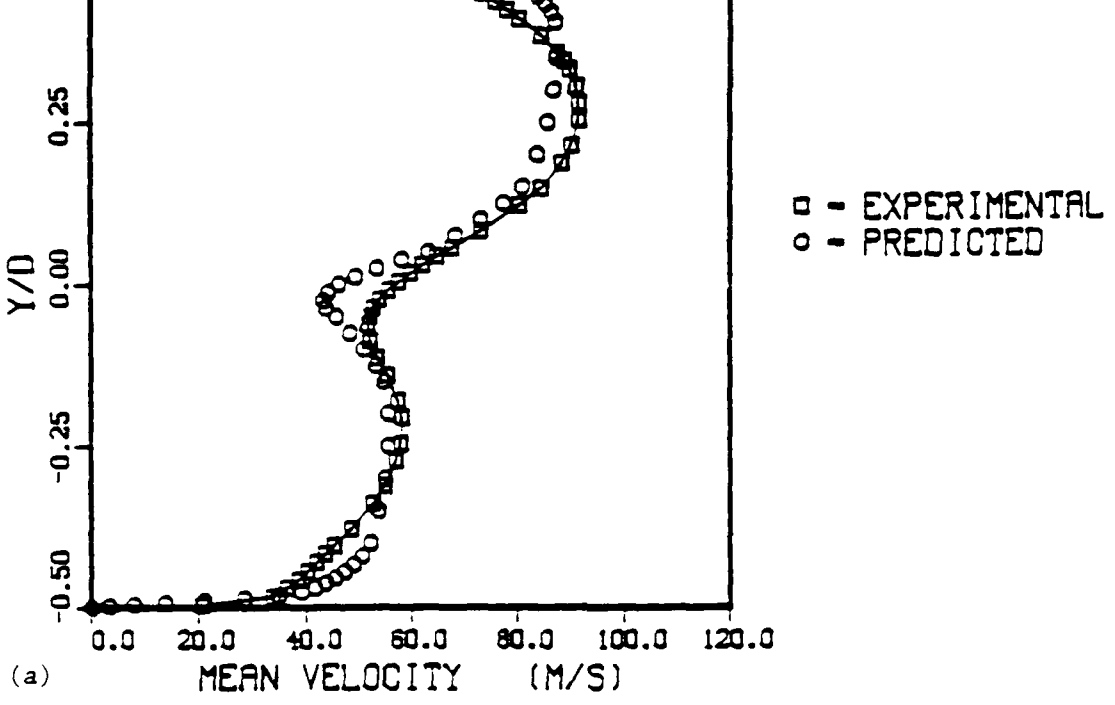

(a)

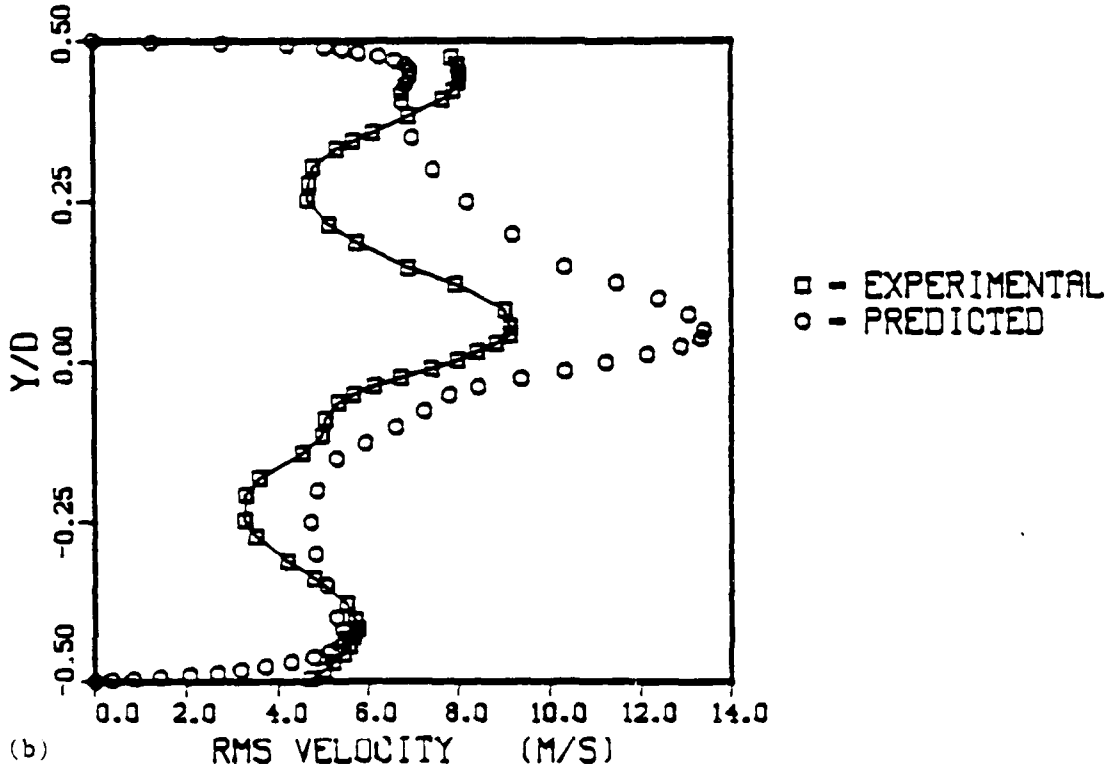

(b)

Figure 4.14 Comparison of Experimental Z-Averaged (a) Mean and (b) rms Velocity with Predicted Values for Case 14 at X/D = 1.5

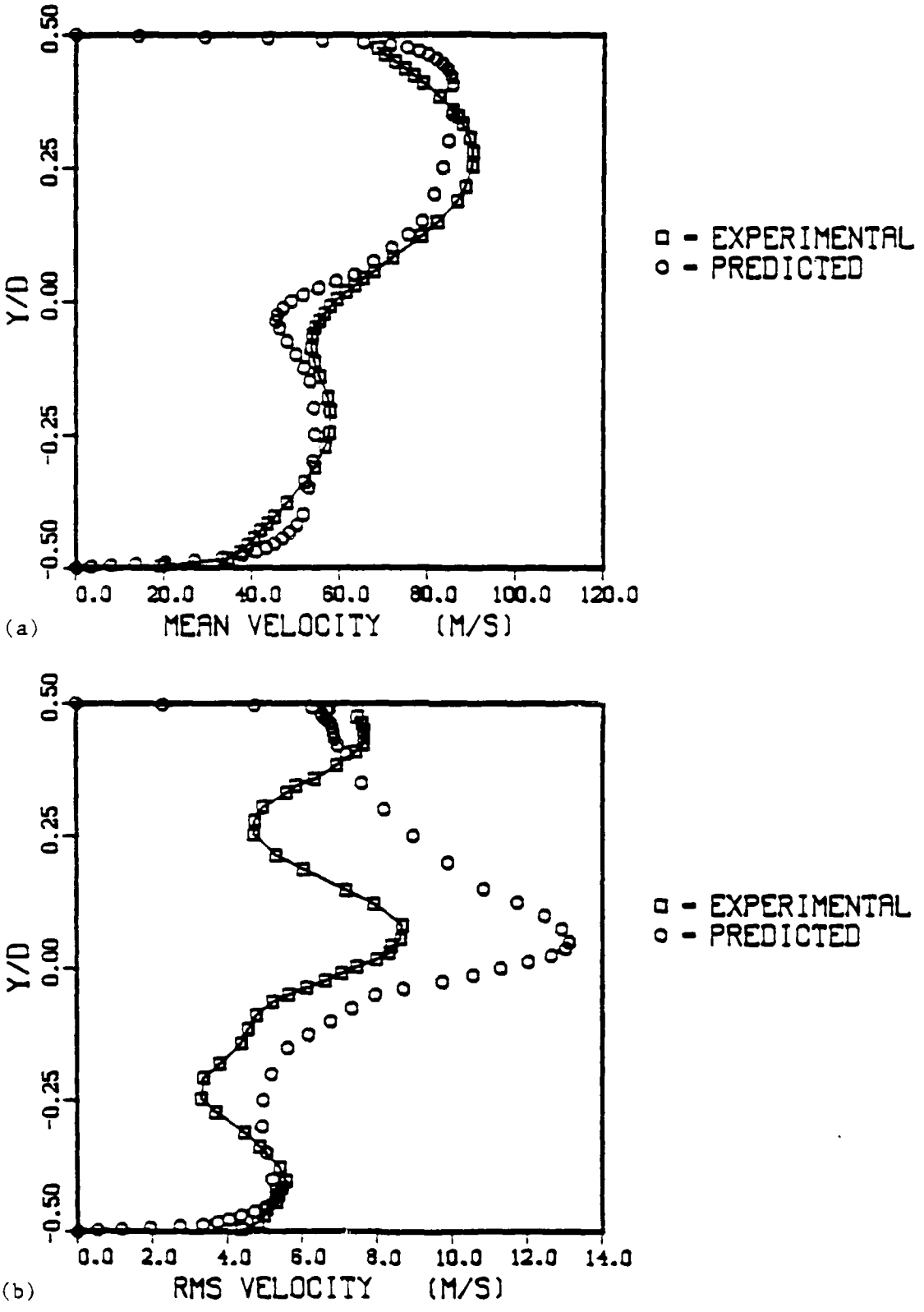

Figure 4.15 Comparison of Experimental Z-Averaged (a) Mean and (b) rms Velocity with Predicted Values for Case 14 at X/D = 2.0

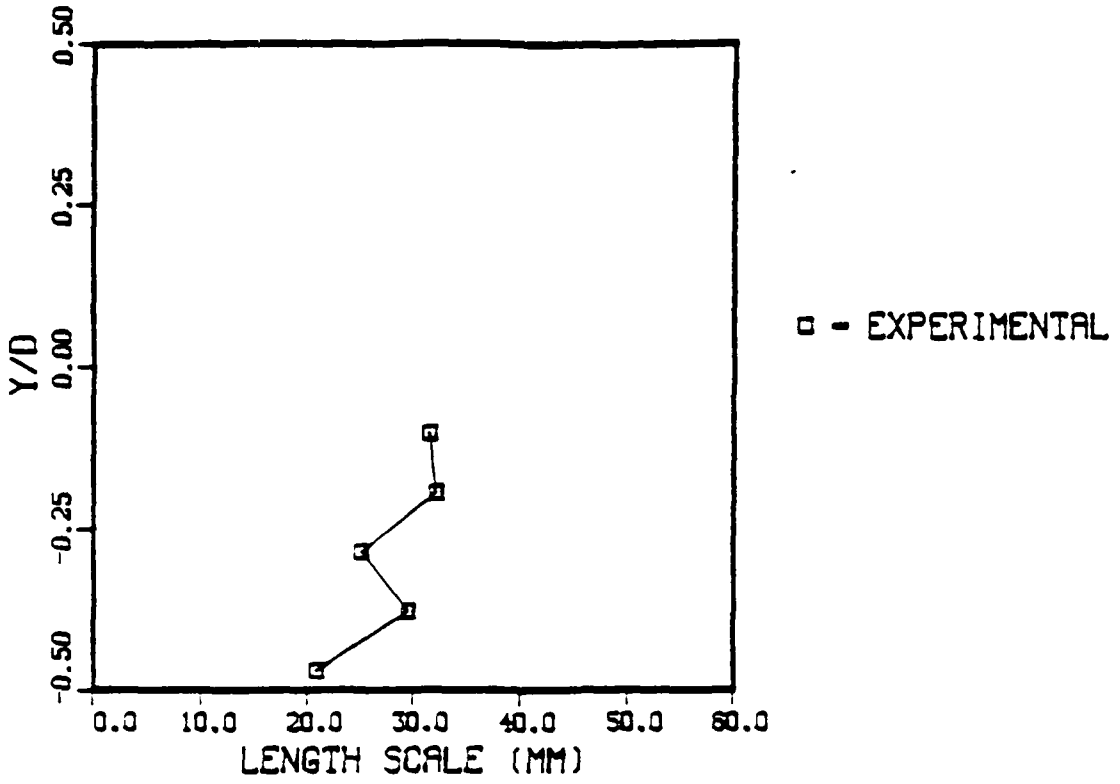

Figure 4.16 Experimental Length Scale for Case 1 at X/D = -0.66

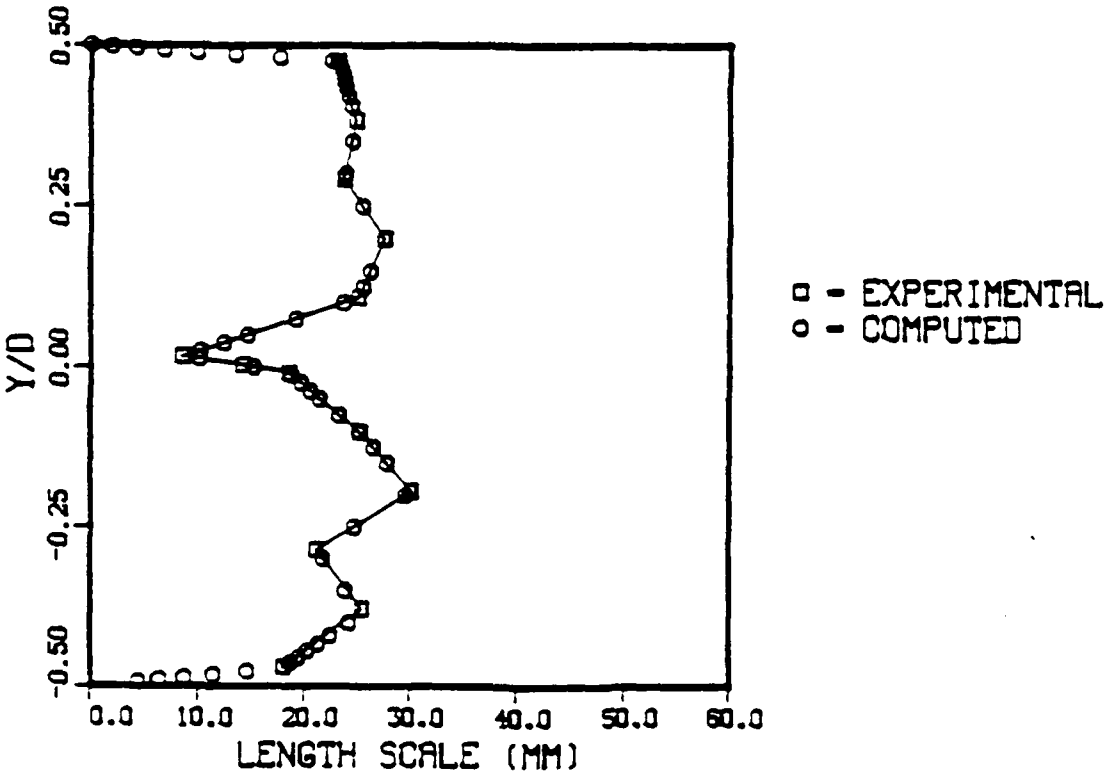

Figure 4.17 Experimental and Computed Length Scale for Case 1 at X/D = 0.03

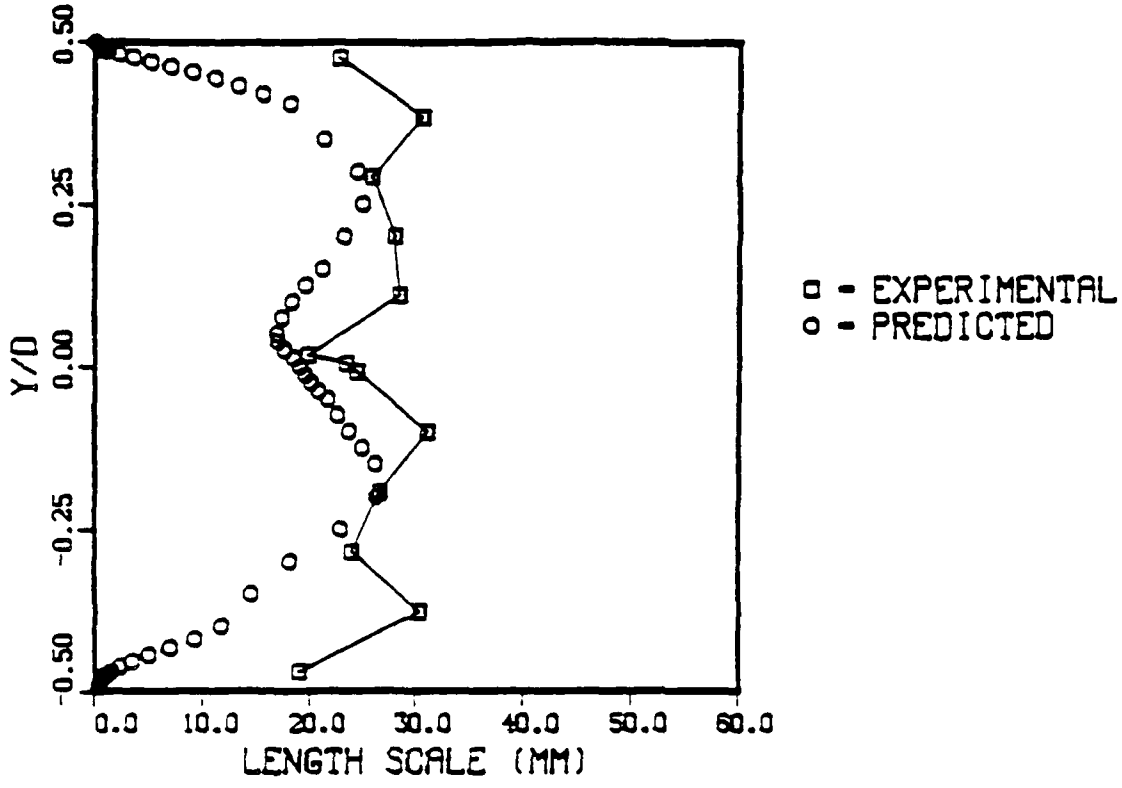

Figure 4.18 Experimental and Predicted Length Scale for Case 1 at X/D = 1.0

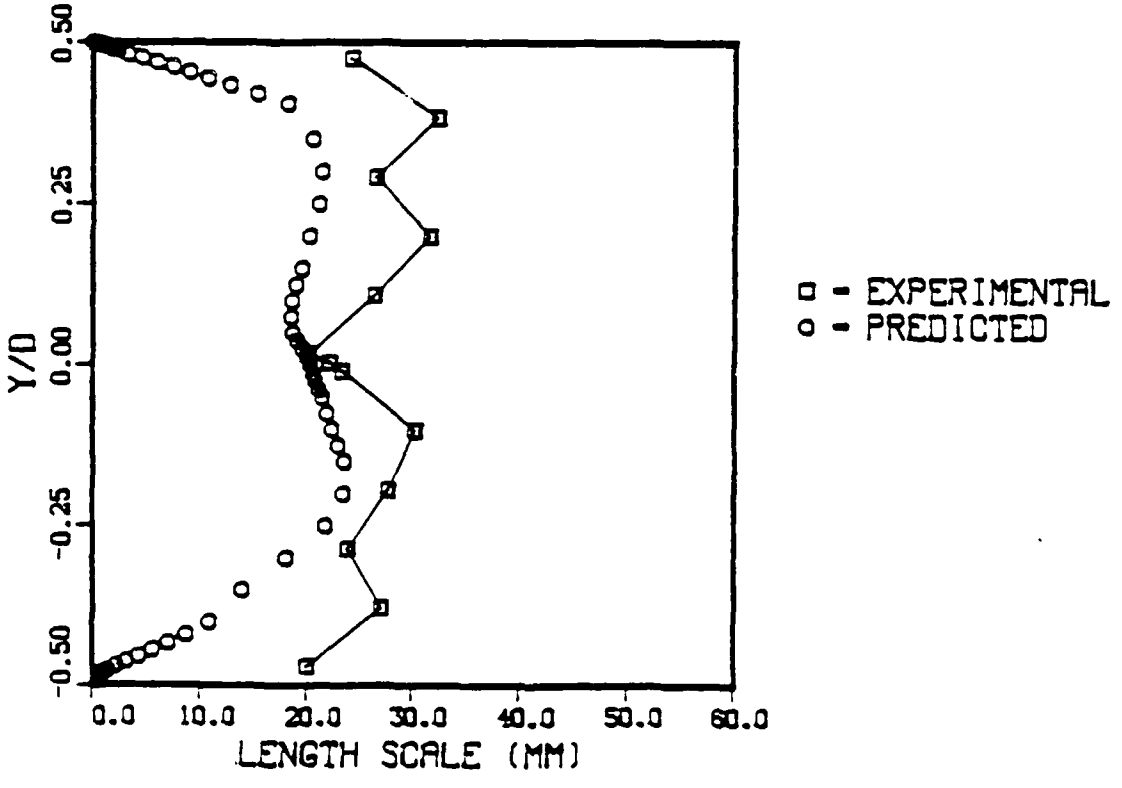

Figure 4.19 Experimental and Predicted Length Scale for Case 1 at X/D = 2.0

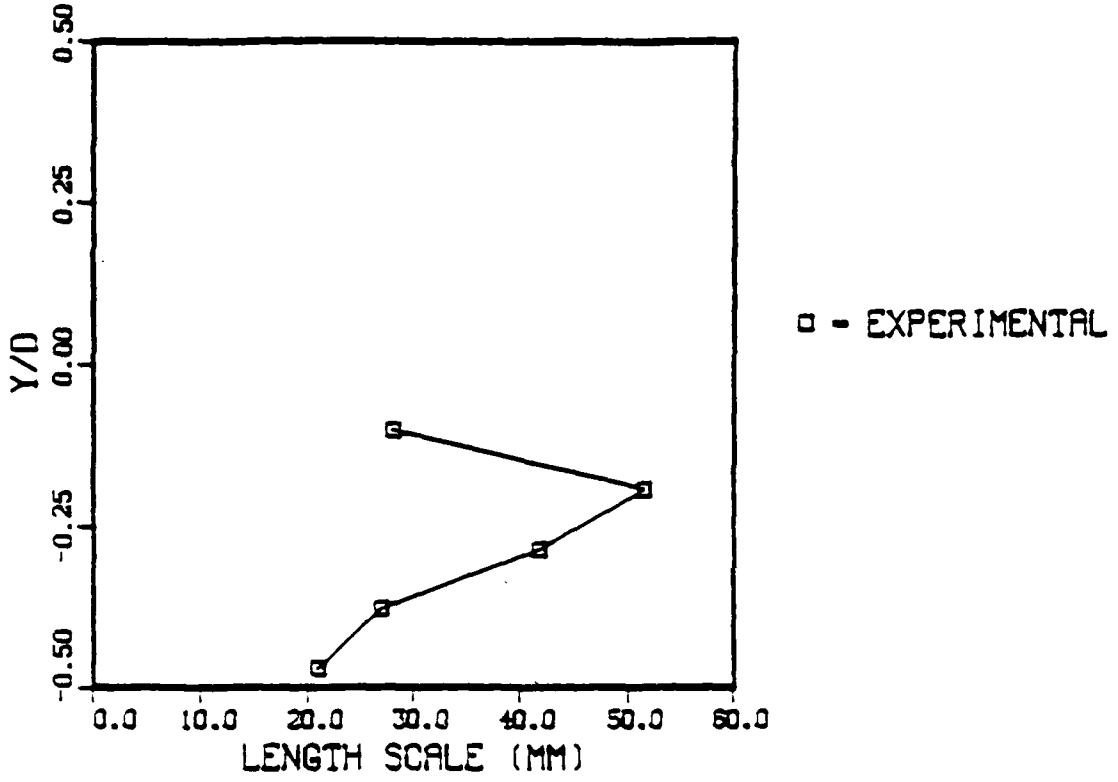

Figure 4.20 Experimental Length Scale for Case 14 at X/D = -0.66

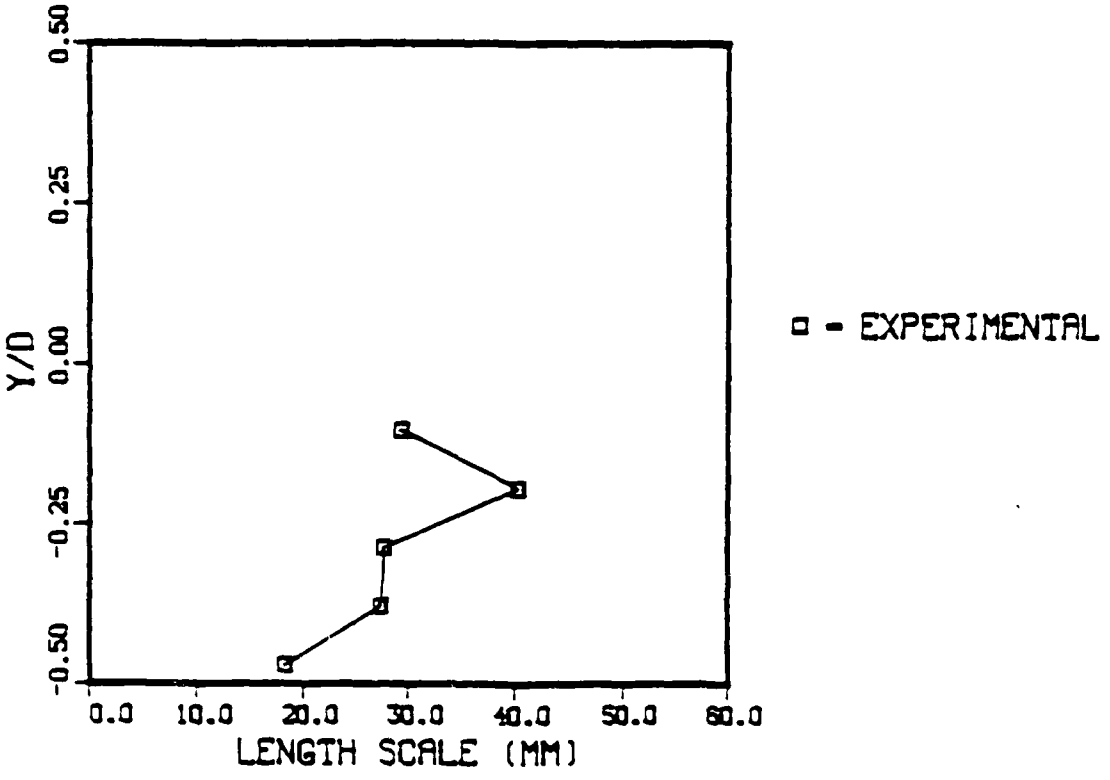

Figure 4.21 Experimental Length Scale for Case 14 at X/D = -0.33

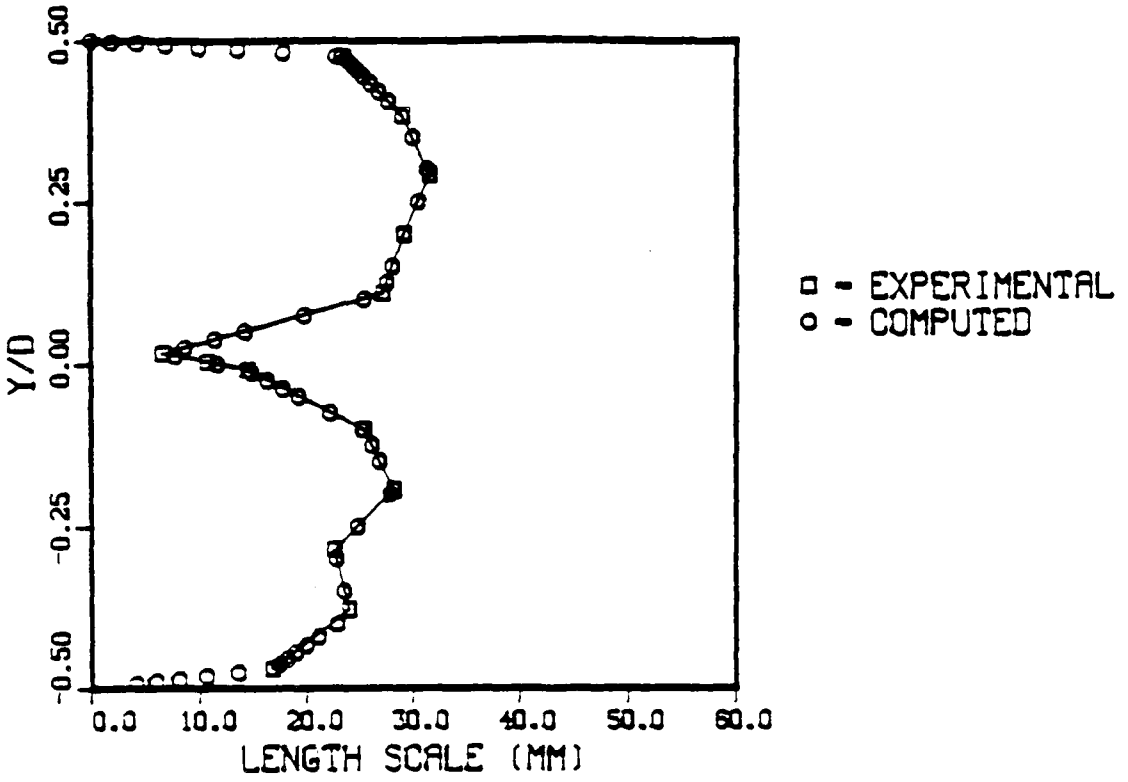

Figure 4.22 Experimental and Computed Length Scale for Case 14 at X/D = 0.03

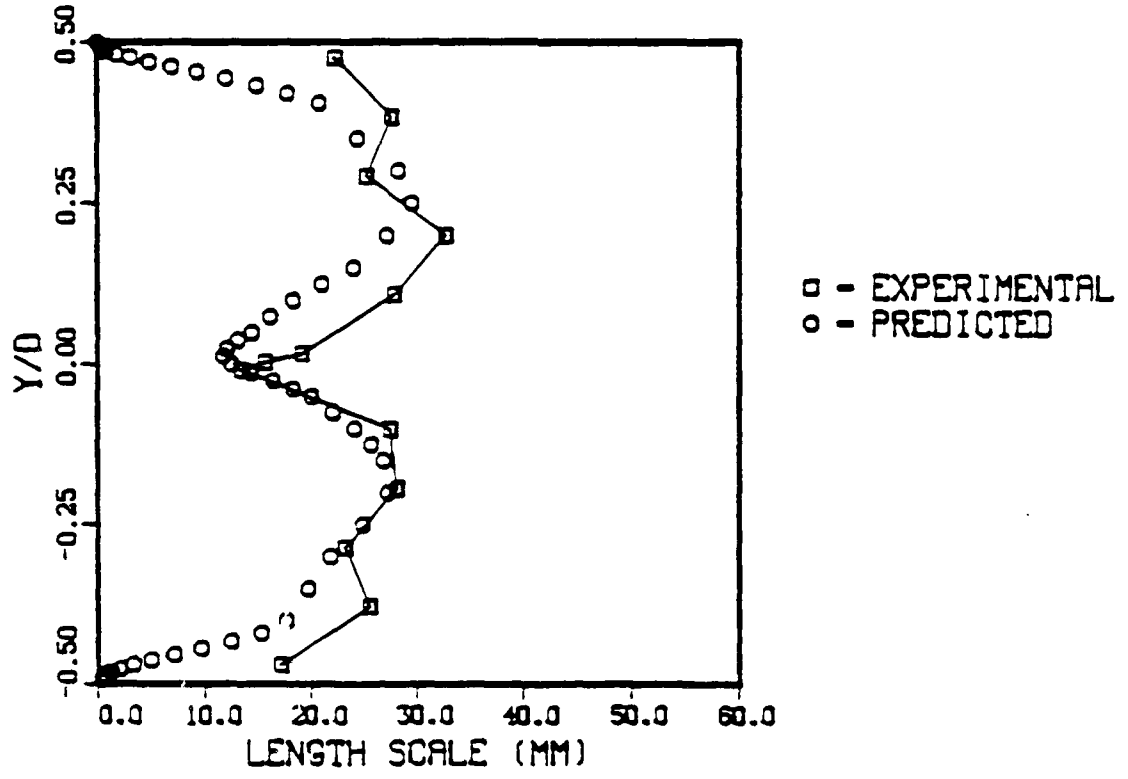

Figure 4.23 Experimental and Predicted Length Scale for Case 14 at X/D = 0.5

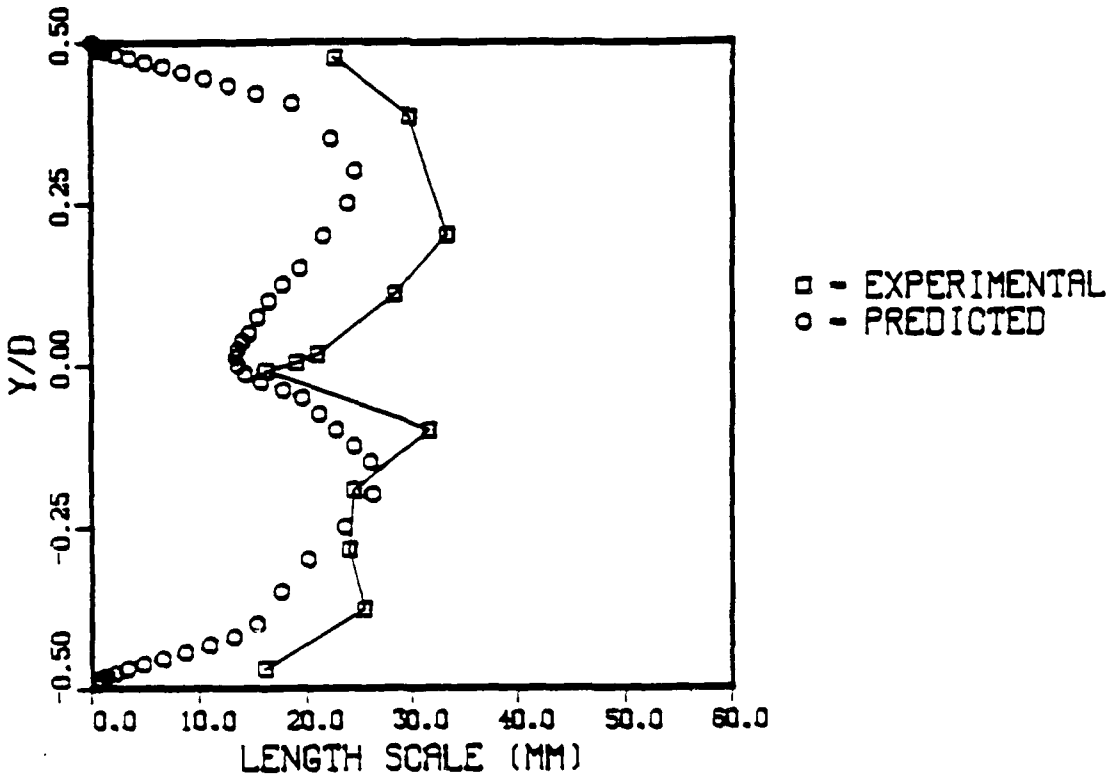

Figure 4.24 Experimental and Predicted Length Scale for Case 14 at X/D = 1.0

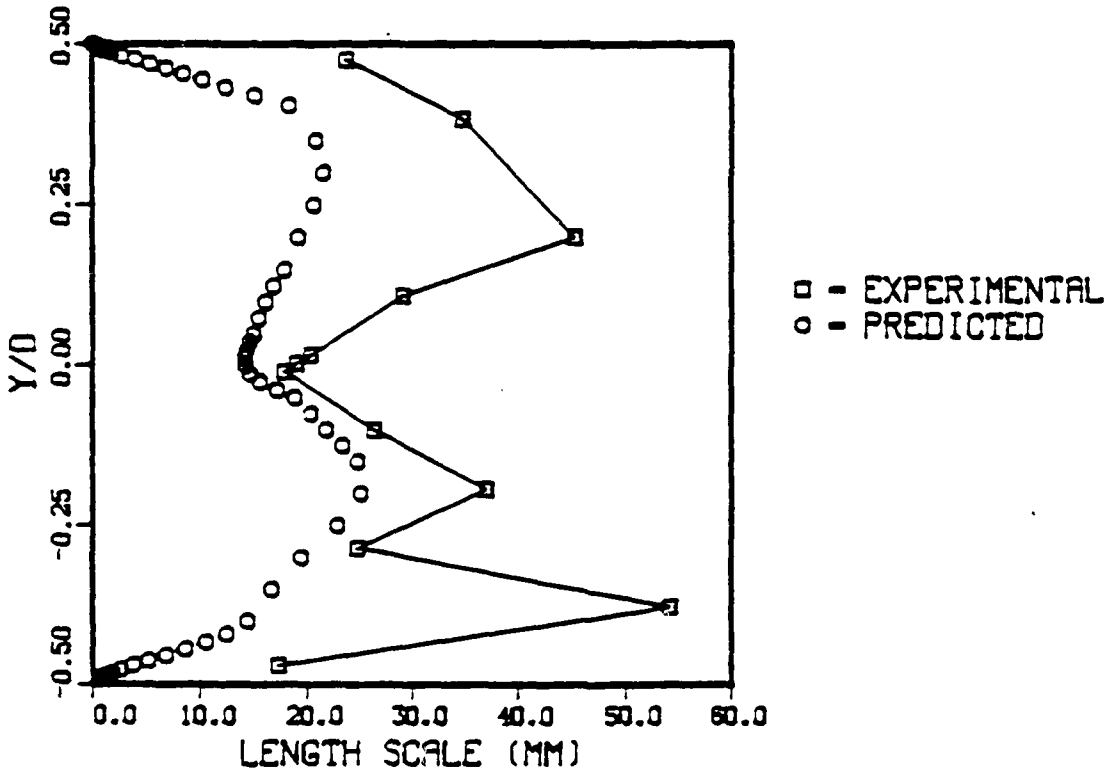

Figure 4.25 Experimental and Predicted Length Scale for Case 14 at X/D = 1.5

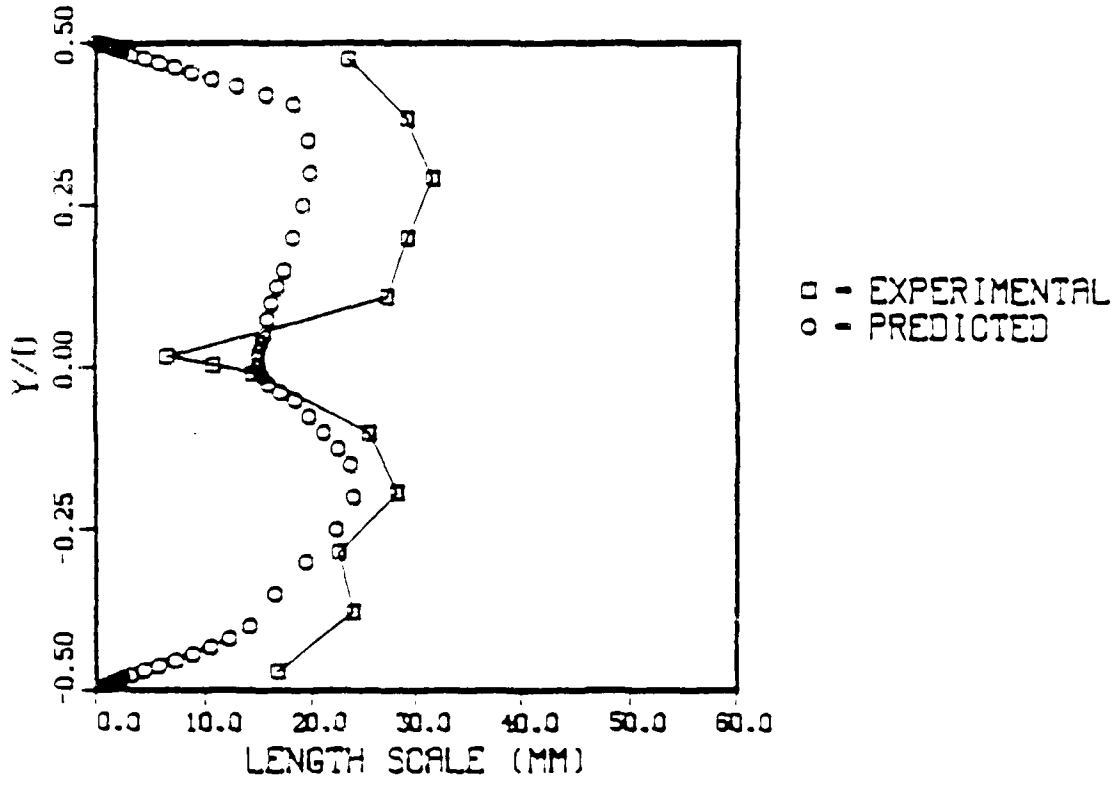

Figure 4.26 Experimental and Predicted Length Scale for Case 14 at X/D = 2.0

predominant direction of transfer is from the high velocity side (fuel side) to the low velocity side (air side), as evidenced by the shift in minimum velocity of the shear layer region toward the lower velocity flow. The peak rms velocity in the shear layer decreases somewhat and spreads slowly in this developing region of the shear layer. The maximum value moves to positive values of Y/D, the region of largest mean velocity gradient.

Length scale measurements reveal good agreement with expected results for both cases 1 and 14 upstream of and at the inlet plane (Figs. 4.16 and 4.17, and 4.20 through 4.22) where measured values in the free stream are roughly one half the difference of the test section width minus the atomizer thickness (33 mm). At the tip of the atomizer, length scales are approximately the thickness of the atomizer (10.3 mm). Downstream length scales (Fig. 4.18 and 4.19, and 4.23 through 4.26) in the free stream remain relatively constant for both cases and at Y/D = 0 increase to 20 mm at X/D = 2.0. Several length scale measurements for case 14 at X/D = -0.66, -0.33, and 1.5 are between 45 mm and 55 mm. The latter values are unrealistic based on test section geometry; however, analysis of the data has not revealed the cause of this discrepancy. The problem is related to the evaluation of the autocorrelation coefficient (Eq. 3.5), but further investigation is necessary to isolate the precise source of deviation from the expected values.

Reproducibility of current test conditions is examined in Fig. 4.27, where experimental average mean and rms velocity profiles at Y/D = 0.03 for cases 1 and 14 are compared. As these cases share the same fuel side mass average air velocity (73.9 m/s), measurements for both cases should be nearly identical for Y/D values greater than zero at the inlet plane. Fig. 4.27 shows that peak mean velocities differ by 2.1% while freestream rms velocities agree within 3%. The comparison of length scales shown in Fig. 4.28 reveals significantly more scatter (as much as 25%) in this measurement. Note full Y-profiles are comparable in this case since scale depends primarily on geometry and should be insensitive to velocity for fully developed turbulent flow.

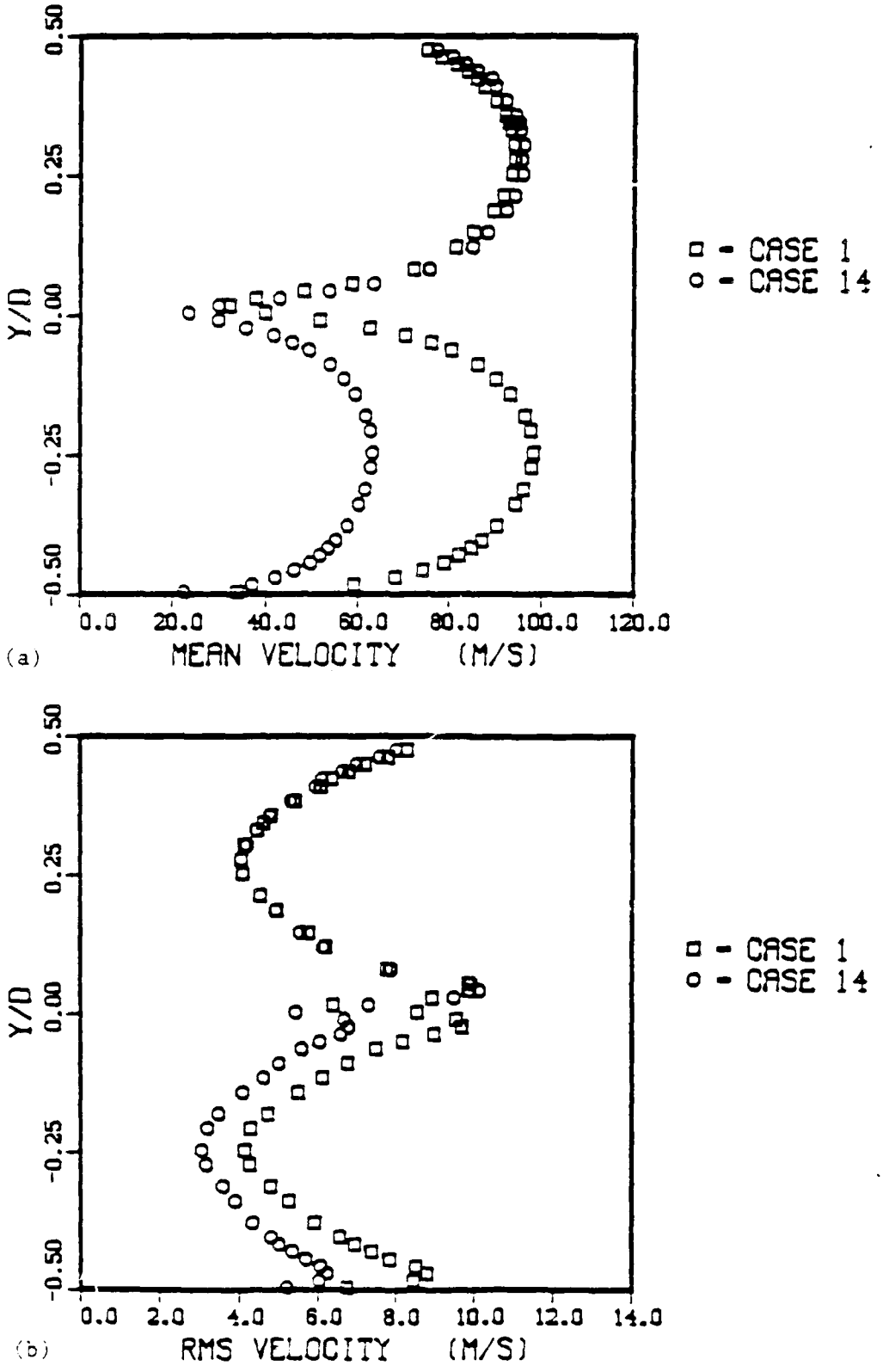

Figure 4.27 Experimental (a) Mean and (b) rms Velocity for Cases 1 and 14 at X/D = 0.03

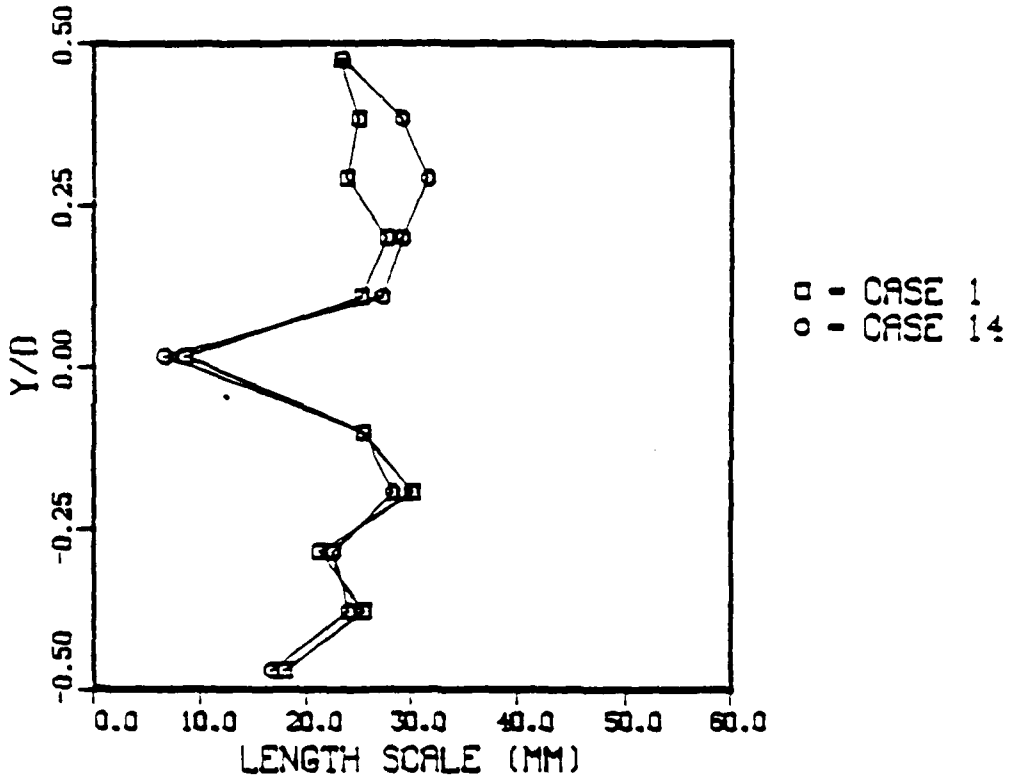

Figure 4.28 Experimental Length Scale for Cases 1 and 14 at X/D = 0.03

4.3.3. Isotropy and Impact of Spray

The computational code assumes isotropic flow throughout the computational regime, and it is therefore necessary to ascertain how isotropic the flow is at the inlet to the test section. Fig. 4.29a shows a centerline (Z/D = 0) rms velocity plot at X/D = 0.03 for cases 1 and 14 of the two-phase flow matrix comparing Y-profiles of u_{rms} with w_{rms}. Fig. 4.29b compares freestream (Y/D = +0.25) u_{rms} and v_{rms} Z-profiles at X/D = 0.03. These two figures reveal that although for each case the profiles are similar, the mean flow in the X-direction dominates the turbulence so that u_{rms} exceeds v_{rms} by approximately a factor of two, as is typically observed in turbulent axisymmetric free jets (see e.g., Faeth, 1987).

Figures 4.29a and 4.29b present another opportunity to establish reproducibility, because cases 1 and 14 share the same fuel side mass average air velocity. From Fig. 4.29a a comparison of u_{rms} and w_{rms} velocity measurements on the fuel side (Y/D > 0) reveals no difference between cases 1 and 14 in the freestream. Likewise, Fig. 4.29b shows similar results for freestream fuel side u_{rms} and v_{rms} profiles from the two cases.

Another topic pertinent to the later computations is the impact of spray on freestream flow. Fig. 4.30a shows a centerline (Z/D = 0) mean velocity profile for case 14 at the inlet plane without spray and a similar profile with spray at the same location. The Y-extent of the latter data was limited by droplet impingement on the hot film probe. A graph of similar case 1 data is given in Fig. 4.30b. The liquid mass flow rate (W_ℓ) for both cases is 16.6 g/s. Mean velocity with spray in the test section increases over that without the spray as the edge of the spray is approached due to the added momentum. These results suggest that decoupling the gas-phase solution from the liquid-phase flow, as is done in Anderson et al. (1982), is a poor assumption, and that measurements should be obtained in the two-phase region of the flow, most likely requiring optical diagnostics.

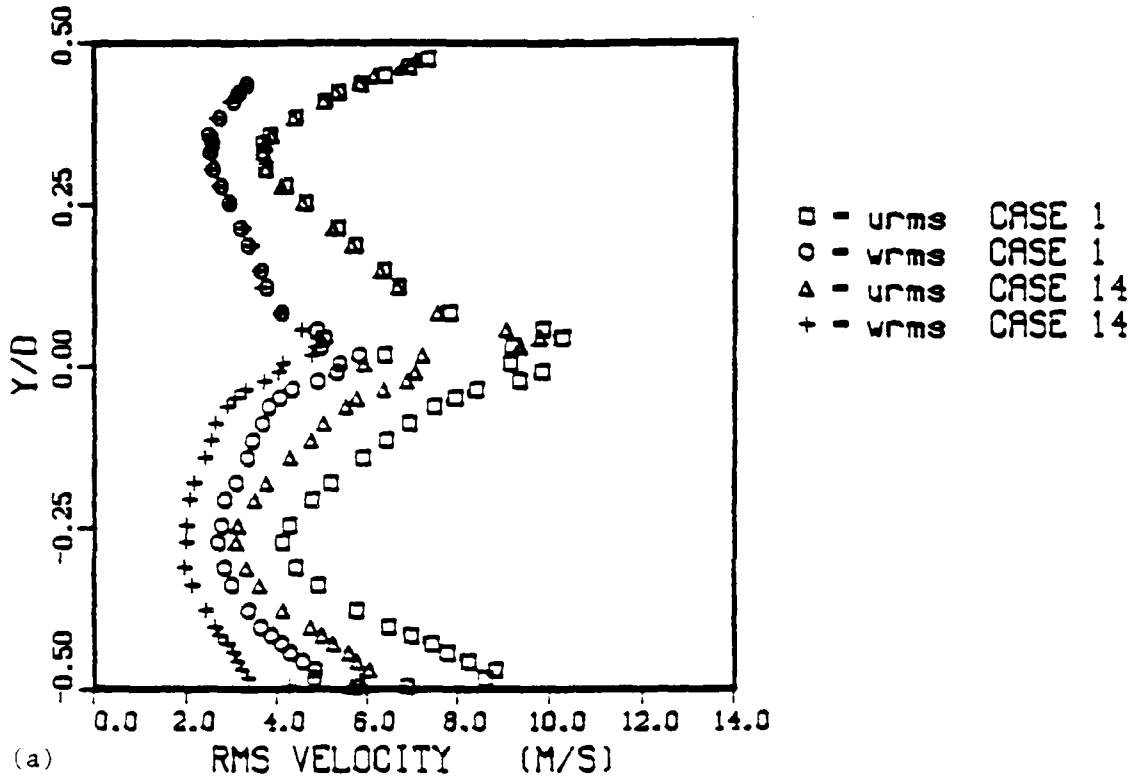

(a)

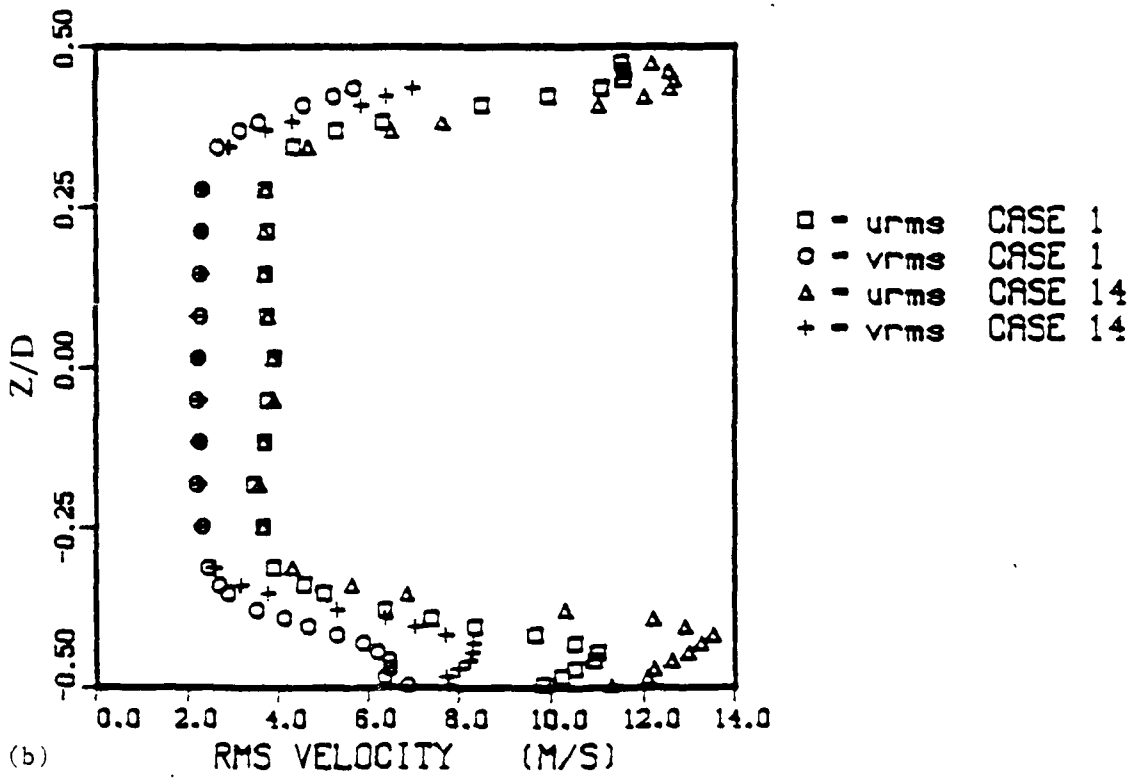

(b)

Figure 4.29 Comparison of Experimental (a) u_{rms} and w_{rms} and (b) u_{rms} and v_{rms} Velocity for Cases 1 and 14 at X/D = 0.03

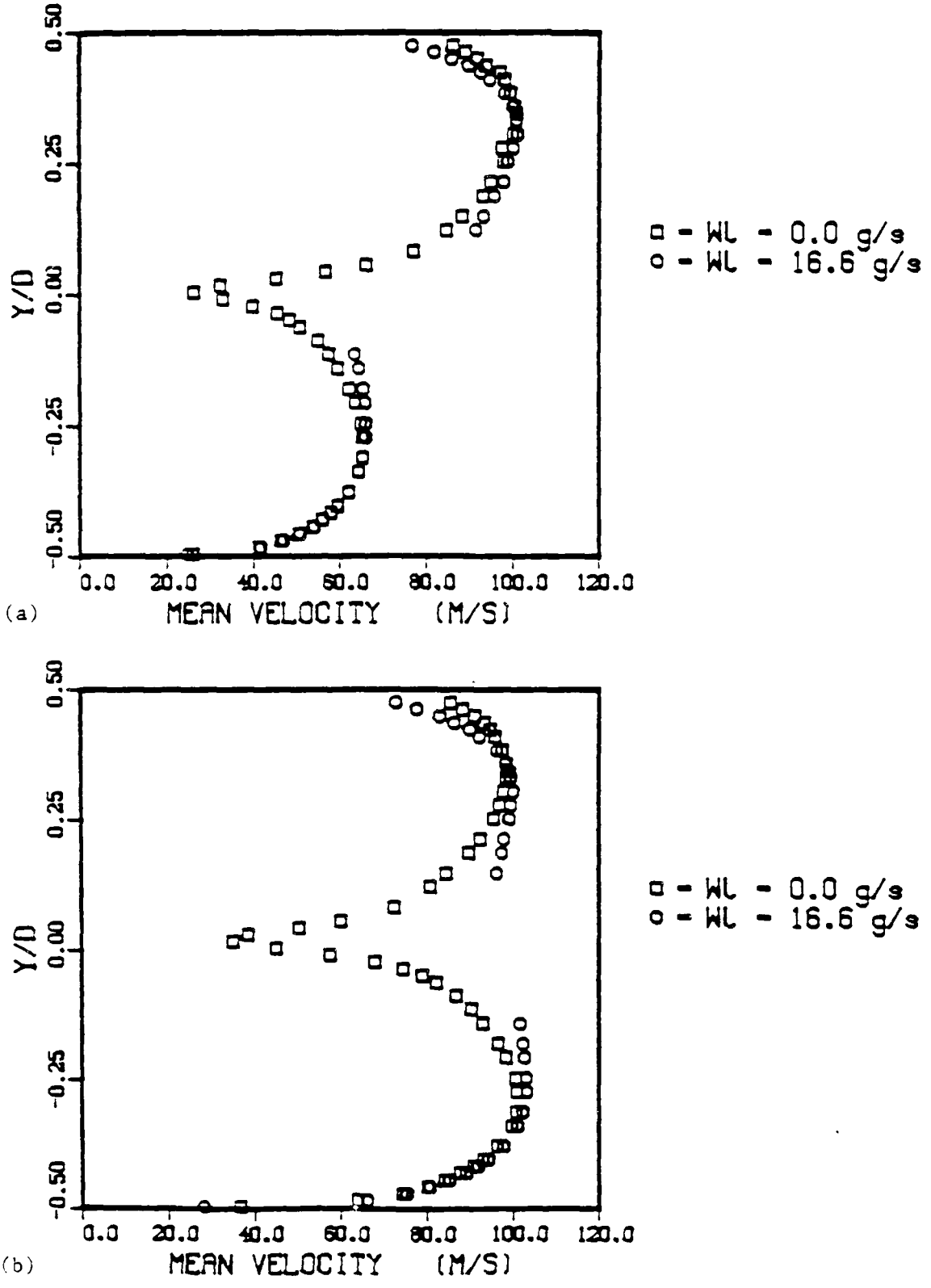

Figure 4.30 Comparison of Experimental Mean Velocity with and without spray for (a) Case 14 and (b) Case 1 at X/D = 0.03

4.3.4. Characteristic Mixing Times

A major thrust of this research was to examine the relationship between various local mixing times, defined in Eq. 2.2:

$$\tau_{s\ell,local} = \ell/u_{rms} \tag{4.1}$$

Here ℓ is turbulent length scale and u_{rms} is the fluctuating velocity component in the direction of flow.

Figs. 4.31a and b show local $\tau_{s\ell}$ normalized with the value at the origin of the shear layer, $\tau_{s\ell,00}$, versus Y/D at those axial postions where length scales were measured. Case 1 in Fig. 4.31a reveals that this parameter is essentially similar in the freestream ($Y/D \geq \pm 0.1$), while shear layer values increase with downstream distance. Case 14 (Fig. 4.31b) exhibits the same trends in the wake region, but in the freestream the scatter is larger than that from Case 1 due to the anomalously large length scales at X/D = 1.50 discussed previously. Ignoring these points on the right hand side of part b of the figure, the remaining scatter shown in Fig. 4.31 appears to result equally from variations both in length scale and rms velocity measurements reported previously.

Outside of the wake or shear layer, similarity of $\tau_{s\ell,xy}$ profiles is expected, because except for boundary layer growth at the Y-walls at Y/D = ±0.5, the length scale, rms velocity, and thus local mixing time should not change with X/D. The latter are larger at Y/D > -0.1 in case 14 because the non-zero value of λ augments the local mixing time through lower mean (and rms) velocities, and thus larger $\tau_{s\ell,xy}$'s. However, on or near the tunnel centerline, i.e., within the wake or shear layer, Fig. 4.32 shows that $\tau_{s\ell,x0}/\tau_{s\ell,00}$ grows linearly in each case.

For case 1, from X/D = 0.03 to 1.00 length scale increases and rms velocity decreases (see also Brown and Roshko, 1974). Downstream the increase in mixing time is primarily due to a decrease in fluctuating velocity. For case 14, eddy size behaves in the same manner as case 1; however, the fluctuating component increases from X/D = 0.03 to 1.00, and then decreases.

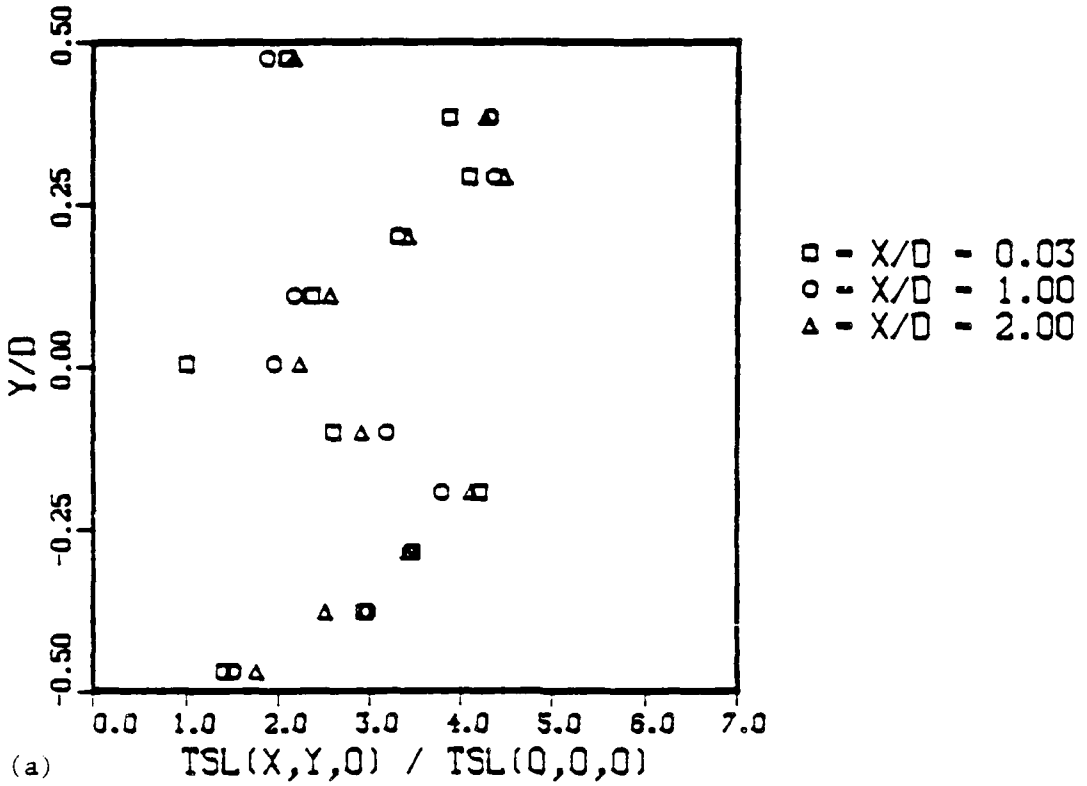

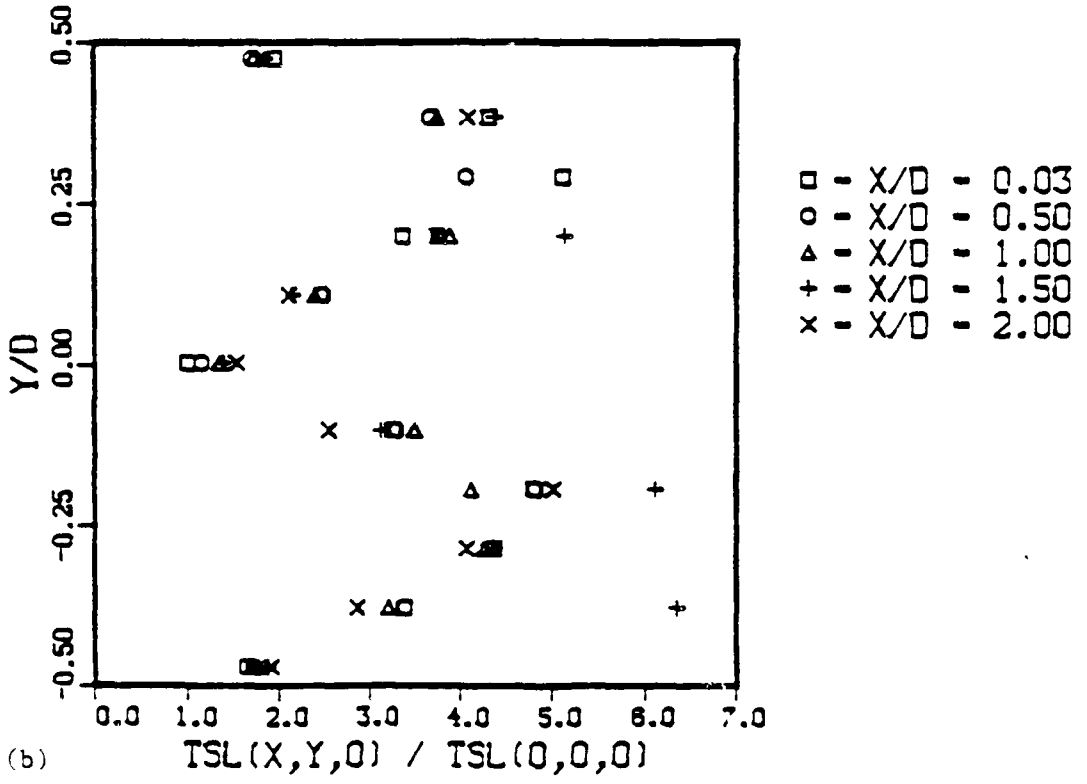

Figure 4.31 Normalized $r_{sl,xy}$ for (a) Case 1 and (b) Case 14 at Various Locations

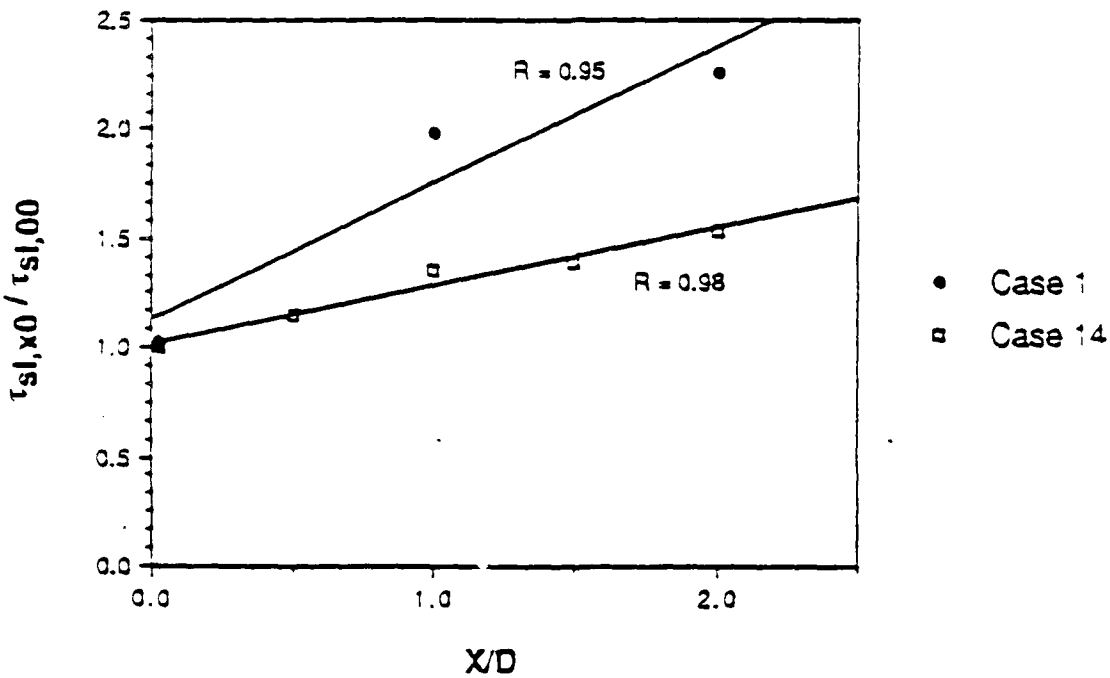

Figure 4.32 Normalized $\tau_{sl,x0}$ versus Axial Position for Cases 1 and 14

Because neither length scale nor rms velocity completely characterizes the mixing, the choice of a combined mixing parameter such as ℓ/u_{rms} may be more appropriate. In addition, Fig. 4.32 shows that downstream wake or shear layer mixing times are proportional to $\tau_{s\ell,00}$, which supports the hypothesis of Tuttle et al. (1977) that the appropriate time scale is proportional to ℓ/u_{rms}. However, the question still to be addressed is whether or not this initial mixing time can be related to the global time defined in the characteristic time model.

Equation 2.6 defines the global time for a gas turbine combustor in terms of reference velocity and a macroscale of turbulence expressed as a function of primary or secondary air addition hole position and combustor diameter at that location. For the origin of the shear layer in the test tunnel, the appropriate macroscale is the atomizer thickness t, and reference velocity is taken as the average of the fuel and air side velocities:

$$\tau_{s\ell,global} = 2t / (U_{AFS} + U_{AAS}) \qquad 4.2$$

Eliminating U_{AFS} via the definition of λ, Eq. 3.1:

$$\tau_{s\ell,global} = t(1 - \lambda) / U_{AAS} \qquad 4.3$$

where a single velocity and the value of λ have been used to characterize the flow for the tunnel geometry. Figure 4.33 presents $\tau_{s\ell,00}$ versus $\tau_{s\ell,global}$ for the eight cases of the two-phase flow matrix. Note the linearity of the data for constant values of λ. Also apparent is the decrease in $\tau_{s\ell,00}$ at constant $\tau_{s\ell,global}$ as shear layer strength increases, as expected.

Figure 4.34 recasts the data with the local mixing times normalized as suggested in Eq. 4.3, that is, divided by $(1 - \lambda)$. This re-expresses the global mixing time in a form exactly equivalent to its definition for a combustor, and thus the x-axis in Fig. 4.34 is relabeled $\tau_{s\ell,co}$, where :

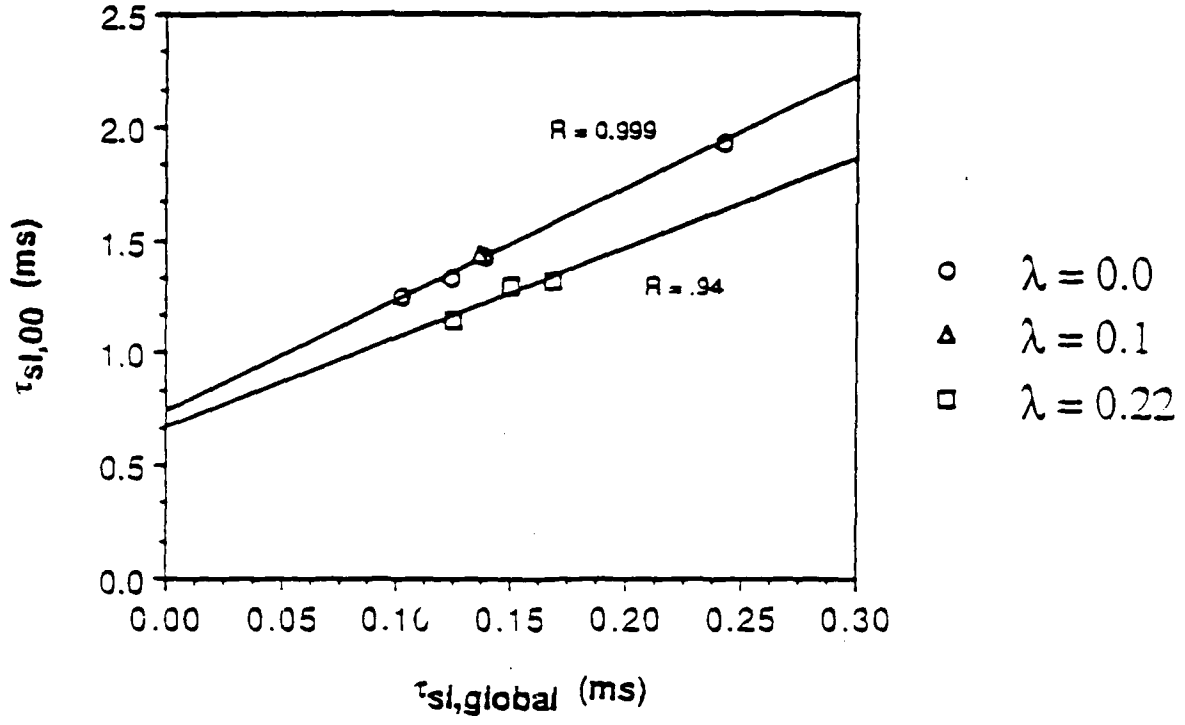

Figure 4.33 Comparison of $\tau_{s\ell,oo}$ and $\tau_{s\ell,global}$ for the Two-Phase Flow Matrix

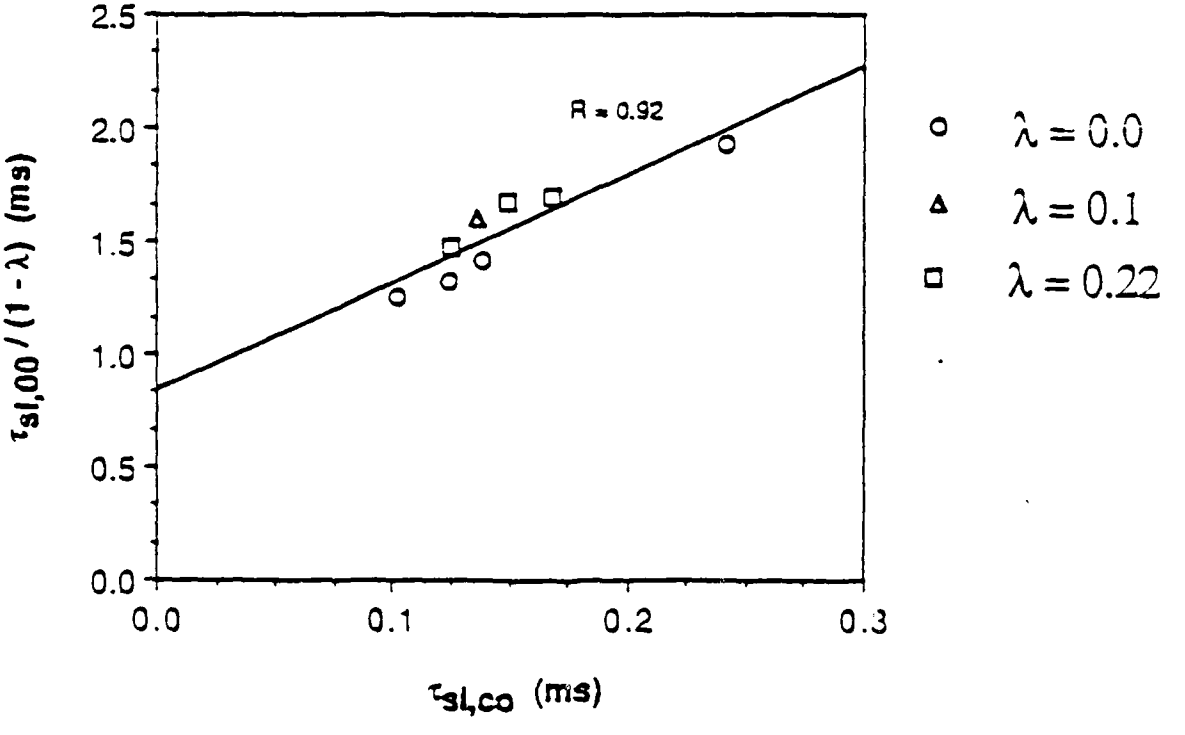

Figure 4.34 Comparison of $\tau_{s\ell,oo}$ Normalized by λ and $\tau_{s\ell,co}$ for the Two-Phase Flow Matrix

$$\tau_{s\ell,co} = t/U_{AAS} = \tau_{s\ell,global}/(1-\lambda) \sim \tau_{s\ell,00}/(1-\lambda) \qquad 4.4$$

The significance of this figure is that local mixing times at the origin of the shear layer are in fact proportional to the initial shear layer mixing time, as formulated for a gas turbine combustor, for all eight cases tested in the present experimental matrix. As indicated by the least squares fit given in Fig. 4.34, the relationship is reasonably accurate considering the small number of data available.

Coupled with Fig. 4.32 and 4.33, the additional conclusion is that $\tau_{s\ell,co}$ does in fact completely characterize the flow fields studied to date, at least for $X/D \leq 2.0$. Thus the original hypothesis of Tuttle et al. (1977) is verified for the region of shear layer growth, which in turn explains the laboratory rig and combustor correlations with $\tau_{s\ell,co}$ for CO (Tuttle et al., 1977; Mellor and Washam, 1979), lean blowoff (Plee and Mellor, 1979; Derr and Mellor, 1987), and combustion efficiency (Leonard and Mellor, 1983).

4.3.5 Discussion of Length Scale

However, no length scale variations have been accomplished to date in the experimental program. Figure 4.16 through 4.26 show that in the freestream they equal approximately the half-height of the tunnel and at the origin of the shear layer the splitter plate thickness. Additional experiments are required to explore the effect of variations in length scale on the results presented in Section 4.3.4. Grids and screens upstream of the atomizer tip will vary freestream scale, but the variation of atomizer thickness is not practical. In the limit of zero thickness, freestream scale is expected to dominate the shear layer: the relationships between these two relevant length scales should be explored in further work.

4.3.6 Relation of $\tau_{s\ell,global}$ to Combustors

Figure 4.35 represents a primary zone half-section of a typical combustor through the plane of a primary jet; for simplicity, no swirler is indicated. A velocity profile showing recirculation

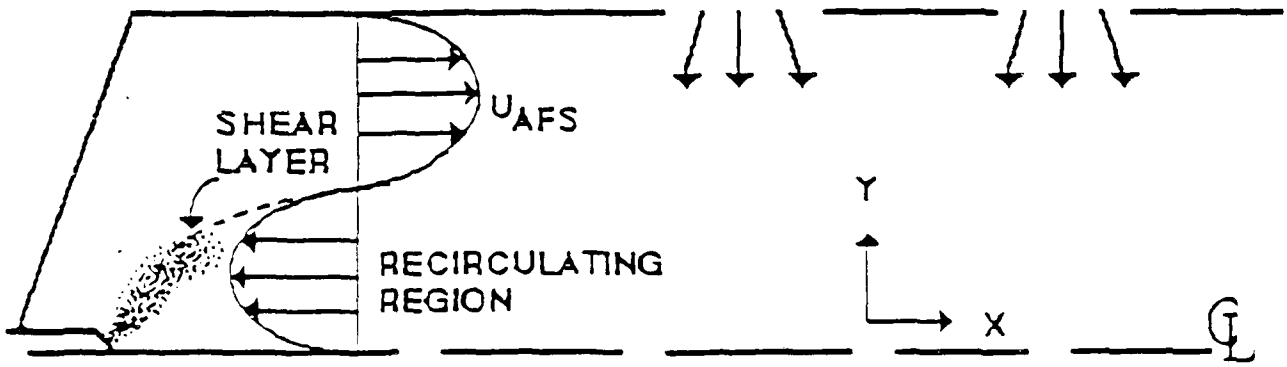

Figure 4.35 Cross-section of a Typical Combustor Through Plane of Primary Jet Showing Modeled Flow Region (No Swirler)

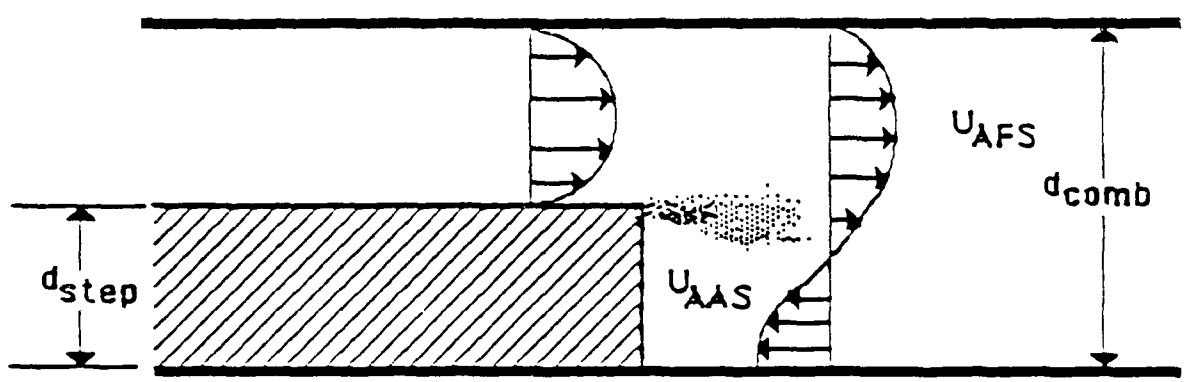

Figure 4.36 Schematic of Proposed Experimental Test Section for Flow Over a Rearward Facing Step

and a possible choice for U_{AFS} are also shown. For a given combustor the shear layer strength is constant as the geometry is fixed. Therefore data for any given combustor should collapse using $\tau_{s\ell,co}$.

As shown by Fig. 2.1, with $\tau_{s\ell,co}$ the CTM collapses data from several combustors on a single curve. Equations 4.3 and 4.4 suggest that some of the vertical scatter in the CTM correlations involving $\tau_{s\ell,co}$ is due to assuming a constant shear layer strength from combustor to combustor. In fact λ will depend on at least ℓ_{pri}/d_{comb}, the fraction of air flowing through the primary holes, and the swirl number (S), if a swirler is included in the design. Although $\tau_{s\ell,co}$ is defined in Eqs. 2.5 and 2.6 as a function of ℓ_{pri} and d_{comb}, the fraction of air flowing through the primary holes and the swirl number are omitted in the mixing time which characterizes the initial shear layer for a combustor.

Returning to Fig. 4.35, it is seen that the choice of λ for an individual combustor is somewhat arbitrary due to the presence of a recirculation zone. For example, if the edge of the shear layer is identified with the edge of the recirculation zone, then $\lambda = 1$, $U_{AAS} = 0$, and $\tau_{s\ell,co} = \infty$, a significant extrapolation of the present experiments for $\lambda \leq 0.22$, leading to a trivial result. Rather, to resolve the issue of evaluating shear layer strength in a recirculating flow, further experiments are recommended, particularly with the flow over a rearward facing step. Fuel injection should be directly into the shear layer surrounding the recirculation zone. It is anticipated that λ will be replaced by a term proportional to the entrainment ratio of the recirculation zone, a function of d_{step}/d_{comb} in Fig. 4.36 but for the turbine combustor related to swirl number and normalized primary hole air flow and position.

Another way to incorporate the effect of shear layer strength in correlations may be a hybrid model as discussed in Section 2. A three-dimensional code can be used to evaluate λ or entrainment ratio for each combustor, which, in conjunction with $\tau_{s\ell,global}$ replacing $\tau_{s\ell,co}$ in the CTM, could lead to improved correlations for CO emissions, combustion efficiency, and lean blowoff limit. Thus the study performed by Rizk and Mongia (1986) using a three-dimensional code in conjunction with Lefebvre's semi-empirical models could be extended to include the

CTM, but at the present time no work of this type is underway known to the authors. This modeling approach coupled with the above experiments for the rearward facing step with measurements of CO emissions, combustion efficiency, and lean-blowoff equivalence ratios may be a prerequisite.

The experimental configuration sketched schematically in Fig. 4.36 requires fuel injection and subsequent atomization in the shear layer originating at the top edge of the step. Present atomization results are discussed in Section 4.4 below, where one aspect is the effect of λ approaching unity on SMD.

4.4 Spray Measurements

4.4.1 Limitations in the Experimental Rig and Instrumentation

Unlike local mixing times it was not possible to measure local droplet lifetimes (τ_{eb}). Recall that the originally proposed method, outlined in Section 3, called for extinction measurements to evaluate total evaporation length and proved to be impossible in the present facility because of spray impingement on the windows and limitations on air temperatures imposed by the tunnel's sealant design. Other methods documented there failed as well.

The focus of the investigation therefore became SMD and I/I_0 measurements as a function of Y/D, as well as turbulent dispersion of the spray in the Y-direction for work with two-phase turbulent flow models. However, the latter study was precluded even utilizing the narrow porous plate described in Section 3 due to spray impingement on the Z-walls (parallel to the Y-axis) at X/D less than 0.5 for most of the two-phase flow matrix cases. Therefore, the focus was reduced to integral (Y-averaged) SMD and I/I_0 measurements as a function of X/D upstream of where impingement occurred on the corresponding Y-windows. In Section 6 proposed modifications to the rig and instrumentation designed to alleviate these problems will be addressed.

4.4.2 Spray Characterization

SMD measurements obtained at X/D = 1.83 and compared with literature correlations were discussed in Tallio (1987). The focus here is on integral SMD measurements resolved spatially in the X-direction, variations in the two-dimensionality of the spray in the Z-direction, and the effect of shear layer strength on integral SMD. Attenuation measurements are examined in Section 4.4.4. SMD and attenuation data are recorded in Appendix B.

Figure 4.37 shows integral SMD versus Z/D for case 8 at X/D = 1.5 for two liquid mass flow rates. Three measurements were obtained at each value of Z/D. The data exhibit scatter of ±3 microns for W_ℓ = 16.6 g/s and ±6 microns for W_ℓ = 9.5 g/s, consistent with preliminary results (Tallio, 1987) and typical of results at all X-locations studied for this case and other cases. Variation in mean drop size across the spray is ±4 microns for W_ℓ = 16.6 g/s and ±9 microns for W_ℓ = 9.5 g/s, indicating uniformity of spray SMD as the data are within the limits of scatter observed for this measurement technique (±10 μm).

Also apparent is that the SMD is not a function of liquid flow rate, a consequence of the low liquid-to-air ratios used in this study (maximum of 0.05). Lefebvre (1980) observed this phenomenon in other prefilming airblast atomizers for liquid-to-air ratios below 0.2.

The development of the spray as a function of axial distance is shown in Fig. 4.38 for cases 8 and 10. Here, each datum point is an average of three measurements obtained at Z/D = 0. This average integral SMD is seen to decrease with increasing distance from the injector; however, because it is not possible to decouple the effects of evaporation from those due to laminar dispersion (see Section 3.4), the precise cause of the observed changes cannot be identified.

4.4.3 Effect of Shear Layer Strength on SMD

Having characterized the spray as two-dimensional and independent of liquid flow rate, the study turned to the effects of shear layer strength on atomization, a parameter not included in current correlations for SMD (e.g., Eq. 2.12). For this purpose, additional cases were added to

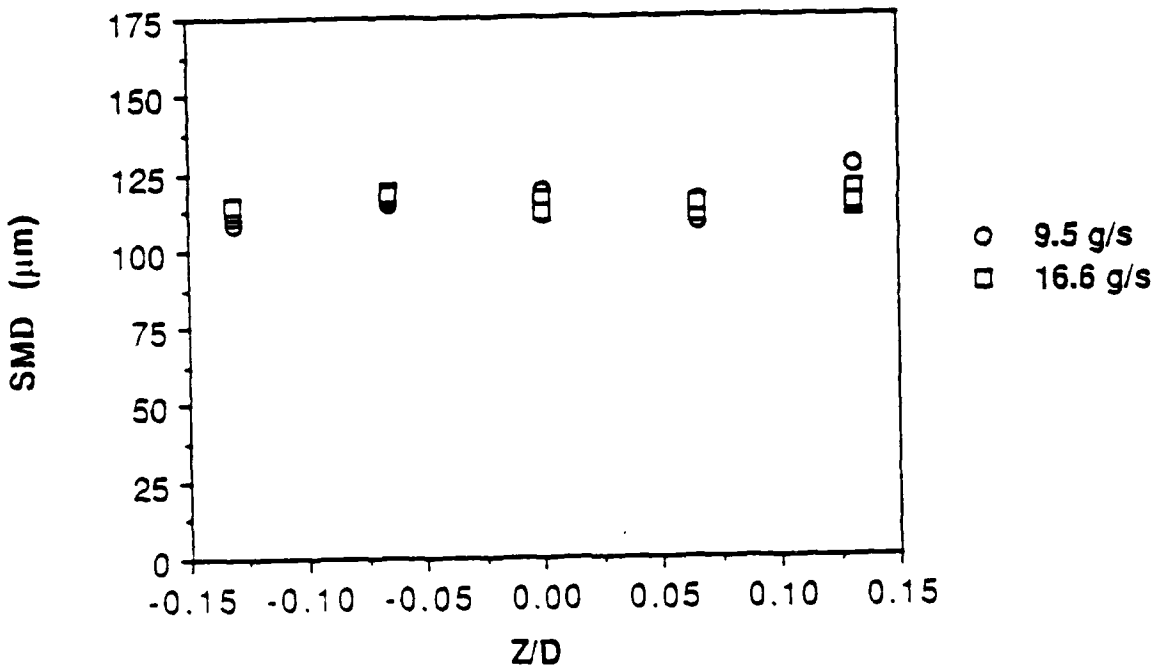

Figure 4.37 Experimental SMD at Various Z/D Locations for Case 8 at X/D = 1.5

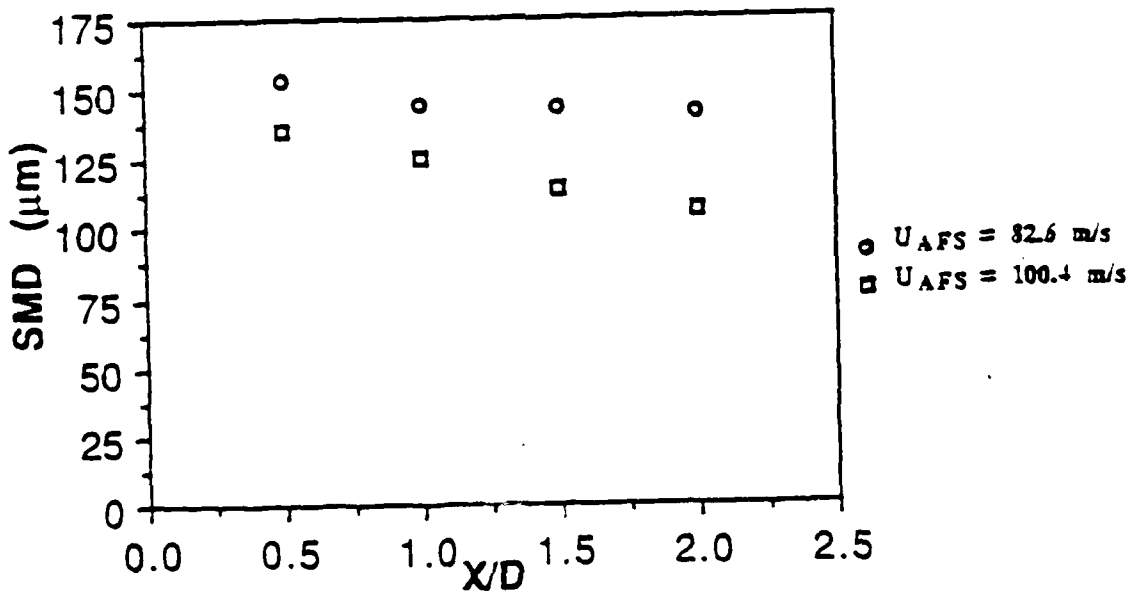

Figure 4.38 Experimental Centerline Average SMD at Downstream Locations for Case 8 and Case 10 (W_ℓ = 16.6 g/s)

the two-phase flow matrix to provide a broader range of U_{AFS}. As shown in Figure 4.39, SMD increases with an increase in λ for all values of U_{AFS}. At a given value of U_{AFS} an increase in SMD of as much as 33 percent, or 40 μm, is observed due solely to increasing shear layer strength from λ = 0 to 0.22. These results are consistent with the findings of other researchers (e.g., Sattlemayer and Wittig, 1987), and are due to momentum transfer from the high velocity airstream deflecting the liquid sheet to the low velocity side (Fig. 4.27a), resulting in a reduction of effective atomizing air velocity and thereby increasing mean drop size. Consequently, direct atomization into the shear layer surrounding a recirculation zone, as suggested by Fig. 4.36, may not be efficient: a more sophisticated design will be necessary.

Also consistent with other researchers is the effect of U_{AFS} on SMD in Fig. 4.39. At constant λ, SMD decreases with increasing values of U_{AFS} because of the additional momentum transfer to the liquid sheet. For zero shear layer strength the experimental data show a 38% decrease in SMD (141 μm to 97 μm) corresponding to an increase in U_{AFS} from 82.6 m/s to 122.0 m/s. Over the same velocity range, Eq. 2.12 predicts a 37% decrease in SMD. Similar decreases in experimental SMD are observed for λ = 0.1 and 0.22 (35 and 31 percent, respectively); however, because the effect of λ is not included in Eq. 2.12 it is not possible to predict SMD at shear layer strengths other than zero.

4.4.4 Attenuation Measurements

In view of the problems associated with spray impingement due to turbulent dispersion and the inability to experimentally determine β, attenuation (I/I_0) measurements are now of interest only from the point of view of the two-dimensionality of the spray. Fig. 4.40 shows individual I/I_0 measurements versus Z/D for case 8 at X/D = 0.5 for two liquid flow rates. As expected lower values of I/I_0 are observed at the higher liquid flow rate as a result of an increase in liquid volume concentration. Also to be noted is the non-uniformity of the transmission measurements across the flow, which suggests that the slight increase in SMD with increasing Z/D in Fig. 4.37 may be real. Although SMD for liquid injected via the porous plate is

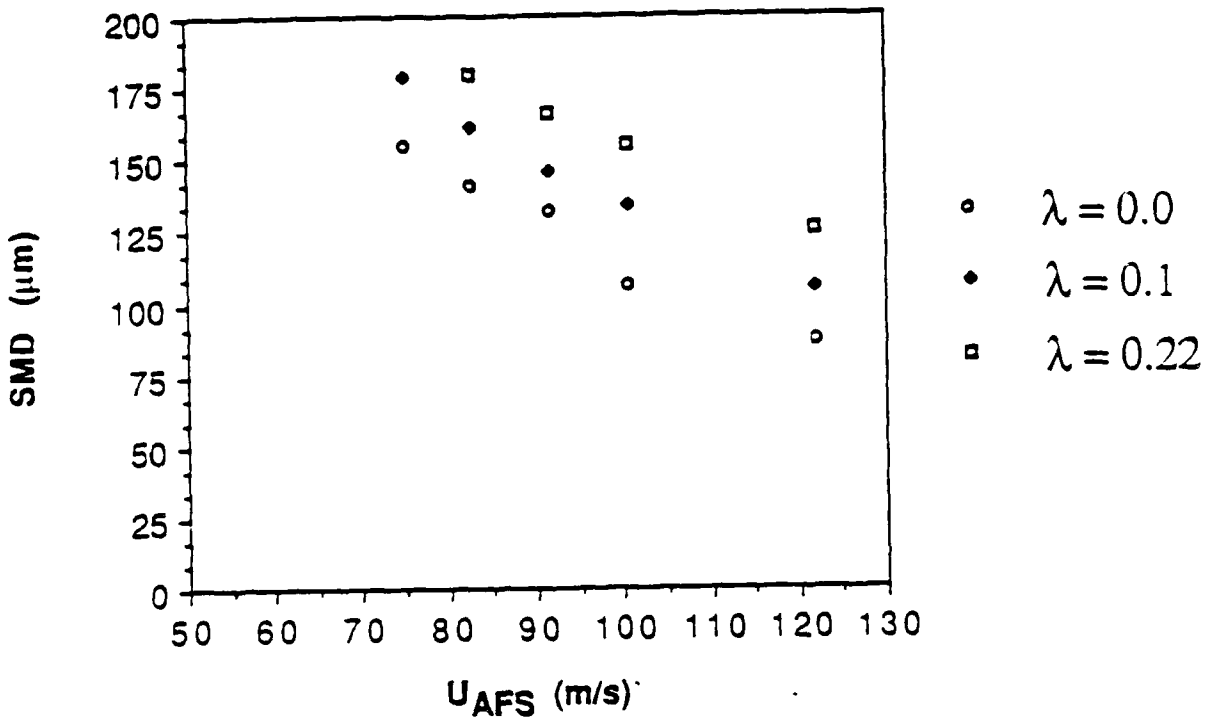

Figure 4.39 Experimental Centerline Average SMD as a Function of U_{AFS} at X/D = 2.0 and Various λ

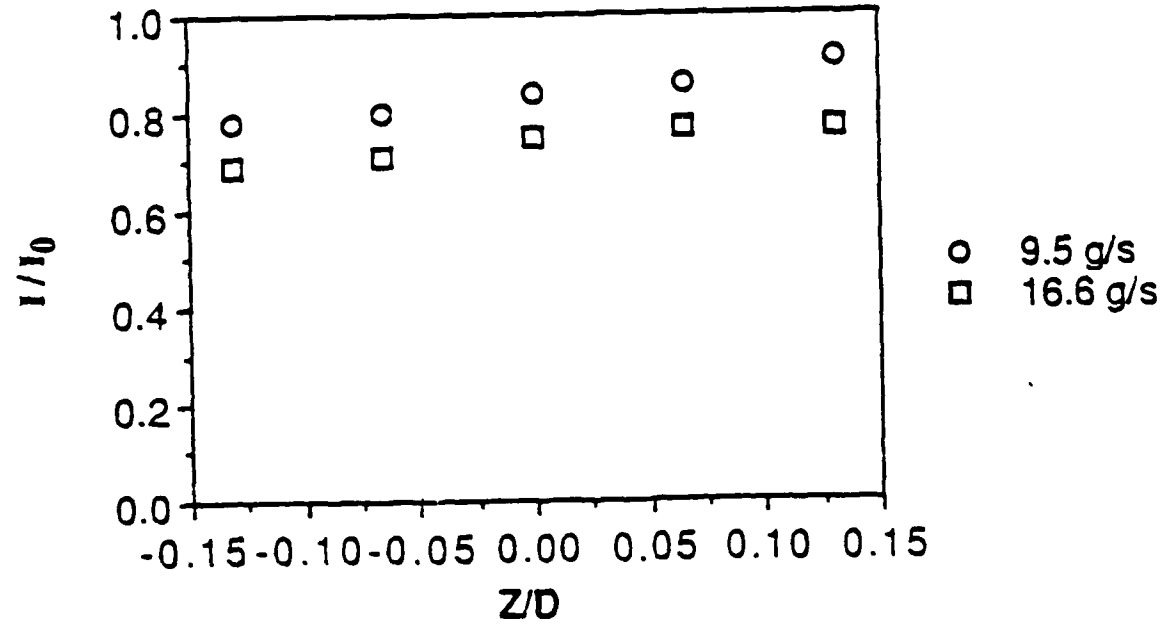

Figure 4.40 Transmission Measurements for Case 8 at X/D = 0.5

independent of liquid flow rate, leaks around the porous plate would not be. At downstream locations (not shown) the Z/D nonuniformity becomes less pronounced due to turbulent dispersion of the spray.

4.4.5 Implications for the Characteristic Time Model

Accurate correlations for SMD are necessary to limit x-axis scatter in droplet lifetime calculations (Eq. 2.7) for the blowoff, ignition, and efficiency CTM's. As discussed in Section 4.1, liquid properties are not correlated to better than 10%, while geometric effects can produce differences of 50% or more, as evidenced by the wide range of efficiency factors required in Eq. 2.12 (Lefebvre, 1980; Tallio, 1987). Although proper inclusion of liquid property effects and forward diffraction measurement scatter are well-known potential sources of ambiguity, geometric and shear layer effects also require consideration in correlations for SMD.

Since errors in predicted SMD can create discrepancies in τ_{eb} as $SMD^{1.4}$ or $SMD^{2.0}$, depending on the convective correlation chosen, it is apparent that they can cause a significant amount of scatter on the ordinate of Fig. 2.1. For example, a 33% error at 100 μm (taking Jet-A fuel in a 750 K environment with a 30 m/s relative velocity) can move a given datum point in Fig. 2.1 $\pm$0.43 ms, or $\pm$1 standard deviation. Thus one improvement in the CTM predictive ability for τ_{eb} requires more accurate correlations for SMD, including effects of shear layer strength as shown by the present work.

This conclusion implies the need for in-situ measurements of SMD in actual combustors. However, this major effort may not be warranted since combustor development tests integrate injector with swirl cup and primary zone design to solve performance problems under realistic operating conditions. Therefore, future research should focus not on SMD, other than to yield relative rankings for injectors as is standard practice, but rather on fundamental studies of the transition from dense to dilute sprays. In the latter case, turbulence-spray interactions, such as turbulent dispersion and modulation, are also of interest for continuum finite difference

computations. One such model, used for predicting the gas-phase flows discussed in Section 4.3.2, is the subject which follows.

5.0. Investigation of Continuum Models for Turbulent Flows

Finite difference modeling techniques for turbulent flows have evolved considerably over the last several decades (e.g., Jones and Launder, 1972; Gosman and Ioannides, 1983; Faeth, 1987) to their present state. The difficulty with modeling this type of flow stems from the closure problem in the time averaged Navier-Stokes equations. Several approaches to solving this problem have been suggested, many of which deal with methods of modeling turbulent, or eddy, viscosity. Since many publications discussing these techniques in detail are available (e.g., Bradshaw et al., 1981), only the points relevant to this program will be discussed. The intent here is not to review available modeling techniques, but rather to investigate the predictive ability of a selected model by comparing the computed flow parameters (mean and rms velocity and length scale) with those measured in a series of well defined experiments. The ultimate objective of this investigation is to evaluate models for two-phase turbulent flows; however, the data reported here are limited to comparison with the gas-flow measurements since they must be predicted accurately before it is meaningful to incorporate the liquid phase flow.

5.1 Model for Turbulent Flows

The finite difference model selected for this study was developed by Anderson (1980) to predict the velocity field of subsonic laminar or turbulent flows in axisymmetric and two-dimensional ducts with or without fuel injection. This code was developed at United Technologies Research Center under the sponsorship of NASA-Lewis/AVSCOM to model flows in prevaporizing-premixing passages of advanced gas turbine combustors. It can be used to model both the gas and liquid-phases of a two-phase turbulent flow.

The Axisymmetric Duct Diffuser (ADD) code employs a parabolic formulation of the governing equations along with a two-equation (k-ϵ) turbulence model to compute the gas-phase flowfield in the first of three codes included in Anderson et al. (1982). The other codes available are PTRAK, a deterministic separated particle trajectory model, in that following Faeth

(1987) all parameters are computed using mean values of the gas-phase flow, and VAPDIF, an analysis centered on an individual droplet which calculates both rate of evaporation and diffusion of vapor into the gas-phase from the droplet. The three codes are separate for numerical convenience, in that the gas-phase solution from ADD is used for solving PTRAK, and so forth, representing rather severe approximations for the computation of a spray flowing in a gas.

Work in the present program focused on ADD, since the experimental limitations identified during the study prevented measurements on vaporizing sprays. The intent was to establish the quality of the ADD code predictions for the gas phase, a prerequisite before incorporation of the spray model. A closely related effort (see Farouk, 1988) concentrated in part on improving the PTRAK analysis by incorporating a stochastic separated flow model (Faeth, 1987), in which droplets randomly encounter turbulent eddies and respond to fluctuations in the gas phase from eddy to eddy.

The coordinate system chosen for the ADD code (Anderson, 1980) is constructed using a potential flow solution of the flowfield within the duct with the stream function forming the coordinate normal to the wall, and the velocity potential the coordinate tangent to it. Since the potential flow streamlines closely approximate those of the viscous flow, the equations of motion can be simplified by assuming that the velocity component normal to the streamlines is small compared to the streamwise velocity. This approach reduces the governing equations for the viscous flow to a system of parabolic partial differential equations which can be solved with a forward marching numerical integration procedure (Anderson, 1980). Errors introduced by terms neglected in the parabolic formulation are on the order of four percent, based on experimental values of these quantities, in the calculations for the shear layer region presented here.

There are several restrictions on the types of flows that can be modeled using the ADD code. First, as stated earlier, the flows must be two-dimensional, or axisymmetric. Second,

since the governing equations have been reduced to a parabolic system it is not possible for this code to handle separated, or recirculating flowfields.

The modeled governing equations can be expressed as:

$$U_s \frac{\partial(\rho\Phi)}{\partial s} - \frac{\partial}{\partial n}\left[\Gamma_\Phi \frac{\partial \Phi}{\partial n} \right] = S_\Phi \qquad 5.1$$

S_Φ and Φ are defined in Table 5.1, along with the appropriate constants.

Table 5.1.

Parameters for Eq. 5.1

Φ	Γ_Φ	S_Φ
1	0	0
U_s	$\mu + \mu_t$	$-\frac{\partial P}{\partial s}$
k	$\mu + \frac{\mu_t}{\sigma_k}$	$\mu_t\left[\frac{\partial U_s}{\partial n}\right]^2 - \rho\varepsilon - 2\mu\frac{k}{Y^2}$
ε	$\mu + \frac{\mu_t}{\sigma_\varepsilon}$	$C_1 \mu_t \left[\frac{\partial U_s}{\partial n}\right]^2 - C_2 \rho \frac{\varepsilon^2}{k} - 2 C_3 \mu \frac{\varepsilon}{Y^2}$

C_μ	C_1	C_2	C_3	σ_k	σ_ε
0.09	1.35	1.8	1	1.0	1.3

The turbulence parameters are coupled with the momentum equation through the turbulent

viscosity.

$$\mu_t = \frac{\rho C_\mu k^2}{\varepsilon} \tag{5.2}$$

The computational technique employed by Anderson et al. (1982) lags these turbulent flow quantities one step behind the mean flow equations. This approach allows the mean flow quantities to be known at each axial station, but requires that the values of k and ϵ be known at the station immediately upstream. This computational strategy is used to reduce the amount of computer storage and computational time required for the calculations.

To circumvent the need to utilize the boundary layer equations to compute the flow near the wall ADD employs an empirical, universal turbulent boundary layer profile, proposed by Coles (1956), to fit the experimental data. This procedure reduces the computational time required to iterate between the freestream and boundary layer solutions from the equations of motion. Initial boundary layer profiles are based on initial conditions for boundary layer displacement thickness and the power law exponent, both inputs provided by the user. In the present study these parameters were determined using experimental velocity profiles.

Initial conditions for all of the computations reported here came directly from the experimental data. The code permits the user to enter the initial profiles of mean velocity, static pressure, and temperature directly as initial conditions. Turbulence quantities can be calculated with a mixing length model for turbulent pipe flow (a model incorporated in the original version of the code), but modifications to the code (discussed below) were required to enter the rms velocity and length scale profiles at the inlet plane directly so that the initial values of k and ϵ can be calculated. Prior to discussing the results of this investigation, an overview of modifications made to enable the code to model a central shear layer and to input the experimental conditions is warranted.

5.2 Modifications to ADD

The finite difference mesh generated by the original version of ADD was not suitable for modeling the flow studied here. The code was developed to model turbulent duct flows with no significant velocity gradients in the freestream; as a result, the grid density across the duct is much larger in the boundary layers (to resolve the large velocity gradients) than in the freestream. The results of ADD's original grid generation scheme can be seen in Fig. 5.1 for the computational domain used in this study with 55 cross-stream grid lines. The lack of gridlines in the central region of the flow did not provide adequate resolution of the shear layer where the velocity gradients are on the same order as those found in the boundary layers. In addition, the accuracy of the finite difference calculations in this region of the flow suffered because of the large cross-stream step sizes.

To resolve these problems, the grid generation scheme incorporated in ADD was modified to allow the user to specify the location of the cross-stream grids used in the computations. This makes it possible to increase the grid density in the shear layer, providing better resolution in this region of the flow. The resulting computational domain and streamlines can be seen in Fig. 5.2. Note that the high grid density in the boundary layers has been retained so that the velocity gradients near the walls can be accurately resolved.

Anderson et al. (1982) suggest that 50 cross-stream grid lines are sufficient to model the flow. The location of the streamwise grid lines are used for outputing results only; the code implements intermediate computational stations to ensure that the solution converges between the specified streamwise locations (Anderson et al., 1982).

The detailed experimental measurements from the two-phase flow matrix (Table 4.2) provided the data necessary to apply the experimental initial conditions for mean and rms velocity and turbulent length scale directly, and thereby eliminate any uncertainty due to assumed initial conditions. Those for the turbulent kinetic energy are calculated using Z-averaged profiles of rms velocity measured at the inlet plane (X/D = 0.03). A typical

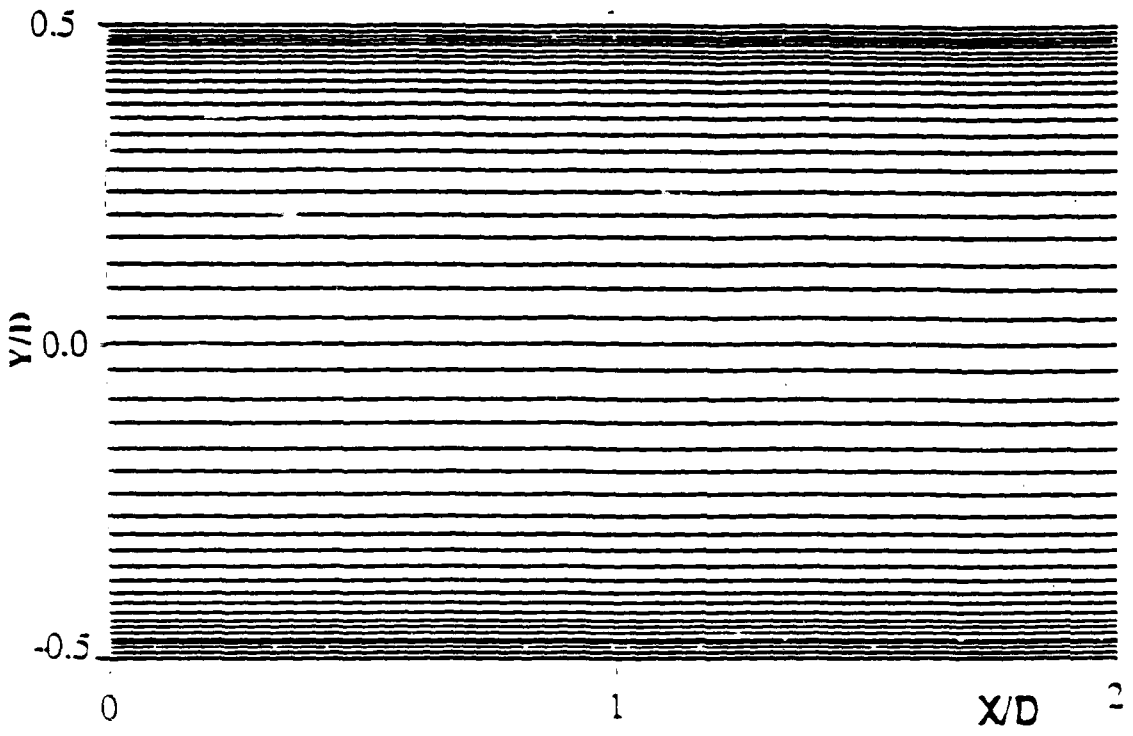

Figure 5.1 Original Computational Mesh for Gas-Phase Flow

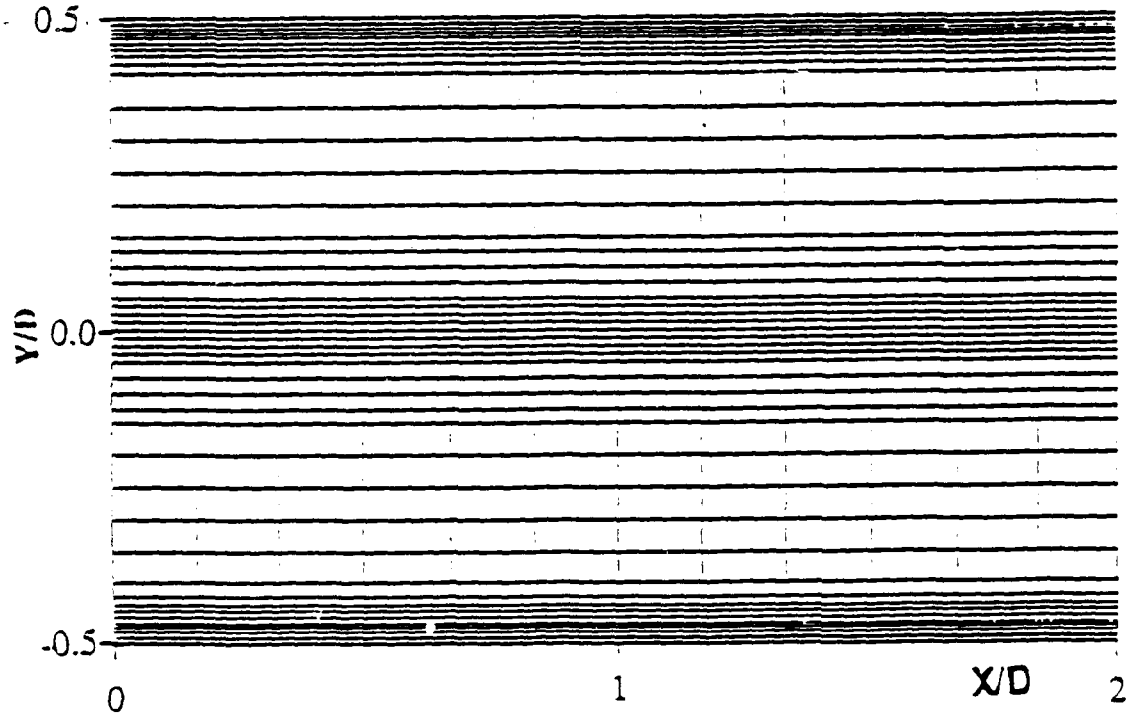

Figure 5.2 Refined Computational Mesh for Gas-Phase Flow

measurement of this parameter can be found in Fig. 4.6b. Since turbulent kinetic energy is defined in terms of the rms velocity its value is computed as:

$$k = \frac{3}{2} u^2_{rms} \tag{5.3}$$

where for the calculations presented here the turbulence is modeled as isotropic. However, as shown in Fig. 4.29, this assumption is a poor approximation in this flow.

The second turbulence modeling parameter to be calculated is the dissipation rate of turbulence, which can be defined in terms of k and the integral length scale as:

$$\varepsilon = \frac{C_\mu^{0.75} k^{1.5}}{l} \tag{5.4}$$

However, there is some ambiguity in the literature (see, for example, Gosman and Ioannides, 1983; Faeth, 1987) as to the preferred value for the exponent on the constant C_μ. Since an eventual objective of the studies reported here is to model the liquid phase flow using the stochastic separated flow approach, a value of 0.75 was selected following Faeth (1987). The effects of varying this parameter have been investigated and the results are presented below.

5.3 Results

The modifications outlined in the previous section were necessary to reduce the difference between the velocity profiles (both mean and rms) predicted by the model and those measured experimentally, but the agreement remains poor. Figures 4.6 through 4.8 and 4.11 through 4.15 show both the experimentally measured and computed velocity profiles for cases 1 and 14, respectively, of the two-phase flow matrix (Table 4.2). As discussed in Section 4, these were the cases studied in detail to generate a datum base that could be used to compare the results predicted by the code with the experimental data.

Figures 4.6 and 4.11 show the experimental values of mean and rms velocity at the X/D = 0.03 station and the values used for initial conditions in the computations for cases 1 and 14, respectively. The initial turbulence quantities, calculated from Eq. 5.3 and 5.4 for X/D = 0.03, are used as the lagged values for computations at the first axial station. The agreement in these figures is expected since the experimental data are used as input to the code. These results simply show that the modifications to the code to permit the initial values of k to be calculated from the rms velocity have been implemented correctly and that grid resolution of the shear layer is adequate. At this point the reader should recall that all of the experimental velocity profiles discussed here are Z-averaged. The error bars shown on these figures represent the maximum and minimum values of experimental velocity included in the average and demonstrate the degree of two-dimensionality of the flow.

Initial conditions for turbulent length scale can be found in Fig. 4.17 and 4.22 for cases 1 and 14. Again, the agreement demonstrates that the modifications to the code to incorporate initial conditions are correct. Unlike the mean and rms velocity measurements, however, all of the experimental values of length scale reported here represent a single traverse at Z/D = 0. Because only one profile is used no error bars appear on the figures.

Figure 4.7 shows both profiles for mean and rms velocity for case 1 at X/D=1, the first measurement station for this case. The difference between the predicted and measured mean velocities is approximately 15 percent near the centerline of the flow (percent difference = 100*(model-experiment)/experiment) while the difference in the rms velocities exceeds 50 percent. As the flow develops further downstream (Fig. 4.8) the difference between the two mean velocity profiles remains relatively constant, but the predicted values of rms velocity show a larger difference over the previous station. The length scales computed at these two locations fall short of the measured values in the freestream, but agree quite well near the center of the shear layer as shown in Fig. 4.18 and 4.19. It is worthwhile to note that in spite of the large quantitative differences between the experimental and numerical mean and rms velocity profiles,

the predicted data qualitatively follow the experimental trends quite well. Qualitative length scale agreement is less satisfactory.

Figure 5.3 summarizes percent differences between the experimental and computational mean and rms velocity profiles for case 1 at all three axial stations. The errors in the mean velocity profiles near the centerline appear to be caused by a lack of momentum transfer from the relatively high speed freestream flow to the wake region. The overpredictions of the rms velocity are most likely caused by the turbulence model, which will be discussed further below. Note also that the experimental discrepancies in rms between this and the earlier work (Marakovits, 1987) cannot account for these overpredictions (compare for example Fig. 4.3b and 4.7b). The large errors observed in the lower boundary layer indicate that the empirical correlation used by Anderson (1980) to model this region of the flow is inadequate.

Percent differences between experimental and computed length scales for this case are shown in Fig. 5.4a. The underpredictions of length scale in the freestream region may indicate that the values of turbulent kinetic energy calculated by the model are too high for the flow conditions encountered here (see Eq. 5.4).

The experimental conditions for case 1 are for $\lambda = 0$, that is, a wake flow condition. To study the effects of imposing a cross-stream velocity gradient on the flow, case 14 with $\lambda = 0.22$ was studied. Measurements for this case were obtained at more frequent intervals to provide additional data for investigating the model. The mean and rms velocity comparisons for the X/D = 0.5, 1.0, 1.5, and 2.0 stations appear in Fig. 4.12 through 4.15. Comparisons for length scale can be found in Fig. 4.23 through 4.26. The same trends of underpredicted mean velocity and length scale and overpredicted rms velocity are observed for this case; however, the presence of the shear layer provides some additional insight into the effects of momentum transfer.

Because of the differences between the fuel and air side velocities there is an exchange of momentum in the direction of the lower speed flow. This effect causes the experimentally measured point of minimum velocity in the shear layer region to shift toward negative Y/D.

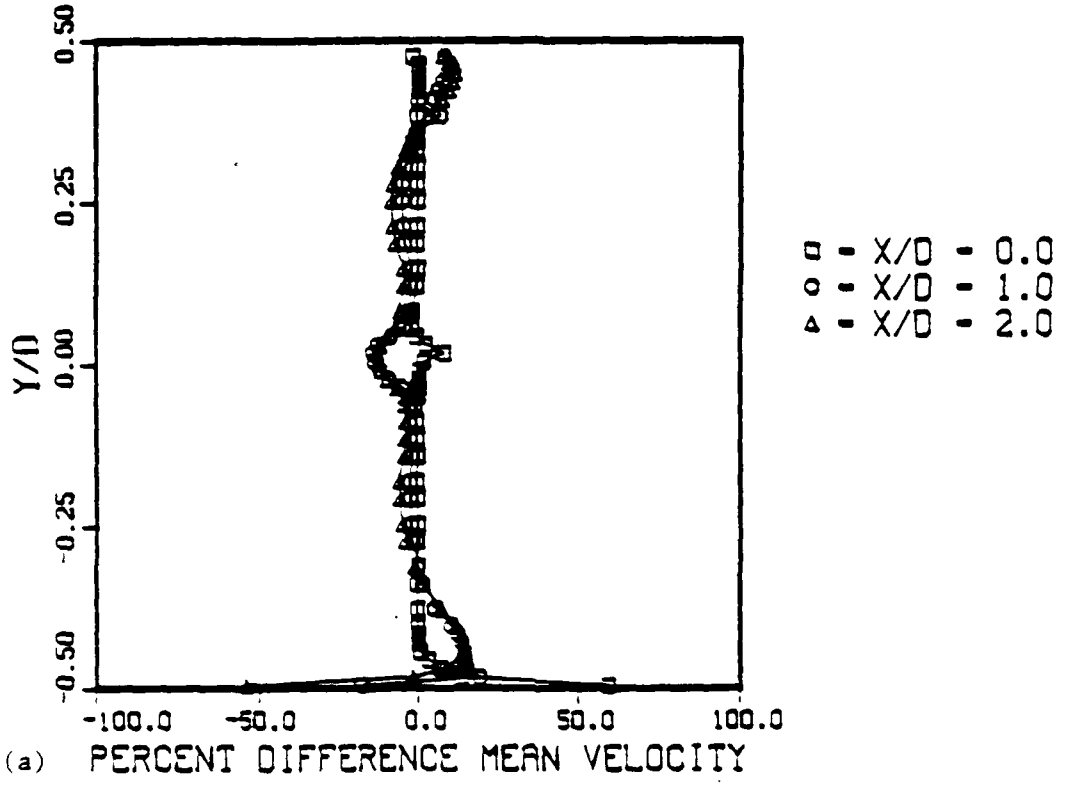

(a)

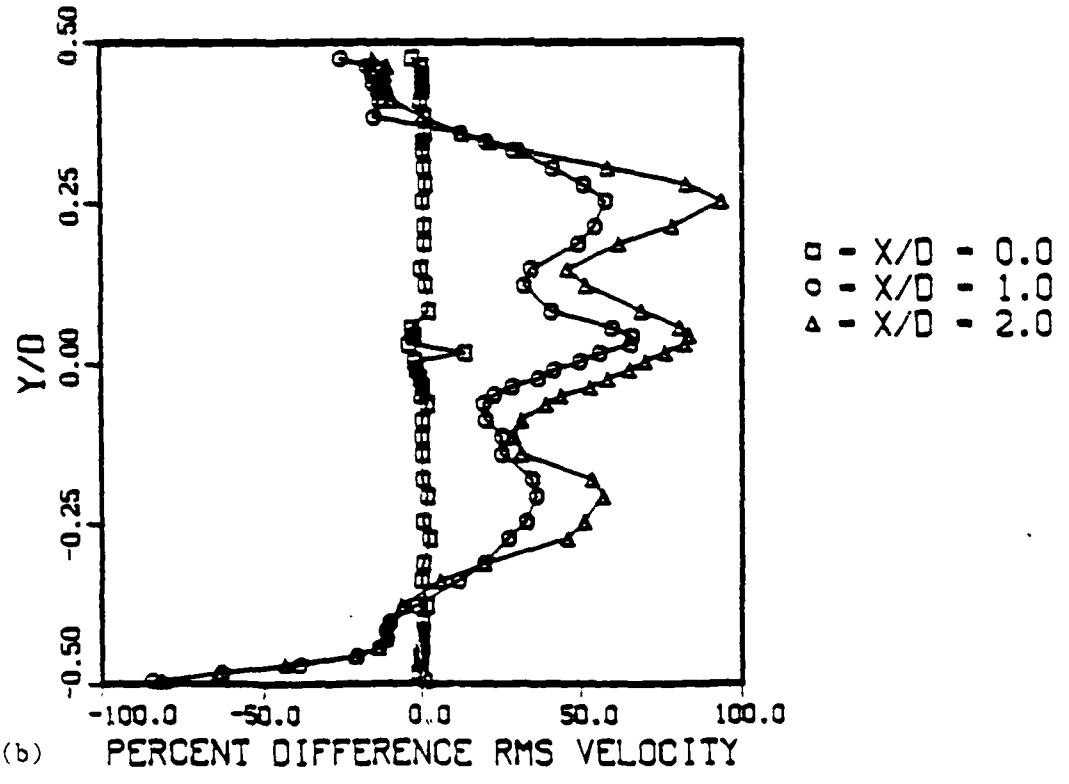

(b)

Figure 5.3 Percent Difference Between Experimental and Predicted (a) Mean Velocity and (b) rms Velocity Profiles for Case 1.

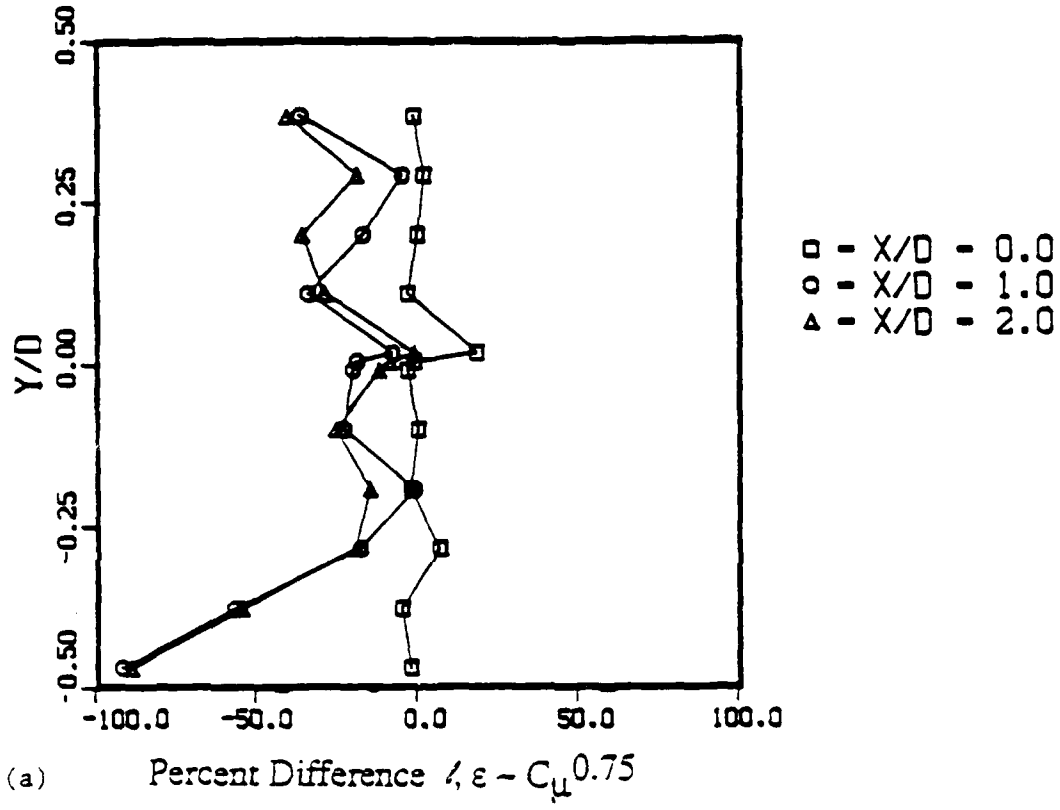

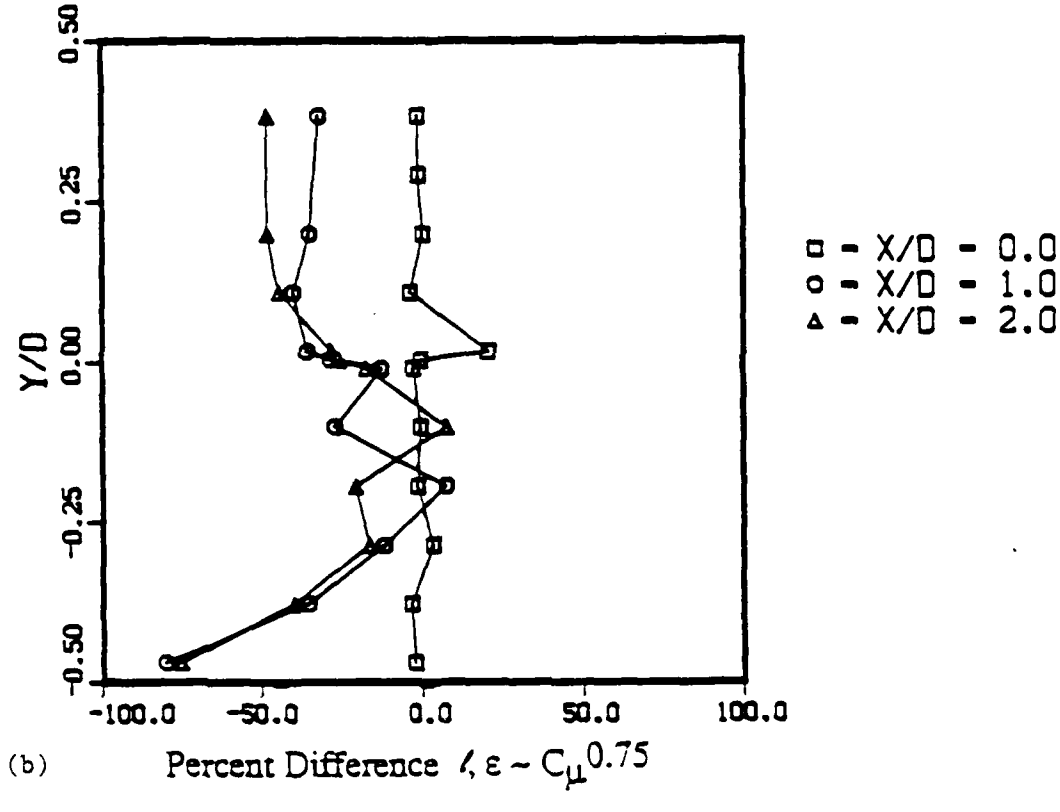

Figure 5.4 Percent Difference Between Experimental and Predicted Length Scale Profiles for (a) Case 1 and (b) Case 14.

This trend, however, does not appear to the same extent in the numerical predictions. This observation is illustrated clearly in Fig. 5.5a which shows the percent differences for this case at X/D = 0, 1 and 2. Notice that the maximum difference shifts away from the center of the flow at X/D = 1.0, and the shift is even more pronounced at X/D = 2.0.

The differences in velocities (Fig. 5.5) and length scale (Fig. 5.4b) for this case are comparable with those found in case 1, indicating that the turbulence model parameters are also not correct for this flow. Furthermore, since the discrepancies are comparable, they are independent of shear layer strength in the range of λ from 0 to 0.22. For case 14 the static pressure decreases from the air to fuel side airflows, which might be expected to increase these discrepancies.

The results presented in the previous paragraphs demonstrate the inability of the ADD code to adequately predict the gas-phase flow in the CTM test tunnel. The error appears to be rooted in the turbulence model, since the differences in rms velocity and length scale approach 100 percent. In order to model the turbulent kinetic energy and rate of dissipation several constants are used (see Table 5.1), but two in ADD have the strongest impact on the results (Anderson, 1988). These are C_μ in Eq. 5.4 and C_2, a constant appearing in the source term for the rate of dissipation. Anderson (1988) suggests that if these parameters are 'calibrated' for the flow in the CTM tunnel, it should be possible to significantly improve the predicted results. As these constants have been evaluated for turbulence behind grids and screens (Bradshaw et al., 1981), their applicability to flows with large cross-stream velocity gradients is questionable.

The value used for C_μ in this investigation was 0.09, the suggested value in the literature (e.g., Jones and Launder, 1972; Pope and Whitelaw, 1976); however, Bradshaw et al, (1981) state that "this parameter is undoubtedly not a constant, but it is hoped that its value will not change much from one flow to another." To date the effect of changing the exponent of C_μ in the model for dissipation rate (Eq. 5.4) has been investigated. Indirectly this change modifies the turbulent viscosity (Eq. 5.2). The variation was achieved using two values other than 0.75 suggested by Faeth (1987): 0.5 was selected based on the work of Gosman and Ioannides (1983),

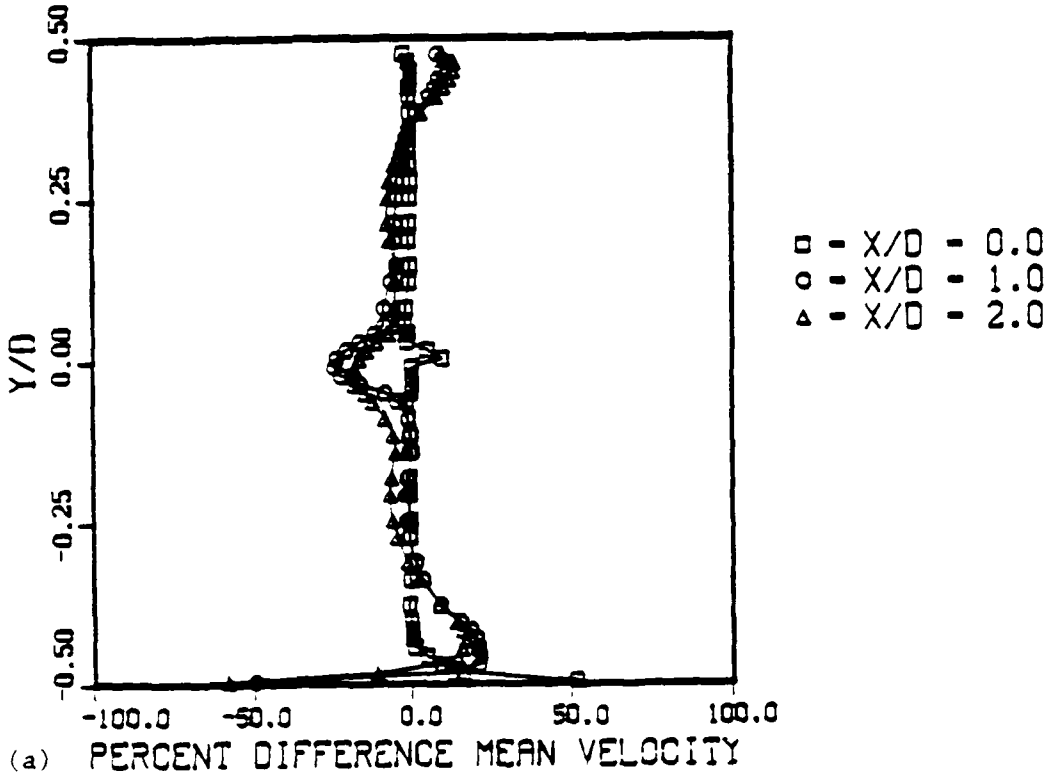

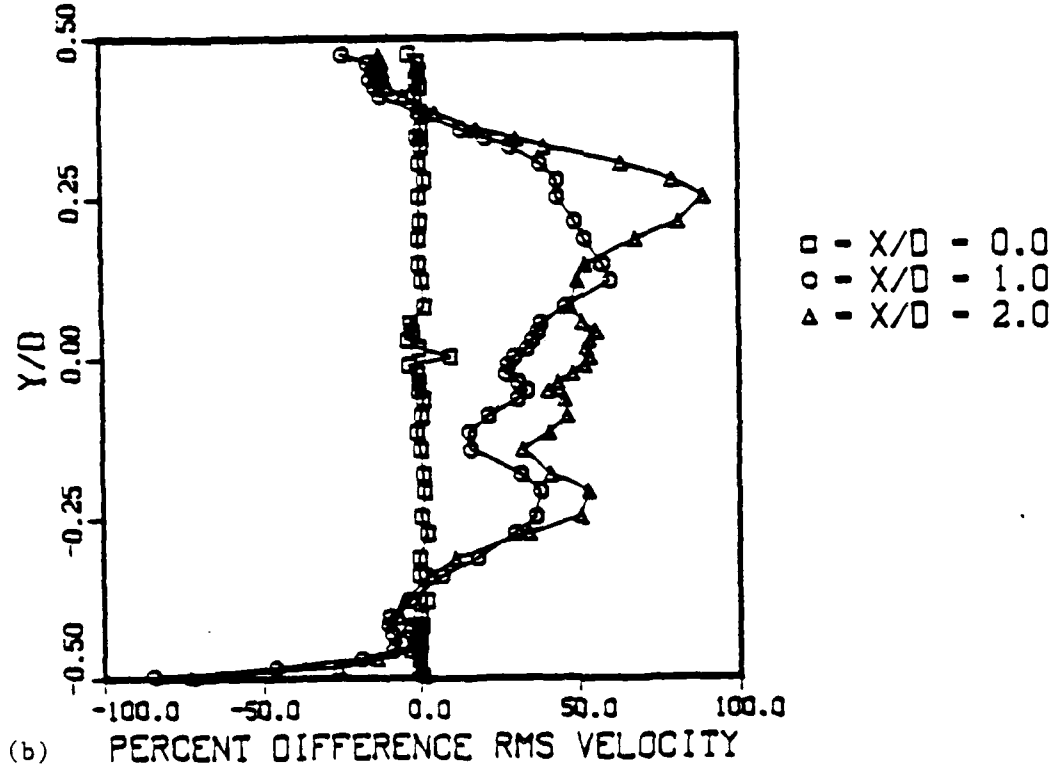

Figure 5.5 Percent Difference Between Experimental and Predicted (a) Mean Velocity and (b) rms Velocity for Case 14.

and to provide a similar variation in the other direction, a value of unity was also studied. The percent errors in mean and rms velocity and length scale for these two computations are shown in Fig. 5.6 through 5.8 for case 1; the results for case 14 (not shown) were similar.

Figure 5.8 shows results for length scale are similar to those for rms velocity;. consequently, in view of the discrepancies with experiment for these parameters, no attempt was made to compute the evolution of $\tau_{s\ell}$ ($= \ell/u_{rms}$) downstream or to compare the downstream computed values with those at the inlet plane. For the mean velocity, predictions in the shear layer improve significantly (from 25 to about 5 percent) as the exponent on C_μ is increased, but the freestream difference degrades to about 8 percent. Using the lower value for the exponent reduces the error in the rms velocity to approximately 25 percent. The opposite trend is observed for the larger exponent and the error in rms velocity is increased to over 100 percent for several locations in the flow. Since low values of exponent improve rms and length scale agreement while no value of exponent optimizes mean velocity agreement, the next step could involve defining both C_μ and its exponent as functions of Y/D, that is, assign values corresponding to the freestream and wake or shear layer. However, first incorporation of experimental deviations from isotropy should be tested in Eq. 5.3, following Faeth (1987).

For the results shown in Fig. 5.3, 5.6, and 5.7, the changes in computed mean velocity in the shear layer, where the droplets are injected in the experiment, can be as large as 25% depending on the choice of the exponent on C_μ. In terms of the calculation of droplet evaporation time, for example, this error is negligible compared to the experimental uncertainty in drop diameter: assuming a Nusselt number directly proportional to the square root of Reynolds number, the convective enhancement of evaporation rate will be uncertain to only 12%. The major error in moving on to calculations using PTRAK modified to include a stochastic approach for turbulent dispersion of droplets will be its overprediction due to the excess in rms velocity, irrespective of the exponent used on C_μ in Eq. 5.4.

The results show that, as suggested by Strahle and Lekoudis (1985), turbulent flow models are not easily extended from one application to another. Further, the decoupling of gas and

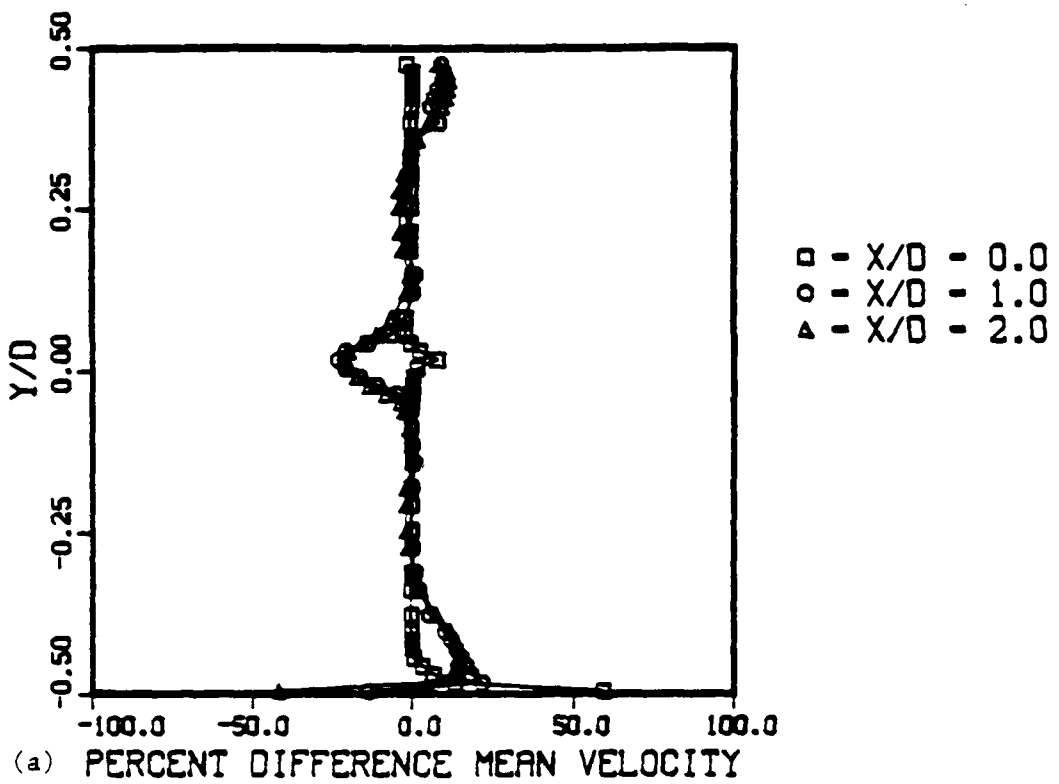

(a) PERCENT DIFFERENCE MEAN VELOCITY

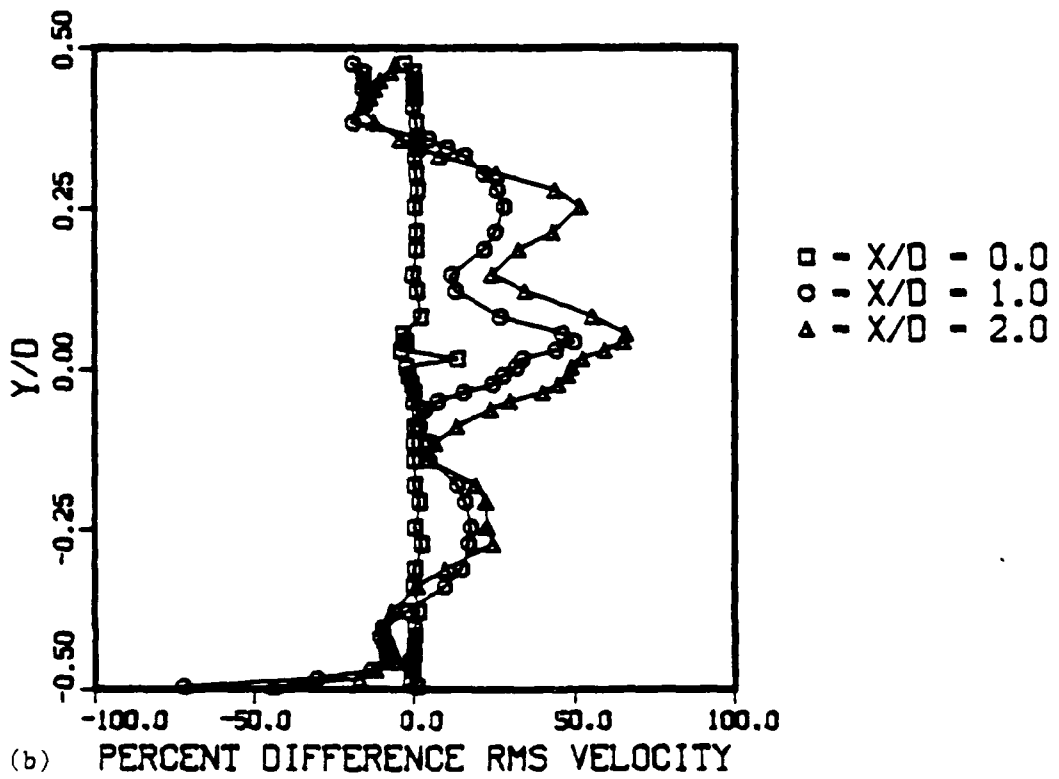

(b) PERCENT DIFFERENCE RMS VELOCITY

Figure 5.6 Percent Difference Between Experimental and Predicted (a) Mean Velocity and (b) rms Velocity for Case 1: $\varepsilon \sim C_\mu^{0.5}$

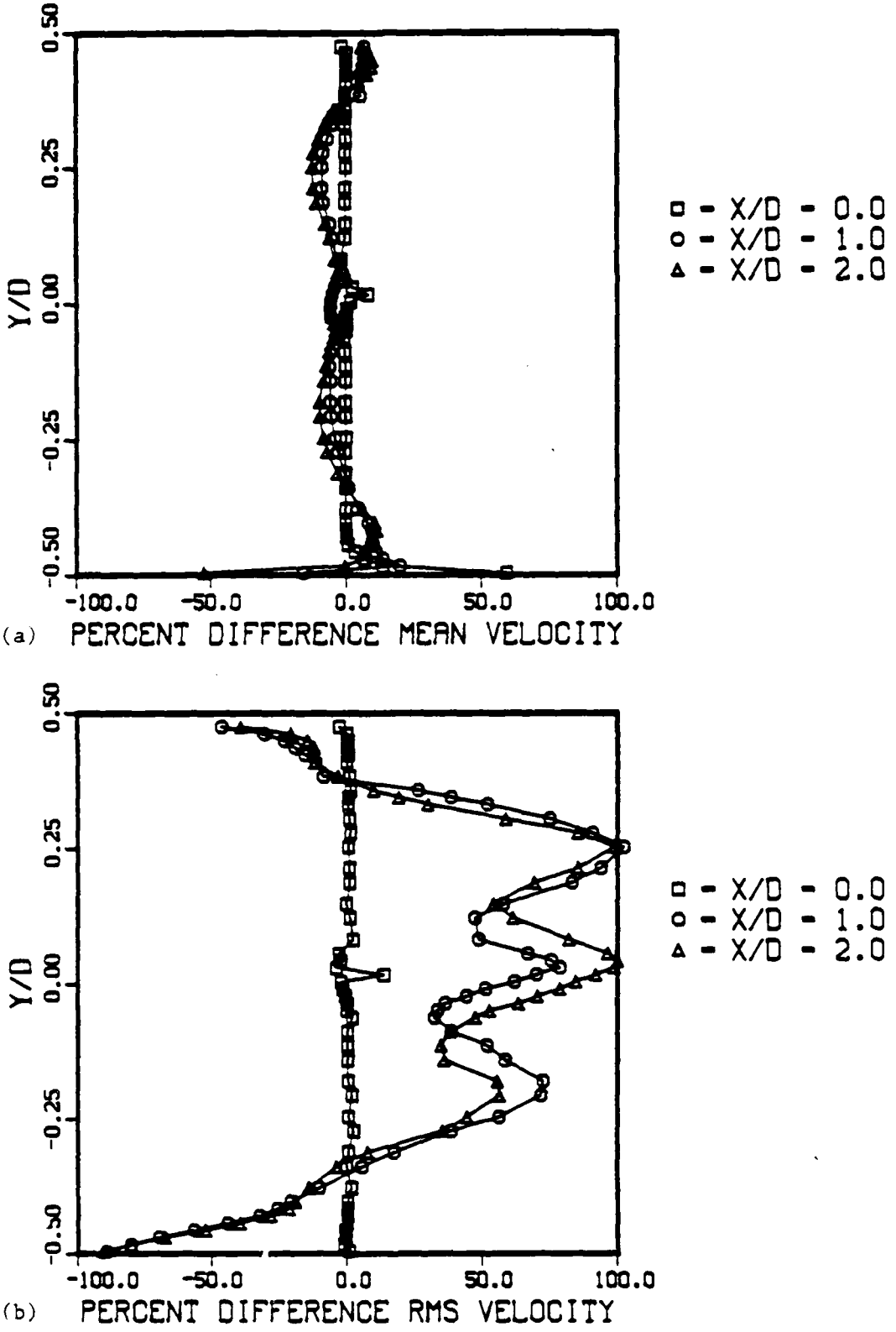

Figure 5.7 Percent Difference Between Experimental and Predicted (a) Mean Velocity and (b) rms Velocity for Case $\varepsilon \sim C_{\mu}{}^{1.0}$

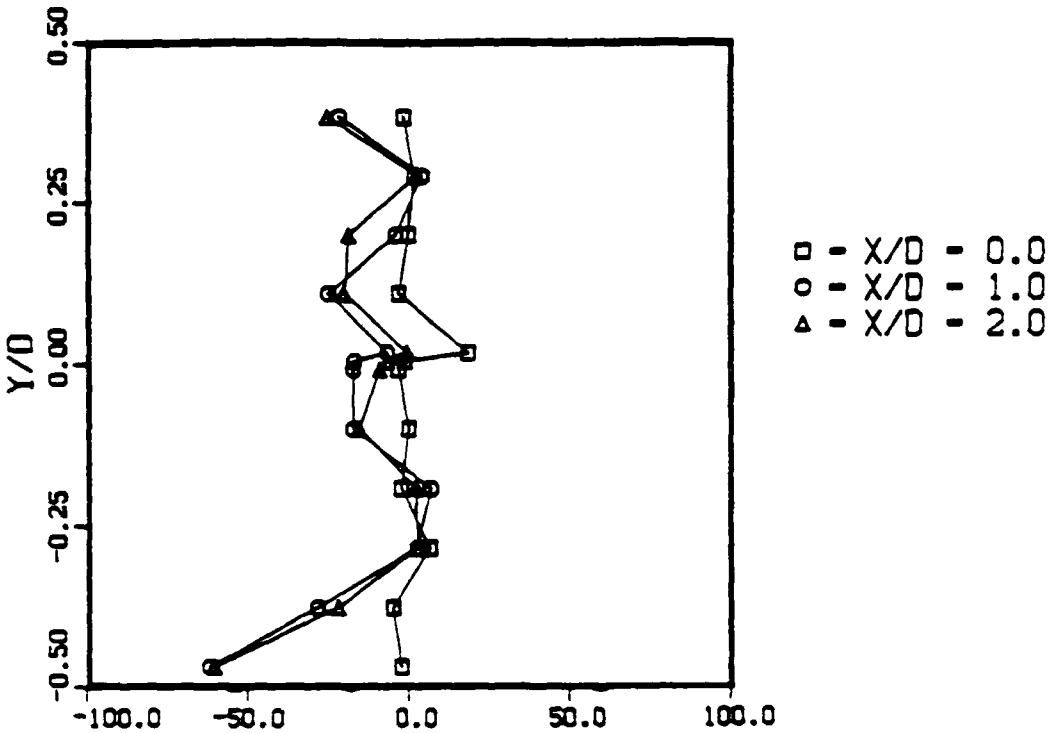

(a) Percent Difference $\ell, \varepsilon \sim C_\mu^{0.5}$

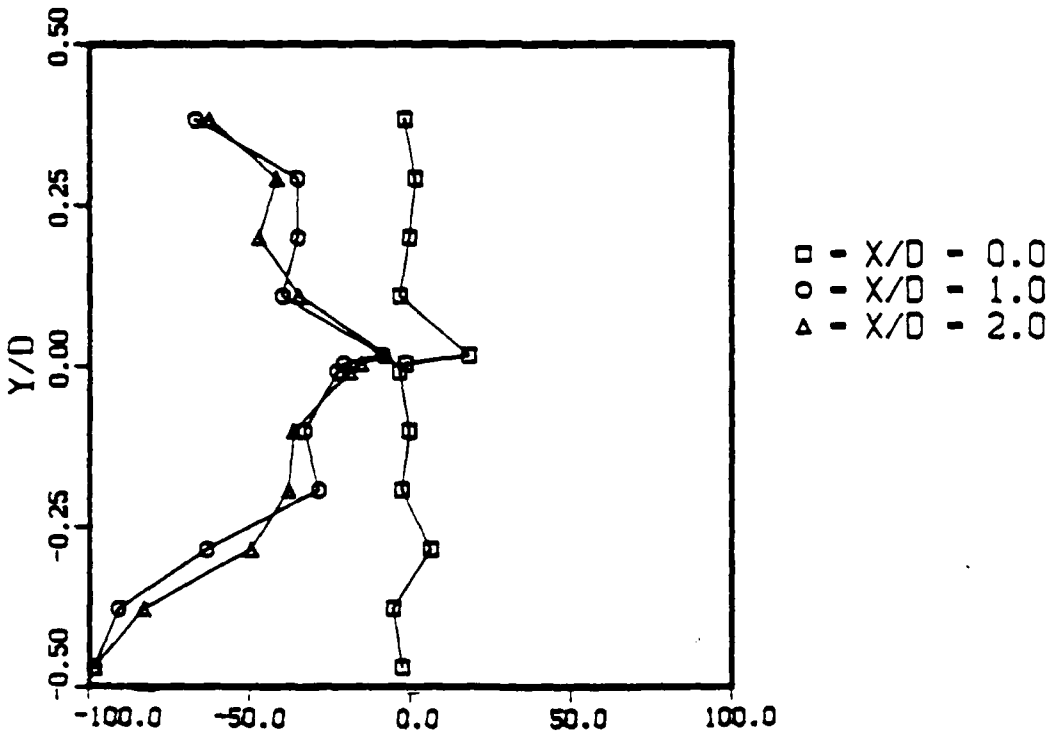

(b) Percent Difference $\ell, \varepsilon \sim C_\mu^{1.0}$

Figure 5.8 Percent Difference Between Experimental and Predicted Length Scales for Case 1: (a) $\varepsilon \sim C_\mu^{0.5}$ and (b) $\varepsilon \sim C_\mu^{1.0}$

liquid computations as utilized by Anderson et al. (1982) in ADD, PTRAK, and VAPDIF is too severe an approximation for modeling prevaporizing/premixing tubes. In many practical designs, wakes and/or shear layers will result from the fuel insertion scheme, and the present studies document the difficulties to be expected with the (as-received or modified) ADD code. Significant improvement in the techniques used to model these and other two-phase flows is required.

6.0. Future Efforts

The primary focus of program continuation is centered on the design and development of an improved experimental facility and implementation of new diagnostic systems. The new turbulent shear layer test section will be designed to permit studies of turbulent dispersion, of atomization using a wider range of liquids, and to extend the existing datum base for investigating two-phase flow models. In addition, improvements in inlet flow design will be made so that the freestream scale of turbulence can be varied to ascertain its effect on turbulent mixing and atomization. The tunnel redesign will incorporate improvements to eliminate the problems encountered in the previous facility (Section 3.1), and the atomizer will be modified to eliminate leakage and spray impingement on the windows.

Diagnostic improvements are also planned to facilitate the study of two-phase turbulent flows. The recent acquisition of a Phase/Doppler Particle Analyzer (P/DPA) (Bachalo and Houser, 1984) will make detailed measurements of droplet size and velocity distributions in the spray possible. P/DPA measurements are based on the flux of droplets passing through the probe volume eliminating the drawbacks associated with number density based drop sizing instruments (Tallio, 1987). The usefulness of this approach for measuring two-phase flow parameters has been demonstrated by Rudoff et al. (1987), who measured drag coefficients as a function of drop diameter in a polydisperse spray.

Turbulent spray dispersion will be studied to examine the methods currently used to model this phenomenon. The P/DPA's ability to correlate size and velocity also facilitates tracking of the gas-phase flow (using droplets sufficiently small to follow the airflow). Droplet flux measurements to locate the edge of the spray sheet, corresponding to a measure of dispersion, can then be obtained by traversing the instrument across the flow in the Y-direction. Finally, using the experimental data obtained near the inlet plane for both the gas and liquid-phase flows where the spray becomes dilute, finite difference computations of the two-phase flowfield as it develops downstream can be compared with the experimental values.

The effect of atomizer aerodynamics on airblast atomization quality is another area of interest. Sattlemayer and Wittig (1986), using a two-dimensional atomizer, found that the presence of a shear layer in the gas-phase at the atomizer tip can have a significant impact on atomization quality. Aigner and Wittig (1987) observed similar results with an axisymmetric atomizer, and, as discussed in Section 4.4, the same effects were observed in this study using a two-dimensional atomizer. To date, no experimental investigations have focused on the effects of freestream turbulence parameters on atomization quality. Wittig et al. (1987) investigated the influence of turbulence on droplet size distributions in sprays; however, their turbulent flowfield quantities were not measured, but rather computed based on mean flow quantities measured at the inlet plane. The effect of rms velocity and turbulent length scale on mean drop size and drop size distribution are areas that warrant investigation.

The redesign of the experimental facility will allow the studies noted above to be performed for a wide range of fuels to investigate liquid property effects. Initially, distilled water will be used for system verification. Later studies will incorporate both single, bi- and multicomponent liquids. Sattlemayer and Wittig (1986) have investigated water/ethanol and water/glycerine mixtures to vary the liquid surface tension and viscosity. Although the water/glycerine mixture will increase the viscosity by one order of magnitude, calculations using Eq. 2.12 show only a seven percent change in SMD. This change is small, but the effect of liquid viscosity on spray penetration normal to the flow should be investigated. Unlike variations in viscosity, increasing the liquid surface tension by adding ethanol can have a significant impact on the SMD. If pure ethanol is used a decrease of fifty percent is predicted by the correlation. These two liquids will be used initially to investigate property effects and later work will be extended to typical aviation type fuels.

Changes in the gas-phase flowfield induced by the presence of the spray is another area of interest. Characterizing these effects will assist in the development of improved models for the disperse phase flow (e.g., SSF models (Faeth, 1987)) which use the turbulent velocities to predict particle trajectories.

Measuring experimental values of the local droplet evaporation coefficient, β, should be possible with the P/DPA which can decouple the effects of evaporation from those of laminar dispersion. A combusting flow test section, similar to Fig. 4.36, is envisioned for this work to provide the large temperature gradients necessary for enhanced evaporation. The shear layer surrounding the recirculation zone formed downstream of the rearward facing step will be used to stabilize the flame. Data obtained in these studies can be used to complete validation of the droplet lifetime parameter, τ_{eb}, in the characteristic time model.

Continuing investigation of the turbulent mixing time parameter in the characteristic time model will focus on freestream turbulence variations. The existing datum base comparing the local values of mixing times at the origin of the shear layer with those defined by the model can be expanded and augmented with the length scale variations to provide additional data for validation of this parameter.

The relationship between shear layer strength for the experimental configuration and entrainment ratio in an actual combustor is another issue to be addressed. A literature review is planned to evaluate the effects of combustor geometry on entrainment ratio. The ultimate objective here is to modify the mixing time parameter based on the results discussed in Section 4.4.6, defined for a combustor, to reduce the scatter in the correlation. Additional experiments using the rearward facing step rig may be warranted for final refinement of the model.

Section 5 identified problems inherent in finite difference modeling of turbulent flows. Further work in this area will focus on obtaining more realistic predictions of mean and rms velocity and length scale. Initially, the effect of anisotropy of the turbulence will be investigated by suitably modifying the initial conditions for the ADD code. Should these studies prove fruitful, fine tuning of the constants in the turbulence model may be warranted; however, it is difficult to justify extensive work in this area since other codes with less-restrictive assumptions, and thus capable of better predictions of the two-phase flowfield, are available.

REFERENCES

Abdalla, A.Y., Ali, B.B., Bradley, D. and Chin, S.B. (1981). "Stratified Combustion in Recirculating Flow," Combust. Flame, 43, 131-143.

Aigner, M. and Wittig, S. (1987). "Swirl and Counterswirl Effects in Prefilming Airblast Atomizers," ASME Paper No. 87-GT-204.

Altenkirch, R.A. and Mellor, A.M. (1975). "Emissions and Performance of Continuous Flow Combustors," Fifteenth Symposium (International) on Combustion, The Combustion Institute, Pittsburgh, 1181-1189.

Anderson, D.A., Tannehill, J.C. and Pletcher, R.H. (1984). Computational Fluid Mechanics and Heat Transfer, Hemisphere, New York.

Anderson, O.L., (1980). "Calculation of Internal Viscous Flows in Axisymmetric Ducts at Moderate to High Reynolds Number," J. Computers and Fluids, 8, 391-411.

Anderson, O.L. (1988). Personal Communication 7/88.

Anderson, O.L., Chiappetta, L.M., Edwards, D.E. and McVey, J.B. (1982). "Analytical Modeling of Operating Characteristics of Premixing-Prevaporizing Fuel-Air Mixing Passages," Vol. 1 and 2 NASACR-167990.

Bachalo, W.D. and Houser, M.J. (1984). "Phase/Doppler Spray Analyzer for Simultaneous Measurements of Drop Size and Velocity," J. Opt. Eng., 23, 583-590.

Bradshaw, P., Cebeci, T., and Whitelaw, J.H. (1981). Engineering Calculation Methods for Turbulent Flow, Academic Press, London.

Brown, G.L. and Roshko, A. (1974). "On Density Effects and Large Scale Structure in Turbulent Mixing Layers," J.Fluid Mech., 64, 775-816.

Coles, D. (1956). "The Law of the Wake in a Turbulent Boundary Layer," J. Fluid Mech., 1, 191-224.

Derr, W.S. and Mellor, A.M. (1987). "Characteristic Times for Lean Blowoff in Turbine Combustors," J. Propulsion Power, 3, 377-380.

Dobbins, R.A., Crocco, L. and Glassman, I. (1963). "Measurement of Mean Particle Size from Diffractively Scattered Light," AIAA Journal, 8, 1882-1886.

Dobbins, R.A. and Jizmagian, G.S. (1966). "Optical Scattering Cross-Sections for Polydispersions of Dielectric Spheres," J. Opt. Soc. Am., 56, 1345-1350.

Dodge, L.G. (1987). "Comparison of Performance of Drop-Sizing Instruments," Applied Optics, 26, 1328-1341.

Dodge, L.G. and Moses, M.A. (1984). "Diagnostics for Fuel Sprays as Applied to Emulsified Fuels," Twentieth Symposium (International) on Combustion, The Combustion Institute, Pittsburgh, 1239-1247.

El Shanawany, M.S. and Lefebvre, A.H. (1980). "Airblast Atomization: The Effect of Linear Scale on Mean Drop Size," ASME Paper No. 80-GT-74.

Faeth, G. (1987). "Mixing, Transport and Combustion in Sprays," Prog. Energy Combust. Sci., 13, 293-345.

Farouk, B. (1988). Final Report for Contract DAAL03-87-K-0015, Army Research Office.

Godsave, G.A.E. (1953). "Studies of the Combustion of Drops in a Fuel Spray--The Burning of Single Drops of Fuel." Fourth Symposium (Intl.) on Combustion, Williams and Williams, Baltimore, 818-830.

Gosman, A.D. and Ioannides, E. (1983). "Aspects of Computed Simulation of Liquid-Fueled Combustors," J. Energy, 7, 482-490.

Gretzinger, I. and Marshall, W.R. (1961). "Characteristics of Pneumatics Atomization," AICHE J., 17, 312-318.

Halliday, D. and Resnick, R. (1974). Fundamentals of Physics, John Wiley and Sons, New York.

Jarymowycz, T.A. and Mellor, A.M. (1986). "Correlation of Lean Blowoff in an Annular Combustor," J. Propulsion Power, 2, 190-192.

Jasuja, A.K. (1979). "Atomization of Crude and Residual Fuel Oils," Trans. ASME, 101, 250-258.

Lefebvre, A.H. (1980). "Airblast Atomization," Prog. Energy Combust. Sci., 6, 233-261.

Lefebvre, A.H. (1983). Gas Turbine Combustion, Hemisphere, Cambridge.

Leonard, P.A. and Mellor, A.M. (1983). "Correlation of Gas Turbine Combustor Efficiency," J. Energy, 7, 596-602.

Marakovits, S. (1987). "Characterization of a Confined Turbulent Shear Layer," MSME Thesis, Dept. of Mechanical Engineering, Drexel University.

Mellor, A.M. (1976). "Gas Turbine Engine Pollution," Prog. Energy Combust. Sci., 1, 111-113.

Mellor, A.M. (1977). "Characteristic Time Emissions Correlations: the T-63 Helicopter Gas Turbine Combustor," J. Energy, 1, 257-262.

Mellor, A.M. (1980). "Semi-Empirical Correlations for Gas Turbine Emissions, Ignition and Flame Stabilization," Prog. Energy Combust. Sci., 6, 347-358.

Peters, J.E. and Mellor, A.M. (1982). "A Spark Ignition Model for Liquid Fuel Sprays Applied to Gas Turbine Engines," J. Energy, 6, 272-274.

Plee, S.L. and Mellor, A.M. (1979). "Characteristic Time Correlations for Lean Blowoff of Bluff-Body-Stabilized Flames," Combust. Flame, 35, 61-80.

Pope, S.B. and Whitelaw, J.H. (1976). "The Calculation of Near Wake Flows," J. Fluid Mech., 73, 9-32.

Ranz, W.E. and Marshall, W.R. (1952). "Evaporation From Drops," Chem. Eng. Prog. 48, 173-180.

Rizk, N.K. (1976). "Studies on Liquid Sheet Disintegration in Airblast Atomizers," Ph.D. Thesis, School of Mechanical Engineering, Cranfield Institute of Technology.

Rizk, N.K. and Lefebvre, A.H. (1982). "Airblast Atomization: Studies on Drop Size Distribution," J. Energy, 6, 823-827.

Rizk, N.K. and Mongia, H.C. (1986). "Gas Turbine Combustor Design Methodology," AIAA Paper No. 86-1531.

Rizkalla, A.A. and Lefebvre, A.H. (1975a). "Influence of Liquid Properties on Airblast Atomizer Spray Characteristics," Trans. ASME, 97, 173-179.

Rizkalla, A.A. and Lefebvre, A.H. (1975b). "The Influence of Air and Liquid Properties on Airblast Atomization," Trans. ASME, 97, 316-320.

Rudoff, R.C. and Bachalo, W.D. (1988). "Measurements of Droplet Drag Coefficients in a Polydispersed Turbulent Flow Field," AIAA Paper No. 88-0235.

Rudoff, R.C., Houser, M.J. and Bachalo, W.D. (1987). "Two-Phase Flow Measurements of a Spray in a Turbulent Flow," AIAA Paper No. 87-0062.

Sattlemayer, T. and Wittig, S. (1987). "Internal Flow Effects in Prefilming Airblast Atomizers: Mechanisms of Atomization and Droplet Spectra," ASME Paper No. 86-GT-150.

Simmons, H.C. (1977). "The Correlation of Drop-Size Distribution in Fuel Nozzle Sprays," J. Eng. Power, 99, pp. 309-319.

Simmons, H.C. (1979). "The Prediction of Sauter Mean Diameter for Gas Turbine Fuel Nozzles of Different Types," ASME Paper No. 79-WA/GT-5.

Strahle, W.C. and Lekoudis, S.G., Editors (1985). "Evaluation of Data on Simple Turbulent Reacting Flows," AFOSR-TR-85-0880.

Swithenbank, J., Beer, J., Taylor, D., Abbot, D. and McCreath, G. (1976). "A Laser Diagnostic Technique for Measurement of Droplet and Particle Size Distributions," AIAA Paper No. 76-69.

Tallio, K.V. (1987). "Atomization in a Turbulent Shear Layer," MSME Thesis, Dept. of Mechanical Engineering, Drexel University.

Tennekes, H. and Lumley, J.L. (1972). A First Course in Turbulence, The MIT Press, Cambridge.

Tuttle, J.H., Colket, M.B., Bilger, R.W. and Mellor, A.M. (1977). "Characteristic Times for Combustion and Pollutant Formation in Spray Combustion," Sixteenth Symposium (International) on Combustion, The Combustion Institute, Pittsburgh, 209-219.

Wigg, J. (1964). "Drop Size Predictions for Twin Fluid Atomizers," J. Inst. Fuels, 27, 500-505.

Wittig, S., Klausmann, W., and Noll, B. (1987). "Turbulence Effects on the Droplet Distribution Behind Airblast Atomizers," AGARD CP-422.

Zukoski, E.E. and Marble, F.E. (1956). "Experiments Concerning the Mechanism of Flame Blowoff from Bluff Bodies," Proceedings of Gas Dynamics Symposium on Aerothermochemistry, Northwestern University, 205-210.

Appendix A:

Experimental Mean and rms Velocity, and Length Scale Results for the Two-Phase Flow Matrix

Case 1 , Y-Profile, Z/D = -0.25, Gas Phase

X/D = -0.66			X/D = 0.03		
Y/D	Ux m/s	urms m/s	Y/D	Ux m/s	urms m/s
0.475	78.60	6.92	0.475	69.44	8.92
0.462	93.48	6.63	0.462	73.31	8.42
0.449	86.97	6.54	0.449	77.00	7.63
0.436	90.21	6.52	0.436	79.13	7.12
0.423	92.62	6.35	0.423	81.29	6.79
0.409	94.65	6.20	0.409	83.01	6.40
0.383	97.86	5.78	0.383	86.28	5.81
0.357	100.65	5.34	0.357	88.48	5.27
0.344	102.16	5.09	0.344	89.61	5.01
0.331	103.37	4.66	0.331	90.60	4.61
0.304	105.21	4.30	0.304	91.88	4.23
0.278	106.29	3.94	0.278	92.51	3.82
0.252	106.43	3.77	0.252	92.71	3.57
0.213	105.03	4.13	0.213	91.58	3.75
0.186	103.82	4.54	0.186	90.26	4.12
0.147	99.23	5.34	0.147	86.63	5.07
0.121	95.44	5.86	0.121	83.12	5.69
0.081	85.30	6.46	0.081	73.83	7.81
-0.089	95.99	5.92	0.055	58.82	10.02
-0.115	100.30	5.52	0.042	47.60	9.85
-0.142	104.00	5.07	0.029	37.92	8.58
-0.181	107.70	4.13	0.016	30.64	5.90
-0.207	108.83	3.63	0.003	38.47	9.55
-0.247	108.85	3.43	-0.010	48.72	9.42
-0.273	108.19	3.70	-0.024	60.25	10.04
-0.312	106.27	3.99	-0.037	68.03	9.52
-0.339	104.52	4.38	-0.050	75.33	8.30
-0.378	101.45	4.85	-0.063	80.45	7.58
-0.404	99.22	5.16	-0.089	86.95	6.52
-0.417	97.61	5.34	-0.115	91.22	5.61
-0.430	96.20	5.62	-0.142	94.38	4.95
-0.444	94.51	5.80	-0.181	97.25	4.14
-0.457	92.27	5.83	-0.207	97.70	3.82
-0.470	87.58	6.18	-0.247	97.09	4.04
-0.483	78.39	6.86	-0.273	96.05	4.44
-0.496	41.55	5.03	-0.312	93.65	4.93
			-0.339	91.87	5.33
			-0.378	88.38	5.91
			-0.404	85.76	6.64
			-0.417	83.71	6.91
			-0.430	81.53	7.30
			-0.444	79.11	7.86
			-0.457	73.97	8.80
			-0.470	67.43	8.89
			-0.483	58.22	8.36
			-0.496	34.37	6.41

Case 1 , Y-Profile, Z/D = -0.25, Gas Phase

X/D = 1.00			X/D = 2.00		
Y/D	Ux m/s	urms m/s	Y/D	Ux m/s	urms m/s
0.475	60.16	8.93	0.475	62.39	7.58
0.462	63.20	9.09	0.462	63.89	7.69
0.449	65.94	9.39	0.449	65.81	8.05
0.436	69.17	9.37	0.436	67.81	8.05
0.423	72.19	9.09	0.423	69.21	8.12
0.409	74.95	8.62	0.409	71.41	8.21
0.383	79.70	7.69	0.383	75.72	7.98
0.357	83.56	6.23	0.357	79.82	7.22
0.344	84.93	5.79	0.344	81.54	6.84
0.331	86.21	5.26	0.331	83.00	6.28
0.304	87.69	4.61	0.304	85.60	5.33
0.278	89.14	4.32	0.278	87.17	4.67
0.252	89.50	3.95	0.252	87.72	4.19
0.213	88.63	4.48	0.213	86.56	4.60
0.186	87.14	4.94	0.186	85.27	5.25
0.147	82.64	6.70	0.147	81.00	6.61
0.121	78.31	7.96	0.121	77.85	6.93
0.081	70.55	8.61	0.081	73.35	7.02
0.055	66.02	7.88	0.055	71.06	6.65
0.042	64.94	7.69	0.042	70.55	6.45
0.029	64.56	7.57	0.029	70.33	6.47
0.016	64.69	7.80	0.016	70.25	6.60
0.003	65.61	8.01	0.003	70.87	6.98
-0.010	67.19	8.69	-0.010	71.41	7.12
-0.024	69.55	9.22	-0.024	72.18	7.62
-0.037	72.18	9.80	-0.037	73.77	8.11
-0.050	75.05	9.89	-0.050	74.70	8.29
-0.063	78.44	9.69	-0.063	76.60	8.54
-0.089	84.38	8.73	-0.089	80.55	8.66
-0.115	88.67	6.89	-0.115	84.34	8.03
-0.142	91.93	5.32	-0.142	87.53	7.08
-0.181	93.71	4.20	-0.181	90.55	5.36
-0.207	93.49	4.25	-0.207	90.90	4.86
-0.247	92.09	4.54	-0.247	89.71	4.95
-0.273	90.18	4.98	-0.273	88.32	5.43
-0.312	87.28	5.66	-0.312	84.32	6.33
-0.339	84.73	6.26	-0.339	81.21	7.09
-0.378	79.83	7.56	-0.378	75.49	7.86
-0.404	74.84	8.68	-0.404	71.56	7.99
-0.417	72.07	9.03	-0.417	69.61	8.06
-0.430	69.13	9.03	-0.430	67.39	8.11
-0.444	65.76	9.04	-0.444	65.72	7.92
-0.457	62.17	8.66	-0.457	62.89	7.64
-0.470	57.93	8.41	-0.470	60.31	7.52
-0.483	51.86	7.65	-0.483	55.88	7.21
-0.496	23.76	4.91	-0.496	28.33	4.92

Case 1 , Y-Profile, Z/D = 0.00, Gas Phase

X/D = -0.66			X/D = 0.03		
Y/D	Ux m/s	urms m/s	Y/D	Ux m/s	urms m/s
0.475	86.41	6.44	0.475	85.43	7.36
0.462	91.11	6.06	0.462	88.20	6.93
0.449	96.05	5.86	0.449	91.01	6.38
0.436	98.76	5.71	0.436	93.23	5.84
0.423	101.39	5.47	0.423	94.75	5.35
0.409	103.51	4.97	0.409	95.87	5.04
0.383	106.43	4.09	0.383	97.56	4.40
0.357	108.11	3.65	0.357	98.52	3.84
0.344	108.67	3.52	0.344	98.51	3.69
0.331	108.78	3.45	0.331	98.36	3.68
0.304	108.61	3.65	0.304	97.76	3.74
0.278	107.48	4.11	0.278	96.78	4.19
0.252	105.93	4.54	0.252	95.43	4.63
0.213	103.13	4.95	0.213	92.31	5.34
0.186	101.03	5.36	0.186	89.63	5.73
0.147	97.42	5.82	0.147	84.52	6.36
0.121	93.89	6.21	0.121	80.75	6.71
-0.089	97.56	6.81	0.081	72.42	7.83
-0.115	101.72	6.46	0.055	60.08	9.85
-0.142	104.78	6.04	0.042	50.40	10.28
-0.181	108.51	5.40	0.029	38.48	9.19
-0.207	110.16	4.97	0.016	35.00	6.39
-0.247	112.23	4.29	0.003	45.17	9.16
-0.273	113.29	4.10	-0.010	57.61	9.85
-0.312	113.84	3.91	-0.024	67.95	9.35
-0.339	112.86	4.14	-0.037	74.43	8.40
-0.378	110.25	4.72	-0.050	78.97	7.95
-0.404	107.36	5.31	-0.063	82.23	7.50
-0.417	105.38	5.76	-0.089	86.76	6.94
-0.430	103.16	5.97	-0.115	90.24	6.41
-0.444	100.29	6.28	-0.142	92.93	5.89
-0.457	97.26	6.27	-0.181	96.46	5.19
-0.470	90.92	6.67	-0.207	98.39	4.78
-0.483	82.23	7.14	-0.247	100.56	4.28
-0.496	47.49	6.29	-0.273	100.93	4.11
			-0.312	100.71	4.43
			-0.339	99.74	4.92
			-0.378	96.24	5.76
			-0.404	93.01	6.48
			-0.417	90.84	6.99
			-0.430	87.69	7.44
			-0.444	84.18	7.77
			-0.457	80.14	8.23
			-0.470	74.28	8.82
			-0.483	64.07	8.59
			-0.496	36.53	6.89

Case 1 , Y-Profile, Z/D = 0.00, Gas Phase

X/D = 1.00			X/D = 2.00		
Y/D	Ux m/s	urms m/s	Y/D	Ux m/s	urms m/s
0.475	79.29	7.62	0.475	77.25	7.37
0.462	81.93	7.58	0.462	80.05	7.19
0.449	85.21	7.05	0.449	82.17	7.05
0.436	87.80	6.50	0.436	84.75	6.85
0.423	89.91	5.86	0.423	86.71	6.23
0.409	91.63	5.41	0.409	88.73	5.88
0.383	80.35	7.42	0.383	91.20	4.88
0.357	94.63	3.94	0.357	92.38	4.17
0.344	94.99	3.73	0.344	92.88	3.89
0.331	95.10	3.71	0.331	93.24	3.83
0.304	94.89	3.69	0.304	93.06	3.76
0.278	94.23	4.12	0.278	92.61	3.98
0.252	92.73	4.65	0.252	90.73	4.62
0.213	89.65	5.30	0.213	87.29	5.59
0.186	87.42	5.75	0.186	84.75	6.35
0.147	82.24	6.96	0.147	79.55	6.97
0.121	77.83	7.95	0.121	76.19	6.93
0.081	69.58	8.12	0.081	71.89	6.11
0.055	65.29	6.94	0.055	70.52	5.83
0.042	64.49	6.57	0.042	70.38	5.71
0.029	64.43	6.40	0.029	70.79	5.91
0.016	65.10	6.99	0.016	71.70	6.32
0.003	67.42	7.63	0.003	72.45	6.59
-0.010	70.11	8.28	-0.010	73.80	7.12
-0.024	73.01	8.59	-0.024	75.31	7.42
-0.037	75.72	8.84	-0.037	76.77	7.52
-0.050	78.80	8.59	-0.050	79.00	7.75
-0.063	81.16	8.09	-0.063	80.37	7.69
-0.089	85.51	6.99	-0.089	84.27	7.38
-0.115	88.58	5.98	-0.115	86.93	6.67
-0.142	90.76	5.61	-0.142	89.80	5.87
-0.181	93.52	4.79	-0.181	92.63	4.83
-0.207	94.64	4.34	-0.207	94.07	4.47
-0.247	96.14	4.15	-0.247	94.93	4.21
-0.273	96.68	4.28	-0.273	94.80	4.38
-0.312	95.87	4.60	-0.312	93.52	5.19
-0.339	94.68	5.19	-0.339	91.87	5.77
-0.378	90.85	6.09	-0.378	86.92	6.96
-0.404	86.88	6.95	-0.404	82.83	7.56
-0.417	84.14	7.38	-0.417	80.26	7.64
-0.430	80.92	7.77	-0.430	77.81	8.03
-0.444	77.03	8.12	-0.444	74.89	7.96
-0.457	72.75	8.28	-0.457	70.92	7.71
-0.470	68.05	8.02	-0.470	67.16	7.65
-0.483	61.60	7.41	-0.483	61.16	7.26
-0.496	34.46	5.89	-0.496	35.25	6.11

Case 1 , Y-Profile, Z/D = 0.25, Gas Phase

X/D = -0.66			X/D = 0.03		
Y/D	Ux m/s	urms m/s	Y/D	Ux m/s	urms m/s
0.475	82.40	5.87	0.475	70.58	8.60
0.462	86.36	5.65	0.462	73.23	8.06
0.449	89.22	5.66	0.449	76.63	7.63
0.436	91.77	5.53	0.436	79.32	7.44
0.423	93.08	5.50	0.423	81.53	6.92
0.409	95.36	5.16	0.409	83.75	6.79
0.383	98.06	4.83	0.383	86.63	6.06
0.357	100.60	4.36	0.357	89.20	5.32
0.344	101.66	4.23	0.344	90.36	5.17
0.331	102.45	3.98	0.331	91.36	5.10
0.304	103.59	3.65	0.304	92.70	4.40
0.278	104.26	3.47	0.278	93.21	4.15
0.252	104.09	3.50	0.252	92.96	4.03
0.213	103.16	3.96	0.213	91.35	4.50
0.186	101.69	4.44	0.186	88.85	5.03
0.147	98.98	5.27	0.147	84.17	5.85
0.121	95.53	5.71	0.121	80.44	6.16
-0.089	94.28	6.46	0.081	70.33	7.68
-0.115	99.96	6.09	0.055	57.37	9.70
-0.142	103.86	5.77	0.042	46.76	9.58
-0.181	108.02	4.89	0.029	37.06	9.04
-0.207	109.60	4.32	0.016	31.06	6.84
-0.247	110.87	3.71	0.003	35.87	6.93
-0.273	110.41	4.07	-0.010	48.53	9.37
-0.312	108.61	4.54	-0.024	59.80	9.71
-0.339	106.33	4.77	-0.037	68.81	9.05
-0.378	102.29	5.13	-0.050	74.36	8.25
-0.404	99.06	5.43	-0.063	79.11	7.39
-0.417	97.22	5.55	-0.089	85.04	6.81
-0.430	95.12	5.70	-0.115	89.35	6.31
-0.444	92.87	5.75	-0.142	92.68	5.64
-0.457	90.19	5.85	-0.181	95.93	4.87
-0.470	86.37	5.97	-0.207	97.23	4.25
-0.483	79.16	6.48	-0.247	97.41	4.10
-0.496	51.95	6.13	-0.273	96.70	4.22
			-0.312	94.06	5.05
			-0.339	91.64	5.56
			-0.378	86.51	6.07
			-0.404	82.91	6.57
			-0.417	80.27	6.94
			-0.430	77.28	7.44
			-0.444	73.69	7.93
			-0.457	68.83	8.52
			-0.470	62.90	8.76
			-0.483	55.23	8.40
			-0.496	30.51	6.92

Case 1 , Y-Profile, Z/D = 0.25, Gas Phase

X/D = 1.00			X/D = 2.00		
Y/D	Ux m/s	urms m/s	Y/D	Ux m/s	urms m/s
0.475	62.38	8.92	0.475	61.84	7.55
0.462	64.67	9.07	0.462	63.22	7.66
0.449	67.57	9.20	0.449	65.62	7.99
0.436	70.73	9.18	0.436	67.47	8.15
0.423	73.58	8.76	0.423	69.94	8.40
0.409	76.64	8.46	0.409	71.90	8.52
0.383	81.01	7.15	0.383	76.61	8.14
0.357	84.32	6.34	0.357	81.34	7.57
0.344	85.70	5.80	0.344	83.37	7.09
0.331	86.75	5.37	0.331	84.55	6.66
0.304	88.77	4.80	0.304	87.61	5.38
0.278	90.17	4.31	0.278	89.47	4.45
0.252	89.91	4.12	0.252	89.70	4.12
0.213	88.35	4.69	0.213	88.50	4.94
0.186	86.25	5.48	0.186	86.14	5.90
0.147	81.51	6.63	0.147	81.36	7.21
0.121	77.21	7.58	0.121	77.23	7.55
0.081	68.74	8.14	0.081	72.42	7.17
0.055	64.21	7.67	0.055	70.19	6.66
0.042	62.62	7.15	0.042	69.79	6.65
0.029	61.36	7.03	0.029	69.40	6.51
0.016	61.34	7.34	0.016	69.62	6.70
0.003	61.73	7.82	0.003	69.81	7.01
-0.010	63.53	8.41	-0.010	70.85	7.25
-0.024	65.74	9.03	-0.024	72.23	7.68
-0.037	68.53	9.60	-0.037	73.06	7.93
-0.050	71.46	9.62	-0.050	74.89	8.52
-0.063	74.18	9.92	-0.063	77.08	8.63
-0.089	80.42	9.16	-0.089	80.42	8.92
-0.115	85.26	7.99	-0.115	84.68	8.79
-0.142	88.67	6.92	-0.142	88.15	7.86
-0.181	91.87	5.66	-0.181	92.55	6.03
-0.207	93.09	5.14	-0.207	92.85	5.77
-0.247	92.53	4.83	-0.247	93.10	5.47
-0.273	91.60	5.09	-0.273	92.50	4.88
-0.312	88.18	5.64	-0.312	89.02	5.81
-0.339	84.95	6.27	-0.339	85.64	6.64
-0.378	78.53	7.60	-0.378	79.55	7.39
-0.404	72.20	8.50	-0.404	74.51	8.09
-0.417	68.89	8.72	-0.417	72.03	8.11
-0.430	65.89	8.64	-0.430	69.63	7.83
-0.444	61.88	8.55	-0.444	67.42	7.86
-0.457	58.90	8.28	-0.457	65.23	7.62
-0.470	54.96	8.14	-0.470	62.04	7.69
-0.483	44.45	6.79	-0.483	58.99	7.42
-0.496	25.40	5.84	-0.496	53.35	6.85

Case 1 , Y-Profile, Z/D = -0.25, Two Phase

X/D = 0.03			X/D = 1.00			X/D = 2.00		
Y/D	Ux m/s	urms m/s	Y/D	Ux m/s	urms m/s	Y/D	Ux m/s	urms m/s
0.475	59.69	9.72	0.475	55.40	9.38	0.475	57.29	8.14
0.462	66.39	9.66	0.462	60.54	9.54	0.462	60.20	8.57
0.449	71.00	9.17	0.449	64.37	9.91	-0.378	78.20	7.82
0.436	74.88	8.55	0.436	68.71	10.19	-0.404	74.69	8.14
0.423	78.52	8.16	0.423	72.09	9.60	-0.417	72.15	7.91
0.409	81.07	7.67	0.409	75.03	9.40	-0.430	69.69	8.17
0 383	85.14	6.96	0.383	79.08	9.17	-0.444	68.07	7.89
0.357	88.24	6.44	0.357	84.03	8.25	-0.457	65.87	7.63
0.344	90.07	6.16	0.344	86.12	7.19	-0.470	62.53	7.47
0.331	91.26	5.83	-0.273	94 39	5.88	-0.483	57.09	7.36
0.304	93.20	5.30	-0 312	90.81	5.59	-0.496	30.78	5.10
0.278	95.08	4.76	-0.339	88.56	6.08			
0.252	95 87	4.21	-0.378	83.79	7.37			
0.213	94.99	4.08	-0.404	78.64	8.76			
0.186	93.84	4.42	-0.417	76.04	9.15			
0 147	90.07	5.01	-0.430	72.62	9.20			
0.121	87.19	6.46	-0.444	69.33	9.17			
-0.050	84.89	7.31	-0.457	64.86	8.91			
-0.063	88.39	6.52	-0.470	61.00	8.50			
-0.089	92.56	5.45	-0.483	56.50	7.82			
-0.115	95.57	4.82	-0.496	28.00	5.53			
-0.142	97.84	5.80						
-0.181	99.40	3.70						
-0.207	99.37	3.77						
-0.247	98.54	4.15						
-0.273	97.43	4.43						
-0.312	94.86	4.90						
-0.339	93.12	5.31						
-0.378	90.13	5.93						
-0.404	87.31	6.35						
-0.417	85.80	6.73						
-0 430	83.44	7.19						
-0 444	80.89	7.83						
-0.457	75.73	8.37						
-0.470	69.55	8.78						
-0.483	59.95	8.42						
-0.496	30.72	5.64						

Case 1 , Y-Profile, Z/D = 0.00, Two Phase

X/D = 0.03			X/D = 1.00		
Y/D	Ux m/s	urms m/s	Y/D	Ux m/s	urms m/s
0.475	72.76	8.15	0.475	70.34	7.42
0.462	77.64	7.78	0.462	74.35	7.53
0.449	83.02	7.36	0.449	78.27	7.67
0.436	86.47	6.93	0.436	81.66	7.30
0.423	89.98	6.36	0.423	84.82	6.92
0.409	92.14	5.94	0.409	87.56	6.43
0.383	96.23	4.93	0.383	91.67	5.39
0.357	98.26	4.33	0.357	94.27	4.54
0.344	99.21	4.16	0.344	95.24	6.49
0.331	99.49	3.87	0.331	95.67	6.01
0.304	100.11	3.56	-0.247	100.02	7.76
0.252	99.17	4.53	-0.312	97.75	6.51
0.213	97.83	3.95	-0.339	96.00	5.26
0.186	97.27	4.42	-0.378	92.34	6.15
0.147	96.09	5.51	-0.404	88.40	7.00
-0.142	101.62	4.48	-0.417	85.42	7.43
-0.181	102.24	4.12	-0.430	82.50	7.97
-0.207	102.72	4.43	-0.444	78.60	8.21
-0.247	103.00	3.83	-0.457	73.84	8.13
-0.273	103.24	3.98	-0.470	69.18	7.94
-0.312	102.27	4.53	-0.483	61.57	7.48
-0.339	101.13	5.01	-0.496	37.66	6.29
-0.378	97.75	5.70			
-0.404	94.28	6.30			
-0.417	91.80	6.83			
-0.430	89.15	7.43			
-0.444	85.26	7.90			
-0.457	80.61	8.52			
-0.470	75.31	8.83			
-0.483	66.15	8.70			
-0.496	27.97	5.40			

Case 1 , Y-Profile, Z/D = 0.25, Two Phase

X/D = 0.03			X/D = 1.00			X/D = 2.00		
Y/D	Ux m/s	urms m/s	Y/D	Ux m/s	urms m/s	Y/D	Ux m/s	urms m/s
0.475	60.57	8.62	0.475	54.30	7.73	0.475	57.86	6.92
0.462	66.02	8.46	0.462	57.85	8.20	0.462	60.54	7.10
0.449	70.24	7.77	0.449	60.72	8.53	0.449	62.94	7.73
0.436	73.90	7.30	0.436	63.92	8.59	0.436	65.27	7.61
0.423	76.18	7.00	0.423	68.76	8.64	0.423	67.29	7.77
0.409	78.28	6.76	0.409	71.25	8.38	0.409	69.74	7.55
0.383	82.80	6.08	0.383	77.46	7.56			
0.357	85.64	5.52	0.357	81.76	6.51			
0.344	86.91	5.27	0.344	83.72	5.99			
0.331	88.19	5.13	0.331	85.26	5.63			
0.304	90.06	4.56	0.304	87.87	7.15			
0.278	91.30	4.00	-0.417	62.82	7.61			
0.252	92.33	3.74	-0.430	60.07	7.74			
0.213	92.34	3.76	-0.444	56.26	7.61			
0.186	91.57	4.02	-0.457	53.48	7.57			
0.147	89.41	4.68	-0.470	50.03	7.26			
-0.115	98.97	5.19	-0.483	45.53	6.67			
-0.142	100.36	4.46	-0.496	27.79	5.87			
-0.181	100.90	4.35						
-0.207	100.71	3.96						
-0.247	99.64	4.15						
-0.273	98.70	4.52						
-0.312	95.21	5.09						
-0.339	92.75	5.52						
-0.378	87.47	6.08						
-0.404	83.66	6.61						
-0.430	78.31	7.30						
-0.444	74.84	7.81						
-0.457	70.51	8.38						
-0.470	62.79	8.72						
-0.483	55.63	8.31						
-0.496	32.65	6.96						

Case 1, Z-Profile, Y/D = -0.25, Gas Phase

X/D = -0.66			X/D = 0.03		
Z/D	Ux m/s	urms m/s	Z/D	Ux m/s	urms m/s
0.475	47.93	10.41	0.475	60.89	11.69
0.462	69.22	9.81	0.449	66.04	11.67
0.449	85.55	8.55	0.436	71.75	11.53
0.436	93.27	7.24	0.423	76.42	10.34
0.423	96.95	6.50	0.409	80.33	9.42
0.409	99.21	5.98	0.383	85.95	6.85
0.383	102.13	5.00	0.370	88.38	5.93
0.370	103.39	4.63	0.344	90.95	4.62
0.344	105.38	3.87	0.278	94.04	3.47
0.278	107.26	3.18	0.213	94.20	3.55
0.213	106.64	3.39	0.147	94.05	3.59
0.147	105.67	3.57	0.081	93.87	3.70
0.081	104.73	3.74	0.016	93.78	3.57
0.016	104.43	3.69	-0.050	93.46	3.57
-0.050	104.88	3.50	-0.115	93.29	3.55
-0.115	104.94	3.18	-0.181	93.16	3.64
-0.181	104.93	2.95	-0.247	93.16	3.69
-0.247	104.57	2.89	-0.312	92.35	3.70
-0.312	103.61	3.08	-0.339	90.96	4.68
-0.339	102.19	3.64	-0.352	88.92	5.69
-0.352	100.86	4.08	-0.378	83.48	8.37
-0.378	97.24	5.27	-0.391	79.42	9.92
-0.391	94.99	5.92	-0.404	74.81	10.87
-0.404	92.14	6.68	-0.417	69.14	11.72
-0.417	87.21	7.60	-0.430	63.76	12.17
-0.430	76.60	8.80	-0.444	58.11	12.01
-0.444	49.45	10.33	-0.457	52.32	11.90
-0.457	26.24	7.33	-0.470	47.79	11.25
-0.470	27.05	7.63	-0.483	42.42	10.80
-0.483	41.74	6.59	-0.496	31.19	8.98
-0.496	29.05	6.07			

Case 1, Z-Profile, Y/D = -0.25, Gas Phase

X/D = 1.00			X/D = 2.00		
Z/D	Ux m/s	urms m/s	Z/D	Ux m/s	urms m/s
0.475	58.98	9.19	0.475	65.75	8.05
0.462	61.10	9.75	0.462	67.02	8.17
0.449	63.49	10.11	0.449	69.12	8.29
0.436	64.96	10.18	0.436	70.21	8.37
0.423	67.24	10.58	0.423	72.39	8.52
0.409	69.67	10.58	0.409	74.32	8.59
0.383	74.98	10.23	0.383	77.99	8.36
0.370	77.80	9.91	0.370	80.00	8.06
0.344	83.12	8.54	0.344	83.13	7.46
0.278	90.16	4.86	0.278	88.64	4.97
0.213	91.46	3.67	0.213	90.37	3.89
0.147	91.56	3.58	0.147	90.91	3.68
0.081	91.34	3.64	0.081	90.90	3.61
0.016	91.32	3.58	0.016	90.51	3.52
-0.050	90.88	3.54	-0.050	90.03	3.55
-0.115	90.29	3.68	-0.115	89.07	3.97
-0.181	89.44	3.98	-0.181	88.18	4.17
-0.247	89.45	3.98	-0.247	87.86	4.31
-0.312	88.30	4.77	-0.312	86.64	5.05
-0.339	85.98	6.11	-0.339	84.86	5.74
-0.352	84.36	6.67	-0.352	83.51	6.29
-0.378	79.71	8.32	-0.378	80.64	7.01
-0.391	77.48	8.50	-0.391	78.58	7.29
-0.404	75.08	8.87	-0.404	76.64	7.53
-0.417	71.98	9.05	-0.417	74.48	7.55
-0.430	69.68	9.22	-0.430	72.42	7.69
-0.444	67.09	9.04	-0.444	70.23	7.67
-0.457	64.62	9.03	-0.457	68.21	7.74
-0.470	61.34	8.85	-0.470	65.44	7.56
-0.483	57.00	8.34	-0.483	60.71	7.17
-0.496	41.39	7.60	-0.496	44.99	7.14

Case 1, Z-Profile, Y/D = 0.00, Gas Phase

X/D = 0.03			X/D = 1.00			X/D = 2.00		
Z/D	Ux m/s	urms m/s	Z/D	Ux m/s	urms m/s	Z/D	Ux m/s	urms m/s
0.475	30.62	8.22	0.475	55.20	7.41	0.475	59.86	6.30
0.462	30.69	7.88	0.462	56.10	7.60	0.462	60.53	6.17
0.449	32.39	8.25	0.449	56.51	7.53	0.449	61.34	6.24
0.436	33.23	8.18	0.436	57.48	7.54	0.436	62.15	6.25
0.423	33.76	8.21	0.423	58.64	7.61	0.423	62.83	6.25
0.409	33.66	8.15	0.409	59.24	7.44	0.409	63.76	6.23
0.383	32.15	8.09	0.383	60.82	7.62	0.383	65.40	6.28
0.370	31.23	8.28	0.370	61.68	7.47	0.370	66.20	6.19
0.344	30.88	7.82	0.344	62.78	7.35	0.344	67.41	6.14
0.278	35.88	7.31	0.278	63.93	6.75	0.278	69.63	5.54
0.213	39.56	7.20	0.213	64.17	6.14	0.213	70.04	5.35
0.147	40.84	7.53	0.147	65.06	6.02	0.147	70.17	5.07
0.081	39.39	7.46	0.081	65.24	5.91	0.081	70.27	5.05
0.016	39.11	7.16	0.016	65.21	5.89	0.016	70.64	5.07
-0.050	40.66	7.24	-0.050	66.20	6.13	-0.050	71.88	5.25
-0.115	39.73	6.74	-0.115	66.26	6.15	-0.115	71.36	5.23
-0.181	36.48	6.48	-0.181	64.21	6.20	-0.181	70.47	5.22
-0.247	32.91	5.73	-0.247	62.75	6.76	-0.247	68.77	5.63
-0.312	39.26	7.72	-0.312	61.19	7.56	-0.312	66.41	6.06
-0.339	40.83	7.97	-0.339	59.48	7.65	-0.339	65.39	6.16
-0.352	40.89	8.23	-0.352	58.56	7.70	-0.352	64.61	6.28
-0.378	39.27	8.43	-0.378	56.45	7.54	-0.378	62.87	6.08
-0.391	37.36	8.18	-0.391	55.19	7.50	-0.391	61.80	6.29
-0.404	35.10	8.32	-0.404	54.13	7.54	-0.404	60.99	6.22
-0.417	32.36	8.73	-0.417	52.72	7.54	-0.417	60.07	6.17
-0.430	30.55	8.58	-0.430	51.72	7.43	-0.430	58.62	6.12
-0.444	27.96	8.48	-0.444	50.79	7.47	-0.444	57.56	6.21
-0.457	25.43	8.51	-0.457	49.14	7.35	-0.457	56.32	6.07
-0.470	23.21	8.27	-0.470	47.73	7.33	-0.470	54.56	6.12
-0.483	20.19	8.09	-0.483	45.58	7.02	-0.483	52.45	6.04
-0.496	15.88	7.43	-0.496	39.38	7.19	-0.496	44.02	6.13

Case 1, Z-Profile, Y/D = 0.25, Gas Phase

X/D = -0.66			X/D = 0.03		
Z/D	Ux m/s	urms m/s	Z/D	Ux m/s	urms m/s
0.475	43.55	10.83	0.475	59.98	11.52
0.462	61.73	10.67	0.462	62.82	11.55
0.449	81.87	9.17	0.449	68.53	11.58
0.436	90.64	8.04	0.436	73.47	11.10
0.423	94.63	7.34	0.423	77.95	9.95
0.409	97.33	6.62	0.409	81.89	8.50
0.383	100.93	5.53	0.383	86.76	6.31
0.370	102.26	4.93	0.370	88.74	5.27
0.344	104.46	4.11	0.344	90.94	4.34
0.278	105.90	3.32	0.278	92.38	3.69
0.213	105.33	3.53	0.213	92.69	3.75
0.147	104.69	3.79	0.147	92.93	3.70
0.081	104.11	3.95	0.081	93.52	3.75
0.016	103.66	4.07	0.016	93.08	3.90
-0.050	103.41	4.06	-0.050	93.05	3.75
-0.115	103.34	3.87	-0.115	92.82	3.69
-0.181	103.55	3.27	-0.181	92.41	3.46
-0.312	100.32	3.75	-0.312	89.30	3.90
-0.339	98.08	4.43	-0.339	87.81	4.58
-0.352	96.42	4.93	-0.352	86.49	5.02
-0.378	93.13	5.81	-0.378	83.39	6.37
-0.391	91.04	6.47	-0.391	80.71	7.41
-0.404	88.21	7.23	-0.404	77.84	8.34
-0.417	85.38	7.70	-0.417	74.73	9.65
-0.430	78.25	8.69	-0.430	69.35	10.51
-0.444	58.30	10.70	-0.444	65.48	11.02
-0.457	30.64	8.84	-0.457	59.92	10.93
-0.470	17.77	5.57	-0.470	54.57	10.51
-0.483	16.54	4.67	-0.483	49.90	10.22
-0.496	18.41	4.51	-0.496	40.35	9.81

Case 1, Z-Profile, Y/D = 0.25, Gas Phase

X/D = 1.00			X/D = 2.00		
Z/D	Ux m/s	urms m/s	Z/D	Ux m/s	urms m/s
0.475	66.44	8.80	0.475	67.36	7.35
0.462	68.09	8.90	0.462	68.85	7.32
0.449	71.12	8.97	0.449	71.26	7.33
0.436	73.85	8.91	0.436	72.88	7.42
0.423	75.59	8.83	0.423	74.39	7.07
0.409	78.11	8.49	0.409	76.13	7.03
0.383	82.28	6.96	0.383	79.33	6.57
0.370	84.50	6.18	0.370	80.46	6.14
0.344	86.57	4.93	0.344	82.51	5.37
0.278	88.05	3.95	0.278	84.93	4.33
0.213	88.52	3.88	0.213	85.72	4.06
0.147	89.09	3.85	0.147	86.52	3.81
0.081	89.52	3.83	0.081	86.88	3.79
0.016	89.28	3.78	0.016	87.00	3.73
-0.050	89.29	3.75	-0.050	86.92	3.85
-0.115	88.83	3.63	-0.115	86.37	3.83
-0.181	87.96	3.74	-0.181	85.56	3.89
-0.247	86.78	3.94	-0.247	84.07	4.18
-0.312	83.46	5.31	-0.312	81.76	4.74
-0.339	80.77	6.55	-0.339	80.15	5.18
-0.352	78.88	7.37	-0.352	79.13	5.40
-0.378	75.37	8.22	-0.378	76.54	6.24
-0.391	72.80	8.63	-0.391	75.05	6.66
-0.404	70.14	8.89	-0.404	72.98	6.89
-0.417	67.80	8.95	-0.417	71.31	6.99
-0.430	65.70	8.96	-0.430	69.44	7.20
-0.444	63.17	9.13	-0.444	67.15	7.07
-0.457	60.54	9.12	-0.457	64.67	7.27
-0.470	58.10	8.80	-0.470	62.05	7.03
-0.483	53.20	8.54	-0.483	57.63	6.73
-0.496	46.87	8.19	-0.496	49.57	6.71

Case 1 , Z-Profiles, Two Phase

Y/D = -0.25			Y/D = 0.25		
X/D = 0.03			X/D = 0.03		
Z/D	Ux m/s	urms m/s	Z/D	Ux m/s	urms m/s
0.475	63.23	11.36	0.475	64.86	11.06
0.462	67.08	11.48	0.462	69.59	11.13
0.449	72.17	11.35	0.449	73.07	10.76
0.436	76.14	10.87	0.436	79.06	9.82
0.423	80.88	9.50	0.423	82.98	8.60
0.409	83.85	8.64	0.409	85.88	7.50
0.383	89.83	6.37	0.383	89.89	5.52
0.370	90.93	5.53	0.370	91.26	5.13
0.344	93.50	4.57	0.344	93.21	4.27
0.278	96.61	3.63	0.278	95.04	3.72
0.213	97.33	3.39	0.213	95.69	3.69
0.147	98.07	3.75	0.147	96.55	3.45
0.016	97.69	3.62	0.016	96.25	3.21
-0.115	95.99	4.54	-0.115	96.02	3.31
-0.181	95.25	3.96	-0.181	93.91	3.49
-0.247	95.40	3.70	-0.247	93.14	3.69
-0.339	91.98	5.09	-0.339	89.72	4.39
-0.352	90.17	6.07	-0.352	88.92	4.68
-0.378	84.38	8.81	-0.378	85.93	5.76
-0.404	74.63	11.91	-0.404	81.09	7.65
-0.430	62.68	12.62	-0.430	73.33	9.69
-0.444	56.79	12.48	-0.444	69.19	10.73
-0.457	51.38	12.51	-0.457	64.49	10.54
-0.470	45.98	11.98	-0.470	59.32	10.52
-0.483	41.10	11.33			
-0.496	30.94	10.11			

Case 14, Y-Profile, Z/D = -0.25, Gas Phase

X/D = -0.66			X/D = -0.33		
Y/D	Ux m/s	urms m/s	Y/D	Ux m/s	urms m/s
0.475	78.72	6.63	0.475	68.53	8.45
0.462	82.82	6.40	0.462	75.70	7.77
0.449	86.38	6.52	0.449	78.95	7.40
0.436	88.97	6.25	0.436	82.81	7.03
0.423	91.55	6.21	0.423	84.74	6.88
0.409	92.79	6.05	0.409	87.08	6.70
0.383	96.14	5.66	0.383	90.74	6.13
0.357	99.46	5.24	0.357	93.86	5.65
0.344	100.51	4.97	0.344	95.49	5.25
0.331	101.63	4.89	0.331	96.85	5.12
0.304	103.34	4.32	0.304	98.71	4.70
0.278	104.10	3.93	0.278	99.98	4.11
0.252	104.69	3.65	0.252	100.59	3.76
0.213	103.51	4.03	0.213	100.23	4.03
0.186	101.78	4.46	0.186	99.10	4.51
0.147	97.73	5.17	0.147	95.67	5.39
0.121	94.09	5.71	0.121	92.30	5.77
0.081	84.15	6.28	0.081	84.41	6.67
-0.089	61.84	4.99	-0.063	51.57	5.87
-0.115	65.56	4.66	-0.089	57.18	5.31
-0.142	68.67	4.28	-0.115	61.06	4.81
-0.181	71.11	3.68	-0.142	63.81	4.29
-0.207	72.71	3.31	-0.181	66.39	3.39
-0.247	72.90	3.01	-0.207	67.29	2.95
-0.273	72.58	3.10	-0.247	67.14	2.89
-0.312	71.28	3.39	-0.273	66.39	3.13
-0.339	70.32	3.61	-0.312	64.60	3.51
-0.378	68.10	3.86	-0.339	63.61	3.70
-0.404	66.57	4.07	-0.378	61.01	4.18
-0.417	65.71	4.22	-0.404	58.86	4.49
-0.430	64.23	4.36	-0.417	57.99	4.62
-0.444	63.32	4.56	-0.430	56.77	4.82
-0.457	61.68	4.67	-0.444	54.96	5.11
-0.470	59.51	4.84	-0.457	51.63	5.62
-0.483	53.85	5.03	-0.470	48.45	5.79
-0.496	31.97	4.92	-0.483	42.54	6.08
			-0.496	25.69	5.15

Case 14, Y-Profile, Z/D = -0.25, Gas Phase

X/D = 0.03			X/D = 0.50			X/D = 1.00		
Y/D	Ux m/s	urms m/s	Y/D	Ux m/s	urms m/s	Y/D	Ux m/s	urms m/s
0.475	73.67	8.66	0.475	67.41	9.39	0.475	63.61	9.00
0.462	77.55	8.13	0.462	70.60	9.44	0.462	65.68	9.17
0.449	80.08	7.40	0.449	74.83	8.95	0.449	68.34	9.11
0.436	83.27	6.87	0.436	78.07	8.44	0.436	71.91	9.31
0.423	85.27	6.52	0.423	81.02	7.86	0.423	74.35	8.98
0.409	86.98	6.31	0.409	83.29	7.30	0.409	76.76	8.54
0.383	89.52	5.62	0.383	86.63	6.37	0.383	81.85	7.44
0.357	92.27	5.06	0.357	89.28	5.72	0.357	85.46	6 30
0.344	93.00	4.92	0.344	90.38	5.41	0.344	87.02	5.78
0.331	93.96	4.74	0.331	91.22	5.31	0.331	87.57	5.42
0.304	95.29	4.44	0.304	92.78	4.76	0.304	89.38	4.97
0.278	95.91	3.90	0.278	93.84	4.43	0.278	90.06	4.81
0.252	96.12	3.72	0.252	94.28	4.39	0.252	90.38	4.85
0.213	95.27	3.88	0.213	93.33	4.65	0.213	90.45	4.93
0.186	94.30	4.11	0.186	92.60	4.91	0.186	89.69	5.18
0.147	91.07	4.71	0.147	90.56	5.57	0.147	87.23	5 58
0.121	88.44	5.40	0.121	88.43	5.81	0.121	84.70	6.74
0.081	80.04	7.01	0.081	82.33	7.61	0.081	77.62	9.01
0.055	66.98	9.29	0.055	73.37	10.43	0.055	69.92	10.56
0.042	58.36	9.37	0.042	67.55	11.35	0.042	66.39	10.61
0.029	46.31	8.67	0.029	61.36	11.52	0.029	62.54	10.70
0.016	29.87	6.40	0.016	55.27	10.79	0.016	59.71	10.12
0.003	20.79	5.38	0.003	50.51	9.50	0.003	55.86	9.10
-0.010	27.37	6.79	-0.010	46.37	8.13	-0.010	53.42	8.45
-0.024	31.90	7.09	-0.024	44.98	7.13	-0.024	51.22	7.51
-0.037	38.68	7.08	-0.037	44.84	6.54	-0.037	50.40	6.88
-0.050	43.66	6.60	-0.050	45.95	6.62	-0.050	49.63	6.12
-0.063	48.94	5.77	-0.063	48.15	6.49	-0.063	49.42	5.99
-0.089	54.29	5.14	-0.089	52.67	5.78	-0.089	50.72	5.53
-0.115	57.99	4.51	-0.115	56.05	4.72	-0.115	53.52	5.12
-0.142	60.85	3.83	-0.142	58.54	3.93	-0.142	55.87	4.20
-0.181	63.00	3.21	-0.181	60.14	3.26	-0.181	57.45	3.21
-0.207	63.73	2.96	-0.207	60.11	3.23	-0.207	57.27	3.13
-0.247	63.36	3.17	-0.247	59.21	3.60	-0.247	56.24	3.43
-0.273	62.44	3.37	-0.273	58.13	3.81	-0.273	54.98	3.83
-0.312	60.60	3.85	-0.312	55.60	4.36	-0.312	52.89	4.22
-0.339	59.11	4.12	-0.339	54.00	4.66	-0.339	50.54	4.94
-0.378	56.87	4.54	-0.378	50.70	5.63	-0.378	47.07	5.64
-0.404	54.54	4.94	-0.404	47.30	6.26	-0.404	43.37	6.35
-0.417	53.18	5.16	-0.417	45.49	6.63	-0.417	41.47	6.44
-0.430	51.55	5.58	-0.430	43.04	6.83	-0.430	39.39	6.44
-0.444	49.77	5.85	-0.444	40.37	6.79	-0.444	37.24	6.16
-0.457	46.22	6.45	-0.457	37.63	6.57	-0.457	35.50	5.95
-0.470	42.03	6.48	-0.470	34.71	6.45	-0.470	33.06	5.59
-0.483	36.45	6.24	-0.483	30.72	5.85	-0.483	29.94	5.35
-0.496	19.22	4.45	-0.496	15.52	4.35	-0.496	14.97	3.97

Case 14, Y-Profile, Z/D = -0.25, Gas Phase

X/D = 1.50			X/D = 2.00		
Y/D	Ux m/s	urms m/s	Y/D	Ux m/s	urms m/s
0.475	62.28	8.04	0.475	64.30	7.63
0.462	64.58	8.33	0.462	65.60	7.95
0.449	66.71	8.70	0.449	67.78	7.98
0.436	69.48	8.89	0.436	69.79	8.00
0.423	71.61	8.82	0.423	71.80	8.24
0.409	74.38	8.66	0.409	73.70	8.27
0.383	79.22	8.03	0.383	77.91	7.88
0 357	83.27	7.01	0.357	81.65	7.17
0 344	85.00	6.42	0.344	83.49	6.58
0.331	86.64	5.93	0.331	84.72	6.34
0 304	88.51	5.18	0.304	87.09	5 26
0 278	89 62	4.81	0.278	88.45	4 93
0.252	90.42	4.54	0.252	89.34	4.52
0.213	90.10	4.69	0.213	88.91	4.72
0.186	88.62	5.12	0.186	87.33	5.53
0 147	85.46	6.38	0.147	83.76	6.67
0 121	81.61	7.66	0.121	80.19	7.67
0 081	74.15	9.21	0.081	73 25	9.06
0 055	68.49	9 67	0.055	68.71	8.96
0 042	65.45	9.70	0.042	66.23	8.85
0 029	62.21	9.47	0.029	64.07	8.71
0.016	60.02	9.04	0.016	62.20	8.62
0.003	57.53	8.37	0.003	59.92	7.98
-0.010	55.81	7.91	-0.010	58.22	7.67
-0.024	54.41	7.20	-0.024	56.92	7.16
-0.037	53.07	6.46	-0.037	55.79	6.63
-0.050	52.40	6.17	-0.050	54.98	6.11
-0.063	52.15	5.54	-0.063	54.31	5.65
-0.089	52.63	5.22	-0.089	54.08	5.01
-0.115	54.08	4.96	-0.115	54.63	4.62
-0.142	56.20	4.39	-0.142	56.09	4.36
-0.181	57.84	3.33	-0.181	57.57	3.66
-0.207	57.94	3.11	-0.207	57.88	3.34
-0.247	56.87	3.48	-0.247	56.60	3.55
-0.273	55.49	3.78	-0.273	55.41	3.91
-0.312	52.95	4 47	-0.312	52.68	4.78
-0.339	50.93	5 09	-0.339	50.26	5.16
-0.378	46.64	5.76	-0.378	46.32	5.68
-0.404	43.90	5.91	-0.404	43.80	5.80
-0.417	42.07	5.95	-0.417	42.14	5.62
-0.430	40.41	5.85	-0.430	40.81	5.55
-0.444	38.91	5.70	-0.444	39.56	5.42
-0.457	37 19	5.56	-0.457	37.97	5.10
-0 470	35.11	5.41	-0.470	36.55	5.06
-0.483	32.88	5.08	-0.483	33.33	4.91
-0.496	19.26	4.37	-0.496	16.38	3.99

Case 14, Y-Profile, Z/D = 0.00, Gas Phase

X/D = -0.66			X/D = -0.33		
Y/D	Ux m/s	urms m/s	Y/D	Ux m/s	urms m/s
0.475	86.56	6.20	0.475	81.27	7.00
0.462	92.21	5.91	0.462	86.98	6.37
0.449	96.31	6.00	0.449	90.55	6.36
0.436	99.29	5.69	0.436	94.05	5.96
0.423	101.83	5.33	0.423	96.56	5.50
0.409	103.89	4.82	0.409	98.33	5.28
0.383	106.43	4.22	0.383	101.95	4.40
0.357	107.73	3.67	0.357	103.21	3.92
0.344	108.45	3.48	0.344	104.01	3.62
0.331	109.05	3.47	0.331	104.72	3.54
0.304	108.50	3.73	0.304	104.31	3.63
0.278	107.07	4.15	0.278	103.89	4.00
0.252	105.65	4.58	0.252	102.41	4.52
0.213	103.11	5.00	0.213	99.88	5.05
0.186	101.23	5.22	0.186	97.78	5.50
0.147	97.18	5.90	0.147	94.47	6.05
0.121	93.64	6.17	0.121	91.38	6.23
-0.089	63.14	4.82	0.081	84.73	6.81
-0.115	66.23	4.71	-0.063	54.56	5.42
-0.142	68.49	4.44	-0.089	59.25	5.02
-0.181	70.96	4.15	-0.115	61.57	4.85
-0.207	72.49	3.64	-0.142	63.85	4.51
-0.247	73.84	3.37	-0.181	66.29	3.99
-0.273	74.40	3.11	-0.207	67.53	3.65
-0.312	74.58	3.00	-0.247	68.87	3.23
-0.339	74.14	3.15	-0.273	69.31	3.11
-0.378	72.51	3.58	-0.312	69.06	3.14
-0.404	70.53	3.97	-0.339	68.14	3.33
-0.417	69.63	4.15	-0.378	66.01	3.92
-0.430	68.13	4.30	-0.404	64.28	4.35
-0.444	66.26	4.60	-0.417	62.78	4.57
-0.457	64.64	4.61	-0.430	61.31	4.73
-0.470	61.17	4.72	-0.444	58.82	5.06
-0.483	56.19	4.84	-0.457	56.26	5.28
-0.496	36.58	5.68	-0.470	52.95	5.62
			-0.483	47.50	5.69
			-0.496	29.56	5.81

Case 14, Y-Profile, Z/D = 0.00, Gas Phase

X/D = 0.03			X/D = 0.50			X/D = 1.00		
Y/D	Ux m/s	urms m/s	Y/D	Ux m/s	urms m/s	Y/D	Ux m/s	urms m/s
0.475	85.97	7.09	0.475	83.28	7.84	0.475	81.27	7.36
0.462	88.77	6.77	0.462	86.63	7.16	0.462	83.35	7.35
0.449	91.54	6.13	0.449	89.47	6.62	0.449	86.72	6.79
0.436	93.68	5.83	0.436	91.78	6.09	0.436	89.19	6.45
0.423	96.94	5.28	0.423	93.57	5.57	0.423	91.14	5.81
0.409	98.06	5.01	0.409	94.93	5.15	0.409	92.53	5.33
0.383	99.41	4.35	0.383	96.92	4.56	0.383	94.78	4.55
0.357	100.38	3.88	0.357	98.08	4.11	0.357	96.16	4.03
0.344	100.80	3.74	0.344	98.00	3.82	0.344	96.45	3.93
0.331	100.57	3.67	0.331	98.33	3.81	0.331	96.78	3.69
0.304	99.98	3.75	0.304	98.04	3.82	0.304	96.80	3.70
0.278	97.29	4.08	0.278	97.17	3.89	0.278	96.72	3.89
0.252	97.68	4.56	0.252	96.53	4.37	0.252	95.78	4.07
0.213	94.72	5.23	0.213	94.51	4.84	0.213	93.85	4.72
0.186	92.87	5.65	0.186	92.26	5.41	0.186	91.75	5.12
0.147	88.17	6.27	0.147	89.01	5.83	0.147	88.28	5.79
0.121	84.55	6.67	0.121	85.48	6.18	0.121	85.18	6.39
0.081	77.01	7.56	0.081	79.57	7.63	0.081	78.43	7.85
0.055	66.08	9.05	0.055	71.92	9.42	0.055	72.25	8.72
0.042	56.71	9.80	0.042	66.78	9.66	0.042	68.82	9.13
0.029	45.40	9.36	0.029	61.69	9.67	0.029	65.34	8.96
0.016	32.26	7.24	0.016	56.55	9.25	0.016	61.60	8.48
0.003	26.07	5.92	0.003	51.58	8.22	0.003	58.48	8.19
-0.010	32.86	7.08	-0.010	47.72	6.78	-0.010	54.92	7.41
-0.024	39.73	6.88	-0.024	45.41	5.42	-0.024	52.50	6.57
-0.037	45.60	6.35	-0.037	45.06	5.61	-0.037	50.72	5.78
-0.050	48.57	5.77	-0.050	46.40	6.08	-0.050	49.65	5.18
-0.063	50.86	5.52	-0.063	48.49	6.13	-0.063	49.66	5.06
-0.089	54.95	5.02	-0.089	52.24	5.62	-0.089	51.59	5.40
-0.115	57.50	4.75	-0.115	54.96	4.85	-0.115	54.13	5.09
-0.142	59.59	4.28	-0.142	57.03	4.23	-0.142	56.35	4.48
-0.181	62.19	3.75	-0.181	59.22	3.67	-0.181	58.66	3.69
-0.207	63.64	3.50	-0.207	60.22	3.39	-0.207	59.98	3.30
-0.247	64.94	3.14	-0.247	61.36	3.09	-0.247	60.68	3.05
-0.273	65.18	3.09	-0.273	61.46	3.11	-0.273	60.66	3.12
-0.312	65.22	3.33	-0.312	60.72	3.55	-0.312	59.63	3.49
-0.339	64.33	3.61	-0.339	59.70	3.88	-0.339	58.56	3.91
-0.378	62.01	4.13	-0.378	57.18	4.62	-0.378	55.86	4.68
-0.404	59.54	4.75	-0.404	54.41	5.24	-0.404	52.45	5.36
-0.417	57.92	5.00	-0.417	52.78	5.59	-0.417	50.28	5.66
-0.430	55.83	5.24	-0.430	50.60	5.90	-0.430	48.22	5.70
-0.444	53.63	5.58	-0.444	47.44	6.03	-0.444	46.51	5.68
-0.457	50.46	5.76	-0.457	44.69	5.89	-0.457	43.79	5.55
-0.470	46.40	6.04	-0.470	41.61	5.94	-0.470	41.29	5.33
-0.483	41.10	5.81	-0.483	37.53	5.52	-0.483	37.69	5.10
-0.496	25.88	5.60	-0.496	20.62	5.05	-0.496	22.36	4.75

Case 14, Y-Profile, Z/D = 0.00, Gas Phase

X/D = 1.50			X/D = 2.00		
Y/D	Ux m/s	urms m/s	Y/D	Ux m/s	urms m/s
0.475	79.39	7.51	0.475	78.37	7.33
0.462	81.86	7.53	0.462	80.53	7.17
0.449	84.81	7.05	0.449	83.27	7.12
0.436	87.27	6.69	0.436	85.67	6.82
0.423	89.30	6.40	0.423	87.59	6.33
0.409	90.99	5.85	0.409	89.65	5.78
0.383	93.26	4.94	0.383	92.13	5.10
0.357	94.88	4.37	0.357	93.54	4.39
0.344	95.33	4.15	0.344	93.90	4.08
0.331	95.37	3.87	0.331	94.12	4.04
0.304	95.62	3.86	0.304	94.66	3.79
0.278	95.42	3.96	0.278	94.43	3.94
0.252	94.32	4.30	0.252	92.99	4.18
0.213	92.07	4.97	0.213	90.89	4.98
0.186	90.05	5.50	0.186	88.77	5.53
0.147	86.66	6.23	0.147	84.36	6.68
0.121	83.09	7.04	0.121	81.05	7.33
0.081	76.35	8.36	0.081	74.47	8.12
0.055	71.39	8.66	0.055	70.34	8.38
0.042	68.07	8.80	0.042	67.89	8.09
0.029	65.56	8.49	0.029	66.04	8.18
0.016	62.94	8.22	0.016	63.81	7.73
0.003	60.52	8.03	0.003	61.66	7.26
-0.010	58.23	7.50	-0.010	60.05	6.90
-0.024	55.84	6.68	-0.024	58.46	6.58
-0.037	54.39	6.17	-0.037	57.10	6.05
-0.050	53.16	5.58	-0.050	55.59	5.50
-0.063	52.45	5.22	-0.063	54.82	4.98
-0.089	52.52	4.94	-0.089	54.10	4.61
-0.115	53.84	5.13	-0.115	54.89	4.50
-0.142	55.97	4.71	-0.142	56.10	4.44
-0.181	58.26	3.76	-0.181	58.23	3.92
-0.207	59.72	3.42	-0.207	59.31	3.45
-0.247	60.48	3.16	-0.247	60.08	3.08
-0.273	60.29	3.21	-0.273	59.79	3.32
-0.312	59.40	3.67	-0.312	58.58	3.77
-0.339	57.76	4.15	-0.339	56.94	4.27
-0.378	54.52	5.01	-0.378	53.79	5.06
-0.404	51.57	5.41	-0.404	50.97	5.47
-0.417	49.77	5.58	-0.417	49.35	5.54
-0.430	48.10	5.57	-0.430	47.41	5.52
-0.444	45.99	5.73	-0.444	45.48	5.46
-0.457	43.97	5.59	-0.457	43.80	5.29
-0.470	41.79	5.35	-0.470	41.73	5.33
-0.483	38.38	5.10	-0.483	38.82	5.08
-0.496	21.81	4.94	-0.496	20.63	4.59

Case 14, Y-Profile, Z/D = 0.25, Gas Phase

X/D = -0.66			X/D = -0.33		
Y/D	Ux m/s	urms m/s	Y/D	Ux m/s	urms m/s
0.475	81.50	5.84	0.475	73.26	7.03
0.462	85.82	5.57	0.462	78.15	6.52
0.449	87.82	5.63	0.449	81.33	6.21
0.436	90.19	5.39	0.436	84.20	5.98
0.423	92.26	5.42	0.423	85.86	5.86
0.409	93.68	5.23	0.409	87.68	5.59
0.383	96.79	4.83	0.383	90.68	5.09
0.357	99.63	4.39	0.357	93.29	4.71
0.344	100.26	4.22	0.344	94.21	4.45
0.331	101.26	3.99	0.331	94.93	4.32
0.304	102.19	3.73	0.304	96.78	3.92
0.278	103.36	3.48	0.278	97.64	3.59
0.252	103.13	3.61	0.252	97.71	3.65
0.213	102.32	3.90	0.213	97.00	3.94
0.186	101.24	4.47	0.186	95.51	4.48
0.147	97.87	5.24	0.147	92.57	5.24
0.121	94.69	5.81	0.121	89.89	5.73
-0.089	59.89	4.50	0.081	81.06	6.65
-0.115	63.45	4.44	-0.063	51.03	5.24
-0.142	66.26	4.05	-0.089	57.24	4.82
-0.181	69.46	3.64	-0.115	60.53	4.63
-0.207	70.64	3.38	-0.142	63.12	4.28
-0.247	71.40	3.02	-0.181	65.94	3.72
-0.273	71.21	2.89	-0.207	66.64	3.40
-0.312	69.86	3.15	-0.247	67.19	3.04
-0.339	68.48	3.33	-0.273	66.77	2.97
-0.378	65.73	3.75	-0.312	65.17	3.30
-0.404	63.72	3.87	-0.339	63.41	3.58
-0.417	62.43	3.99	-0.378	60.39	3.94
-0.430	61.12	4.02	-0.404	57.82	4.32
-0.444	59.55	4.12	-0.417	56.24	4.32
-0.457	58.03	4.21	-0.430	54.66	4.42
-0.470	55.47	4.25	-0.444	53.09	4.61
-0.483	51.84	4.34	-0.457	50.68	4.70
-0.496	32.66	4.60	-0.470	47.08	5.09
			-0.483	42.29	5.31
			-0.496	22.69	4.95

Case 14, Y-Profile, Z/D = 0.25, Gas Phase

X/D = 0.03			X/D = 0.50			X/D = 1.00		
Y/D	Ux m/s	urms m/s	Y/D	Ux m/s	urms m/s	Y/D	Ux m/s	urms m/s
0.475	72.15	8.28	0.475	67.54	8.92	0.475	63.67	8.52
0.462	75.63	7.83	0.462	70.45	8.93	0.462	66.03	8.56
0.449	78.61	7.40	0.449	74.87	8.52	0.449	69.84	8.80
0.436	80.90	7.12	0.436	77.44	8.10	0.436	72.70	8.79
0.423	85.01	6.51	0.423	79.86	7.70	0.423	75.16	8.45
0.409	85.01	6.51	0.409	82.68	7.13	0.409	78.30	8.19
0.383	87.68	5.95	0.383	86.07	6.39	0.383	83.33	7.10
0.357	90.37	5.34	0.357	89.36	5.91	0.357	86.90	6.38
0.344	91.31	5.19	0.344	90.25	5.56	0.344	87.57	6.00
0.331	91.68	4.89	0.331	91.41	5.26	0.331	88.98	5.81
0.304	93.21	4.38	0.304	92.56	4.89	0.304	90.24	5.49
0.278	93.87	4.20	0.278	94.15	4.54	0.278	90.97	5.51
0.252	94.01	4.01	0.252	93.62	4.42	0.252	90.65	5.92
0.213	92.47	4.49	0.213	92.51	4.86	0.213	89.74	6.15
0.186	90.26	5.01	0.186	91.26	5.27	0.186	88.53	6.38
0.147	85.73	5.68	0.147	88.36	5.71	0.147	86.31	6.78
0.121	82.36	6.29	0.121	85.78	6.19	0.121	82.95	7.35
0.081	70.25	9.08	0.081	78.29	8.14	0.081	75.14	9.24
0.055	57.36	11.41	0.055	68.77	9.76	0.055	68.50	9.67
0.042	46.04	11.26	0.042	63.91	9.93	0.042	64.40	9.68
0.029	37.26	10.44	0.029	58.43	9.93	0.029	61.30	9.42
0.016	27.86	8.27	0.016	52.69	8.89	0.016	57.05	8.81
0.003	23.49	4.99	0.003	47.85	7.53	0.003	54.49	8.31
-0.010	29.31	6.13	-0.010	44.73	6.42	-0.010	52.15	7.56
-0.024	35.43	6.44	-0.024	43.24	5.58	-0.024	50.40	6.83
-0.037	40.84	6.30	-0.037	43.81	5.74	-0.037	49.14	6.00
-0.050	45.06	5.76	-0.050	45.35	5.96	-0.050	48.99	5.76
-0.063	48.30	5.45	-0.063	47.16	6.03	-0.063	49.10	5.71
-0.089	52.25	4.86	-0.089	50.88	5.38	-0.089	50.67	5.41
-0.115	55.26	4.57	-0.115	53.74	4.68	-0.115	52.50	5.00
-0.142	57.83	4.12	-0.142	56.04	4.24	-0.142	54.33	4.42
-0.181	60.15	3.50	-0.181	57.95	3.55	-0.181	56.58	3.54
-0.207	60.93	3.17	-0.207	58.58	3.10	-0.207	57.26	3.21
-0.247	61.49	2.91	-0.247	58.23	3.12	-0.247	56.65	3.18
-0.273	60.97	3.07	-0.273	57.36	3.42	-0.273	55.48	3.48
-0.312	58.98	3.61	-0.312	54.79	4.07	-0.312	52.74	4.36
-0.339	57.12	3.97	-0.339	52.50	4.54	-0.339	50.17	5.05
-0.378	53.98	4.31	-0.378	47.89	5.58	-0.378	44.86	5.81
-0.404	51.22	4.74	-0.404	43.46	6.24	-0.404	40.96	6.16
-0.417	49.20	4.88	-0.417	40.92	6.57	-0.417	38.46	6.23
-0.430	47.49	5.24	-0.430	38.54	6.65	-0.430	36.58	6.21
-0.444	45.20	5.63	-0.444	36.10	6.71	-0.444	34.49	5.87
-0.457	42.03	5.96	-0.457	33.04	6.58	-0.457	32.87	5.81
-0.470	37.80	6.18	-0.470	30.77	6.28	-0.470	30.74	5.54
-0.483	33.54	6.00	-0.483	27.59	5.94	-0.483	28.03	5.09
-0.496	22.37	5.56	-0.496	18.01	5.38	-0.496	19.76	5.24

Case 14, Y-Profile, Z/D = 0.25, Gas Phase

X/D = 1.50			X/D = 2.00		
Y/D	Ux m/s	urms m/s	Y/D	Ux m/s	urms m/s
0.475	63.57	8.02	0.475	62.69	7.42
0.462	65.41	8.10	0.462	64.37	7.65
0.449	68.09	8.30	0.449	66.56	7.83
0.436	70.58	8.42	0.436	68.94	8.07
0.423	73.09	8.46	0.423	71.16	8.31
0.409	75.52	8.45	0.409	73.51	8.24
0.383	80.73	7.73	0.383	78.30	7.81
0.357	84.16	6.91	0.357	81.95	7.43
0.344	85.99	6.40	0.344	83.50	6.86
0.331	87.16	6.09	0.331	85.06	6.39
0.304	89.07	5.30	0.304	87.50	5.86
0.278	89.83	5.29	0.278	88.49	5.38
0.252	89.90	5.14	0.252	88.44	5.45
0.213	88.41	5.75	0.213	86.47	6.25
0.186	86.44	6.59	0.186	84.13	7.07
0.147	81.50	8.07	0.147	79.18	8.20
0.121	76.67	9.08	0.121	74.64	8.74
0.081	68.51	9.52	0.081	68.45	8.86
0.055	63.23	9.10	0.055	64.11	8.56
0.042	60.89	8.89	0.042	61.60	8.19
0.029	58.57	8.54	0.029	60.13	8.04
0.016	56.39	7.97	0.016	58.45	7.59
0.003	54.67	7.53	0.003	56.86	7.15
-0.010	52.85	6.80	-0.010	55.37	6.60
-0.024	51.54	6.28	-0.024	54.10	6.13
-0.037	50.71	5.76	-0.037	53.33	5.69
-0.050	50.67	5.27	-0.050	52.70	5.33
-0.063	50.47	5.25	-0.063	52.37	5.07
-0.089	51.48	4.98	-0.089	52.64	4.76
-0.115	52.71	4.82	-0.115	53.35	4.57
-0.142	54.31	4.52	-0.142	54.53	4.35
-0.181	56.45	3.69	-0.181	56.35	3.79
-0.207	57.04	3.37	-0.207	56.73	3.32
-0.247	56.71	3.17	-0.247	56.52	3.28
-0.273	55.38	3.53	-0.273	55.04	3.84
-0.312	52.42	4.47	-0.312	51.66	4.85
-0.339	49.24	5.12	-0.339	48.77	5.18
-0.378	44.24	5.79	-0.378	43.90	5.51
-0.404	40.53	5.80	-0.404	40.77	5.46
-0.417	38.92	5.74	-0.417	39.26	5.24
-0.430	37.27	5.57	-0.430	37.91	5.07
-0.444	35.66	5.33	-0.444	36.69	5.10
-0.457	34.22	5.20	-0.457	35.21	4.78
-0.470	32.09	4.89	-0.470	33.53	4.58
-0.483	29.96	4.81	-0.483	31.29	4.48
-0.496	20.36	4.76	-0.496	19.96	4.53

Case 14, Y-Profile, Z/D = -0.25, Two Phase

X/D = 0.03			X/D = 0.50			X/D = 1.00		
Y/D	Ux m/s	urms m/s	Y/D	Ux m/s	urms m/s	Y/D	Ux m/s	urms m/s
0.475	64.62	9.65	0.475	59.03	9.50	0.475	53.75	8.87
0.462	71.25	9.16	0.462	62.76	9.70	0.462	58.49	9.36
0.449	74.78	8.60	0.449	66.98	9.73	0.449	63.05	9.55
0.436	77.31	8.08	0.436	70.72	9.65	0.436	68.00	9.87
0.423	80.02	7.60	0.423	74.66	9.21	0.423	71.76	9.49
0.409	82.50	7.25	0.409	77.45	8.73	0.409	74.87	9.51
0.383	86.22	6.79	0.383	82.88	7.53	0.383	80.75	8.73
0.357	89.49	6.27	0.357	87.06	6.83	0.357	85.31	7.42
0.344	91.06	6.06	0.344	88.58	6.23	-0.378	52.87	5.70
0.331	92.19	5.80	0.331	89.83	5.99	-0.404	49.71	6.07
0.304	94.38	5.31	0.304	92.45	5.56	-0.417	48.14	6.75
0.278	96.10	4.61	0.278	94.30	5.77	-0.430	46.36	6.08
0.252	96.73	4.26	0.252	94.85	4.81	-0.444	44.32	6.28
0.213	96.69	3.93	-0.273	60.69	4.62	-0.457	42.03	6.20
0.186	95.87	4.00	-0.312	58.17	4.05	-0.470	38.99	5.92
0.147	93.48	4.56	-0.339	56.68	4.44	-0.483	35.93	5.56
0.121	91.29	5.06	-0.378	53.84	5.00	-0.496	18.05	4.60
-0.037	48.92	6.85	-0.404	50.67	5.94			
-0.050	52.64	5.89	-0.417	48.16	6.28			
-0.063	55.27	5.36	-0.430	46.03	6.65			
-0.089	58.30	4.54	-0.444	43.22	6.77			
-0.115	61.08	4.07	-0.457	40.10	6.50			
-0.142	62.65	3.70	-0.470	37.01	6.21			
-0.181	64.20	3.16	-0.496	14.66	3.97			
-0.207	64.51	3.02						
-0.247	63.60	3.41						
-0.273	62.71	3.63						
-0.312	60.94	3.99						
-0.339	59.32	4.22						
-0.378	56.74	4.58						
-0.404	54.73	5.10						
-0.417	53.89	5.18						
-0.430	52.16	5.51						
-0.444	50.00	5.98						
-0.457	46.68	6.26						
-0.470	42.46	6.47						
-0.483	37.06	6.25						
-0.496	19.56	4.59						

Case 14, Y-Profile, Z/D = -0.25, Two Phase

X/D = 1.50			X/D = 2.00		
Y/D	Ux m/s	urms m/s	Y/D	Ux m/s	urms m/s
0.475	56.89	8.03	0.475	57.58	7.91
			0.462	61.36	7.92
0.449	64.14	8.85	0.449	64.93	9.02
0.436	67.12	9.23	0.436	67.29	8.88
0.423	69.98	9.22			
0.409	72.49	8.99			
-0.470	37.20	5.74			
-0.483	34.64	5.31			
-0.496	10.01	3.44			

Case 14, Y-Profile, Z/D = 0.00, Two Phase

X/D = 0.03			X/D = 0.50			X/D = 1.00		
Y/D	Ux m/s	urms m/s	Y/D	Ux m/s	urms m/s	Y/D	Ux m/s	urms m/s
0.475	76.55	8.22	0.475	70.94	7.89	0.475	69.44	7.25
0.462	81.67	7.66	0.462	76.85	7.76	0.462	75.54	7.30
0.449	85.75	7.36	0.449	81.05	7.59	0.449	80.91	7.40
0.436	89.58	6.70	0.436	84.66	7.22	0.436	84.62	7.17
0.423	92.28	6.40	0.423	87.36	6.71	0.423	86.67	6.83
0.409	94.46	5.93	0.409	90.36	6.07	0.409	89.55	6.31
0.383	97.93	5.01	0.383	95.21	5.22	0.383	93.72	6.14
0.357	99.76	4.32	0.357	97.49	4.57	0.357	96.77	5.44
0.344	100.52	4.11	0.344	97.63	4.09	0.344	97.15	4.36
0.331	100.70	3.93	0.331	98.18	3.93	0.331	97.75	4.14
0.304	101.10	3.71	0.304	97.88	3.84	-0.378	57.99	6.40
0.278	100.04	3.82	0.278	98.29	3.78			
0.252	98.77	3.97	0.252	98.22	3.79	-0.417	52.72	5.85
0.213	97.81	4.48	-0.312	62.86	4.41	-0.430	50.90	5.95
0.186	95.55	4.66	-0.339	61.59	4.37	-0.444	48.38	5.84
0.147	93.10	5.00	-0.378	58.54	4.42	-0.457	45.70	5.69
0.121	91.26	5.18	-0.404	55.99	5.02	-0.470	42.88	5.32
-0.115	63.49	3.67	-0.417	53.74	5.40	-0.483	39 60	5.34
-0.142	64.47	3.44	-0.430	52.09	5.76	-0.496	20.25	4.36
-0.181	65.51	3.10	-0.444	49.68	5.89			
-0.207	65.90	2.95	-0.457	46.63	5.85			
-0.247	66.14	2.85	-0.470	43.46	5.91			
-0.273	66.08	2.96	-0.483	39.46	5.48			
-0.312	65.30	3.29	-0.496	22.59	5.30			
-0.339	64.43	3.62						
-0.378	62.06	4.14						
-0.404	59.60	4.60						
-0.417	58.12	4.95						
-0.430	56.07	5.15						
-0.444	54.11	5.51						
-0.457	50.96	5.74						
-0.470	47.09	5.86						
-0.483	41.70	5.87						
-0.496	24.51	5.31						

Case 14, Y-Profile, Z/D = 0.00, Two Phase

X/D = 1.50			X/D = 2.00		
Y/D	Ux m/s	urms m/s	Y/D	Ux m/s	urms m/s
0.475	70.29	7.14	0.475	71.09	7.34
0.462	75.00	7.30	0.462	74.41	7.18
0.449	78.83	7.41			
0.436	81.92	7.26	0.436	81.58	7.93
0.423	85.15	7.07	0.423	84.47	7.45
0.409	87.87	6.43			
0.383	91.32	5.47			

Case 14, Y-Profile, Z/D = 0.25, Two Phase

X/D = 0.03			X/D = 0.50			X/D = 1.00		
Y/D	Ux m/s	urms m/s	Y/D	Ux m/s	urms m/s	Y/D	Ux m/s	urms m/s
0.475	65.43	8.04	0.475	58.89	8.04	0.475	59.32	7.64
0.462	69.57	7.79	0.462	63.86	8.61	0.462	63.09	7.99
0.449	74.16	7.43	0.449	68.15	8.32	0.449	65.74	8.29
0.436	78.12	6.92	0.436	72.10	8.27	0.436	68.78	8.56
0.423	80.81	6.55	0.423	75.26	7.99	0.423	71.48	8.54
0.409	82.47	6.24	0.409	78.47	7.31	0.409	75.04	8.27
0 383	86.23	5.79	0.383	83.29	6.35	0.383	81.63	7.34
0.357	88.55	5.35	0.357	85.77	5.68	0.357	85.78	6.24
0.344	89.30	5.09	0.344	86.74	5.46	0.344	87.09	5.77
0.331	90.86	4.95	0.331	88.68	5.18	0.331	88.70	5.74
0.304	92.42	4.49	0.304	90.78	4.67	0.304	90.81	4.94
0.278	93.87	4.04	0.278	92.00	4.28	-0.378	48.66	6.21
0.252	94.67	3.78	0.252	93.16	3.98	-0.404	44.18	6.24
0.213	94.76	3.73	0.213	93.99	3.90			
0 186	94.47	3.85	0.186	93.49	4.12	-0.430	40.08	6.05
0.147	93.13	4.37	-0.273	60.58	4.49	-0.444	37.59	6.12
-0.089	61.52	4.58	-0.312	57.83	3.91	-0.457	34.88	5.62
-0.115	62.69	3.65	-0.339	55.63	4.31	-0.470	32.88	5.49
-0.142	63.59	3.44	-0.378	51.45	5.39	-0.483	30.31	5.11
-0.181	64.06	3.09	-0.404	47.27	6.05	-0.496	17.23	4.90
-0.207	64.14	2.89	-0.417	44.74	6.28			
-0.247	63.41	3.02	-0.430	42.06	6.66			
-0.273	62.13	3.28	-0.444	39.29	6.54			
-0.312	60.19	3.71	-0.457	36.42	6.35			
-0.339	58.23	4.04	-0.470	33.08	6.13			
-0.378	54.91	4.41	-0.483	29.62	5.73			
-0.404	52.34	4.76	-0.496	19.55	5.46			
-0.417	50.79	4.91						
-0.430	48.86	5.30						
-0.444	46.24	5.60						
-0.457	43.22	5.84						
-0.470	39.33	6.05						
-0.483	34.23	5.85						
-0.496	19.73	5.10						

Case 14, Y-Profile, Z/D = 0.25, Two Phase

X/D = 1.50			X/D = 2.00		
Y/D	Ux m/s	urms m/s	Y/D	Ux m/s	urms m/s
0.475	58.92	7.24	0.475	58.93	7.01
0.462	62.57	7.52	0.462	62.35	7.24
0.449	65.06	7.74	0.449	64.47	7.36
0.436	67.70	7.89	0.436	67.40	7.46
0.423	70.28	7.83			
0.409	73.12	7.84			
0.383	78.16	7.43			
0.357	82.10	6.71			
0.344	84.50	6.10			
0.331	85.86	5.69			
-0.496	19.81	5.63			

Case 14, Z-Profile, Y/D = -0.25, Gas Phase

X/D = -0.66			X/D = -0.33		
Z/D	Ux m/s	urms m/s	Z/D	Ux m/s	urms m/s
0.475	38.58	7.62	0.475	44.94	7.77
0.462	48.87	6.92	0.462	49.34	7.11
0.449	58.10	5.92	0.449	53.22	6.03
0.436	62.65	5.32	0.436	56.22	5.39
0.423	64.58	4.87	0.423	57.84	4.70
0.409	65.92	4.47	0.409	59.51	4.40
0.383	67.77	3.91	0.383	62.14	3.82
0.370	68.56	3.53	0.370	63.04	3.39
0.344	69.97	3.01	0.344	64.69	2.90
0.278	70.72	2.44	0.278	66.18	2.45
0.213	70.03	2.63	0.213	66.18	2.65
0.147	69.04	2.79	0.147	66.06	2.76
0.081	68.61	2.79	0.081	65.62	2.76
0.016	68.65	2.70	0.016	65.64	2.67
-0.050	68.95	2.58	-0.050	66.11	2.52
-0.115	69.19	2.41	-0.115	66.00	2.48
-0.181	69.26	2.33	-0.181	65.64	2.38
-0.247	69.08	2.34	-0.247	65.42	2.40
-0.312	68.60	2.41	-0.312	64.50	2.48
-0.339	67.65	2.81	-0.339	63.54	2.82
-0.352	66.46	3.23	-0.352	62.63	3.20
-0.378	64.28	3.94	-0.378	60.49	3.87
-0.391	62.57	4.47	-0.391	58.96	4.33
-0.404	60.38	4.99	-0.404	56.56	5.06
-0.417	58.39	5.30	-0.417	53.70	5.94
-0.430	53.16	6.38	-0.430	49.28	7.53
-0.444	40.91	8.07	-0.444	42.41	8.67
-0.457	24.02	7.59	-0.457	34.76	9.29
-0.470	13.22	4.51	-0.470	26.89	8.40
-0.483	11.01	3.50	-0.483	20.13	6.96
-0.496	10.30	3.15	-0.496	13.93	5.52

Case 14, Z-Profile, Y/D = -0.25, Gas Phase

X/D = 0.03			X/D = 0.50			X/D = 1.00		
Z/D	Ux m/s	urms m/s	Z/D	Ux m/s	urms m/s	Z/D	Ux m/s	urms m/s
0.475	60.89	11.69	0.475	43.04	6.29	0.475	44.42	5.74
0.449	66.04	11.67	0.462	44.88	6.34	0.462	45.89	5.74
0.436	71.75	11.53	0.449	46.55	6.34	0.449	47.51	5.82
0.423	76.42	10.34	0.436	48.66	6.05	0.436	48.79	5.69
0.409	80.33	9.42	0.423	50.24	5.66	0.423	50.75	5.51
0.383	85.95	6.85	0.409	52.09	5.18	0.409	52.09	5.17
0.370	88.38	5.93	0.383	54.62	4.20	0.383	54.41	4.34
0.344	90.95	4.62	0.370	55.69	3.79	0.370	55.37	4.01
0.278	94.04	3.47	0.344	57.10	3.17	0.344	56.68	3.32
0.213	94.20	3.55	0.278	58.43	2.65	0.278	57.82	2.82
0.147	94.05	3.59	0.213	58.47	2.66	0.213	58.07	2.76
0.081	93.87	3.70	0.147	58.67	2.70	0.147	58.20	2.72
0.016	93.78	3.57	0.081	58.44	2.70	0.081	58.17	2.70
-0.050	93.46	3.57	0.016	58.31	2.62	0.016	58.12	2.69
-0.115	93.29	3.55	-0.050	58.24	2.58	-0.050	57.98	2.65
-0.181	93.16	3.64	-0.115	57.74	2.74	-0.115	57.25	2.87
-0.247	93.16	3.69	-0.181	57.27	2.89	-0.181	56.60	2.99
-0.312	92.35	3.70	-0.247	56.85	2.97	-0.247	56.28	3.14
-0.339	90.96	4.68	-0.312	56.69	2.88	-0.312	56.04	3.13
-0.352	88.92	5.69	-0.339	56.24	3.17	-0.339	55.36	3.57
-0.378	83.48	8.37	-0.352	55.49	3.42	-0.352	54.69	3.85
-0.391	79.42	9.92	-0.378	53.16	4.69	-0.378	52.52	4.68
-0.404	74.81	10.87	-0.391	51.44	5.26	-0.391	51.14	5.15
-0.417	69.14	11.72	-0.404	50.05	5.58	-0.404	49.47	5.29
-0.430	63.76	12.17	-0.417	47.77	6.02	-0.417	48.08	5.44
-0.444	58.11	12.01	-0.430	45.61	6.21	-0.430	46.45	5.61
-0.457	52.32	11.90	-0.444	43.61	6.16	-0.444	44.54	5.52
-0.470	47.79	11.25	-0.457	41.27	6.11	-0.457	42.38	5.49
-0.483	42.42	10.80	-0.470	39.28	6.08	-0.470	40.81	5.40
-0.496	31.19	8.98	-0.483	36.11	5.94	-0.483	38.31	5.31
0.000	0.00	0.00	-0.496	25.03	5.44	-0.496	28.12	5.19

Case 14, Z-Profile, Y/D = -0.25, Gas Phase

X/D = 1.50			X/D = 2.00		
Z/D	Ux m/s	urms m/s	Z/D	Ux m/s	urms m/s
0.475	45.19	5.15	0.475	65.75	8.05
0.462	46.12	5.36	0.462	67.02	8.17
0.449	47.59	5.40	0.449	69.12	8.29
0.436	49.20	5.35	0.436	70.21	8.37
0.423	50.66	5.11	0.423	72.39	8.52
0.409	52.10	4.80	0.409	74.32	8.59
0.383	54.20	4.22	0.383	77.99	8.36
0.370	55.10	3.83	0.370	80.00	8.06
0.344	56.30	3.30	0.344	83.13	7.46
0.278	57.53	2.77	0.278	88.64	4.97
0.213	57.84	2.77	0.213	90.37	3.89
0.147	57.94	2.67	0.147	90.81	3.68
0.081	57.91	2.74	0.081	90.90	3.61
0.016	57.79	2.68	0.016	90.51	3.52
-0.050	57.31	2.70	-0.050	90.03	3.55
-0.115	56.81	2.84	-0.115	89.07	3.97
-0.181	56.26	2.99	-0.181	88.18	4.17
-0.247	56.05	3.09	-0.247	87.86	4.31
-0.312	55.73	3.12	-0.312	86.64	5.05
-0.339	54.94	3.47	-0.339	84.86	5.74
-0.352	54.09	3.88	-0.352	83.51	6.29
-0.378	52.40	4.53	-0.378	80.64	7.01
-0.391	51.27	4.78	-0.391	78.58	7.29
-0.404	49.95	4.95	-0.404	76.64	7.53
-0.417	48.23	5.18	-0.417	74.48	7.55
-0.430	46.83	5.27	-0.430	72.42	7.69
-0.444	45.26	5.21	-0.444	70.23	7.67
-0.457	43.33	5.07	-0.457	68.21	7.74
-0.470	41.73	5.11	-0.470	65.44	7.56
-0.483	39.20	5.04	-0.483	60.71	7.17
-0.496	28.36	5.27	-0.496	44.99	7.14

Case 14, Z-Profile, Y/D = 0.00, Gas Phase

X/D = 0.03			X/D = 0.50			X/D = 1.00		
Z/D	Ux m/s	urms m/s	Z/D	Ux m/s	urms m/s	Z/D	Ux m/s	urms m/s
0.475	24.92	5.32	0.475	42.12	6.30	0.475	46.57	6.22
0.462	25.30	5.30	0.462	42.75	6.51	0.462	47.33	6.33
0.449	25.46	5.59	0.449	43.96	7.16	0.449	48.47	6.65
0.436	25.92	5.69	0.436	45.38	7.60	0.436	49.39	6.88
0.423	26.14	6.31	0.423	46.68	8.22	0.423	50.96	7.44
0.409	26.14	6.61	0.409	47.71	8.58	0.409	52.33	7.89
0.383	25.77	6.72	0.383	49.50	9.22	0.383	53.98	8.21
0.370	25.56	6.49	0.370	49.66	9.67	0.370	54.79	8.46
0.344	25.49	5.88	0.344	49.27	9.37	0.344	55.86	8.75
0.278	26.23	4.53	0.278	48.27	8.20	0.278	56.00	8.81
0.213	26.65	4.37	0.213	50.80	7.72	0.213	56.34	8.36
0.147	26.52	4.40	0.147	53.11	7.64	0.147	58.50	8.02
0.081	26.84	4.44	0.081	54.86	7.95	0.081	60.63	8.03
0.016	27.32	4.59	0.016	54.40	7.79	0.016	60.56	7.82
-0.050	27.87	4.62	-0.050	53.64	7.88	-0.050	59.71	7.94
-0.115	28.88	4.92	-0.115	53.61	7.97	-0.115	59.01	8.07
-0.181	28.73	5.19	-0.181	53.42	8.32	-0.181	59.11	8.98
-0.247	28.45	5.68	-0.247	54.05	9.90	-0.247	59.21	10.09
-0.312	30.78	7.34	-0.312	53.34	11.25	-0.312	58.04	10.16
-0.339	32.43	8.20	-0.339	52.19	11.08	-0.339	55.86	9.60
-0.352	32.40	7.96	-0.352	50.62	10.50	-0.352	54.60	9.34
-0.378	30.58	7.51	-0.378	47.80	9.41	-0.378	52.07	8.62
-0.391	29.66	7.41	-0.391	46.26	9.13	-0.391	50.25	8.19
-0.404	28.03	6.98	-0.404	45.02	8.55	-0.404	49.23	8.13
-0.417	26.76	6.87	-0.417	43.40	7.87	-0.417	47.36	6.99
-0.430	24.79	6.56	-0.430	41.85	7.22	-0.430	46.37	6.80
-0.444	23.02	5.94	-0.444	40.65	6.55	-0.444	44.73	6.44
-0.457	21.21	5.69	-0.457	39.16	5.97	-0.457	43.40	5.82
-0.470	19.97	5.38	-0.470	37.87	5.56	-0.470	41.62	5.50
-0.483	18.22	5.01	-0.483	35.79	5.50	-0.483	39.70	5.42
-0.496	13.83	4.64	-0.496	31.50	5.65	-0.496	34.60	5.71

Case 14, Z-Profile, Y/D = 0.00, Gas Phase

X/D = 1.50			X/D = 2.00		
Z/D	Ux m/s	urms m/s	Z/D	Ux m/s	urms m/s
0.475	47.93	5.86	0.475	49.41	5.83
0.462	48.94	6.03	0.462	50.58	6.09
0.449	49.82	6.25	0.449	51.10	6.04
0.436	50.68	6.36	0.436	52.26	6.42
0.423	51.81	6.58	0.423	53.24	6.41
0.409	52.74	6.92	0.409	54.10	6.48
0.383	54.10	7.17	0.383	55.53	6.87
0.370	54.68	7.24	0.370	56.36	6.97
0.344	55.62	7.47	0.344	57.26	7.02
0.278	56.40	7.59	0.278	58.23	7.08
0.213	56.76	7.43	0.213	58.50	7.25
0.147	58.86	7.73	0.147	59.89	7.33
0.081	61.18	7.49	0.081	61.74	7.17
0.016	61.79	7.37	0.016	62.33	7.16
-0.050	61.07	7.36	-0.050	61.47	6.98
-0.115	60.78	7.75	-0.115	61.51	7.39
-0.181	60.44	8.35	-0.181	61.49	7.87
-0.247	59.20	8.67	-0.247	61.01	8.04
-0.312	57.95	8.87	-0.312	59.40	8.16
-0.339	56.92	8.54	-0.339	58.23	8.20
-0.352	55.84	8.41	-0.352	57.36	8.13
-0.378	54.12	8.23	-0.378	55.88	8.01
-0.391	52.58	7.98	-0.391	54.87	7.94
-0.404	51.52	7.77	-0.404	53.32	7.64
-0.417	49.87	7.34	-0.417	52.38	7.47
-0.430	48.44	7.02	-0.430	50.97	7.44
-0.444	47.19	6.68	-0.444	49.38	7.10
-0.457	45.82	6.52	-0.457	48.34	7.11
-0.470	44.09	5.99	-0.470	46.91	6.74
-0.483	41.98	5.89	-0.483	44.42	6.62
-0.496	36.77	5.99	-0.496	34.82	6.76

Case 14, C-Profile, Y/D = 0.25, Gas Phase

X/D = -0.66			X/D = -0.33		
Z/D	Ux m/s	urms m/s	Z/D	Ux m/s	urms m/s
0.475	30.72	8.84	0.475	55.02	13.27
0.462	50.28	10.67	0.462	60.32	13.53
0.449	73.30	10.14	0.449	68.92	13.58
0.436	87.61	8.61	0.436	77.01	12.95
0.423	94.06	7.66	0.423	84.88	10.62
0.409	98.02	6.76	0.409	89.19	9.05
0.383	102.26	5.72	0.383	94.85	6.26
0.370	103.80	5.27	0.370	96.62	5.43
0.344	106.18	4.42	0.344	99.33	4.46
0.278	107.68	3.62	0.278	101.92	3.54
0.213	107.08	3.71	0.213	102.09	3.72
0.147	106.78	4.01	0.147	102.18	3.68
0.081	106.57	4.16	0.081	102.94	3.91
0.016	105.73	4.28	0.016	102.61	3.98
-0.050	105.57	4.29	-0.050	102.68	3.92
-0.115	105.75	3.98	-0.115	102.49	3.83
-0.181	105.74	3.56	-0.181	102.13	3.61
-0.247	105.21	3.35	-0.247	101.09	3.64
-0.312	102.42	3.98	-0.312	97.91	4.17
-0.339	99.26	4.73	-0.339	95.59	4.99
-0.352	98.48	5.19	-0.352	93.71	5.51
-0.378	94.76	6.12	-0.378	89.14	7.08
-0.391	92.47	6.66	-0.391	85.25	8.80
-0.404	89.66	7.26	-0.404	79.13	11.18
-0.417	84.68	8.11	-0.417	70.54	13.00
-0.430	74.33	10.21	-0.430	61.77	13.48
-0.444	49.48	11.71	-0.444	51.50	13.55
-0.457	26.42	8.36	-0.457	44.31	12.74
-0.470	25.56	8.22	-0.470	36.11	11.51
-0.483	36.93	8.10	-0.483	29.68	10.55
-0.496	25.26	7.57	-0.496	23.49	9.69

Case 14, Z-Profile, Y/D = 0.25, Gas Phase

X/D = 0.03			X/D = 0.50			X/D = 1.00		
Z/D	Ux m/s	urms m/s	Z/D	Ux m/s	urms m/s	Z/D	Ux m/s	urms m/s
0.475	58.07	12.17	0.475	59.13	11.77	0.475	59.55	11.20
0.462	61.68	12.55	0.462	61.36	12.18	0.462	61.74	11.48
0.449	65.60	12.66	0.449	64.35	12.11	0.449	63.80	11.59
0.436	70.84	12.58	0.436	67.65	12.17	0.436	66.39	11.80
0.423	76.37	12.02	0.423	70.55	12.16	0.423	68.79	11.73
0.409	80.47	11.04	0.409	73.47	12.03	0.409	71.32	11.89
0.383	88.21	7.65	0.383	79.98	11.13	0.383	76.31	11.57
0.370	90.55	6.51	0.370	83.08	10.03	0.370	78.72	11.23
0.344	93.37	4.68	0.344	88.08	7.96	0.344	83.04	10.11
0.278	95.92	3.71	0.278	92.70	4.35	0.278	90.46	5.88
0.213	96.14	3.68	0.213	93.46	3.95	0.213	92.02	4.13
0.147	96.55	3.68	0.147	94.00	3.96	0.147	92.99	3.82
0.081	97.06	3.79	0.081	95.03	3.90	0.081	93.73	3.80
0.016	97.25	3.87	0.016	95.51	3.83	0.016	94.06	3.76
-0.050	97.05	3.89	-0.050	95.50	3.84	-0.050	94.25	3.62
-0.115	96.98	3.69	-0.115	94.72	3.73	-0.115	93.31	3.62
-0.181	96.61	3.58	-0.181	93.94	3.92	-0.181	92.41	3.87
-0.247	95.42	3.66	-0.247	92.50	4.07	-0.247	90.43	4.72
-0.312	92.82	4.33	-0.312	88.08	6.47	-0.312	83.20	8.69
-0.339	89.92	5.63	-0.339	83.95	8.89	-0.339	78.12	10.13
-0.352	87.88	6.88	-0.352	80.58	10.38	-0.352	75.46	10.83
-0.378	80.15	10.31	-0.378	74.14	11.95	-0.378	69.80	11.23
-0.391	75.16	12.20	-0.391	70.39	12.67	-0.391	66.83	11.54
-0.404	69.75	12.90	-0.404	67.43	13.07	-0.404	63.70	11.49
-0.417	63.17	13.53	-0.417	63.78	13.18	-0.417	61.60	11.41
-0.430	57.56	13.25	-0.430	60.11	13.05	-0.430	58.79	11.53
-0.444	52.09	12.98	-0.444	56.45	13.21	-0.444	56.46	11.39
-0.457	47.57	12.61	-0.457	52.87	13.06	-0.457	54.07	11.29
-0.470	42.80	12.22	-0.470	49.44	12.76	-0.470	51.07	10.79
-0.483	39.49	12.07	-0.483	45.15	12.35	-0.483	47.94	10.58
-0.496	31.77	11.29	-0.496	38.27	12.05	-0.496	39.59	9.88

Case 14, Z-Profile, Y/D = 0.25, Gas Phase

X/D = 1.50			X/D = 2.00		
Z/D	Ux m/s	urms m/s	Z/D	Ux m/s	urms m/s
0.475	61.58	9.71	0.475	61.97	9.21
0.462	63.40	9.90	0.462	63.02	9.26
0.449	65.41	10.40	0.449	64.98	9.47
0.436	67.50	10.57	0.436	66.78	9.36
0.423	69.62	10.46	0.423	68.59	9.75
0.409	71.47	10.50	0.409	70.27	9.66
0.383	76.28	10.18	0.383	74.44	9.43
0.370	78.46	9.86	0.370	75.87	9.15
0.344	82.12	9.24	0.344	79.03	8.46
0.278	88.66	5.96	0.278	84.94	6.57
0.213	90.51	4.38	0.213	87.77	4.79
0.147	91.35	4.02	0.147	89.03	4.14
0.081	92.15	3.90	0.081	89.75	3.78
0.016	92.50	3.71	0.016	90.16	3.65
-0.050	92.30	3.72	-0.050	90.12	3.64
-0.115	91.13	3.69	-0.115	89.60	3.77
-0.181	90.02	3.90	-0.181	88.46	3.94
-0.247	87.93	4.39	-0.247	86.56	4.51
-0.312	83.66	6.20	-0.312	83.14	5.65
-0.339	80.79	7.30	-0.339	80.58	6.25
-0.352	79.07	7.76	-0.352	79.55	6.71
-0.378	74.79	8.68	-0.378	75.87	7.45
-0.391	72.51	8.91	-0.391	74.08	7.61
-0.404	70.19	9.09	-0.404	72.20	7.80
-0.417	68.35	9.18	-0.417	70.15	8.23
-0.430	66.19	9.32	-0.430	68.53	8.14
-0.444	63.80	9.29	-0.444	66.27	8.37
-0.457	61.34	9.37	-0.457	63.40	8.26
-0.470	59.14	9.12	-0.470	61.06	8.23
-0.483	55.33	8.80	-0.483	56.59	7.78
-0.496	49.57	8.24	-0.496	49.03	7.54

Case 14, Z-Profiles, Two Phase

Y/D = -0.25 X/D = 0.03			Y/D = 0.25 X/D = 0.03		
Z/D	Ux m/s	urms m/s	Z/D	Ux m/s	urms m/s
0.475	44.09	7.29	0.475	63.81	12.01
0.462	46.09	7.38	0.462	67.43	12.06
0.449	49.12	6.66	0.449	72.94	12.14
0.436	51.50	6.22	0.436	77.97	11.53
0.423	53.55	5.48	0.423	82.41	10.41
0.409	55.14	4.93	0.409	84.83	9.58
0.383	57.83	4.17	0.383	90.58	7.10
0.370	58.78	3.88	0.370	92.52	5.80
0.344	60.35	3.20	0.344	94.78	4.54
0.278	62.29	2.57	0.278	96.99	3.80
0.213	63.03	2.47	0.213	97.90	3.71
0.147	63.26	2.51	0.147	98.33	3.57
0.016	63.01	2.31	0.016	98.90	3.40
-0.050	62.54	2.44	-0.050	98.67	3.42
-0.115	61.67	2.72	-0.115	98.26	3.41
-0.181	61.03	3.04	-0.181	97.23	3.58
-0.247	60.88	2.85	-0.247	96.13	3.75
-0.312	60.31	2.80	-0.312	93.52	4.28
-0.339	59.51	3.07	-0.339	90.65	5.14
-0.352	58.70	3.60	-0.352	89.50	6.22
-0.378	55.84	8.87	-0.378	82.85	9.28
-0.391	54.02	5.98	-0.391	78.39	11.03
-0.404	50.88	7.23	-0.404	71.48	12.37
-0.417	47.87	8.04	-0.417	66.23	12.94
-0.430	44.18	8.43	-0.430	60.48	12.84
-0.444	40.93	8.62			
-0.457	37.16	8.37			
-0.470	33.86	8.28			
-0.483	29.86	7.72			
-0.496	19.87	6.08			

Case 1 Length Scale Results

X/D = -0.66

Y/D	U (m/s)	u_{rms} (m/s)	ℓ (mm)
-0.47	89.00	6.03	20.86
-0.378	106.68	4.34	29.49
-0.286	109.98	3.21	25.13
-0.194	106.71	4.31	32.16
-0.102	97.23	5.80	31.56

X/D = 0.03

Y/D	U (m/s)	u_{rms} (m/s)	ℓ (mm)
-0.47	68.92	7.83	17.98
-0.378	91.13	5.30	25.48
-0.286	95.46	3.73	21.25
-0.194	92.77	4.36	30.16
-0.102	84.31	5.94	25.35
-0.01	56.27	9.14	18.55
0.003	45.99	8.68	14.20
0.016	34.28	5.99	8.53
0.108	74.81	6.48	25.16
0.199	87.39	5.09	27.63
0.291	94.16	3.54	23.82
0.383	94.51	3.92	24.95
0.475	83.14	6.71	23.19

X/D = 1.00

Y/D	U (m/s)	u_{rms} (m/s)	ℓ (mm)
-0.47	66.62	7.66	18.98
-0.378	89.75	6.21	30.33
-0.286	95.81	4.26	23.93
-0.194	94.98	4.26	26.54
-0.102	88.20	5.98	31.14
-0.01	71.38	8.01	24.46
0.003	68.11	7.33	23.42
0.016	66.19	6.68	19.79
0.108	74.07	8.01	28.48
0.199	57.87	5.16	27.99
0.291	93.73	3.61	25.89
0.383	92.48	4.32	30.66
0.475	78.37	7.38	27.77

X/D = 2.00

Y/D	U (m/s)	u_{rms} (m/s)	ℓ (mm)
-0.47	65.28	6.95	20.02
-0.378	84.77	6.59	27.06
-0.286	92.24	4.27	23.88
-0.194	91.67	4.12	27.74
-0.102	83.79	6.35	30.31
-0.01	71.93	6.33	23.42
0.003	70.71	6.08	22.25
0.016	69.58	5.62	20.13
0.108	72.41	6.25	26.40
0.199	84.26	5.64	31.71
0.291	91.12	3.60	26.52
0.383	90.37	4.62	32.38
0.475	77.54	6.81	24.26

Case 14 Length Scale Results

X/D = -0.66

Y/D	U (m/s)	u_{rms} (m/s)	ℓ (mm)
-0.47	56.61	4.06	20.94
-0.378	67.68	3.20	26.94
-0.286	70.32	2.50	41.80
-0.194	67.77	3.22	51.53
-0.102	60.96	4.09	28.09

X/D = -0.33

Y/D	U (m/s)	u_{rms} (m/s)	ℓ (mm)
-0.47	50.77	4.91	18.26
-0.378	63.47	3.57	27.37
-0.286	66.57	2.57	27.68
-0.194	64.68	3.25	40.29
-0.102	58.37	4.30	29.38

X/D = 0.03

Y/D	U (m/s)	u_{rms} (m/s)	ℓ (mm)
-0.47	44.34	5.63	16.72
-0.378	58.65	3.93	23.98
-0.286	62.15	2.86	22.59
-0.194	60.04	3.25	28.17
-0.102	53.39	4.30	25.41
-0.01	31.99	6.58	14.46
0.003	25.02	5.95	10.76
0.016	27.44	6.02	6.57
0.108	78.50	6.11	27.17
0.199	90.04	4.79	29.17
0.291	96.31	3.41	31.59
0.383	96.89	3.71	29.04
0.475	85.80	6.61	23.41

X/D = 0.50

Y/D	U (m/s)	u_{rms} (m/s)	ℓ (mm)
-0.47	41.08	5.47	17.06
-0.378	55.56	4.17	25.53
-0.286	59.95	2.97	23.20
-0.194	58.61	3.22	28.11
-0.102	52.53	4.62	27.49
-0.01	44.50	5.81	13.42
0.003	48.75	7.5	15.59
0.016	53.04	8.48	19.13
0.108	81.17	6.22	27.87
0.199	90.37	4.82	32.70
0.291	95.64	3.43	25.22
0.383	94.60	4.18	27.63
0.475	81.82	7.23	22.30

Case 14 Length Scale Results (con'd)

X/D = 1.00

Y/D	U (m/s)	u_{rms} (m/s)	ℓ (mm)
-0.47	40.73	5.20	16.12
-0.378	54.53	4.39	25.43
-0.286	59.32	3.11	24.00
-0.194	58.37	3.28	24.44
-0.102	51.45	4.99	31.62
-0.01	53.45	7.23	16.21
0.003	55.91	7.78	19.02
0.016	59.40	8.49	20.99
0.108	81.23	6.53	28.32
0.199	90.37	4.73	33.32
0.383	93.83	4.39	29.74
0.475	80.24	7.22	22.69

X/D = 1.50

Y/D	U (m/s)	u_{rms} (m/s)	ℓ (mm)
-0.47	41.80	5.11	17.31
-0.378	54.19	4.72	54.17
-0.286	59.51	3.13	24.78
-0.194	58.85	3.35	37.02
-0.102	52.82	4.67	26.38
-0.01	57.15	7.07	17.96
0.003	59.31	7.56	19.07
0.016	61.73	8.02	20.37
0.108	79.54	7.49	29.11
0.199	90.10	4.87	45.35
0.383	92.93	4.39	34.79
0.475	78.97	7.04	23.71

X/D = 2.00

Y/D	U (m/s)	u_{rms} (m/s)	ℓ (mm)
-0.47	41.52	5.01	17.27
-0.378	52.98	4.88	25.28
-0.286	58.99	3.29	24.29
-0.194	58.47	3.34	30.35
-0.102	53.88	4.26	19.70
-0.01	58.71	6.79	18.48
0.003	60.63	7.28	20.25
0.016	62.74	7.62	20.90
0.108	77.91	7.72	29.47
0.199	89.60	5.18	35.11
0.383	92.38	4.90	36.21
0.475	78.95	6.95	23.13

Length Scale Results for All Cases (X/D = 0.03, Z/D = 0.00)

Case 1

Y/D	U (m/s)	u_{rms} (m/s)	ℓ (mm)
0.475	81.61	7.06	21.16
0.409	92.39	4.97	28.17
0.344	95.16	3.59	26.37
0.278	93.38	3.82	24.93
0.213	88.34	4.92	27.83
0.147	80.59	5.86	26.53
0.081	68.33	7.33	26.27
0.016	33.21	5.55	7.88
-0.05	74.67	7.31	27.16
-0.115	85.68	5.94	27.56
-0.181	91.93	4.87	25.59
-0.247	95.61	3.87	27.93
-0.312	95.75	4.08	24.85
-0.378	91.55	5.32	26.02
-0.444	79.72	7.24	20.63
-0.496	34.84	6.06	6.98

Case 7

Y/D	U (m/s)	u_{rms} (m/s)	ℓ (mm)
0.475	45.80	4.20	24.72
0.409	51.99	2.98	46.28
0.344	53.48	2.24	74.49
0.278	52.85	2.44	61.28
0.213	49.98	3.03	50.48
0.081	39.02	4.19	29.30
0.016	19.40	3.57	6.89
-0.05	42.79	4.40	28.79
-0.115	49.73	3.70	35.46
-0.181	53.52	3.11	47.89
-0.247	55.34	2.49	64.32
-0.312	55.26	2.63	61.18
-0.378	52.76	3.36	43.09
-0.444	46.49	4.26	22.54
-0.496	22.85	4.39	6.27

Case 8

Y/D	U (m/s)	u_{rms} (m/s)	ℓ (mm)
0.475	107.88	8.54	23.41
0.409	121.02	5.74	32.00
0.344	124.77	3.94	25.72
0.278	121.37	4.37	28.21
0.213	114.82	5.63	29.49
0.147	105.49	6.97	29.42
0.081	89.96	9.08	27.00
0.016	44.03	7.42	9.28
-0.05	98.66	8.87	26.02
-0.115	112.64	7.05	28.29
-0.181	120.09	5.68	27.93
-0.247	124.49	4.38	28.39
-0.312	123.94	4.43	23.45
-0.378	119.16	5.90	26.74
-0.444	104.47	8.58	22.79
-0.496	63.53	9.32	11.54

Case 10

Y/D	U (m/s)	u_{rms} (m/s)	ℓ (mm)
0.475	90.35	7.68	22.55
0.409	101.57	5.35	29.48
0.344	104.26	3.69	28.81
0.278	102.70	4.03	29.32
0.213	96.84	5.18	28.69
0.147	89.35	6.27	29.58
0.081	75.30	8.07	26.99
0.016	36.44	5.97	7.91
-0.05	82.96	7.80	26.47
-0.115	94.64	6.36	28.28
-0.181	101.43	5.16	26.77
-0.247	105.36	4.06	24.26
-0.312	105.61	4.29	24.71
-0.378	100.72	5.70	27.83
-0.444	88.26	7.77	22.81
-0.496	41.04	6.81	7.45

Length Scale Results for All Cases (X/D = 0.03, Z/D = 0.00)

Case 11

Y/D	U (m/s)	u_{rms} (m/s)	ℓ (mm)
0.475	87.52	7.30	21.05
0.409	99.26	5.11	27.55
0.344	102.35	3.69	26.51
0.278	100.56	3.92	26.84
0.213	96.10	4.99	26.91
0.147	88.36	5.94	28.04
0.081	76.25	7.33	25.05
0.016	33.51	6.47	9.28
-0.05	61.91	6.89	25.17
-0.115	72.92	5.52	24.43
-0.181	78.76	4.48	24.04
-0.247	82.25	3.53	25.55
-0.312	82.52	3.65	20.95
-0.378	78.84	4.65	25.06
-0.444	68.59	6.45	19.91
-0.496	37.42	6.34	8.13

Case 12

Y/D	U (m/s)	u_{rms} (m/s)	ℓ (mm)
0.475	87.14	7.08	24.38
0.409	97.81	4.97	25.52
0.344	100.66	3.58	25.31
0.278	98.74	3.80	28.47
0.213	94.24	4.82	26.95
0.147	87.48	5.78	26.96
0.081	76.00	7.01	24.37
0.016	34.13	7.35	9.56
-0.05	47.17	5.68	22.10
-0.115	56.48	4.60	25.33
-0.181	61.81	3.76	23.49
-0.247	64.88	2.98	22.37
-0.312	64.99	3.14	20.71
-0.378	61.84	4.05	23.45
-0.444	53.15	5.44	19.78
-0.496	25.52	5.01	5.78

Case 13

Y/D	U (m/s)	u_{rms} (m/s)	ℓ (mm)
0.475	106.89	8.23	22.59
0.409	119.48	5.53	27.10
0.344	122.56	3.87	24.22
0.278	120.40	4.17	28.53
0.213	115.11	5.39	29.38
0.147	106.57	6.53	30.77
0.081	93.68	8.01	26.11
0.016	39.91	8.52	9.83
-0.05	55.37	6.64	22.59
-0.115	66.36	5.28	25.22
-0.181	72.26	4.33	25.89
-0.247	75.84	3.38	23.41
-0.312	75.96	3.54	20.14
-0.378	72.28	4.63	23.49
-0.444	62.09	6.42	20.00
-0.496	29.48	5.64	6.48

Case 14

Y/D	U (m/s)	u_{rms} (m/s)	ℓ (mm)
0.475	79.68	6.65	28.10
0.409	89.85	4.95	44.61
0.344	92.53	3.55	77.10
0.278	90.55	3.69	73.72
0.213	86.39	4.60	55.40
0.147	79.72	5.43	38.35
0.081	69.19	6.51	26.89
0.016	31.25	6.77	8.95
-0.05	41.62	5.00	22.20
-0.115	49.91	4.11	24.90
-0.181	54.33	3.38	50.52
-0.247	56.33	2.64	58.71
-0.312	56.06	2.76	50.88
-0.378	53.23	3.51	30.60
-0.444	46.17	4.61	18.30
-0.496	26.53	5.02	7.95

Appendix B:

SMD and Attenuation Results for Cases of the Two-Phase Flow Matrix*

*No SMD or attenuation measurements were obtained for cases 1 and 7 due to U_{AFS} values too low for sufficient atomization. For cases 12 and 14, spray impingement on the Z-walls due to large shear layer strengths (λ = 0.22) prevented these measurements.

Case 8 SMD Results

SMD (μm) (WI = 9.5 g/s)

Z/D	X/D = 0.50	X/D = 1.00	X/D = 1.50	X/D = 2.00
-0.131	127	119	113	114
-0.131	126	125	108	112
-0.131	126	119	112	112
-0.066	129	120	115	102
-0.066	135	120	114	101
-0.066	130	120	115	108
0	128	122	111	110
0	131	128	115	113
0	130	123	119	107
0.066	135	125	108	113
0.066	136	123	111	110
0.066	136	123	115	114
0.131	132	125	115	114
0.131	139	129	118	122
0.131	138	134	126	116

SMD (μm) (WI = 16.6 g/s)

Z/D	X/D = 0.50	X/D = 1.00	X/D = 1.50	X/D = 2.00
-0.131	132	112	111	104
-0.131	135	115	113	103
-0.131	134	116	114	103
-0.066	137	117	119	105
-0.066	137	122	117	111
-0.066	137	121	118	112
0	131	123	115	104
0	135	129	116	110
0	139	124	112	105
0.066	126	121	111	104
0.066	124	119	114	102
0.066	121	120	114	101
0.131	129	119	119	111
0.131	133	122	113	111
0.131	132	120	114	112

Case 10 SMD Results

SMD (μm) (WI = 9.5 g/s)

Z/D	X/D = 0.50	X/D = 1.00	X/D = 1.50	X/D = 2.00
-0.131	144	148	133	127
-0.131	147	156	132	131
-0.131	155	151	133	126
-0.066	166	151	140	142
-0.066	170	167	146	140
-0.066	168	147	145	136
0	165	158	146	144
0	167	155	149	143
0	150	151	152	133
0.066	167	149	142	138
0.066	165	148	140	137
0.066	165	156	136	143
0.131	161	156	153	142
0.131	167	156	153	148
0.131	161	147	156	148

SMD (μm) (WI = 16.6 g/s)

Z/D	X/D = 0.50	X/D = 1.00	X/D = 1.50	X/D = 2.00
-0.131	150	139	136	127
-0.131	148	143	138	132
-0.131	150	150	138	127
-0.066	161	148	141	144
-0.066	157	142	139	141
-0.066	165	150	139	141
0	148	144	142	142
0	158	141	144	138
0	154	149	143	143
0.066	158	148	138	126
0.066	169	149	138	128
0.066	159	140	136	131
0.131	159	147	143	148
0.131	172	148	152	145
0.131	164	153	143	147

Case 11 SMD Results

SMD (μm) (WI = 9.5 g/s)

Z/D	X/D = 0.50	X/D = 1.00	X/D = 1.50	X/D = 2.00
-0.131	160	162	166	155
-0.131	167	164	155	157
-0.131	167	163	168	165
-0.066	170	166	163	168
-0.066	177	176	174	166
-0.066	179	173	169	165
0	171	166	160	154
0	176	173	157	161
0	167	163	162	157
0.066	169	162	167	163
0.066	178	170	167	168
0.066	174	169	167	156
0.131	177	171	164	168
0.131	182	177	170	169
0.131	185	183	172	169

SMD (μm) (WI = 16.6 g/s)

Z/D	X/D = 0.50	X/D = 1.00	X/D = 1.50	X/D = 2.00
-0.131	166	148	160	160
-0.131	183	158	161	159
-0.131	168	164	165	160
-0.066	170	170	157	169
-0.066	174	170	158	166
-0.066	180	169	163	162
0	176	168	174	160
0	173	167	165	163
0	174	168	170	159
0.066	170	168	161	163
0.066	178	164	165	156
0.066	174	159	161	166
0.131	189	164	159	159
0.131	189	168	160	169
0.131	187	170	160	168

Case 13 SMD Results

SMD (μm) (WI = 9.5 g/s)

Z/D	X/D = 0.50	X/D = 1.00	X/D = 1.50	X/D = 2.00
-0.131	152	148	153	134
-0.131	161	153	139	145
-0.131	168	155	150	160
-0.066	173	155	153	173
-0.066	180	164	152	176
-0.066	171	155	158	162
0	164	152	159	161
0	171	168	158	160
0	164	166	156	160
0.066	174	162	164	155
0.066	174	164	171	158
0.066	177	154	182	153
0.131	173	168	164	168
0.131	172	164	168	184
0.131	178	170	160	170

SMD (μm) at WI = 16.6 g/s

Z/D	X/D = 0.50	X/D = 1.00	X/D = 1.50	X/D = 2.00
-0.131	163	153	144	141
-0.131	166	160	149	143
-0.131	173	153	149	135
-0.066	162	156	156	160
-0.066	166	153	158	160
-0.066	166	155	148	161
0	158	153	152	154
0	169	159	154	157
0	165	165	146	153
0.066	162	161	142	159
0.066	162	153	158	158
0.066	165	150	154	168
0.131	172	154	161	164
0.131	170	158	160	173
0.131	178	157	159	169

Case 8 Attenuation Results

I/Io

WI (g/s)	Z/D	X/D = 0.50	X/D = 1.00	X/D = 1.50	X/D = 2.00
9.50	-0.131	0.78	0.83	0.74	0.84
9.50	-0.066	0.80	0.85	0.84	0.85
9.50	0	0.84	0.84	0.87	0.86
9.50	0.066	0.86	0.87	0.88	0.87
9.50	0.131	0.91	0.91	0.90	0.91
16.60	-0.131	0.69	0.73	0.73	0.76
16.60	-0.066	0.71	0.76	0.77	0.76
16.60	0	0.75	0.76	0.77	0.78
16.60	0.066	0.77	0.80	0.79	0.80
16.60	0.131	0.74	0.80	0.81	0.82

Case 10 Attenuation Results

I/Io

WI (g/s)	Z/D	X/D = 0.50	X/D = 1.00	X/D = 1.50	X/D = 2.00
9.50	-0.131	0.83	0.83	0.85	0.85
9.50	-0.066	0.85	0.84	0.87	0.87
9.50	0	0.85	0.85	0.87	0.87
9.50	0.066	0.86	0.89	0.89	0.89
9.50	0.131	0.84	0.89	0.89	0.89
16.60	-0.131	0.70	0.71	0.77	0.76
16.60	-0.066	0.74	0.78	0.78	0.80
16.60	0	0.77	0.80	0.77	0.80
16.60	0.066	0.80	0.79	0.82	0.83
16.60	0.131	0.80	0.80	0.83	0.84

Case 11 Attenuation Results

I/Io

WI (g/s)	Z/D	X/D = 0.50	X/D = 1.00	X/D = 1.50	X/D = 2.00
9.50	-0.131	0.79	0.83	0.86	0.84
9.50	-0.066	0.81	0.83	0.88	0.89
9.50	0	0.83	0.83	0.84	0.89
9.50	0.066	0.85	0.85	0.87	0.88
9.50	0.131	0.86	0.85	0.90	0.88
16.60	-0.131	0.69	0.72	0.78	0.78
16.60	-0.066	0.71	0.73	0.79	0.79
16.60	0	0.74	0.75	0.79	0.78
16.60	0.066	0.77	0.78	0.81	0.83
16.60	0.131	0.76	0.80	0.83	0.83

Case 13 Attenuation Results

I/Io

WI (g/s)	Z/D	X/D = 0.50	X/D = 1.00	X/D = 1.50	X/D = 2.00
9.50	-0.131	0.77	0.80	0.84	0.85
9.50	-0.066	0.77	0.81	0.84	0.85
9.50	0	0.78	0.82	0.85	0.85
9.50	0.066	0.83	0.85	0.88	0.86
9.50	0.131	0.84	0.89	0.89	0.89
16.60	-0.131	0.63	0.69	0.74	0.74
16.60	-0.066	0.67	0.71	0.74	0.75
16.60	0	0.69	0.72	0.75	0.76
16.60	0.066	0.70	0.74	0.78	0.78
16.60	0.131	0.72	0.78	0.80	0.81

SMD (Z/D = 0) versus Fuel Side Air Velocity for various Axial Locations (WI = 16.6 g/s)

SMD (μm) at X/D = 0.5

λ	74.9 m/s	82.6 m/s	91.6 m/s	100.4 m/s	122.0 m/s
0.00	165	148	143	131	111
0.00	163	158	144	135	111
0.00	166	154	139	139	112
0.10	179	176	164	151	125
0.10	177	173	163	147	123
0.10	184	174	164	147	125
0.22	*	190	159	158	149
0.22	*	191	174	169	145
0.22	*	190	173	165	154

SMD (μm) at X/D = 1.0

λ	74.9 m/s	82.6 m/s	91.6 m/s	100.4 m/s	122.0 m/s
0.00	161	144	140	123	99
0.00	162	141	136	129	99
0.00	162	149	137	124	103
0.10	176	168	147	140	117
0.10	173	167	153	143	112
0.10	175	168	147	141	116
0.22	*	173	166	153	138
0.22	*	178	168	159	139
0.22	*	173	164	165	135

* Value greater than the measurement capability of the instrument

SMD (Z/D = 0) versus Fuel Side Air Velocity for various Axial Locations (WI = 16.6 g/s)

SMD (μm) at X/D = 1.5

λ	74.9 m/s	82.6 m/s	91.6 m/s	100.4 m/s	122.0 m/s
0.00	158	142	135	115	89
0.00	159	144	133	116	90
0.00	157	143	142	112	90
0.10	175	174	140	132	104
0.10	177	165	145	137	108
0.10	168	170	145	140	103
0.22	*	164	167	152	122
0.22	*	170	164	154	129
0.22	*	171	165	146	125

SMD (μm) at X/D = 2.0

λ	74.9 m/s	82.6 m/s	91.6 m/s	100.4 m/s	122.0 m/s
0.00	156	142	129	104	87
0.00	155	138	134	110	89
0.00	155	143	132	105	88
0.10	175	160	144	133	104
0.10	181	163	149	137	105
0.10	181	159	146	131	106
0.22	*	176	166	154	125
0.22	*	174	168	157	124
0.22	*	171	165	153	126

* Value greater than the measurement capability of the instrument